Mechanical Engineering

Principles of Ship Buoyancy and Stability

Pekka Ruponen

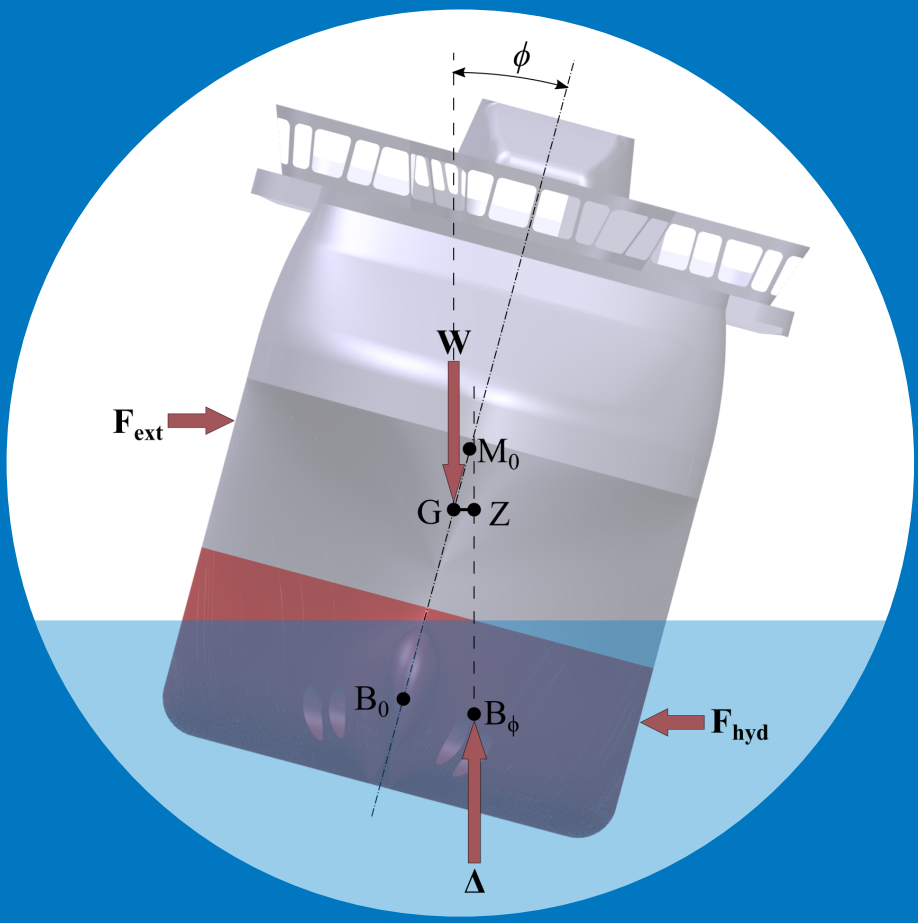

Aalto University
SCIENCE + TECHNOLOGY
LEARNING MATERIAL

Aalto University publication series
SCIENCE + **TECHNOLOGY** 8/2021

Principles of Ship Buoyancy and Stability

Pekka Ruponen

Aalto University
School of Engineering
Mechanical Engineering
Marine Technology

Aalto University publication series
SCIENCE + **TECHNOLOGY** 8/2021

ISBN 978-952-64-0579-7 (printed)
ISBN 978-952-64-0580-3 (pdf)
ISSN 1799-4896 (printed)
ISSN 1799-490X (pdf)
http://urn.fi/URN:ISBN:978-952-64-0580-3

Unigrafia Oy
Helsinki 2021

Finland

Printed matter
4041-0619

Principles of Ship Buoyancy and Stability

Pekka Ruponen

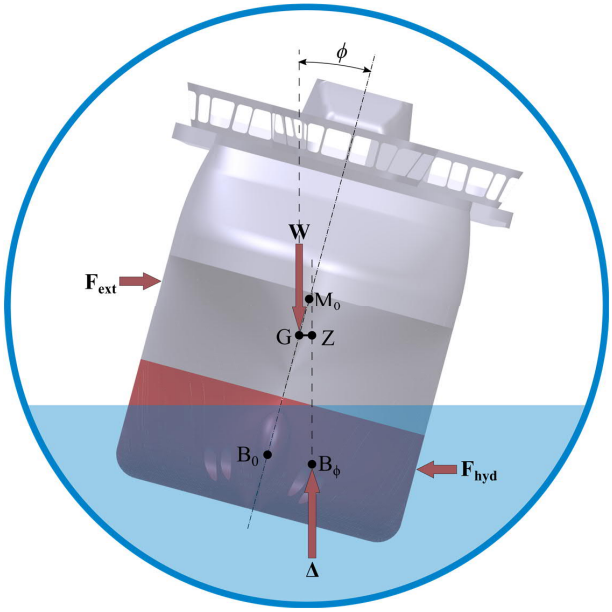

Cover image ship project courtesy of Wärtsilä Ship Design Norway AS,
visualization by Pekka Ruponen and Francesco Oneto

Preface

This book is mainly aimed for students of the course MEC-E2002 “Ship Buoyancy and Stability” at Aalto University. The physical background for ship stability is presented, including several practical examples. The relevant regulations of the International Maritime Organization (IMO), for both intact and damage stability, are also briefly reviewed, with focus on the underlying physics and description of the applied assumptions and simplifications. Therefore, the material is believed to be useful also for graduated naval architects in the industry.

The chapters 3-6 and 9 are based on the excellent textbook *Laivan kelluvuus ja vakavuus* (*Ship buoyancy and stability*) in Finnish by Prof. Jerzy Matusiak, with some updates and additional practical examples.

Several examples have been calculated with NAPA software, using various public demo ships, courtesy of NAPA, which is gratefully acknowledged. The cruise ship design was kindly provided by Mrs. Anna-Lea Routi from Meyer Turku. Graphic output from the software has been partly edited for better visualization for educational purposes.

I would like to thank Prof. Jerzy Matusiak and Mr. Daniel Lindroth for their valuable comments and suggestions. Mr. Alexander Rogers is thanked for checking the language of the very first version of the book.

Pekka Ruponen

Professor of Practice, Aalto University
Lead Research Engineer, NAPA

Contents

Nomenclature

Symbols:

A	attained subdivision index,
	area
A_{k}	bilge keel area
A_{L}	lateral wind area
A_{w}	waterplane area
a_{w}	wave amplitude
B	breadth (of the ship)
$\overline{B_0M_0}$	metacentric radius
$\overline{B_0M_{\mathrm{L}}}$	longitudinal metacentric radius
b	breadth (of a tank)
C_{B}	block coefficient
C_{d}	discharge coefficient (of an opening)
C_{m}	midship section area coefficient
C_{w}	aerodynamic wind resistance coefficient
D	depth of the hull
d	draft (in IMO regulation context)
e	distance,
	dynamic righting lever
F	force,
	flow reduction coefficient
Fn	Froude number
$\boldsymbol{f}$	body force vector
$\overline{GM_0}$	metacentric height
$\overline{GM}_{\mathrm{corr}}$	corrected metacentric height (free surface effect included)
$\overline{GM_{\mathrm{L}}}$	longitudinal metacentric height
$\overline{GZ}$	righting lever
g	gravitational acceleration
H	height
H_{s}	significant wave height
H_{w}	water height
h	height,
	righting lever
I_{L}	longitudinal surface moment of inertia of the waterplane area
I_{T}	transverse surface moment of inertia of the waterplane area
i_{T}	transverse surface moment of inertia of the free surface area in tank
K	coefficient of roll damping effect in the weather criterion,
	coefficient for effect of heeling on the survivability (“s-factor”) for damaged ship
$\overline{KB_0}$	vertical centre of buoyancy
$\overline{KG}$	vertical centre of gravity

k	wave number
k_{xx}	radius of transverse inertia
L	length (of the ship)
L_{pp}	length between perpendiculars
L_{oa}	length over all
L_{s}	subdivision length
L_{wl}	waterline length
l	length (of a tank or a wire),
	lever of a moment
M	moment
M_{ext}	external (heeling) moment
M_{fs}	free surface moment
M_{st}	static righting moment
$\overline{M_0 S}$	residual stability lever
M_{CT}	moment to trim one meter
m	mass
N	number of passengers/cases/etc.
P	contact force (of grounding),
	wind pressure
p	pressure
p_{h}	hydrostatic pressure
p_i	probability ("p-factor") for damage case i
Q	volumetric flow
R	required subdivision index
r	distance,
	steel reduction (factor),
	wave steepness
$\boldsymbol{r}$	distance vector
$range$	range of (positive) stability
S	(wet) surface area,
	cross-sectional area of a cross-flooding device
S_{b}	bottom area
s	cross-sectional area (of a wedge),
	wave slope
s_i	survivability ("s-factor") for damage case i
t	time,
	trim in meters
T	draft
T_{A}	draft at aft perpendicular
T_{F}	draft at fore perpendicular
T_{z}	zero-crossing period
T_ϕ	natural roll period
T^*	characteristic draft

U_{w}	wind velocity
V_{net}	net volume (of a compartment)
V_{s}	velocity of the ship
V_{tot}	total volume (of a compartment)
V_{w}	volume of floodwater
v	volume
v_i	"v-factor" for damage case i
W	weight (of the ship)
W_{f}	cross-flooded volume
W_i	weight factor for case i
x, y, z	coordinates of the right-handed ship-fixed Cartesian coordinate system
Z	wind moment lever

Greek symbols:

α	linear roll damping coefficient
β	encounter angle, quadratic roll damping coefficient
γ	cubic roll damping coefficient
Δ	lifting force of displacement
ε	phase angle
θ	trim or pitch angle
Λ	tuning factor
λ	wavelength
μ	permeability
ξ	critical damping ratio
ρ	density (of water)
ρ_{a}	air density
ρ_{t}	density of liquid load in tank
ϕ	heel or roll angle
ϕ_{A}	roll amplitude
ϕ_{f}	flooding angle (opening immersion)
ψ	yaw angle
ω	angular frequency
ω_{e}	angular encounter frequency
ω_{ϕ}	natural angular frequency of roll motion
∇	volume of displacement

Symbols in bold font denote vectors and matrices.
Dots above variables denote time derivatives.

Abbreviations:

AHTS	anchor handling tug supply (vessel)
AP	aft perpendicular
CFD	computational fluid dynamics
DOF	degree-of-freedom
DSA	direct stability assessment
DSS	decision support system
DW	deadweight
EMSA	European Maritime Safety Agency
FP	forward perpendicular
FWA	freshwater allowance
IACS	International Association of Classification Societies
ICLL	International Convention on Load Lines
IMO	International Maritime Organization
IS Code	International Code on Intact Stability, 2008
ITTC	International Towing Tank Conference
LW	lightweight
OG	operational guidelines
PCTC	pure car/truck carrier
Ro-Ro	Roll on / Roll off
RoPax	Ro-Ro/Passenger (ship)
SGISC	Second Generation Intact Stability Criteria
SOLAS	(International Convention for the) Safety of Life at Sea
SRtP	Safe Return to Port
SWATH	small waterplane area twin hull (vessel)
WL	waterline
WT	watertight

1 Introduction

Ship buoyancy and stability are fundamental parts of Naval Architecture that need to be considered throughout the life cycle of a ship. The ship design process is traditionally visualized as a spiral, where different analyses are recalculated as the design of the ship progresses from early concept stage to detail design. Although, this is a somewhat old-fashioned approach, the design spiral illustrates the importance of ship buoyancy and stability, Figure 1.1. Moreover, after construction, buoyancy and stability calculations are needed every day to ensure safe operation throughout the life cycle of the ship.

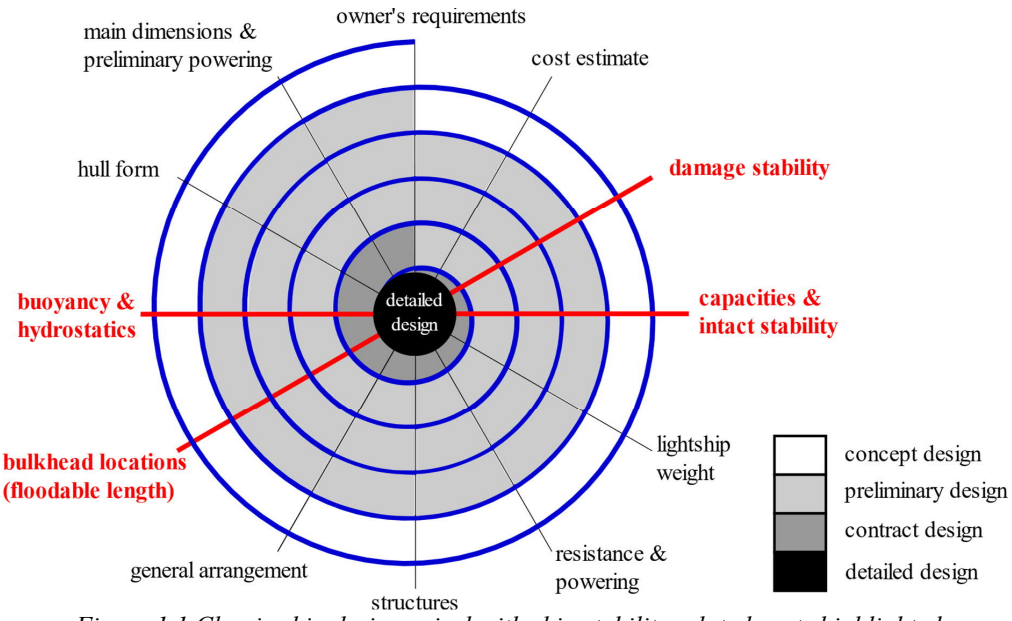

Figure 1.1 Classic ship design spiral with ship stability related parts highlighted

Ship stability assessments require proper understanding of both related laws of physics and relevant international regulations. The term stability has a different meaning, depending on whether the considered ship is intact or damaged. According to a traditional definition:

> ***intact stability*** *means the ability to withstand external moments without interference to the operation of the ship,*

whereas:

> ***damage stability*** *represents ability to withstand external moments without capsizing.*

For centuries, naval architecture was an art based mainly on experience. The successful hull forms and design practices were copied, without really understanding the underlying physics. During the 19th century, the mathematical formulation for ship stability was developed, but the

first proper criteria for intact stability were developed as late as 1939 by Jaakko Rahola. This pioneering work is still the basis for the current international regulations. Recently, the focus has been on rare but dangerous stability failures in waves, with the introduction of the Second Generation Intact Stability Criteria (SGISC), IMO (2020).

The regulatory development for damage stability has been influenced by several catastrophic accidents of large passenger ships. With increased computing capacity, it is nowadays possible to calculate a very large number of different damage cases, and by using probabilistic methods, it is possible to ensure that the ship design meets the required level of survivability. Furthermore, the use of time-domain simulation, for calculation of realistic flooding progression, is nowadays feasible, and can be used to design arrangements that further improve the survivability of the ship in case of damage.

Ship stability calculations are strongly related to regulations by the International Maritime Organization (IMO) and various other administrations and classification societies. These regulations are normally extended and updated at certain intervals, often as a reaction to a catastrophic accident. New methods may be introduced, or alternatively, the safety level standards could be increased. This book focuses on the current IMO Code on Intact Stability and SOLAS (Safety of Life at Sea) edition.

The following chapters present the principles of buoyancy and stability of ships, considering also various stability failure modes in waves, as well as subdivision and damage stability. Finally, various special stability problems are briefly introduced, including the stability of floating offshore structures. In general, the underlying physics and mathematics of the IMO regulations, valid at the time of writing, are described, both for intact and damage stability of new ships.

2 Definitions

2.1 Coordinate system

The current standard in naval architecture is to use a right-handed coordinate system, with the x-axis pointing towards the bow, the z-axis oriented positive-upwards, and the y-axis pointing to port side. Usually, the origin is placed in the baseline at the location of the aft perpendicular (AP). This body-fixed coordinate system moves with the ship, i.e. it is ship-fixed. The axes and the angular motions, heel angle ϕ, trim angle θ and yaw angle ψ, are illustrated in Figure 2.1. Unless otherwise stated, this coordinate system is used in this book.

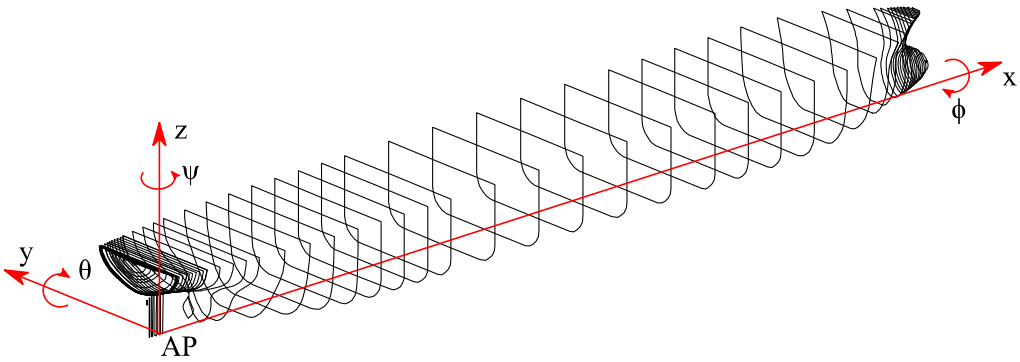

Figure 2.1 Applied right-handed ship-fixed coordinate system

The ship floats *upright* when the heel angle is (practically) zero; the situation where the trim is (practically) zero is known as an *even keel* condition. It should also be noted that the yaw angle ψ does not affect the buoyancy and stability of the ship in calm water.

In literature, other coordinate systems have also been used, including left-handed systems. The selection of the coordinate system does not affect the main equations of ship buoyancy and stability, but special attention is always needed, e.g. when reviewing stability calculation results.

The draft of the ship is usually associated with the readings on the *draft marks* in the sides of the ship at AP (aft perpendicular), amidships and at FP (forward perpendicular)[1], Figure 2.2. However, when the ship is considered as a rigid body, the floating position can be presented with only three variables: draft, trim and heel. Longitudinally the mean draft is measured amidships, perpendicular to the base line, but transversally the draft value is considered to be perpendicular to the sea level, as illustrated in Figure 2.3. It should be noted that this value does not represent the maximum draft of the ship, and the corresponding draft mark values must be calculated separately.

[1] AP and FP are defined in ICLL (International Convention on Load Lines)

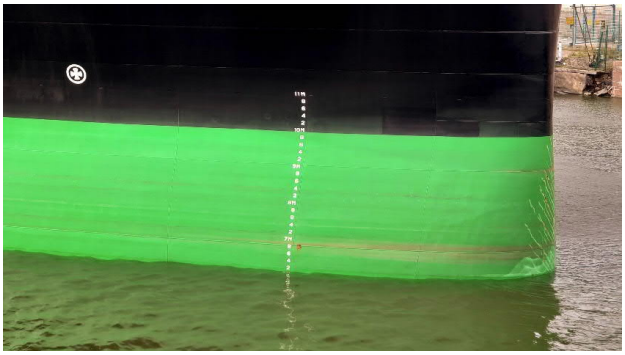

Figure 2.2 Draft marks at forward perpendicular of a bulk carrier

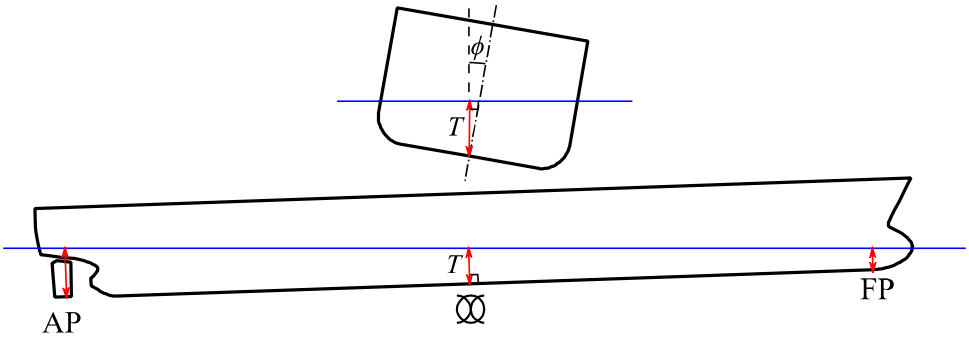

Figure 2.3 Definition of mean draft T for a heeled and trimmed ship

In practice, positive heel angles are preferred, and instead of the sign (+/-), the heeling direction, i.e. either starboard (SB) or port side (PS), is given. In addition, the trim angle is rarely used, and trim in meters is preferred as a more descriptive quantity. Trim is defined as the difference between the fore and aft drafts, T_A and T_F at AP and FP, Figure 2.4, so that the relation to trim angle involves the length between perpendiculars, L_{pp}:

$$\tan\theta = \frac{(T_F - T_A)}{L_{pp}} \tag{2.1}$$

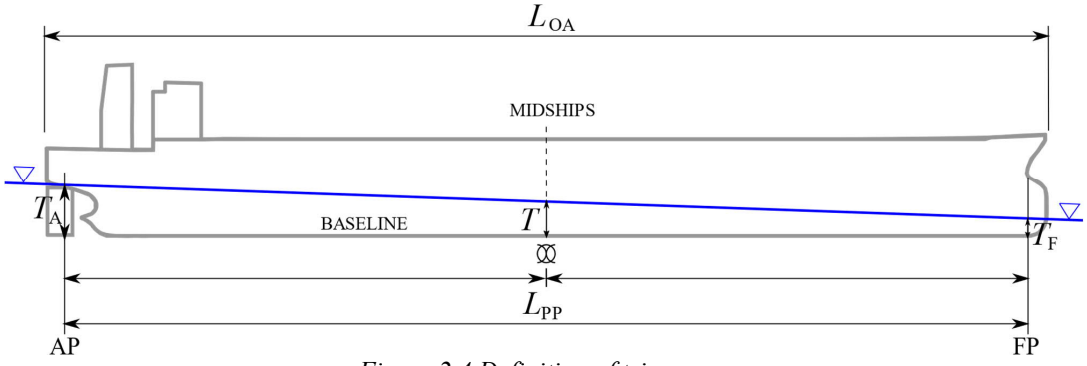

Figure 2.4 Definition of trim

2.2 Buoyant hull and freeboard height

In normal stability calculations the ship is considered to be a rigid body. In rare cases the hull deflection (hogging/sagging) is taken into account by using a deformed hull form as the buoyant hull.

Non-watertight parts, such as the superstructure, are usually excluded from the buoyant hull, Figure 2.5. This is a conservative approach, since, at large heel angles, these parts would also provide some additional buoyancy, at least temporarily.

Figure 2.5 Examples of buoyant hull (shaded area) for a bulk carrier and a cruise ship

The minimum distance from the waterline to the upper deck level is the *freeboard height*, Figure 2.6. It is measured at the lowest point of sheer, where water can enter the ship. In the regulatory context, the calculation of the freeboard deck edge curve is defined in The International Convention on Load Lines (ICLL).

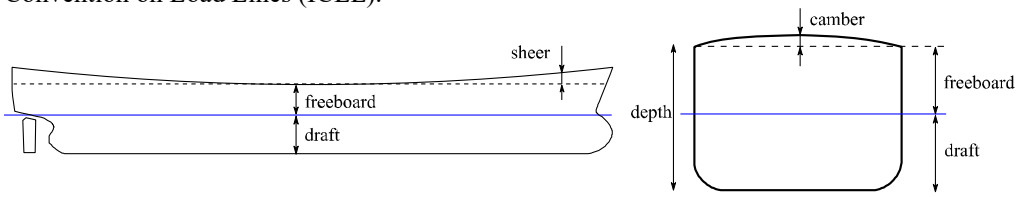

Figure 2.6 Freeboard height

2.3 Equilibrium

An object is in equilibrium if it is not subjected to accelerations. According to Newton's second law, this means that the sum of all forces acting on the object is zero:

$$\sum \boldsymbol{F}_i = 0 \tag{2.2}$$

and that the sum of the moments of those forces is zero:

$$\sum \boldsymbol{r}_i \times \boldsymbol{F}_i = 0 \tag{2.3}$$

where $\boldsymbol{r}$ is the distance vector from the force reaction point to the reference point.

In general, three distinctive types of equilibrium are identified. An object is *stable* when any sort of small movement will increase the object's potential energy, and after a small perturbation, the body falls back to its initial equilibrium position. The object is *unstable* if any sort of small movement decreases the object's potential energy, meaning that it is not returned to the original position without some exertion of energy. Instead, the body tends to fall away from to its initial equilibrium position. If any sort of small movement does not affect the object's potential energy, and the body remains in equilibrium in the new position, the stability condition is *neutral*. All three types of stability are illustrated in Figure 2.7.

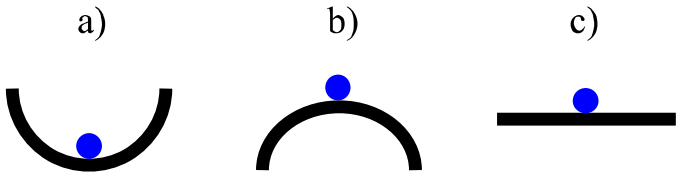

Figure 2.7 Examples of a) steady, b), unsteady and c) neutral equilibrium conditions

As an example, the case in Figure 2.7a is explained in detail. When the ball is disturbed by a small external force so that it is moved to a new position along the circular arc, as visualized in Figure 2.8. When the external force is removed, there is a restoring force due to gravity, acting tangential to the arc:

$$F = -mg \sin \phi \tag{2.4}$$

where m is mass of the ball, g is acceleration due to gravity and ϕ is the angle corresponding to the length of the arc. The travelled distance along the arc is:

$$s = r\phi \tag{2.5}$$

where r is the radius of the arc. The disturbance is small, and therefore also the angle ϕ is small, and the restoring force can be presented as:

$$F \approx -mg\phi = -\frac{mgs}{r} \tag{2.6}$$

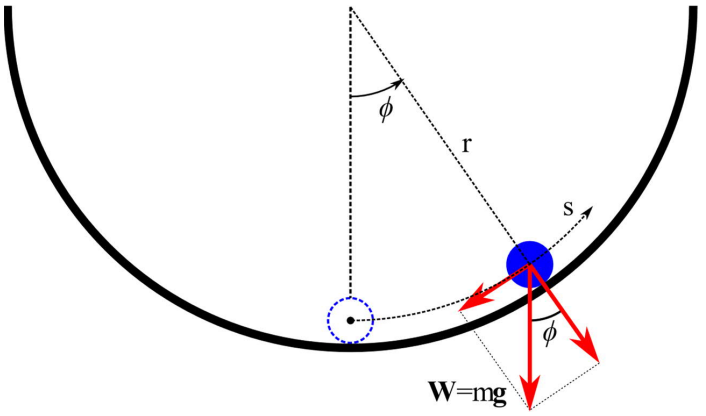

Figure 2.8 Example of restoring force due to gravity

The restoring force will return the ball towards its initial position. Considering the distance s along the arc as a coordinate of the ball position, it can be seen that the derivative of the restoring force is:

$$\frac{\partial F}{\partial s} = -\frac{mg}{r} < 0 \tag{2.7}$$

Therefore, the initial position is a stable equilibrium.

A schematic presentation of the forces acting on a floating ship is shown in Figure 2.9. The equilibrium condition, equations (2.2) and (2.3), is stable if there is a restoring force that returns the ship to the original position. This can be presented as:

$$\sum_i \frac{\partial F_{\mathrm{x},i}}{\partial x} < 0,\ \sum_i \frac{\partial F_{\mathrm{y},i}}{\partial y} < 0,\ \sum_i \frac{\partial F_{\mathrm{z},i}}{\partial z} < 0,\ \sum_i \frac{\partial M_{\mathrm{x},i}}{\partial \phi} < 0,\ \sum_i \frac{\partial M_{\mathrm{y},i}}{\partial \theta} < 0 \text{ and } \sum_i \frac{\partial M_{\mathrm{z},i}}{\partial \psi} < 0 \tag{2.8}$$

Note that external forces are not included when analysing whether the equilibrium condition is stable or not.

Planar motion of the ship does not affect the centre of gravity, nor the centre of buoyancy. Thus the static stability in x and y directions is neutral, and there are no restoring forces. The same applies for the yaw motion, and consequently:

$$\sum_i \frac{\partial F_{\mathrm{x},i}}{\partial x} = 0,\ \sum_i \frac{\partial F_{\mathrm{y},i}}{\partial y} = 0 \text{ and } \sum_i \frac{\partial M_{\mathrm{z},i}}{\partial \psi} = 0 \tag{2.9}$$

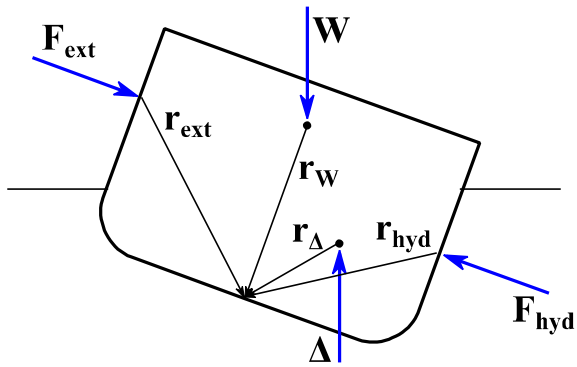

Figure 2.9 Schematic illustration of forces and moments on a floating ship

3 Hydrostatics and buoyancy

3.1 Archimedes' principle

The starting point for hydrostatics is the conservation of momentum for inviscid and incompressible fluid, i.e. the so-called Euler's equation:

$$\frac{\mathrm{D}\boldsymbol{v}}{\mathrm{D}t} = -\frac{1}{\rho}\mathrm{grad}(p) + \boldsymbol{f} \tag{3.1}$$

The left-hand side denotes total acceleration of the fluid. Here $\boldsymbol{v}$ is the flow velocity vector, t is time, ρ is fluid density, p is pressure and $\boldsymbol{f}$ is the so-called body force vector.

Ship hydrostatics are based on the assumption that the pressure variations, associated with the flow around the hull, are small. Consequently, the left-hand side of the equation (3.1) is considered to be zero.

The gravitational force, oriented normally to an undisturbed free surface, is the only distributed force acting on a fluid. In a coordinate system with the z-axis oriented vertically and pointing upwards, this means that the only non-zero body force component is:

$$f_z = -g \tag{3.2}$$

where g is the acceleration due to gravity[2]. Consequently, a single ordinary linear differential equation for the pressure is:

$$\frac{\mathrm{d}p}{\mathrm{d}z} = -\rho g \tag{3.3}$$

This means that the pressure in a fluid at rest varies linearly with the water depth h, Figure 3.1. At sea level the pressure equals to the atmospheric pressure p_0.

Integration gives the pressure:

$$p = p_0 + \rho g h \tag{3.4}$$

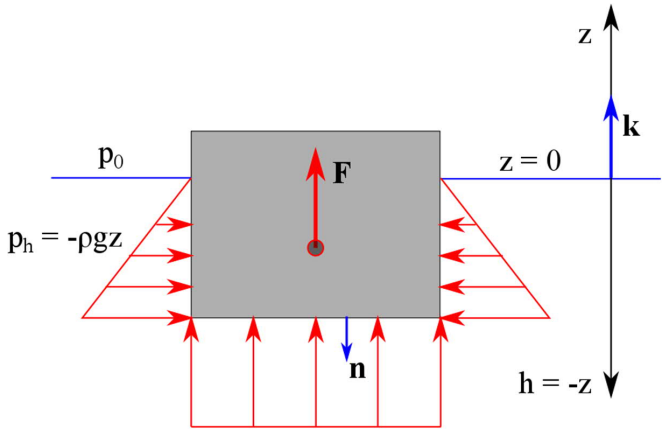

Figure 3.1 Hydrostatic pressure on a floating object

[2] Normally in buoyancy and stability calculations an approximation of 9.81 m/s^2 is used.

The force vector $\boldsymbol{F}$, acting on a submerged or a floating body, can be evaluated by integrating the pressure acting on the body surface in contact with water S, called as the *wet surface*:

$$\boldsymbol{F} = -\int_S p\mathbf{n}\mathrm{d}S = -\int_\nabla \operatorname{grad} p \,\mathrm{d}\nabla = -\mathbf{k}\int_\nabla \frac{\mathrm{d}p}{\mathrm{d}z}\mathrm{d}\nabla = \mathbf{k}\rho g\nabla = \boldsymbol{\Delta} \tag{3.5}$$

Here the Gauss theorem is used in substitution of integrals, so that a surface integral is changed to a volume integral. The vector normal to the body surface and pointing outwards is denoted by **n**. The unit vector, in-line with the vertical axis z, is marked by **k**. The result of integration is the so-called *Archimedes law*, stating that:

"the apparent loss in weight of a body immersed in a fluid is equal to the weight of the displaced fluid".

The only force acting on a body at rest emerged in still fluid, is the vertically oriented force called buoyancy. This force equals the weight of the fluid displaced by the body.

The buoyancy force acts on the point where all moments vanish. This means that the x-coordinate of this point x_B can be solved from the following equation:

$$x_\mathrm{B}\rho g\nabla = \int_\nabla x\rho g\mathrm{d}\nabla \tag{3.6}$$

And consequently:

$$x_\mathrm{B} = \frac{1}{\nabla}\int_\nabla x\mathrm{d}\nabla \tag{3.7}$$

and similarly, for y_B and z_B. This means that the buoyancy acts in the point that is the centre of the volume of the displaced fluid.

In principle, there are two alternative methods for stability calculations, as visualized in Figure 3.2. The most common one is to apply the Archimedes law and integrate submerged volumes based on calculation sections. Alternatively, the hull surface can be divided into panels; the buoyancy force is obtained by direct pressure integration over the submerged panels. The panel models are more suitable for the analysis of ship motions in waves, and for the stability analyses of offshore structures with complex geometry. For ship-shaped objects, the use of Archimedes law is both fast and accurate.

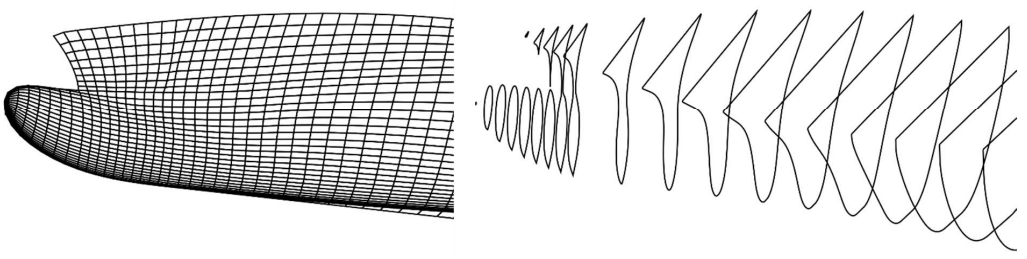

Figure 3.2 Examples of a panel model (left) and calculation sections (right) for hydrostatic calculations

One benefit of using calculations sections and Archimedes law is the possibility to easily account for hull *deflection*. In practice the sections are then shifted vertically, based on the calculated deflection value at the respective x-coordinates. It should be noted that usually in stability calculations the hull is considered to be a rigid body, but in certain conditions, such as the inclining test (see section 8), the deflection should be taken into account.

3.2 Hydrostatic calculations

Modern computer software for naval architectural calculations can accurately calculate the hydrostatics of the ship at any floating position by using a 3D geometry model of the hull. In the past, so-called *Bonjean curves*, were often used for that purpose. This method was originally proposed by French naval engineer Antoine Bonjean in the beginning of the 19th century, and it is still a practical way to present the hydrostatics of a ship. Consequently, these curves are still occasionally prepared, e.g. for use onboard smaller vessels.

The calculated quantities are sectional area as a function of draft T:

$$A(T) = 2\int_0^T y\mathrm{d}z \tag{3.8}$$

and the moment of the sectional area about the baseline:

$$M(T) = 2\int_0^T zy\mathrm{d}z \tag{3.9}$$

Here it is assumed that the baseline of the ship is at $T = 0$ and the hull form is symmetric. The format and reading of the sectional areas from the curves for a ship with stern trim is visualized in Figure 3.3. An example of Bonjean curves for sectional area and moment in the same graph is shown in Figure 3.4.

For calculations in a spread sheet, numeric values from hydrostatic calculation software can be obtained in a tabular format. The precalculated curves are used in calculating the volume of displacement and the centre of buoyancy at any waterline, or angle of trim. The profile of the hull and the waterline can also be plotted in the same graph.

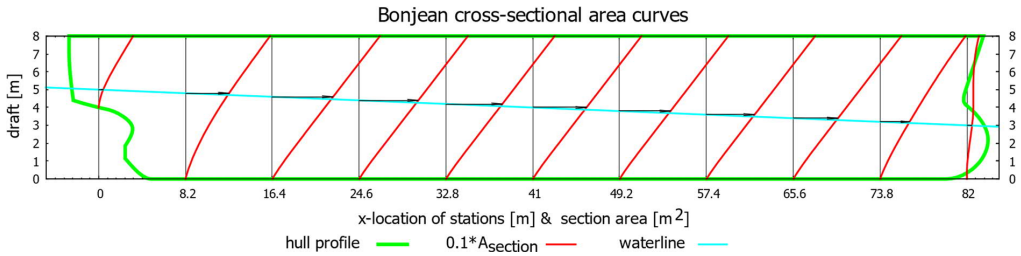

Figure 3.3 Example of reading the sectional areas from Bonjean curves for calculation of displacement when the ship has a stern trim

Many hydrostatic quantities, such as volume of displacement, longitudinal and vertical centres of buoyancy can be plotted as functions of draft. These *hydrostatic curves* can be used for manual stability calculations onboard. Therefore, such data in graphical and numerical format is still prepared for all ships. An example of such curves is shown in Figure 3.5.

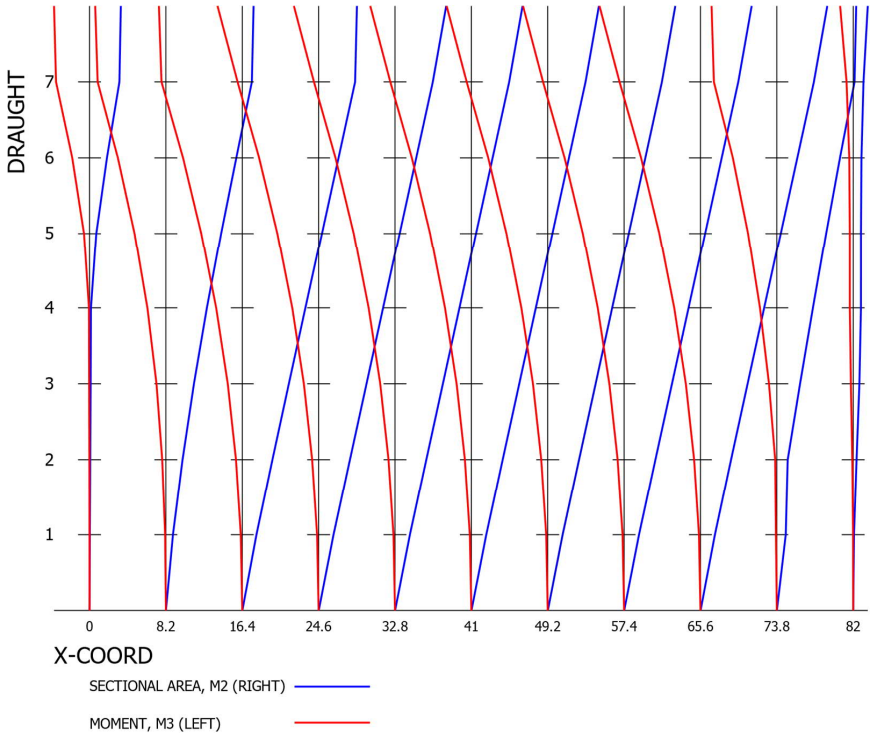

Figure 3.4 Bonjean curves for a small cargo vessel

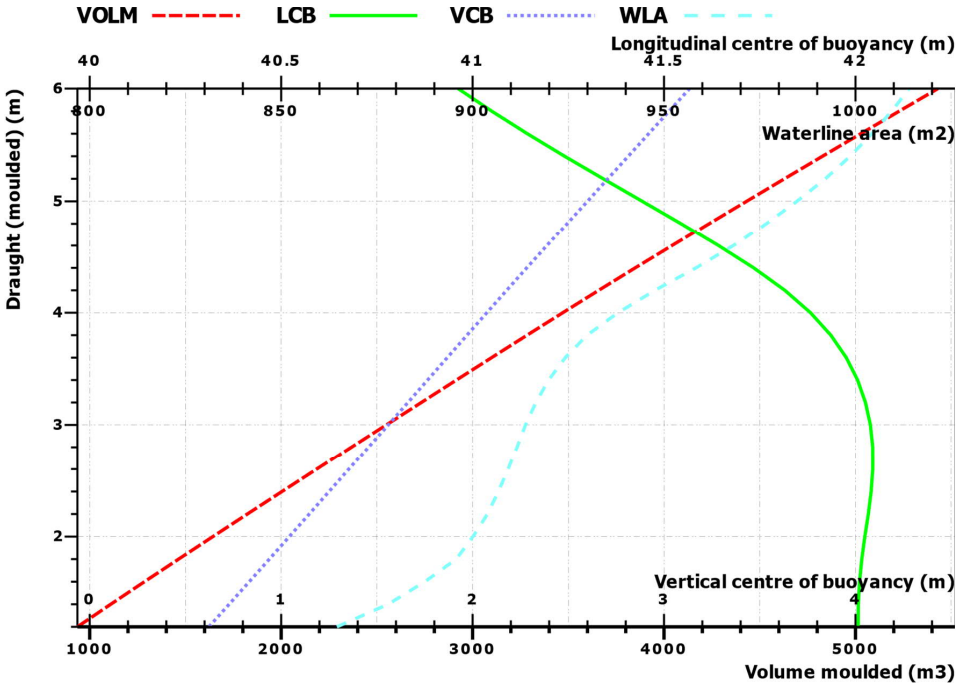

Figure 3.5 Example of typical hydrostatic curves

3.3 Submerged objects in contact with the seabed

The hydrostatics of a fully submerged object are easy to calculate using the Archimedes law. However, the situation is more complex if an object, such as a submarine, is in contact with the seabed. This situation is illustrated in Figure 3.6. The water depth is H and the weight of the submarine is W. The part S_b of the total surface area S is in contact with the seabed.

The lifting force is evaluated by integrating over the wet surface $S - S_b$ by using equation (3.5), resulting in:

$$\boldsymbol{F} = -\int_{S-S_\mathrm{b}} p\mathbf{n}\mathrm{d}S = -\int_{\nabla} \operatorname{grad} p \,\mathrm{d}\nabla + \int_{S_\mathrm{b}} p\mathbf{n}\mathrm{d}S = \mathbf{k}\rho g\nabla + \int_{S_\mathrm{b}} p\mathbf{n}\mathrm{d}S = \boldsymbol{\Delta} + \boldsymbol{\delta\Delta} \tag{3.10}$$

The integral $\int_{S_\mathrm{b}} p\mathbf{n}\mathrm{d}S$ represents the "suction effect" of the seabed. This can be evaluated by using the projected area $S_{b,z}$ of the contact between the submarine and the seabed:

$$\boldsymbol{\delta\Delta} = \int_{S_\mathrm{b}} p\mathbf{n}\mathrm{d}S = \int_{S_\mathrm{b}} (p_0 - \rho g z)\mathbf{n}\mathrm{d}S = -\mathbf{k}(p_0 + \rho g H)S_{\mathrm{b,z}} \tag{3.11}$$

It should be noted that depending on the type of the seabed, the suction force may be reduced due to pore water pressure.

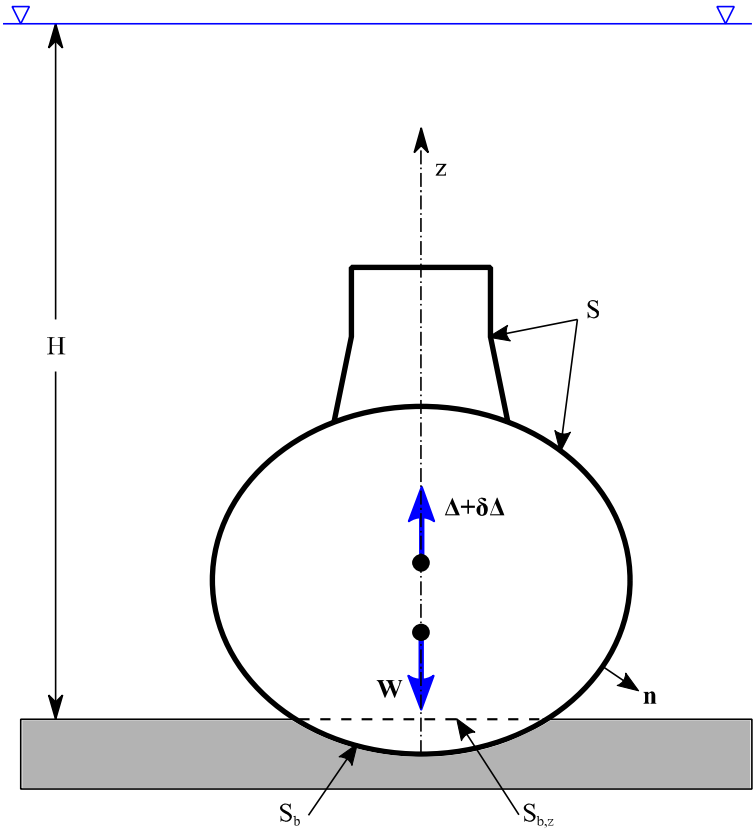

Figure 3.6 Calculation of hydrostatics for a submarine in contact with the seabed

3.4 Forces and moments on floating objects

Firstly, it is essential to note that in naval architecture, the forces and moments are sometimes presented in tons and ton·m, i.e. divided by the gravitational acceleration g. However, in this document, the SI units are used, unless otherwise stated.

The total weight of the ship is:

$$W = g\left(m_{\mathrm{LW}} + \sum_i m_{\mathrm{DW},i}\right) \tag{3.12}$$

where m_{LW} is the mass of the *lightweight* (LW), i.e. ship structures and equipment, m_{LW} and the masses of *deadweight* (DW) components, i.e. cargo, tank loads, provisions and people, are denoted by $m_{\mathrm{DW},i}$.

The buoyancy force is:

$$\Delta = \rho g \nabla \tag{3.13}$$

Both forces are perpendicular to the sea level.

The floating position of a ship can be calculated numerically, so that:

$$\sum \boldsymbol{F}_i = 0 \tag{3.14}$$

$$\sum \boldsymbol{M}_i = \sum \boldsymbol{r}_i \times \boldsymbol{F}_i = 0 \tag{3.15}$$

When there are no external forces, this means that the weight and displacement are equal, and the centre of gravity and centre of buoyancy are vertically aligned (in a global coordinate system with the XY plane parallel to the sea level).

In practice, numerical and iterative methods are needed. Usually a rough estimate (e.g. upright condition) or the previous floating position is used as the starting point. In this condition the weight and buoyancy are not in balance, see Figure 3.7a. Based on these differences a numerical iteration procedure can be used to find a new better estimate for the floating position. The iteration has converged when the weight and buoyancy are in balance, and the centre of gravity and centre of buoyancy are vertically aligned, as illustrated in Figure 3.7b.

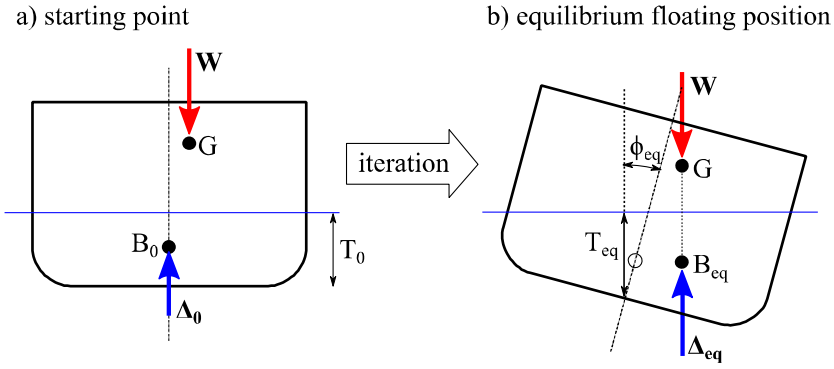

Figure 3.7 Principle of iteration for solving the equilibrium floating position, where weight and buoyancy are in balance

If there are moving masses (e.g. liquid loads in partially filled tanks), the centre of gravity must be updated at each iteration step. For conventional ship hull forms, a reasonable tolerance for a steady equilibrium is 0.001% for displacement and 0.001 m for the differences in the longitudinal and transversal centres of gravity and buoyancy, in the global Earth-fixed coordinate system.

3.5 Vertical stability

Let us consider a freely floating ship without any external forces. There are only two forces acting on the ship, the gravitational force, weight W, and the lifting force of buoyancy Δ. Both are perpendicular to the water level. The ship is in equilibrium if:

$$\sum_i F_{z,i} = W + \Delta = 0 \tag{3.16}$$

The part of the buoyant hull above the water level is referred to as the *reserve buoyancy*. If the weight exceeds the maximum buoyancy the hull can provide, the ship sinks.

With a small increase δW in the weight of the ship, the draft is increased by:

$$\delta T = \frac{\delta W}{\rho g A_{\mathrm{w}}} \tag{3.17}$$

where A_{w} is the waterplane area. It is assumed that this area is practically constant with small variation in the draft.

The consequent increase in the lifting force of the buoyancy is:

$$\delta\Delta = \rho g A_{\mathrm{w}} \delta T \tag{3.18}$$

The situation is illustrated in Figure 3.8. When the additional weight δW is removed, the ship will lift back to the original floating position. A surface ship is vertically stable, as long as the weight does not exceed the total possible buoyancy of the hull, as presented in Figure 2.5.

It should be noted that the above equations are valid only for small changes of draft δT, since with larger changes the waterplane area changes, and consequently, numerical integration and iterative methods are needed to evaluate the new floating position of the ship.

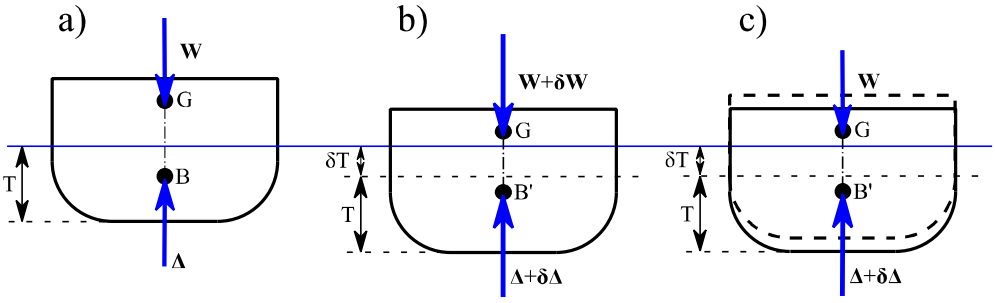

Figure 3.8 Vertical stability

3.6 Effect of sea water density

The lifting force of buoyancy, equation (3.5), depends on the density of the sea water ρ. The *load line* indicates the maximum draft of the ship, i.e. the legal limit to which the ship may be loaded for specific water types and temperatures, in order to safely maintain buoyancy. The original "*Plimsoll mark*" is a circle with a horizontal line through it, indicating the maximum draft of a ship. Additional marks have been added over the years, allowing for different water densities and expected sea conditions, Figure 3.9. The calculation of the required freeboard is defined in the *International Convention on Load Lines* (ICLL).

The amount that the mean draft changes when a ship passes from salt water to fresh water, or vice-versa, when the ship is loaded to the summer (S) displacement, is the so-called *fresh water allowance* (FWA). This regulation obviously refers to a case where the ship is loaded in a river and then sails to the ocean. But the applicability of the freshwater allowance for a ship being loaded in the Gulf of Bothnia and bound for England is not that clear. This is an example of a case, where the regulations leave quite much room for interpretation, as discussed in Pennanen et al. (2019).

The correlation between the displacement and draft is often presented as a monogram, called *loading scale*, Figure 3.10. For practical purposes, also corresponding deadweight values can be shown. The weight quantities are shown separately for sea water and fresh water, together with a grid to help interpolation for different water densities. Also other hydrostatic quantities can be presented in the same graph.

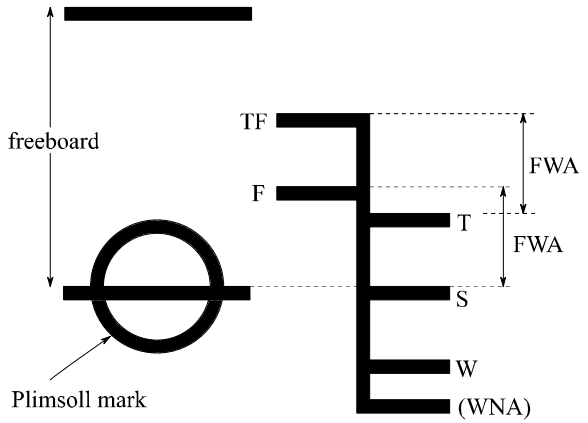

Figure 3.9 Plimsoll and load line markings

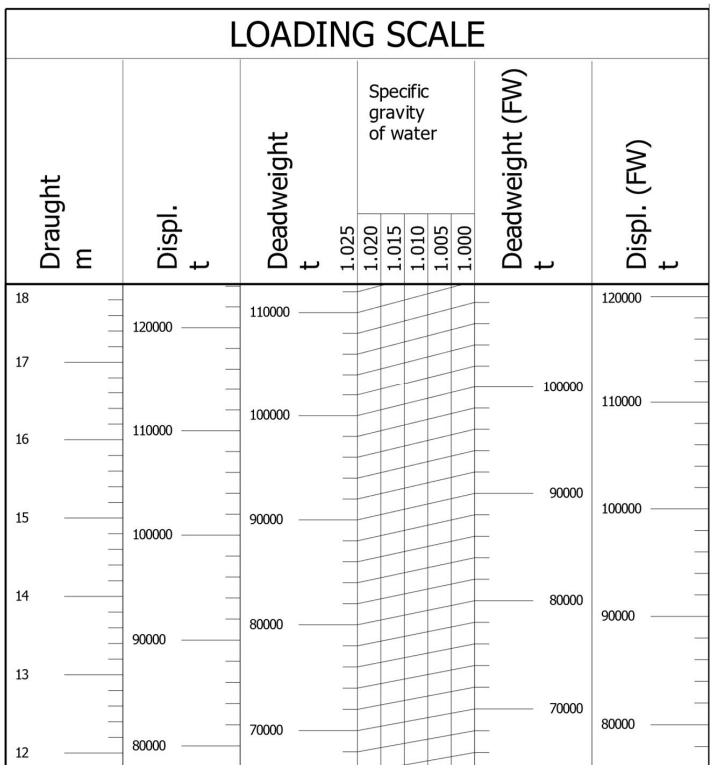

Figure 3.10 Example of a loading scale monogram for a bulk carrier

4 Static stability at small heel angles

4.1 Background

The concept of initial stability is based on the assumption that the heel angle is small. The theory of hydrostatic stability of ships was introduced independently, and almost simultaneously, by Pierre Bouguer in 1746 and by Leonhard Euler in 1749. A comprehensive historical review of this development is given in Nowacki and Ferreiro (2003).

The initial hydrostatics, based on metacentre and restoring moment at small heel angles, were applied for assessment of ship stability for more than a century. Although, more comprehensive stability calculations are nowadays done, it is important to understand also the basic concepts and underlying assumptions of the so-called initial stability at small angles of heel. In the following sections, the relevant theory of initial stability is derived and thoroughly explained.

4.2 Waterplane quantities

Consider a pure angular motion of a floating ship, by a small trim angle $\delta\theta$, as illustrated in Figure 4.1. Volume v_1 is immersed and volume v_2 is emerged from water. There is no change in the displacement, and therefore, $v_1 = v_2$.

The submerged volume can be integrated from the unknown point F to the stem:

$$v_1 = \int_{L_F} \mathrm{d}v = 2\delta\theta \int_0^{L_F} y(x')x'\mathrm{d}x' \tag{4.1}$$

since:

$$\mathrm{d}v = x'\mathrm{d}A_w\delta\theta = 2y(x')x'\mathrm{d}x'\delta\theta \tag{4.2}$$

Here L_F is the length of the ship forward from the point F and A_w is the waterplane area. An auxiliary coordinate system $x'y'$ is used, with origin at F.

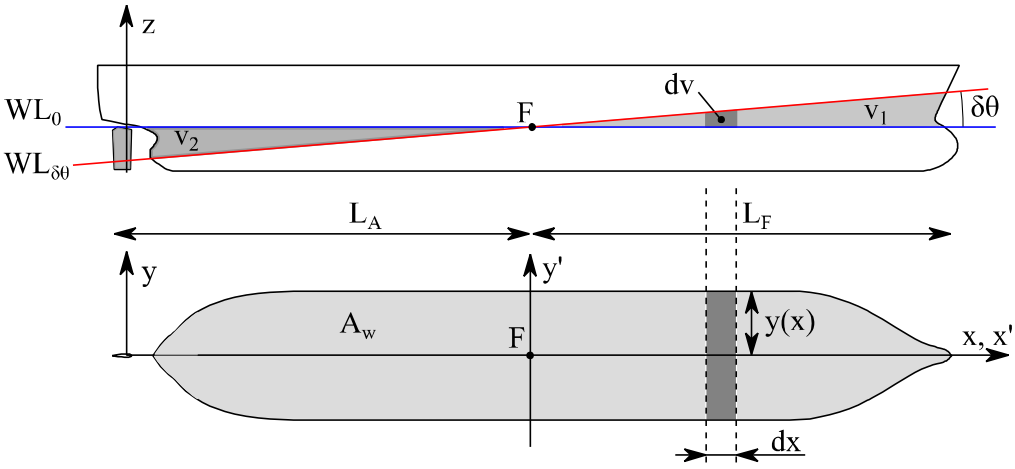

Figure 4.1 Waterplane related quantities

Similarly, the volume that emerges from water is:

$$v_2 = \int_{L_A} \mathrm{d}v = 2\delta\theta \int_0^{L_A} y(\xi')\xi' \mathrm{d}\xi' \tag{4.3}$$

where L_A is the length of the ship aft from the point F and the auxiliary coordinate $\xi' = -x'$. Based on these equations, the following is obtained:

$$v_2 = 2\delta\theta \int_0^{L_A} y(\xi')\xi' \mathrm{d}\xi' = 2\delta\theta \int_0^{-L_A} y(x')x' \mathrm{d}x' = -2\delta\theta \int_{-L_A}^{0} y(x')x' \mathrm{d}x' \tag{4.4}$$

Since the volumes v_1 and v_2 are equal, the longitudinal location of the point F, i.e. the start of the
x'-axis, can be solved from the following equation:

$$\int_{-L_A}^{0} y(x')x' \mathrm{d}x' + \int_0^{L_F} y(x')x' \mathrm{d}x' = \int_{-L_A}^{L_F} y(x')x' \mathrm{d}x' = 0 \tag{4.5}$$

Consequently, the point F is the centroid of the waterplane area, and it is known as the *centre of flotation.* The x' and y'-axes are the main axes of rotation for a floating object.

In addition to the area and the centroid of the waterplane area, also the surface moments of inertia are significant quantities for stability calculations. For the elementary part of the waterplane area dA_w these are:

$$\mathrm{d}I_{xx} = \frac{1}{12}[2y(x)]^3 \mathrm{d}x \tag{4.6}$$

and

$$dI_{yy} = x^2 \mathrm{d}A_w = x^2 2y(x) \mathrm{d}x \tag{4.7}$$

Integration along the x-axis results in:

$$I_{xx} = \int \mathrm{d}I_{xx} = \frac{2}{3}\int_L [y(x)]^3 \mathrm{d}x \tag{4.8}$$

and

$$I_{yy} = \int \mathrm{d}I_{yy} = 2\int_L x^2 y(x) \mathrm{d}x \tag{4.9}$$

These moments of inertia are in the coordinate system x-y, where the origin is at AP. The angular motions take place around the centre of flotation, point F, and the moments need to be transferred by applying Steiner's theorem, resulting in:

$$I_T = I_{xx} \tag{4.10}$$

and

$$\begin{aligned} I_L &= \int (x - x_F)^2 \, \mathrm{d}A_w = \int x^2 \mathrm{d}A_w - 2x_F \int x \mathrm{d}A_w + x_F^2 \int \mathrm{d}A_w \\ &= I_{yy} - 2x_F x_F A_w + x_F^2 A_w \\ &= I_{yy} - x_F^2 A_w \end{aligned} \tag{4.11}$$

If the waterplane area is not symmetric, as in the case of some floating offshore structures or a heeled ship, the x'-axis is not parallel to the x-axis, Figure 4.2. In addition to the transverse and longitudinal moments of inertia, also a product of inertia term is introduced:

$$I_{x'y'} = \int x'y' \, \mathrm{d}A_w \tag{4.12}$$

This means that the main axes of inertia x^* and y^* are not parallel to x' and y' axes, and the angle between these axes is:

$$\alpha = \frac{1}{2}\arctan\left(\frac{I_{x'y'}}{I_{y'y'} - I_{x'x'}}\right) \tag{4.13}$$

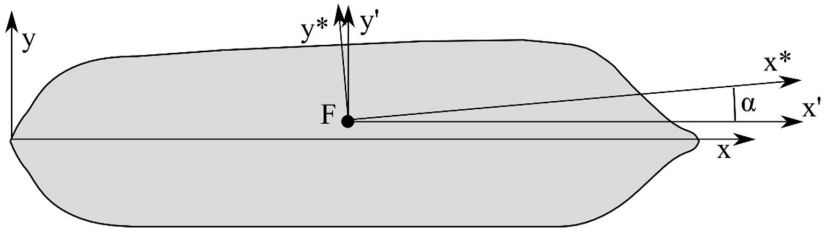

Figure 4.2 Main axes of inertia for an asymmetric waterplane area

The heel and trim motions take place around the x^* and y^* axes. For normal ship hull shapes (length much larger than breadth), the angle α is usually very small, and the assumption of a constant heeling direction is well justified. However, for floating offshore structures the twisting effect can be notable, even in intact stability calculations. This is discussed later in section 16.8.

4.3 Method of wedge volumes

Let us consider a ship with a volume of displacement ∇, heeled around the x-axis by a small angle $\delta\phi$, as illustrated in Figure 4.3. Due to the heeling, a volume v_1 is emerged from water, and volume v_2 is submerged. The centroids of these wedge volumes are marked with g_1 and g_2. As the ship is heeled, the centre of buoyancy shifts from B_0 to B_ϕ. An important relation between these points can be derived by using this so-called method of wedge volumes.

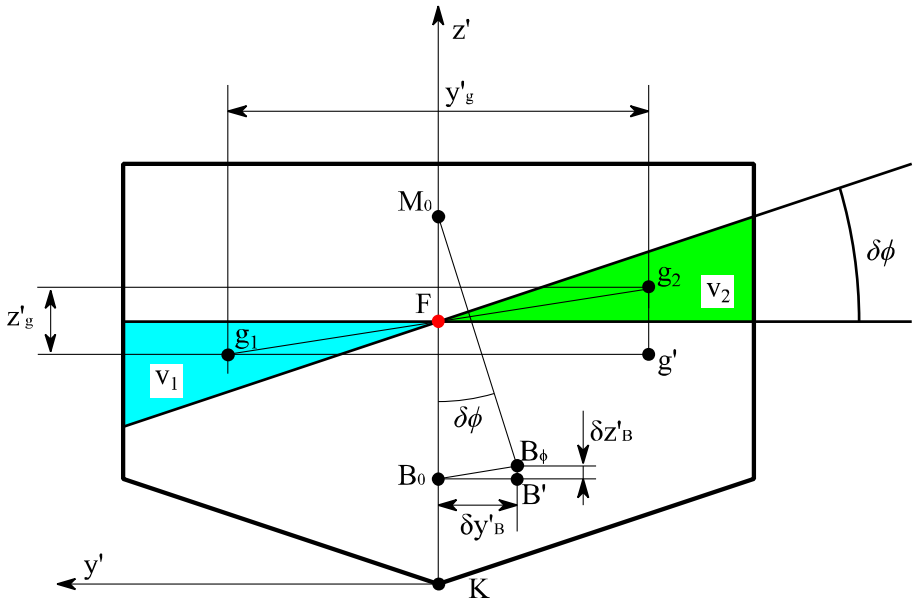

Figure 4.3 Method of wedge volumes

A coordinate system $x'y'z'$ that is heeled with the ship is applied for calculation of the moments of the buoyancy forces.

The balance of the moments around the $x'z'$ plane is:

$$\nabla \cdot (-\delta y'_B)\cos\delta\phi = \nabla \cdot 0 \cdot \cos\delta\phi + v_2\left(-\frac{1}{2}y'_g\right)\cos\delta\phi - v_1\frac{1}{2}y'_g\cos\delta\phi \quad (4.14)$$

and hence:

$$\nabla \cdot \delta y'_B = v \cdot y'_g \quad (4.15)$$

since:

$$v_1 = v_2 = v \quad (4.16)$$

In addition, the balance of the moments around the $x'y'$plane is:

$$\nabla \cdot (z'_B + \delta z'_B)\sin\delta\phi = \nabla \cdot z'_B \sin\delta\phi + v_2\left(T + \frac{1}{2}z'_g\right)\sin\delta\phi - v_1\left(T - \frac{1}{2}z'_g\right)\sin\delta\phi \quad (4.17)$$

Based on this, the following is obtained:

$$\nabla \cdot z'_B = v \cdot z'_g \quad (4.18)$$

By combining these, the following relation is obtained:

$$\frac{\delta y'_B}{\delta z'_B} = \frac{y'_g}{z'_g} \quad (4.19)$$

Meaning that the triangles $B_0B'B_\phi$ and $g_1g'g_2$ are of the same shape.

4.4 Metacentre

Let us consider a ship floating upright with water line WL_0. When the ship is heeled to a new water line WL, the centre of buoyancy is shifted from point B_0 to point B. If heeling is further increased to waterline WL', the buoyancy point is further shifted to B'. The situation is illustrated in Figure 4.4.

The *metacentre* is the point M, where the direction lines of the buoyancy force with a small change of heel angle intersect.

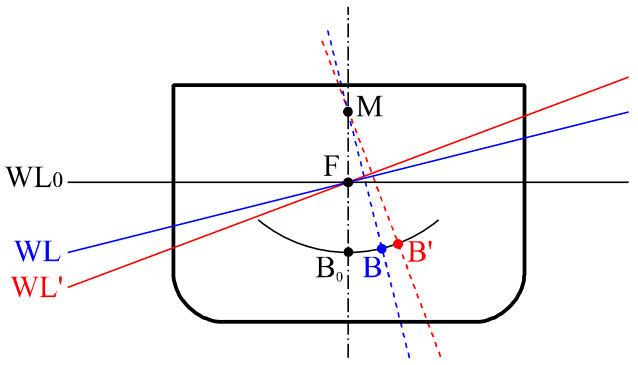

Figure 4.4 Metacentre and metacentric radius

4.5 Metacentric radius

An important quantity related to the stability of the ship is *metacentric radius*. It is the distance between the centre of buoyancy and the metacentre, i.e. $\overline{B_0M_0}$, when the ship is upright, so that $\phi = 0$.

Let us consider a small heel angle $\delta\phi$, with wedge shaped volumes immersed and emerged, as shown in Figure 4.5. Based on the method of wedge volumes, equation (4.19):

$$\overrightarrow{B_0B_1} \uparrow\uparrow \overrightarrow{g_1g_2} \tag{4.20}$$

and therefore, the shift of the centre of buoyancy is:

$$\overrightarrow{B_0B_1} = \frac{\mathrm{v}}{\nabla}\overrightarrow{g_1g_2} \tag{4.21}$$

With a very small heel angle $\delta\phi$ the metacentric radius is:

$$\overline{B_0M_0} = \frac{\overline{B_0B_1}}{\delta\phi} = \frac{\mathrm{v}}{\nabla}\frac{\overline{g_1g_2}}{\delta\phi} \tag{4.22}$$

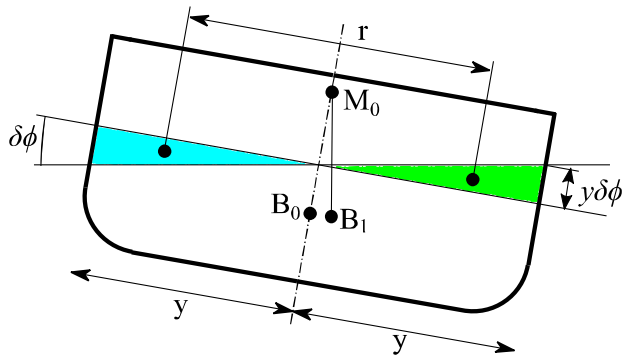

Figure 4.5 Metacentric radius and wedge-shaped volumes with a small heel angle

The half breadth at location x is $y(x)$, Figure 4.6, and consequently, the cross-sectional area of the wedge is:

$$s = \frac{1}{2}y(y \cdot \delta\phi) \tag{4.23}$$

And the distance between the centroids of the wedges is:

$$r = 2\frac{2}{3}y \tag{4.24}$$

The moment of the wedge volumes is obtained by integrating over the length of the ship:

$$v\overline{g_1g_2} = \int_{x_\mathrm{a}}^{x_\mathrm{f}}\left(\frac{1}{2}y^2\delta\phi\right)2\frac{2}{3}y\mathrm{d}x = \delta\phi\frac{2}{3}\int_{x_\mathrm{a}}^{x_\mathrm{f}}y^3\mathrm{d}x \tag{4.25}$$

Here the transverse moment of inertia of the waterplane area is:

$$I_\mathrm{T} = \frac{2}{3}\int_{x_\mathrm{a}}^{x_\mathrm{f}}y^3\mathrm{d}x \tag{4.26}$$

Consequently, by substituting these into equation (4.22), the following simple definition is obtained for the metacentric radius:

$$\overline{B_0M_0} = \frac{I_\mathrm{T}}{\nabla} \tag{4.27}$$

Thus the metacentric radius depends solely on the submerged hull form. Since the volume of displacement is $\nabla = C_B LBT$, where C_B is the block coefficient, the metacentric radius can be presented as a function of ship breadth B and draft T:

$$\overline{B_0 M_0} = f\left(C_B, y(x)\right)\frac{B^2}{T} \tag{4.28}$$

Consequently, the breadth of the ship has a very large effect on the stability of the ship. The function $f\left(C_B, y(x)\right)$ reaches the maximum for a box shaped barge:

$$f\left(1.0, \frac{B}{2}\right) = \frac{1}{12} \tag{4.29}$$

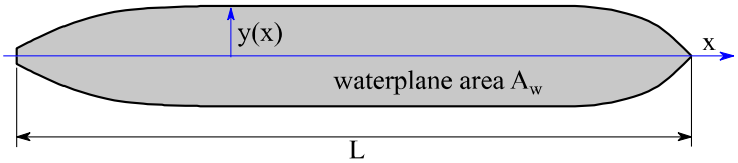

Figure 4.6 Waterplane area and half breadth of a monohull ship

4.6 Stability at small heel angles, metacentric height

At small heel angles (less than 10°), the assumption of *initial stability* is valid for conventional ship hull forms. This means that the location of the metacentre does not change notably, and the centre of buoyancy changes along a curve that is a circular arc. Figure 4.7 shows a ship that is subjected to an external moment, and consequently heeled to a small angle ϕ. The weight and buoyancy force pair result in a righting moment. With this assumption, the shift of the centre of buoyancy can be calculated. The principle is illustrated in Figure 4.8.

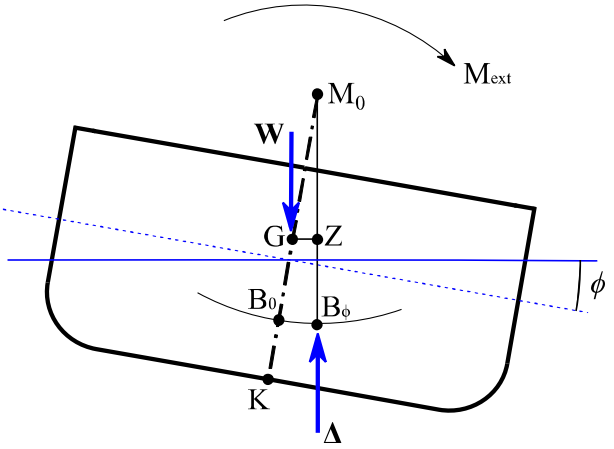

Figure 4.7 Initial stability

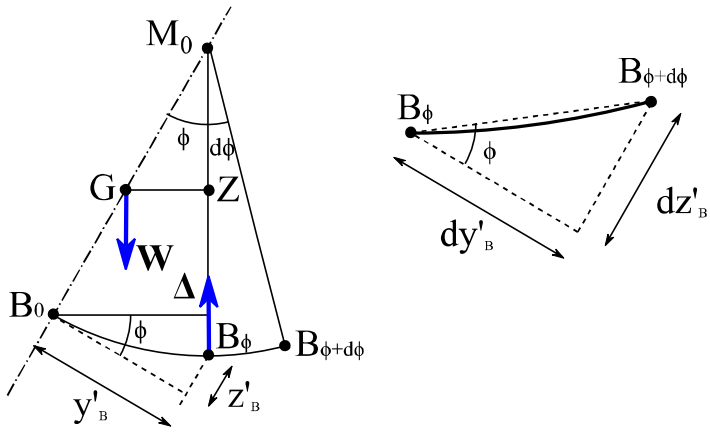

Figure 4.8 Righting lever and shift of centre of buoyancy in initial stability

When the heel is increased by a small angle $\mathrm{d}\phi$, the resulting shift of the centre of buoyancy is:

$$\mathrm{d}y'_{\mathrm{B}} = \overline{B_0M_o}\cos\phi\,\mathrm{d}\phi \quad \text{and} \quad \mathrm{d}z'_{\mathrm{B}} = \overline{B_0M_o}\sin\phi\,\mathrm{d}\phi \tag{4.30}$$

Since the metacentric radius $\overline{B_0M_o}$ does not depend on the heel angle, this can be integrated:

$$y'_{\mathrm{B}} = \overline{B_0M_o}\int_0^{\phi}\cos\phi\,\mathrm{d}\phi = \overline{B_0M_o}\sin\phi \tag{4.31}$$

and

$$z'_{\mathrm{B}} = \overline{B_0M_o}\int_0^{\phi}\sin\phi\,\mathrm{d}\phi = \overline{B_0M_o}(1-\cos\phi) \tag{4.32}$$

The external heeling moment M_{ext} must be compensated by the force pair Δ and W so that the ship remains in equilibrium, i.e. $\sum M = M_{\mathrm{ext}} + M_{\mathrm{st}} = 0$. The resulting static righting moment is:

$$M_{\mathrm{st}} = -\Delta\overline{GZ} \tag{4.33}$$

where $\overline{GZ}$ is the *righting moment lever*. Occasionally, this is also denoted with symbol h. Based on Figure 4.8, the lever is:

$$\overline{GZ} = \overline{B_0M_0}\sin\phi - \overline{B_0G}\sin\phi = \overline{GM_0}\sin\phi \tag{4.34}$$

The measure of initial stability is *metacentric height*, and it can be presented as:

$$\overline{GM_0} = \overline{KB_0} + \overline{B_0M_0} - \overline{KG} \tag{4.35}$$

where $\overline{KB_0}$ is the height of the centre of buoyancy from the baseline.

At small heel angles, the static righting moment can be approximated with:

$$M_{\mathrm{st}} \approx -\Delta\overline{GM_0}\sin\phi \tag{4.36}$$

4.7 Application of initial stability approximation

As mentioned, the approximation of initial stability is valid only at small heel angles. Usually, the heel angle is unknown, and needs to be calculated based on the external heeling moment. Let us consider a simple case, where a weight with mass m is moved transversally a distance e, Figure 4.9. This can be treated as an external heeling moment:

$$M_{\mathrm{ext}} = mge\cos\phi \tag{4.37}$$

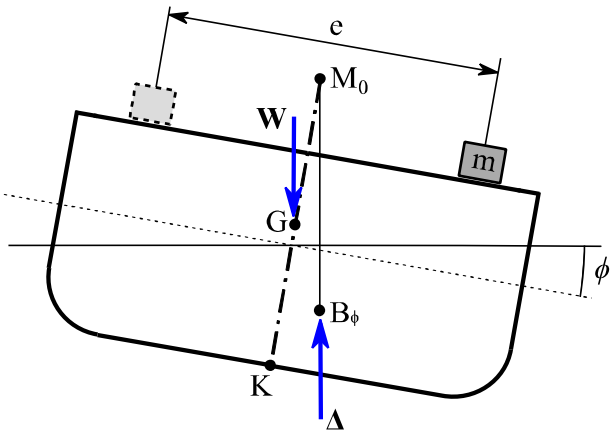

Figure 4.9 Heel due to transverse shift of a weight

At equilibrium the moments are in balance:

$$\sum M = M_{\text{ext}} + M_{\text{st}} = mge\cos\phi - \Delta\overline{GM_0}\sin\phi = 0 \tag{4.38}$$

and the heel angle can be solved:

$$\phi \approx \arctan\left(\frac{mge}{\Delta\overline{GM_0}}\right) \tag{4.39}$$

The initial stability approximation is based on an unchanged metacentre, and consequently, the centre of buoyancy is assumed to move along a circular arc. An example comparison between the actual and assumed shift (up to 30° heel) is shown in Figure 4.10. For a conventional displacement ship hull form, the curves start to deviate significantly when the heel is larger than 10°.

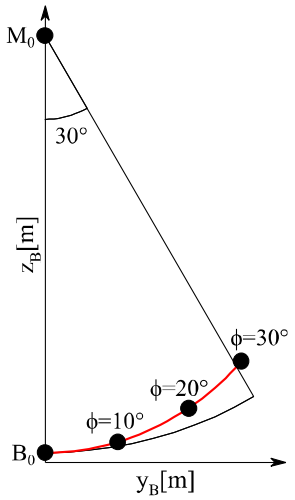

Figure 4.10 Comparison of actual shift of centre of buoyancy and the circular arc assumption

In practice, this means that when the initial stability approximation with equation (4.39) is used, the results need to be critically reviewed. If the resulting heel angle is less than 10°, then the use of the initial stability approximation is usually justified. Otherwise, a more comprehensive analysis is needed, as presented in the next chapter.

5 Stability at large angles of heel

5.1 Background

For a long time, the initial metacentric height $\overline{GM_0}$ was the only measure of stability. The insufficiency of this assumption was grimly demonstrated in a storm in 1870. Two similar British ships with almost identical metacentric heights, the CAPTAIN and the MONARCH, were sailing in the same sea area. The CAPTAIN capsized but the MONARCH survived since she had a higher freeboard, providing better stability at large heel angles. This incident triggered further discussion and research on ship stability, as described in Ferreiro (2020), and eventually led to development of proper criteria for sufficient stability, albeit several decades later.

5.2 Metacentric evolute

At large heel angles the initial stability approximation is not valid since the location of the metacentre is changed. This is caused by changes in the waterplane area and in its moment of inertia. The shift of the centre of buoyancy also depends on the submerged hull form, which changes notably at large heel angles.

The curve representing the location of the centre of buoyancy at different heel angles is the buoyancy curve (or simply B-curve). In the differential geometry of curves, the evolute of a curve is the locus of all its centres of curvature. Meaning that, when the centre of curvature of each point on a curve is drawn, the resultant shape will be the evolute of that curve. Consequently, the curve of the metacentre (the M-curve) is the evolute of the B-curve, and the M-curve is referred as the *metacentric evolute*. Figure 5.1 shows these curves for a parabola-shaped section. Comprehensive examples on calculation of the metacentric evolute with various analytical hull forms are presented in Mégel and Kliava (2010).

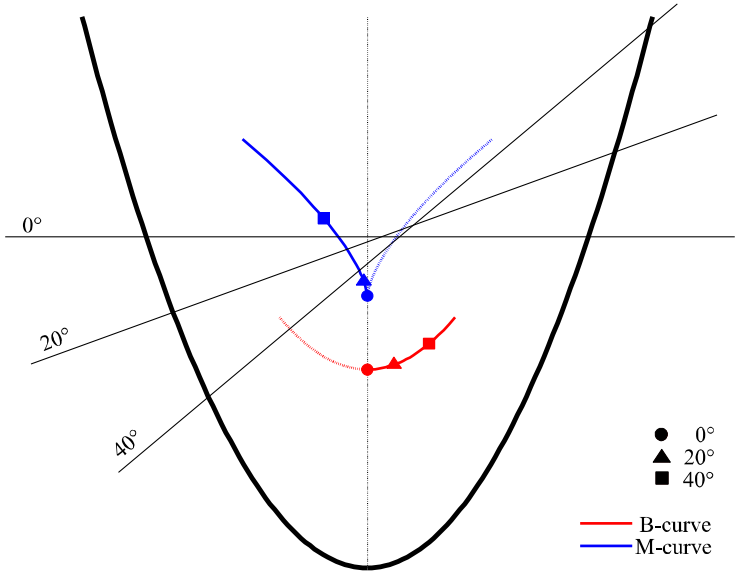

Figure 5.1 Buoyancy curve and metacentric evolute for a parabola-shaped section

5.3 Righting lever curve

At a large heel angle ϕ, the vertical line between the shifted centre of buoyancy B_ϕ and the corresponding metacentre M_ϕ intersects the symmetry plane of the ship in point N_ϕ, which is known as the "false metacentre", Figure 5.2.

In this case the static righting moment at heel angle ϕ is:

$$M_{st}(\phi) = -\Delta\overline{GZ}(\phi) = -\Delta\overline{GN_\phi}\sin\phi = -\Delta\left(\overline{B_0N_\phi}\sin\phi - \overline{B_0G}\sin\phi\right) \quad (5.1)$$

where the part $\overline{B_0N_\phi}\sin\phi$ is called the *form stability lever* since it depends solely on the hull form and the heel angle. Correspondingly, the part $\overline{B_0G}\sin\phi$ is known as *weight stability lever* since it is dependent on the vertical centre of gravity.

As illustrated in Figure 5.2, the righting lever can also be presented as:

$$\overline{GZ} = \overline{GM_0}\sin\phi + \overline{M_0S} \quad (5.2)$$

where the component $\overline{M_0S}$ is called the *residual stability*. For normal ship hull forms this is usually positive, up the heel angle when the deck edge is immersed, and the bilge is emerged from water. With larger heel angles the residual stability becomes negative.

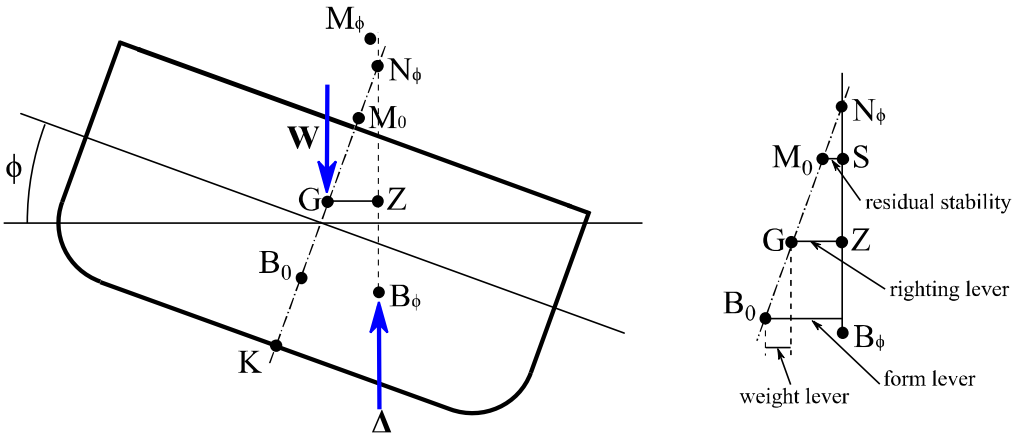

Figure 5.2 Righting lever and its components

5.4 Righting lever for wall-sided ships

If the sides of a ship are parallel and perpendicular to the sea level, i.e. wall-sided, it is possible to calculate analytically the righting lever values up to the angle of deck immersion or the bilge emergence angle, whichever is smaller. The equation can be derived with the method of wedge volumes (see section 4.3), as illustrated in Figure 5.3.

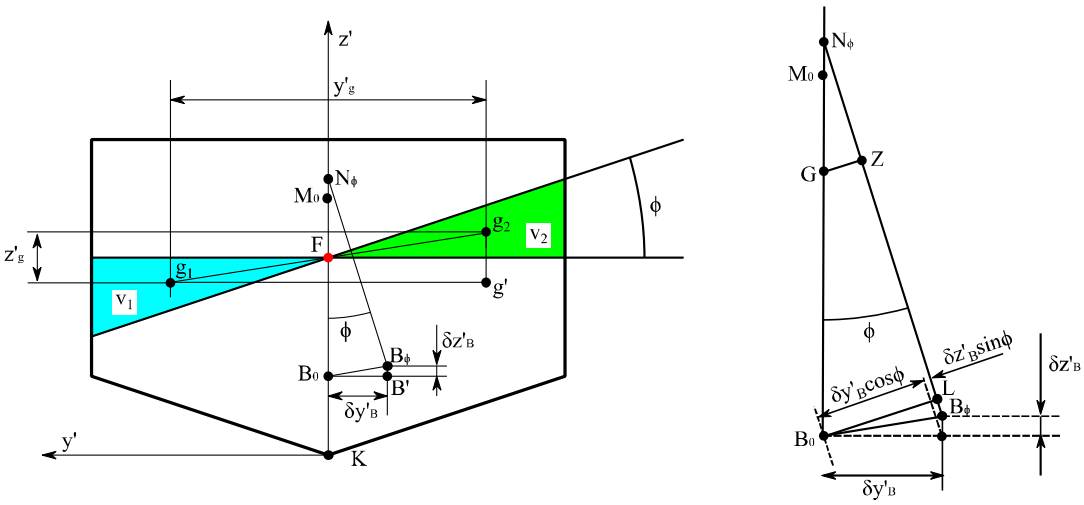

Figure 5.3 Righting lever for a wall-sided ship

Based on the method of wedge volumes, equations (4.15) and (4.18):

$$\delta y'_{\mathrm{B}} = \frac{v}{\nabla} y'_{\mathrm{g}} \quad \text{and} \quad \delta z'_{\mathrm{B}} = \frac{v}{\nabla} z'_{\mathrm{g}} \tag{5.3}$$

the moments of the wedge volumes are obtained by integration over the ship length L:

$$v y'_{\mathrm{g}} = \int_L \; 2\frac{2}{3} y \frac{y}{2} \tan\phi \, \mathrm{d}x = \frac{2}{3} \tan\phi \int_L \; y^3 \, \mathrm{d}x = I_{\mathrm{T}} \tan\phi \tag{5.4}$$

$$v z'_{\mathrm{g}} = \int_L \; \frac{2}{3} y \tan\phi \frac{y^2}{2} \tan\phi \, \mathrm{d}x = \frac{1}{3} \tan^2\phi \int_L \; y^3 \, \mathrm{d}x = \frac{1}{2} I_{\mathrm{T}} \tan^2\phi \tag{5.5}$$

By substituting these into (5.3), the following equations are obtained for the shift of centre of buoyancy:

$$\delta y'_{\mathrm{B}} = \frac{I_{\mathrm{T}}}{\nabla} \tan\phi = \overline{B_0 M_o} \tan\phi \tag{5.6}$$

$$\delta z'_{\mathrm{B}} = \frac{I_{\mathrm{T}}}{\nabla} \frac{\tan^2\phi}{2} = \overline{B_0 M_o} \frac{\tan^2\phi}{2} \tag{5.7}$$

Furthermore, based on Figure 5.3:

$$\overline{B_0 L} = \delta y'_{\mathrm{B}} \cos\phi + \delta z'_{\mathrm{B}} \sin\phi = \left(\frac{\delta y'_{\mathrm{B}}}{\tan\phi} + \delta z'_{\mathrm{B}} \right) \sin\phi \tag{5.8}$$

and by substituting the equations for the shift of centre of buoyancy, (5.6) and (5.7), the following is obtained:

$$\overline{B_0 L} = \overline{B_0 M_0} \left(1 + \frac{\tan^2\phi}{2} \right) \sin\phi \tag{5.9}$$

And consequently, the righting lever is:

$$\overline{GZ} = \overline{B_0 M_0} \left(1 + \frac{\tan^2\phi}{2} \right) \sin\phi - \overline{B_0 G} \sin\phi \tag{5.10}$$

which can be presented as:

$$\overline{GZ} = \overline{GM_0} \sin\phi + \overline{B_0 M_0} \frac{\tan^2\phi}{2} \sin\phi \tag{5.11}$$

The first term is the assumption of initial stability, and the second term represents the effect of the immersed wall-sided hull. Note that this equation is valid only for heel angles up to the angle of deck immersion. Furthermore, it is assumed that the trim is not changed, which is valid only for prismatic hull forms. However, in practice the changing in trim is quite small for heel angles up to 20° for conventional hull forms.

5.5 Calculation of righting lever curve

Traditionally, the ship stability calculations have relied on pre-calculated data, such as the so-called *cross curves of stability*, where $\overline{KN_\phi}$ values are presented as functions of draft for different heel angles. An example is shown in Figure 5.4. Similar curves need to be calculated for different trims. The righting lever curve for various loading conditions (draft, trim and centre of gravity) can then be evaluated from these cross curves of stability.

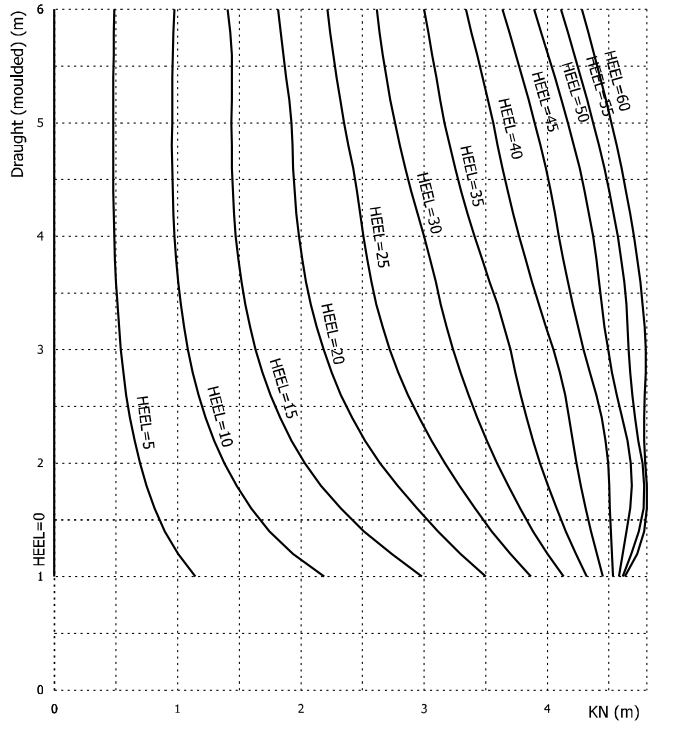

Figure 5.4 Example of cross curves of stability

Nowadays, the increase in computing capacity has completely replaced these auxiliary pre-calculated curves. Instead, the righting lever is calculated directly with numerical iteration by balancing the draft and trim, while keeping the heel angle fixed. This procedure is repeated for a set of heel angles and the actual righting lever curve is obtained by fitting a smooth curve through the calculated points, Figure 5.5. Note that the general least squares fit of any function cannot be applied since the righting lever curve does not follow any general function, such as a polynomial. Moreover, the fitted curve must go through all the calculated points.

Furthermore, the derivative of the righting lever curve at upright condition equals to the initial metacentric height:

$$\frac{\mathrm{d}}{\mathrm{d}\phi}\overline{GZ}(\phi)\Big|_{\phi=0} = \overline{GM_0} \tag{5.12}$$

Also this is illustrated in Figure 5.5. However, it should be noted that this is applicable only to cases, where the ship is floating upright. Occasionally, the derivative of the righting lever curve at the steady non-zero heel angle is referred to as the "actual metacentric height".

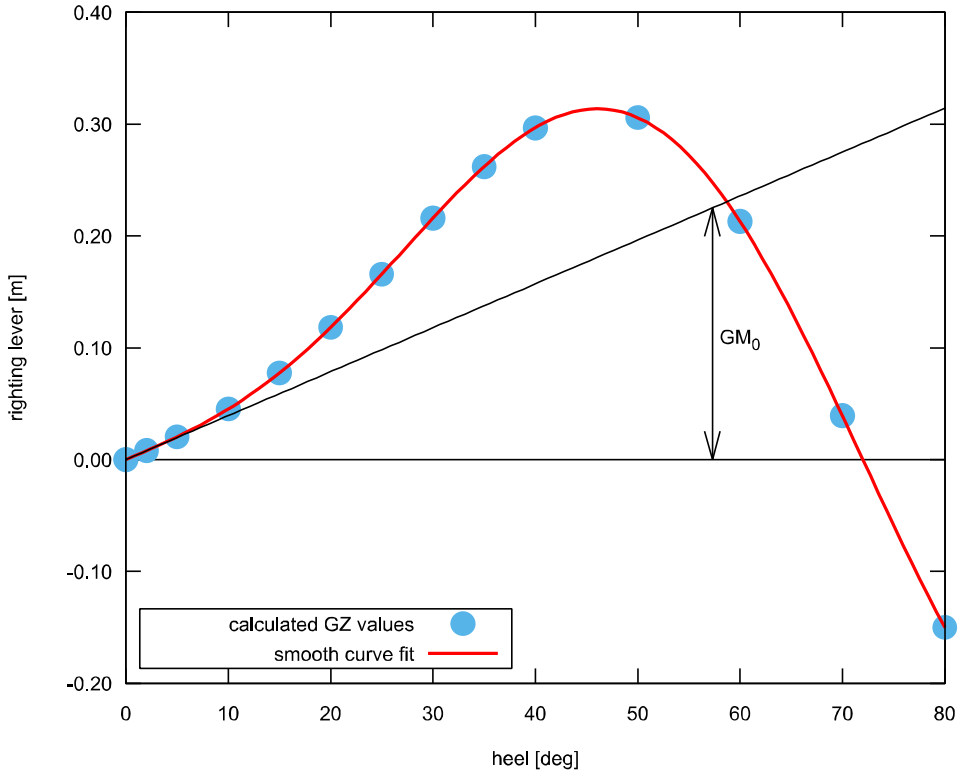

Figure 5.5 GZ curve fitting to the calculated values at the argument heel angles

It is essential to account for changes in trim in the calculation of the righting lever curve. This approach is often called the *free trim* method. The assumption of *fixed trim* often results in much too large righting lever values at large heel angles.

An example of notable trim changes is shown in Figure 5.6. The ship has an extended lower weather deck, typical e.g. for offshore supply vessels. For small heel angles (less than 10°), trim is practically constant. Thereafter, the ship trims slightly to bow, but for heel angles larger than 30° the deck edge is immersed, resulting in large stern trim. Assumption of a fixed trim in the calculation of the righting lever results in overestimation of the stability, especially at large heel angles.

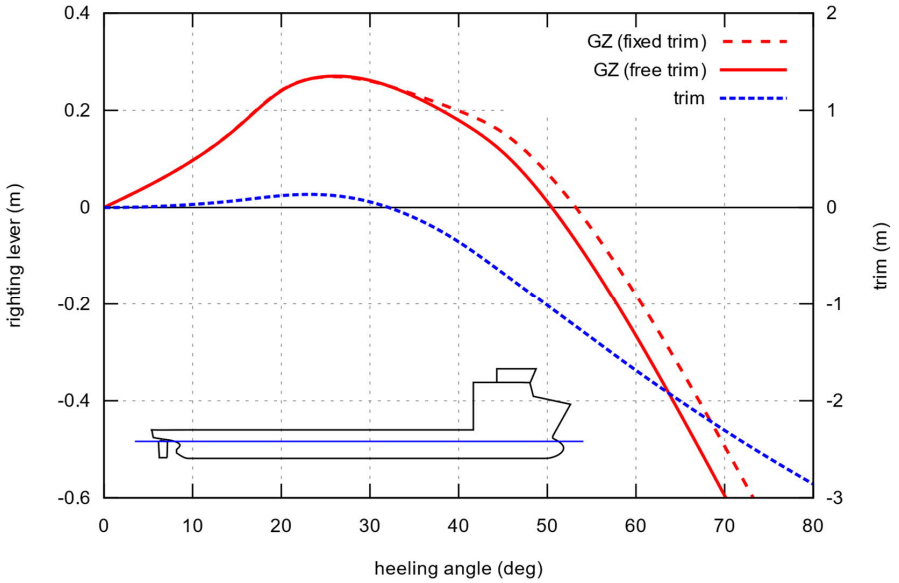

Figure 5.6 Change of trim in the calculation of righting lever for a ship with extended lower weather deck

5.6 Stability analysis with a righting lever curve

Consider an external heeling moment M_{ext} that appears gradually, so that the inertial forces and moments can be neglected. This moment may be a function of the heel angle ϕ, and the effective lever is obtained by dividing the external heeling moment by the displacement force Δ, so that:

$$l_{\text{ext}}(\phi) = \frac{M_{\text{ext}}(\phi)}{\Delta} \tag{5.13}$$

The ship is in equilibrium if the sum of the moments is zero:

$$M_{\text{ext}}(\phi) + M_{\text{st}}(\phi) = 0 \tag{5.14}$$

where the static righting moment is:

$$M_{\text{st}}(\phi) = -\Delta \overline{GZ}(\phi) \tag{5.15}$$

and consequently, at equilibrium heel angle ϕ_{eq}:

$$\overline{GZ}(\phi_{\text{eq}}) = l_{\text{ext}}(\phi_{\text{eq}}) \tag{5.16}$$

This can be solved graphically by plotting both levers, as in Figure 5.7. The above-mentioned condition for equilibrium is met at two points A and B, where the heeling and righting lever curves cross. The equation (2.8) gives the requirement for a stable equilibrium as:

$$\frac{\mathrm{d}M_{\text{st}}(\phi)}{\mathrm{d}\phi} < 0 \tag{5.17}$$

which means:

$$\frac{\mathrm{d}\overline{GZ}(\phi)}{\mathrm{d}\phi} > 0 \tag{5.18}$$

In the point A this condition is met, and therefore, the equilibrium is stable, whereas in the point B it is not met, and therefore, this equilibrium is unstable. Also the point C, where the maximum

righting lever is reached, is of interest since it represents the maximum static heeling lever that the ship can withstand without capsizing.

Normally the righting curve is presented for heel angles from 0° (upright) to sufficiently large angle that is rarely larger than 90° (capsize). Heel angles are positive, and direction is presented as PS or SB. This is convenient since stability criteria are often evaluated separately to both sides. However, physically righting lever is a continuous function, extending from -180° to +180°, as shown in Figure 5.8.

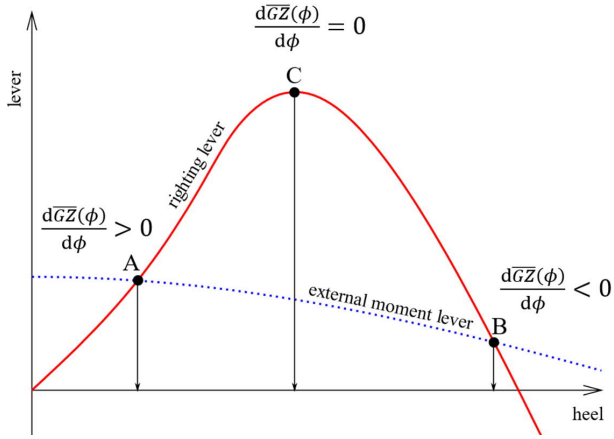

Figure 5.7 Evaluation of equilibrium heel angle under static external moment

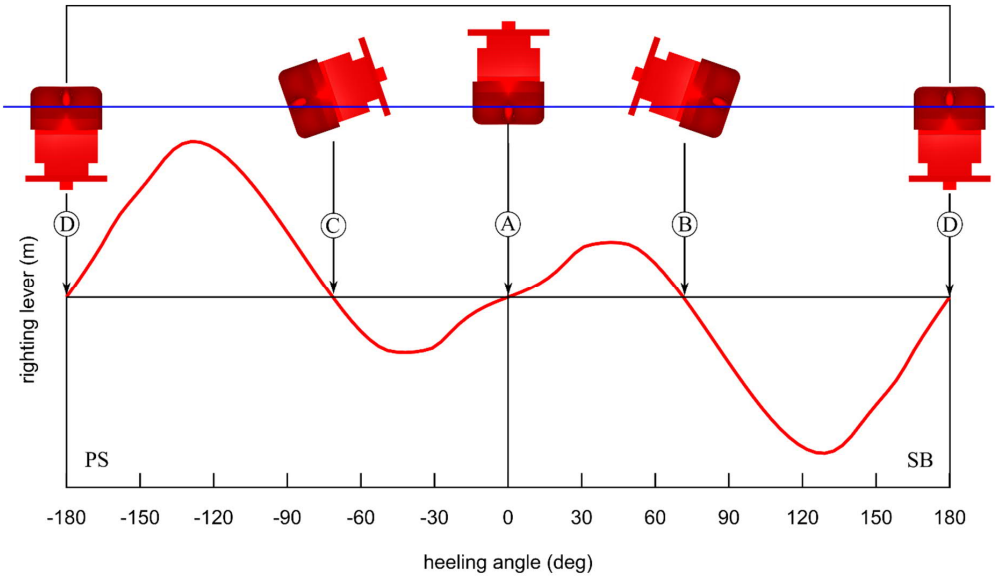

Figure 5.8 Full righting lever curve with all equilibrium conditions (A, B, C and D)

Normally, there are four equilibrium points, where $\overline{GZ}(\phi) = 0$. The stable equilibrium at upright, denoted with A in Figure 5.8, is the actual floating position of the ship in calm water, without any external moments. The points B and C are unstable since $\mathrm{d}\overline{GZ}/\mathrm{d}\phi < 0$, and consequently, $\mathrm{d}M_{\mathrm{st}}/\mathrm{d}\phi > 0$. There is also another stable equilibrium floating position, the point D at heel angle ±180°. It is noteworthy, that this upside-down condition often more "stronger" equilibrium than the upright condition, since the derivative of the righting lever curve is larger.

5.7 Static heel vs. angle of loll

If the transverse centre of gravity is not located in the same y-coordinate as the transverse centre of buoyancy, the ship will have a steady heel angle. This condition is often referred to as "listing". The transverse shift of the centre of gravity, δy_{G}, reduces the righting lever:

$$\overline{GZ}(\phi) = \overline{GZ}_{\mathrm{orig}}(\phi) - \delta y_{\mathrm{G}} \cos\phi \tag{5.19}$$

This is illustrated in Figure 5.9, and an example of the effect of a transverse shift of the centre of gravity on the righting lever curve is shown in Figure 5.10. It should be noted that the resulting asymmetry in the curve might be notable, as the GZ values for the opposite heeling direction are increased.

Evaluating the heel angle from the intersection of the original righting lever curve $\overline{GZ}_{\mathrm{orig}}(\phi)$ and external moment lever caused by the shift of centre of gravity $l_{\mathrm{ext}} = \delta y_{\mathrm{G}} \cos\phi$ obviously coincides with the "listing" angle, where the $\overline{GZ}(\phi) = 0$. Therefore, "listing" and "heeling" are physically the same condition.

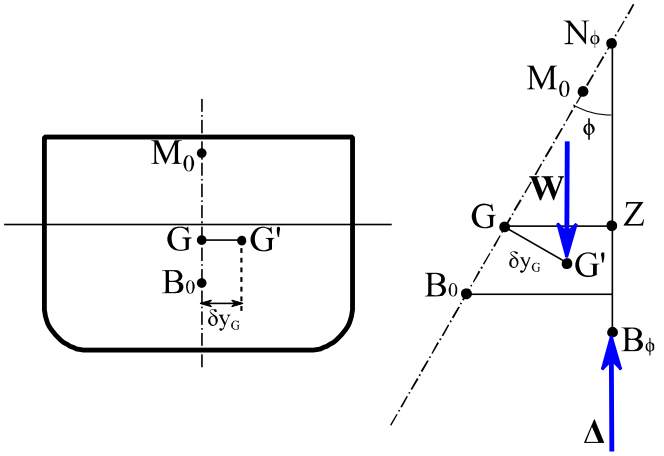

Figure 5.9 Transverse shift of centre of gravity

The ship can have a heel angle even if the centre of gravity is located directly above the centre of buoyancy B_0. In this case the metacentric height is negative, and the heel angle is called the *angle of loll*. An example of this condition is illustrated in Figure 5.11. It should be noted that the international regulations for intact stability of ships do not allow a loading condition with a negative metacentric height.

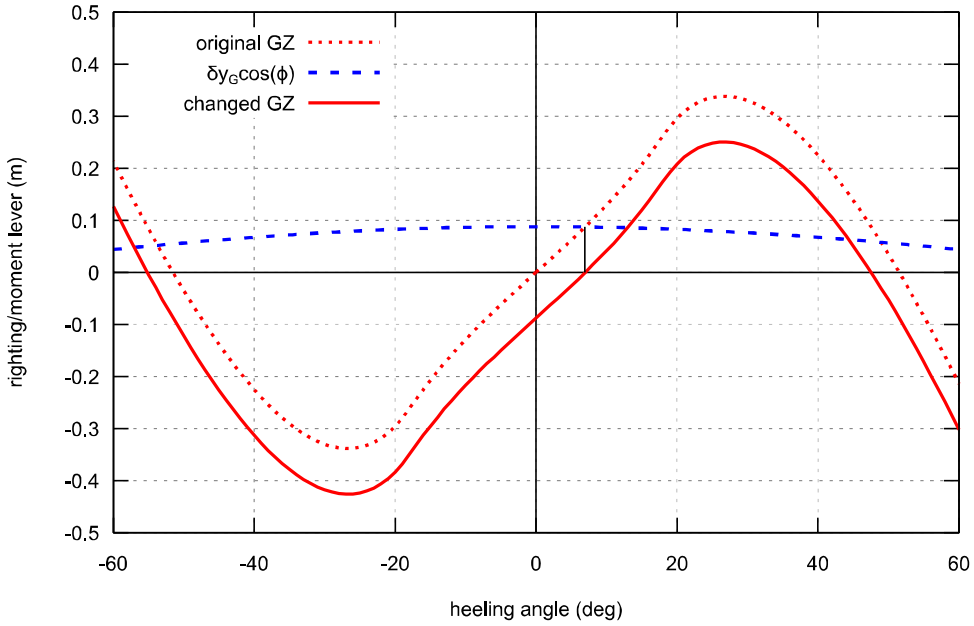

Figure 5.10 Effect of transverse shift of centre of gravity on the righting lever curve

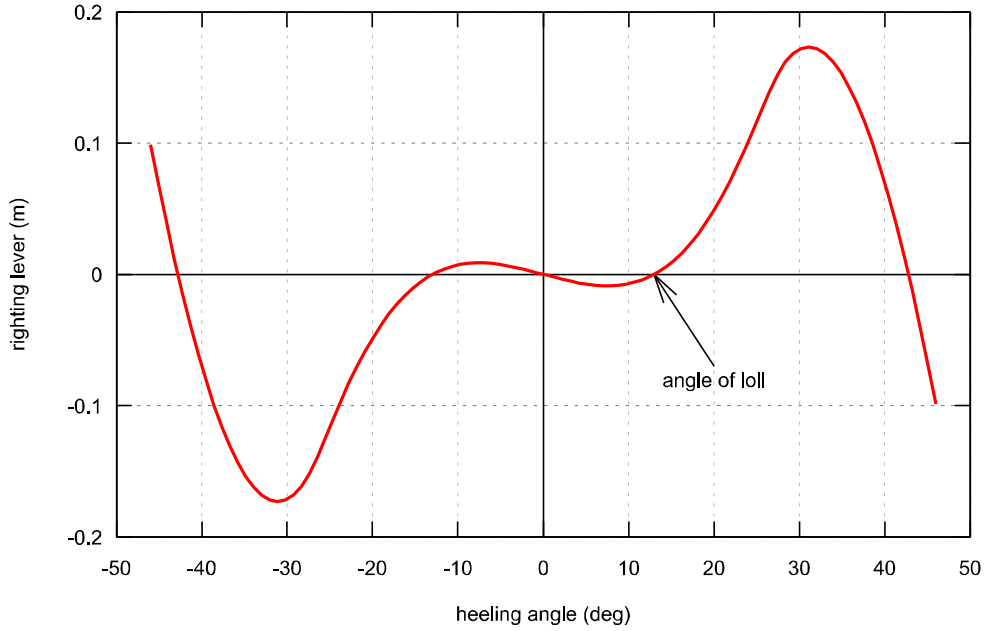

Figure 5.11 Example of angle loll when metacentric height is negative

Since the ship has a stable equilibrium at the angle of loll, and analogically to equation (5.12), the derivative of the righting lever curve at that angle can be considered as the actual metacentric height:

$$\overline{GM}_{\text{act}} = \frac{\mathrm{d}\overline{GZ}(\phi)}{\mathrm{d}\phi}\bigg|_{\phi=\phi_{\text{loll}}} \tag{5.20}$$

since this quantity represents the ability to withstand external moments in the stable heeled floating position.

5.8 Factors affecting the righting lever curve

Typical characteristics of the righting lever curve are visualized in Figure 5.12. Usually the maximum righting lever is obtained at the heel angle when the bilge emerges. For narrow ships with high freeboard height, the bilge emerges first and the GZ maximum occurs when the deck edge is immersed. At the angle of vanishing stability, where GZ becomes negative, the centres of gravity and buoyancy are again vertically aligned, since this is an unstable equilibrium condition.

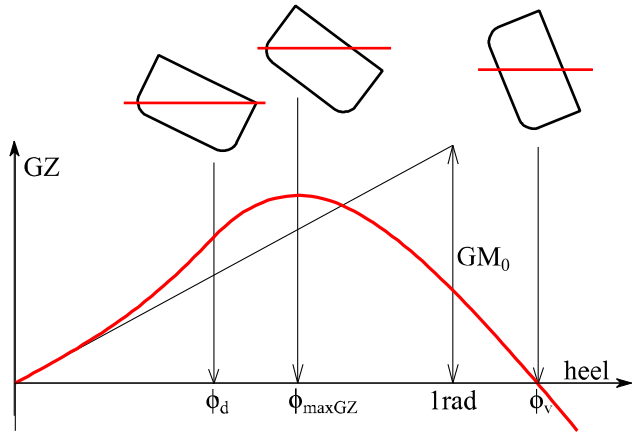

Figure 5.12 Typical characteristics of a righting lever curve

The vertical centre of gravity (KG) has a notable effect on both the initial stability (GM_0) and the characteristics of the stability curve at large heel angles. A lower KG will result in a higher maximum GZ, and a larger range of positive stability, Figure 5.13.

The freeboard height is probably the most important factor affecting the stability of a ship. Obviously, increased freeboard will increase the heel angle when the deck edge is immersed, and therefore, results in a larger range. In practice, the increase in freeboard will likely raise the centre of gravity. Yet, the positive effects on the maximum GZ and stability range may well compensate the decrease in the metacentric height, Figure 5.14.

As discussed earlier, the breadth of the ship has a significant effect on the initial stability. However, if the freeboard, centre of gravity and vertical centre of displacement are unchanged, the deck edge is immersed at a smaller heel angle. Consequently, the effect on the range of positive stability is not as significant as on the initial stability, Figure 5.15.

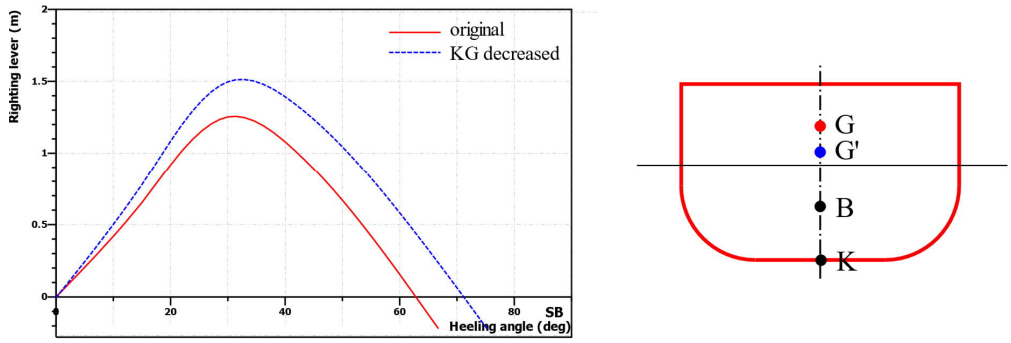

Figure 5.13 Effect of lower KG on the righting lever curve

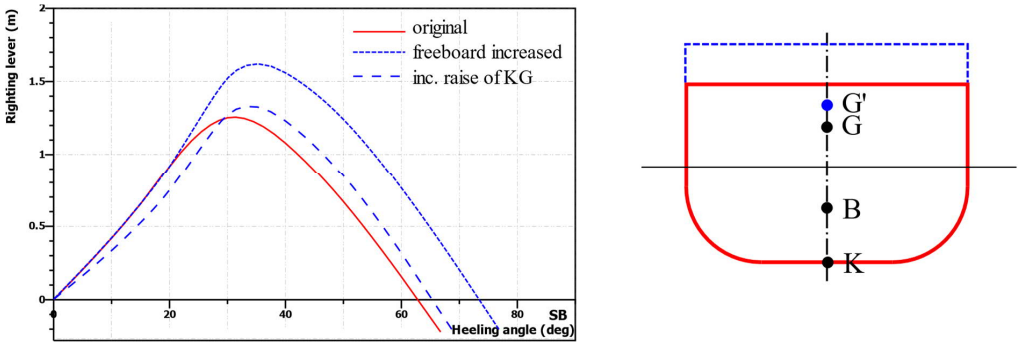

Figure 5.14 Effect of increased freeboard on the righting lever curve; note that increased of freeboard often also increases KG

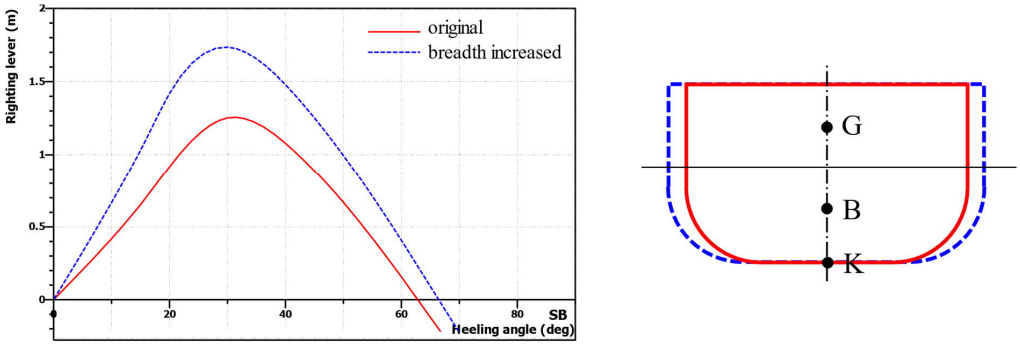

Figure 5.15 Effect of increased breadth on the righting lever curve when the vertical centre of buoyancy is unchanged

5.9 Use of sponsons to improve stability

A *sponson* is a projection that extends outward from the hull to improve stability. Side sponsons (Figure 5.16) increase the breadth, and thus have a notable effect on the stability. However, the sponsons do not usually extend much above the water line, and consequently the improvement of stability at large heel angles is smaller, Figure 5.17. This is relevant both for damage stability (draft increases) and stability in waves (wave above sponsons). In addition, large side sponsons mean challenges for arrangement of the lifesaving appliances. Sponsons may be needed to compensate the rise of the centre of gravity due to a major conversion, or due to new and stricter regulations, such as the Stockholm Agreement (water on deck for passenger ferries) that was introduced in the late 1990s, see section 14.2.

Figure 5.16 A train ferry with large side sponsons

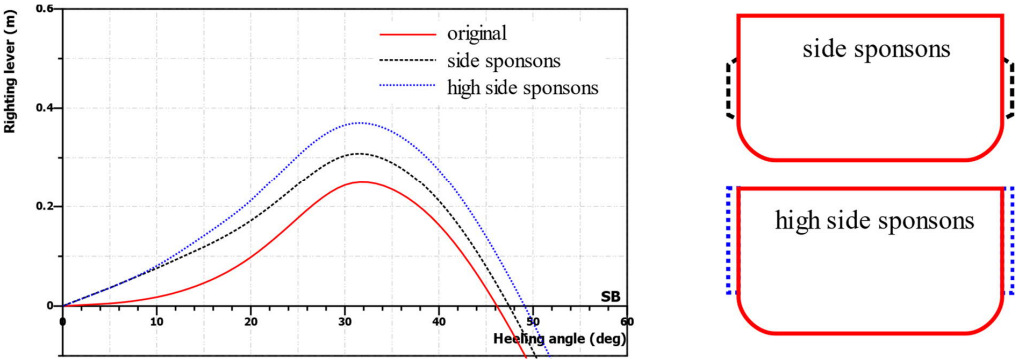

Figure 5.17 Effects of side sponsons on the righting lever curve

5.10 Asymmetric buoyant hull

Textbook examples for the righting lever curve are usually for a symmetric hull form with a symmetric loading condition. In reality, ships rarely operate with an exact upright condition, i.e. with zero heel. In addition, the buoyant hull may not be exactly symmetric. An extreme example of such a ship is the so-called oblique icebreaker. However, smaller asymmetry, especially above the waterline, is quite common, e.g. due to a quartering stern ramp or cranes and other equipment installed only on one side. Some examples of ships with asymmetric buoyant hulls are shown in Figure 5.18.

If the buoyant hull is asymmetric, the direction where the ship is heeling may not always be the critical one, as illustrated in Figure 5.19. Therefore, it is highly recommended to evaluate stability criteria separately to both starboard and port side. Moreover, even if the buoyant hull is fully symmetric, the critical openings that limit the range of positive stability may be different on starboard and port sides.

Figure 5.18 Examples of different levels of asymmetry in the buoyant hull

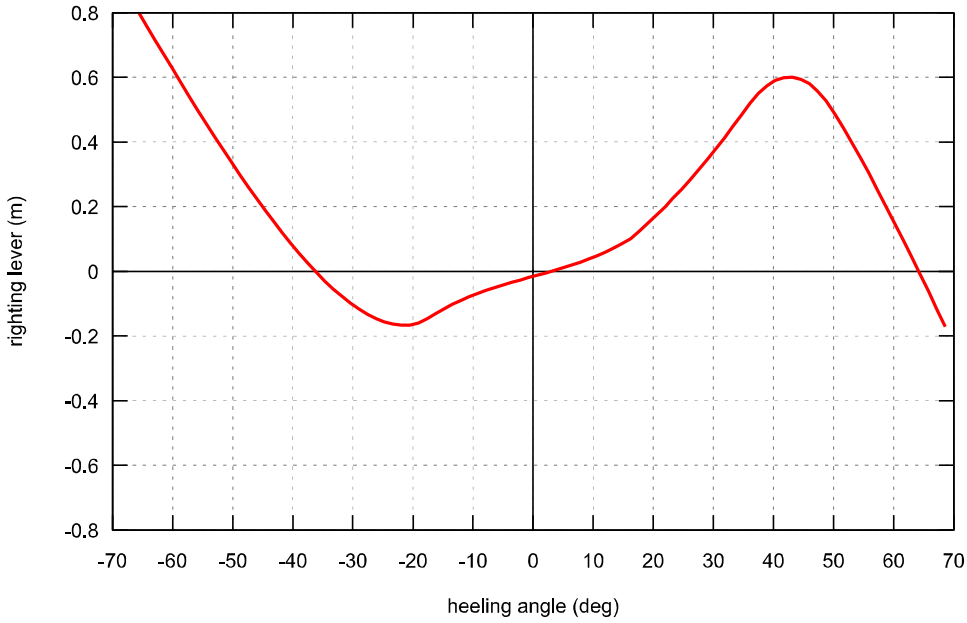

Figure 5.19 Example of a significantly asymmetric righting lever curve due to asymmetric buoyant hull

6 Longitudinal stability

6.1 Longitudinal metacentric height

When a ship trims by an angle θ, the longitudinal centre of buoyancy shifts, as illustrated in Figure 6.1. Analogically to the transverse metacentric radius, equation (4.27), the longitudinal metacentric radius, is calculated from the longitudinal moment of inertia of the waterplane area I_L:

$$\overline{B_0M_\mathrm{L}} = \frac{I_\mathrm{L}}{\nabla} \tag{6.1}$$

And correspondingly, the longitudinal metacentric height is:

$$\overline{GM_\mathrm{L}} = \overline{KB_0} + \overline{B_0M_\mathrm{L}} - \overline{KG} \tag{6.2}$$

For displacement ships the length to breadth ratio, L/B, is usually quite large, and consequently:

$$\overline{GM_\mathrm{L}} \gg \overline{GM_0} \tag{6.3}$$

Therefore, the assumption of initial stability, i.e. unchanged longitudinal metacentre, is justified. In addition, the longitudinal centre of flotation is considered to remain at the same location, and consequently, the longitudinal righting moment is:

$$M_\mathrm{st,L} = -\Delta\overline{GM_\mathrm{L}}\sin\theta \tag{6.4}$$

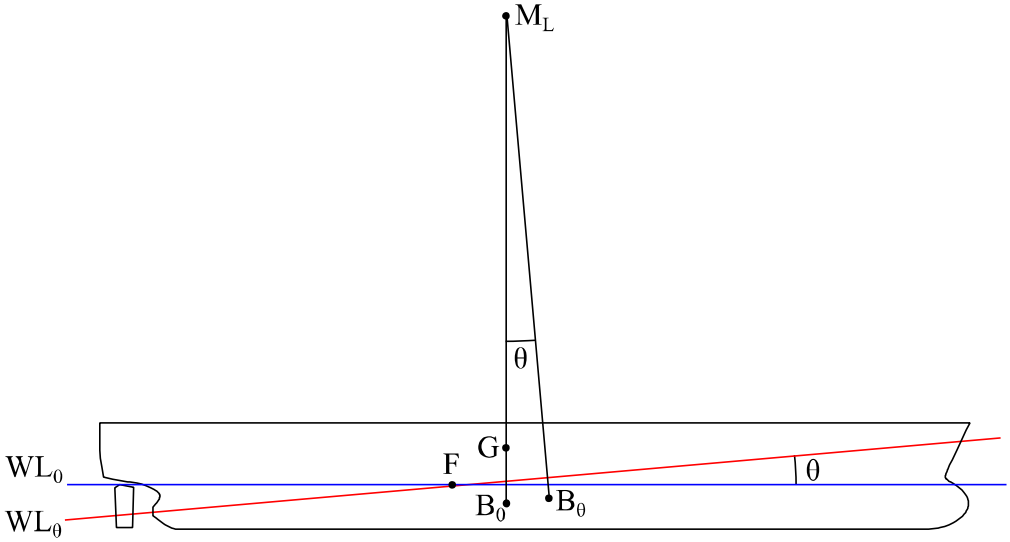

Figure 6.1 Longitudinal metacentre

6.2 Change of trim due to longitudinal shift of a load

An important application of longitudinal stability is the calculation of trim due to the changes in loading condition. Consider a load component with mass m that is initially placed in the aft part of the ship. When this mass is moved forward, the trim of the ship will change, as illustrated in Figure 6.2.

The "external" trimming moment, caused by the longitudinal shift e_L of the mass m is:

$$M_\mathrm{ext} = mge_\mathrm{L}\cos\theta \tag{6.5}$$

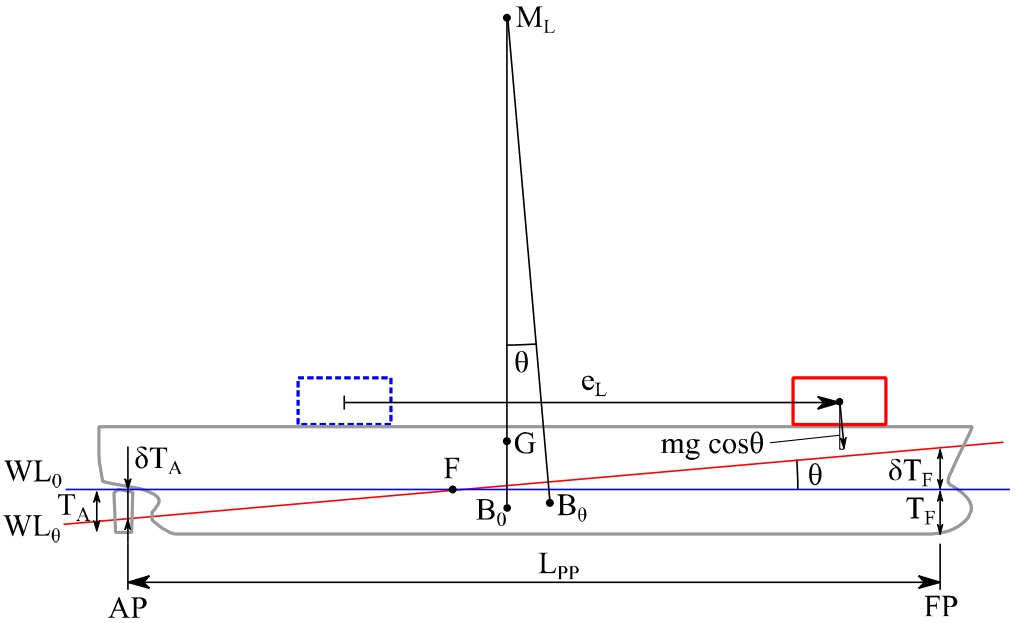

Figure 6.2 Effect of longitudinal transfer of a mass on the trim of the ship

With the assumption of initial stability, the longitudinal righting moment is:

$$M_{\mathrm{st,L}} = -\Delta\overline{GM_{\mathrm{L}}}\sin\theta \tag{6.6}$$

At equilibrium, the sum of the moments is zero, and the tangent of the trim angle is:

$$\tan\theta = \frac{mge_{\mathrm{L}}}{\Delta\overline{GM_{\mathrm{L}}}} = \frac{t}{L_{\mathrm{pp}}} \tag{6.7}$$

where $t = \delta T_{\mathrm{F}} + \delta T_{\mathrm{A}}$ is the change of the trim. Note that, in the applied coordinate system, an increase of fore draft δT_{F} and a decrease of aft draft δT_{A} are positive.

A commonly used auxiliary quantity is *moment to trim one meter*, M_{CT}. By assuming a small trim angle, this is obtained from equation (6.7) by setting $t = 1.0\mathrm{m}$, resulting in:

$$M_{\mathrm{CT}} = \frac{\Delta\overline{GM_{\mathrm{L}}}}{L_{\mathrm{pp}}} \tag{6.8}$$

However, this is not very relevant anymore since most ships are equipped with a loading computer that can accurately calculate the trim based on the hull form, displacement, and centre of gravity.

6.3 Loading and unloading

During the loading and unloading of a ship, both the draft and the trim are changed. The principle is illustrated in Figure 6.3. The change of draft is calculated by considering that the loaded mass is placed longitudinally at the centre of flotation, i.e. at $x = x_F$, and therefore, both the fore and aft drafts are increased by:

$$\delta T = \frac{m}{\rho A_{\mathrm{w}}} \tag{6.9}$$

Then the mass is moved to the actual location $x = x_m$. The trimming moment is calculated relative to the centre of flotation, so that:

$$M_{\text{ext}} = mg(x_{\text{m}} - x_{\text{F}})\cos\theta \tag{6.10}$$

The presented simplified approach for the calculation of trim is based on the assumption that the longitudinal centre of flotation is unchanged. For cargo ships this is usually reasonable, but especially for ferries and cruise ships, even small changes in trim can have a large effect on the waterplane area.

Examples of the waterplane area of a RoPax (RoRo/Passenger) ship at different trim values are illustrated in Figure 6.4. The corresponding quantitative results are listed in Table 6.1. The longitudinal centre of flotation changes significantly between the extreme for and aft trim conditions. Therefore, the trim changes during loading or unloading are not reliably estimated by applying the theory of longitudinal stability.

In practice, ships are equipped with a loading computer, where the floating position (draft, trim and heel) is solved numerically with iterative methods so that the buoyancy equals to the total weight, and the centre of buoyancy and centre of gravity are vertically aligned in a global coordinate system.

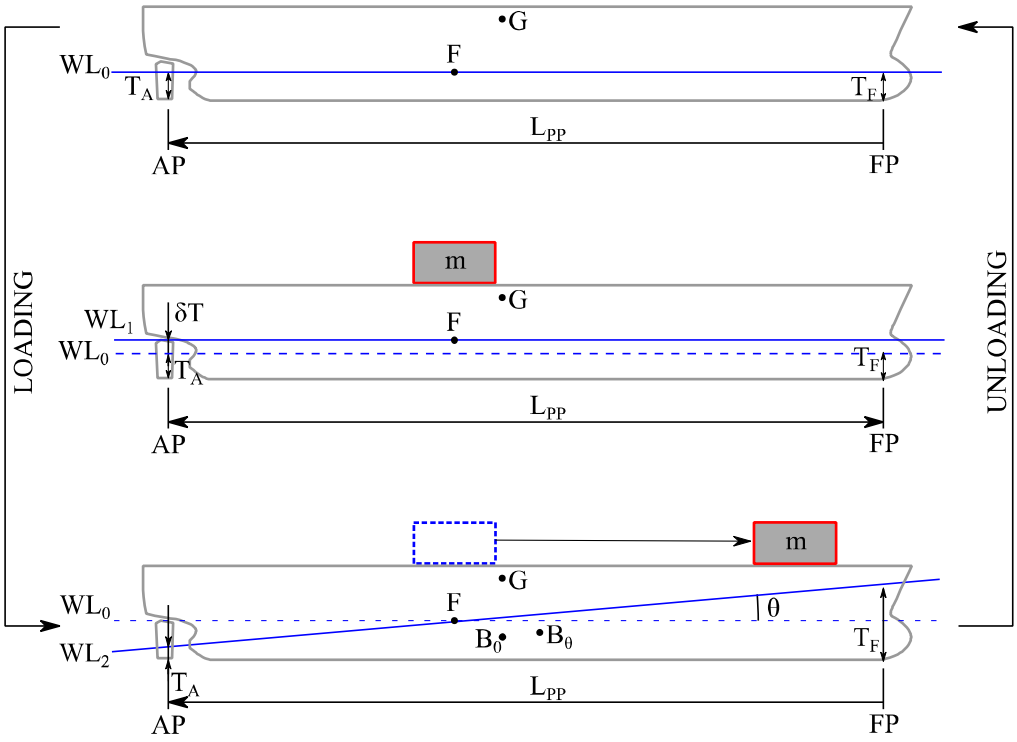

Figure 6.3 Effect of loading and unloading on the trim, based on Matusiak (1995)

Figure 6.4 Waterplane areas at even keel and ±2m trim for a RoPax ship

Table 6.1 Changes in waterplane area related quantities due to trim for a RoPax ship with constant displacement

trim [m]		$\overline{KM_T}$ **[m]**	A_w **[m²]**	x_F **[m]**
-2.0	(aft)	18.085	5353.8	86.33
-1.0	(aft)	17.778	5271.0	88.58
0.0	(even keel)	17.588	5201.7	90.71
1.0	(fore)	17.379	5108.3	93.28
2.0	(fore)	17.221	5051.6	95.55

7 Effects of loads on stability

7.1 Lightweight and deadweight

In the previous sections the centre of gravity was considered independent of the heel and trim. However, this assumption is valid only for an empty ship (lightweight only) or when all load components (deadweight) are solid and well lashed. Real ships always have various loads in the tanks and cargo holds, Figure 7.1. Therefore, it is essential to study the effects of the loads on the stability, as described in the following sub-sections.

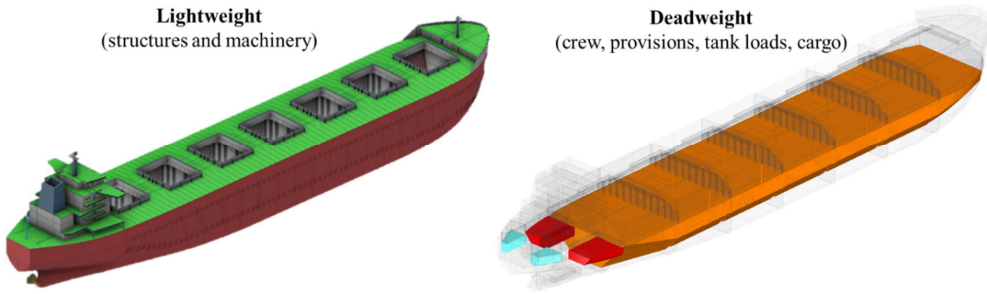

Figure 7.1 Lightweight and deadweight

7.2 Liquid loads with a free surface

All ships normally carry liquid loads, including fresh water and fuels. Some ships, such as tankers, carry also liquid cargo. The tanks containing consumable liquids are often only partly filled, and the filling ratio changes during the voyage. When the ship is heeled, the liquid loads also move, and consequently, the centre of gravity is changed. In this context, the movement is considered as quasi static, and the free surface remains horizontal. Therefore, possible sloshing of the liquid loads in heavy seas is ignored. A tank with liquid load having a free surface is called *slack tank*.

The free surface effect of a liquid load in a partly filled tank is illustrated in Figure 7.2. The ship is heeled to a small angle $\delta\phi$, and the centre of gravity of the load moves from point b to point $b_{\delta\phi}$. Analogically to the initial stability assumption, at small heel angles the centre of load moves along a circular arc with radius $\overline{bm}$. Consequently, the resulting heeling moment is:

$$M_{\mathrm{fs}} = v\rho_{\mathrm{t}} g \overline{bm} \sin\delta\phi \tag{7.1}$$

where v and ρ_{t} are the volume and density of the liquid load in the tank. Analogically to the initial stability of the ship, equation (4.27), the metacentric radius of the tank load is:

$$\overline{bm} = \frac{i_{\mathrm{T}}}{v} \tag{7.2}$$

where i_{T} is the transverse moment of inertia of the free surface in the tank.
The static righting moment of a ship is:

$$M_{\mathrm{st}} = M_{\mathrm{st0}} + M_{\mathrm{fs}} = -\left(\Delta\overline{GM}_0 - v\rho_{\mathrm{t}} g \overline{bm}\right)\sin\delta\phi \tag{7.3}$$

where M_{st0} is the static righting moment with “frozen” liquid loads.

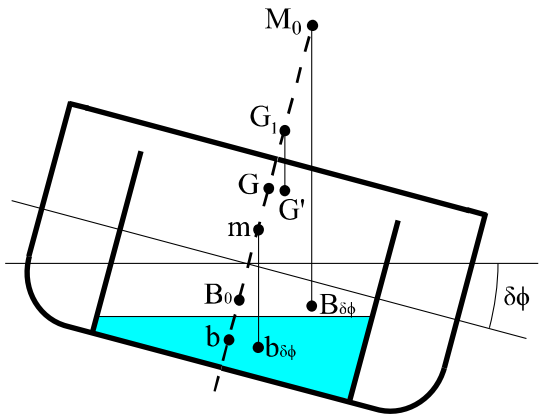

Figure 7.2 Effect of free surface on the righting moment lever

Consequently, the righting moment can be presented as:

$$M_{\mathrm{st}} = -\Delta\left(\overline{GM_0} - \frac{\rho_{\mathrm{t}}}{\rho}\frac{i_{\mathrm{T}}}{\nabla}\right)\sin\delta\phi = -\Delta\overline{GM}_{\mathrm{corr}}\sin\delta\phi \tag{7.4}$$

where ρ is (sea) water density, ∇ is volume of displacement and $\overline{GM}_{\mathrm{corr}}$ is the *corrected metacentric height*.

For a ship with N partly filled tanks, the corrected metacentric height is:

$$\overline{GM}_{\mathrm{corr}} = \overline{GM_0} - \frac{1}{\rho\nabla}\sum_{j=1}^{N}\rho_{\mathrm{t},j}i_{\mathrm{T},j} \tag{7.5}$$

The free surface effect does not depend on the location of the tank, only on the tank geometry, filling ratio and density of the liquid load.

The transverse moment of inertia for the liquid free surface in a tank is calculated based on the modelled 3D geometry. In reality, the steel structures limit the maximum net volume of the tank, Figure 7.3. It is usually assumed that the maximum net volume of a tank is:

$$V_{\mathrm{net}} = (1-r)\cdot V \tag{7.6}$$

where r is the so-called *steel reduction*, typically 2% is assumed, and V is the moulded total volume of the tank. The reduction in volume is normally considered to be equally distributed, whereas in reality, the structural stiffeners and brackets are located on the bottom, top and sides of the tank.

A similar assumption is often applied in the calculation of the free surface moments:

$$\overline{GM}_{\mathrm{corr}} = \overline{GM_0} - \frac{1}{\rho\nabla}\sum_{j=1}^{N}\rho_{\mathrm{t},j}i_{\mathrm{T},j}\left(1-r_j\right) \tag{7.7}$$

So that instead of calculating the actual effect of the structures on the free surface moment in the tank, a simple steel reduction factor is applied. In practice, this approach is conservative since the structures are located in the outer limits of the free surface, and the reduction effect on the surface inertia moment is actually larger than the effect on the free surface area.

It is trivial to evaluate the free surface effect for an actual loading condition, where the exact amounts of liquid loads in all tanks are known. However, some tanks contain consumables, such as fresh water or fuel. The filling rate of these tanks can change during a voyage, and some simplified, yet conservative, approach is needed for planning of the loading conditions when designing the ship. A conservative assumption is to use the maximum free surface effect, as illustrated in Figure 7.4. However, using the maximum effect for all tanks in the ship can be much too conservative, since a condition where all tanks are partly filled is not realistic.

Figure 7.3 Structures inside a tank, adopted from Ruponen et al. (2010)

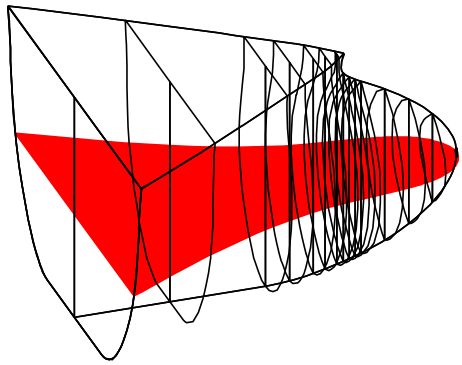

Figure 7.4 Example of the largest free surface in a fore peak tank

Figure 7.5 shows the various tanks on a large passenger ship. Applying the maximum free surface correction to all tanks would lead to a GM reduction of 0.428 m. However, when accounting for only the maximum free surface for each tank purpose (fresh water, fuel oil, etc.), the reduction is only 0.138 m. This is a much more realistic approach, since in real operation all tanks are not consumed simultaneously. Furthermore, it should be noted that this approach is applicable only to consumable liquids. For ballast water and liquid cargo, the actual filling ratio should be used in the calculation of the free surface effect. IMO IS Code provides detailed guidance on how the free surface corrections should be calculated.

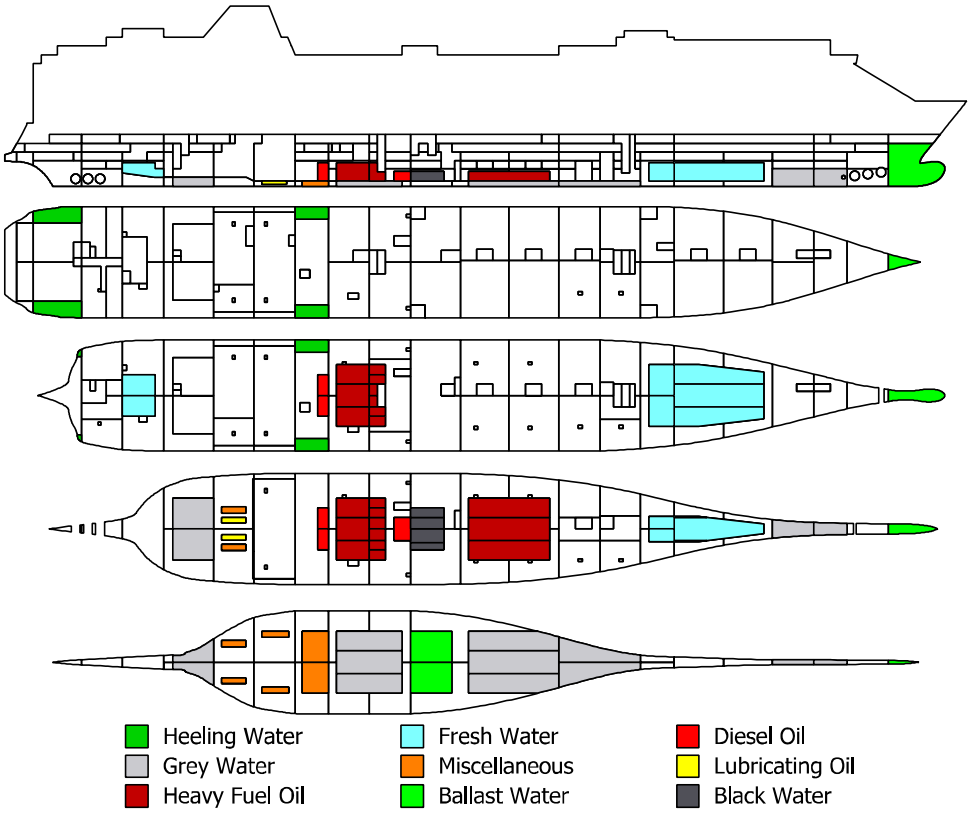

Figure 7.5 Tanks for different purposes on a large passenger ship design

For loading computers on board ships, the actual filling level should be used for all tanks, including consumable liquids, since the intention is to analyse the stability at the actual current loading condition. This is different compared to the "worst-case scenario" approach used when designing the loading capacity of the ship.

The free surface correction to the metacentric height presents the negative effect of liquid loads on the initial stability of the ship. However, as described in chapter 4, the initial stability is not a sufficient measure of the stability of the ship. Therefore, the effect of the free surface needs to be accounted for in the righting lever curve as well.

Similarly to the initial stability approximation, the free surface correction to the righting lever at heel angle ϕ for each partially filled tank i can be estimated as:

$$GZ_{\mathrm{corr},i}(\phi) = \frac{\rho_i}{\rho\nabla} i_{\mathrm{T},i} \sin\phi \tag{7.8}$$

However, this approach does not account for the actual geometry of the tank, nor the changes in the free surface, especially with a small or large fill ratio, Figure 7.6. For box-shaped tanks the estimate is good up to the heel angle, when either tank bottom emerges or the top of the tank is immersed, Figure 7.7.

An example of the effects of different free surface correction methods on the righting lever curve is shown in Figure 7.8. Ignoring the liquid loads results in overestimation of the stability characteristics, especially at large heel angles.

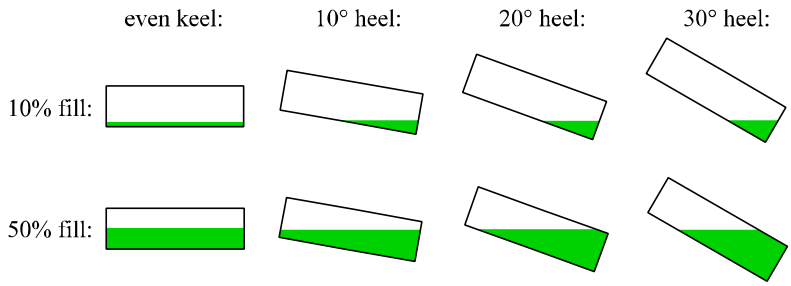

Figure 7.6 Shift of liquid load in a partially filled tank at different heel angles

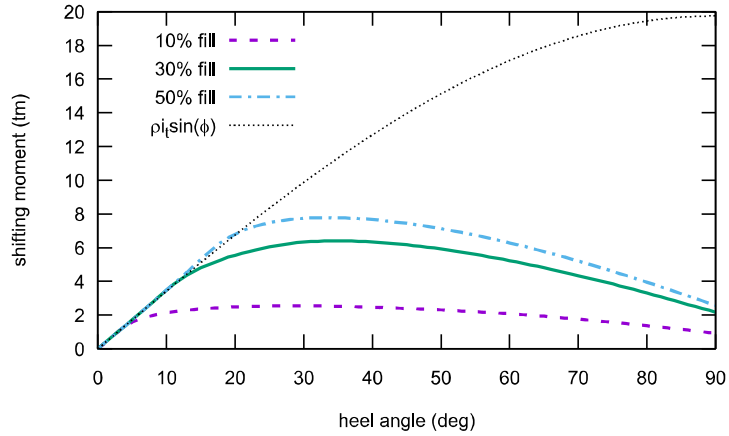

Figure 7.7 Example of real shifting moments at different filling ratios for a box-shaped tank presented in Figure 7.6

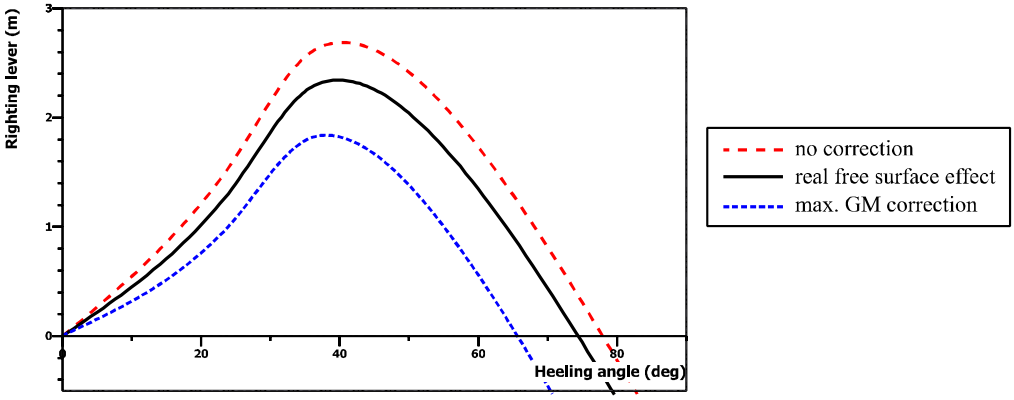

Figure 7.8 Example of free surface corrections on the GZ curve

To maintain a good stability, the free surfaces of tanks must be kept to a minimum. The GM reduction, due to the free surface effect, is highly affected by the breadth of the tank. Instead of a single large tank, several narrower tanks can be used to significantly decrease the free surface effect, as illustrated in Figure 7.9. When the length of the tank is l and the total breadth is b. Thus, the original maximum transverse moment of inertia of the free surface is:

$$i_{\mathrm{T}} = \frac{1}{12} l b^3 \tag{7.9}$$

When divided into n equally wide separate tanks, each with the breadth b/n, the total transverse moment of inertia of the free surfaces is:

$$i_{\mathrm{T}} = n \cdot \frac{1}{12} l \left(\frac{b}{n}\right)^3 = \frac{1}{n^2} \cdot \frac{1}{12} l b^3 \tag{7.10}$$

Consequently, the free surface effect is reduced to $1/n^2$.

It should be noted that for a divided tank, the tank contents need to be consumed symmetrically in order to avoid heeling. For example, in Figure 7.5 the port and starboard side parts of the divided tank form a *tank pair*, and if the maximum free surface moment for each load purpose is calculated, the sum of the components of the tank pairs must be considered.

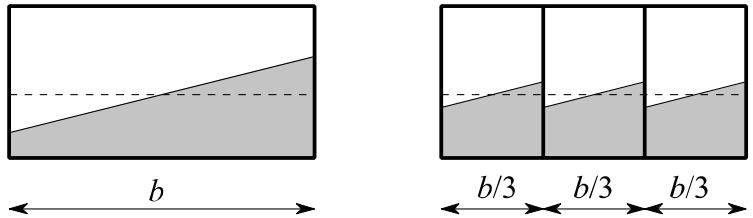

Figure 7.9 Example of reducing the free surface effect by dividing the tank longitudinally

7.3 Suspended loads

Also, suspended (i.e. hanging) loads have a negative effect on the stability of the ship. Similarly to partially filled tanks, heeling of the ship will result in a transverse shift of centre of gravity.

Consider a ship that is subjected to a small static external heeling moment dM_{ext}. Based on the initial stability approximation, the ship will heel to an angle:

$$\delta\phi' = \frac{dM_{\mathrm{ext}}}{\Delta \overline{GM}_0} \tag{7.11}$$

A suspended weight with a mass m, as illustrated in Figure 7.10, will further increase the heeling by an angle $\delta\phi''$, since the cargo shift creates an additional heeling moment:

$$M_{\mathrm{shift}} = mgl \cdot \delta\phi \tag{7.12}$$

where l is the length of the cable, and small heel angles are assumed. Consequently, the total heel angle is:

$$\delta\phi = \delta\phi' + \delta\phi'' = \frac{dM_{\mathrm{ext}}}{\Delta \overline{GM}_0} + \frac{mgl}{\Delta \overline{GM}_0} \delta\phi \tag{7.13}$$

Consequently, the new heel angle can be solved and presented as:

$$\delta\phi = \frac{dM_{\text{ext}}}{\Delta\left(\overline{GM_0} - \frac{mgl}{\Delta}\right)} \tag{7.14}$$

Therefore, the suspended load decreases the effective metacentric height, in a similar way as a liquid load in partially filled tank. However, the effect of a suspended load is the same as if the weight was located at the end of the derrick. In order to simplify the stability calculations, it is a common practice to place suspended weights at the top of the derrick, instead of applying a GM correction.

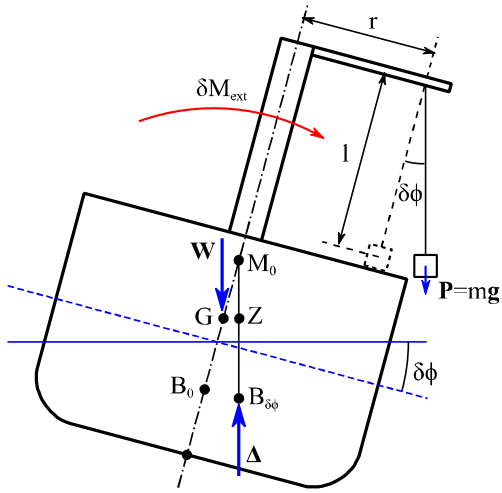

Figure 7.10 Suspended load

7.4 Grain loads

Grain loads are also prone to cargo shift if there are voids in the cargo hold. Thus, IMO has published regulations for *grain loads* in the International Code for the Safe Carriage of Grain in Bulk (International Grain Code), IMO (1991). The grain shift moment is calculated from the geometry of the hold, accounting for the structures that may cause voids. The basics of this approach are illustrated in Figure 7.11. For partially filled holds the shift angle is considered to be 25°, and for hatches and structural gaps the angle is taken as 15°.

The related stability criteria are based on the calculated lever of the grain shift moment at upright l_0. The heeling lever is assumed to decrease linearly so that it equals $0.8l_0$ at 40° heel. It is required that

- Heel angle due to shift of grain shall not be greater than 12°
- The area between the heeling lever and righting lever shall be not less than 0.075 m·rad, when limited to the minimum of the flooding angle and 40°
- Initial metacentric height, with free surface correction, shall not be less than 0.30 m

The grain shift moment lever and related stability criteria are visualized in Figure 7.12. It should be noted that the presented description of grain stability criteria are generalized, and the International Grain Code contains also several other requirements.

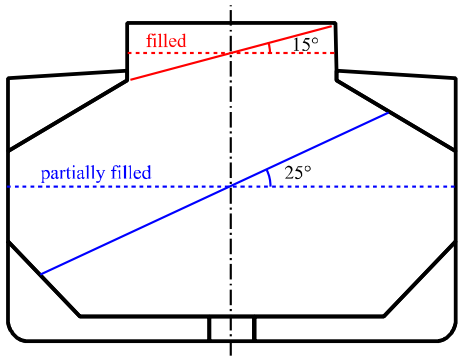

Figure 7.11 Principle for calculation of grain shift moment

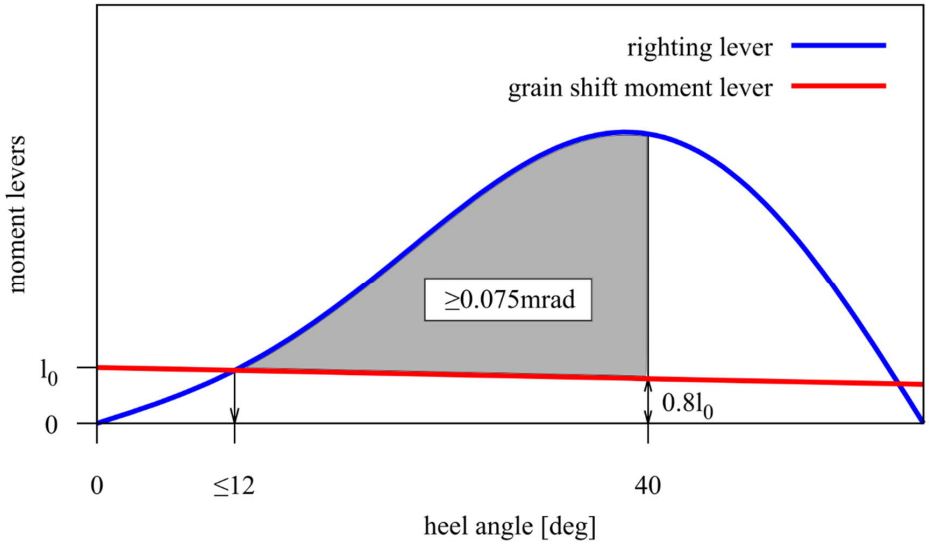

Figure 7.12 Stability criteria based on the grain shift moment

7.5 Other bulk loads

Grain loads are not the only non-liquid load type that needs special attention to ensure sufficient stability of bulk carriers. Moisture mixed with some minerals, such as iron and nickel ore, can sometimes exceed a certain limit, after which the load behaves like a liquid. This phenomenon is known as *liquefaction*, and it has caused several fatal accidents on bulk carriers over the decades. The capsizing of the pusher-barge FINN-BALTIC near Hanko in 1990 is one example.

During loading, the cargo is usually in a solid state. The liquefaction process appears when, in a fine-grained cargo, the spaces between cargo grains are filled with both air and water. The problem occurs in mineral cargoes of predominantly fine particles, in conditions which allow

the soaking up of large amounts of water. The cargo can turn into muddy slush if the amount of moisture is too high. The motions of the ship at sea cause the inter-grain spaces to contract, resulting in the compaction of the cargo. If compaction is such that there is more water inside the cargo than there are spaces between the particles, the water in the spaces between particles is subject to a compressive force, but as it is liquid, it cannot be compressed. The water pressure inside the cargo can rise sharply and press the particles apart. If there is enough moisture, the reduction in inter-grain friction due to the ship motion and vibration can be sufficient to cause the cargo to flow like a liquid, i.e. to liquefy. A comprehensive description of this process and its effects on ship stability is given by Andrei and Hanzu Pazara (2013).

According to Intercargo (2019), cargo shift or liquefaction was the reason for the loss of nine bulk carriers of over 10 000 dwt between the years 2009 and 2018, and a total of 101 lives were lost in these accidents.

8 Inclining test

8.1 Background

Calculations for the intact stability of ships have been presented in the previous chapters, with the assumption that the centre of gravity is known. A good estimation can normally be based on dedicated weight calculations, especially if an accurate 3D model of the structures is prepared. However, there are always notable uncertainties even in the best weight calculation data. Consequently, a more reliable estimate is needed for the stability booklet, and this is evaluated experimentally by utilizing the assumption of initial stability.

The *inclining test* is normally carried out by moving solid weights on the deck. A recommended shifting order, using four weights, is illustrated in Figure 8.1, resulting in total of 9 measurement points, when the initial condition before the first shift is also taken into account.

The floating position is evaluated based on the draft mark readings. The hull form is known, so the volume of displacement can be calculated based on the draft mark readings. Possible hull deflection is also usually accounted for in these analyses. In practice this means that the hydrostatic quantities need to be calculated for a deflected hull object. The curve of deflection is obtained by fitting a smooth curve to the draft mark readings at different longitudinal locations, typically at aft perpendicular, at midships and at fore perpendicular.

The mass of the ship in the test condition is obtained simply multiplying the calculated volume of displacement with the measured water density. The density is analysed from water samples. For a high accuracy, also the water temperature should be measured.

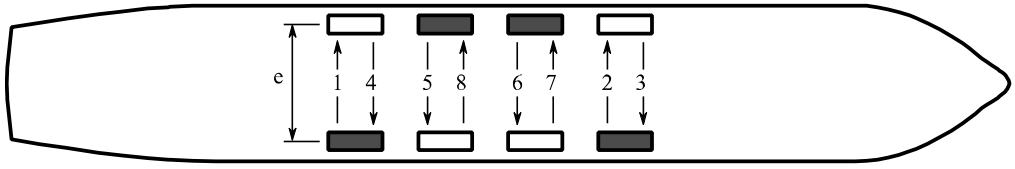

Figure 8.1 Recommended order for weight shifts in an inclining test

8.2 Standard method

The standard method for analysis of the inclining test results is based on the assumption of initial stability. This approach is preferred by the major classification societies, and the calculations can easily be done with a spreadsheet.

Transverse shift e of a weight with mass m results in a heeling moment:

$$M_{\text{ext}} = mge\cos\phi \tag{8.1}$$

It is assumed that all heel angles ϕ during the test are small. Furthermore, the assumption of initial stability implicitly means that the waterplane area is not notably changed. Consequently, the righting moment can be estimated as:

$$M_{\mathrm{st}} = -\Delta \overline{GM_0} \sin \phi \tag{8.2}$$

In inclining test the heel angle ϕ is measured with inclinometers and/or pendulums. Therefore, the initial metacentric height $\overline{GM_0}$ can be calculated from the moment balance at equilibrium:

$$\overline{GM_0} = \frac{mge}{\Delta \tan \phi} \tag{8.3}$$

In order to ensure sufficient accuracy, several different heeling moments to both sides are needed, as shown in Figure 8.1. The $\overline{GM_0}$ can be solved by a least square fit of a straight line to the measurement points, when the heeling moment is plotted as function of $\Delta \tan \phi$. The initial metacentric height can then be obtained easily from the slope of the linear fit. Note that usually moments are given in ton·m and displacement in tons, as illustrated in Figure 8.2. With this method also the measurement points in upright conditions during the test procedure have an impact on the result.

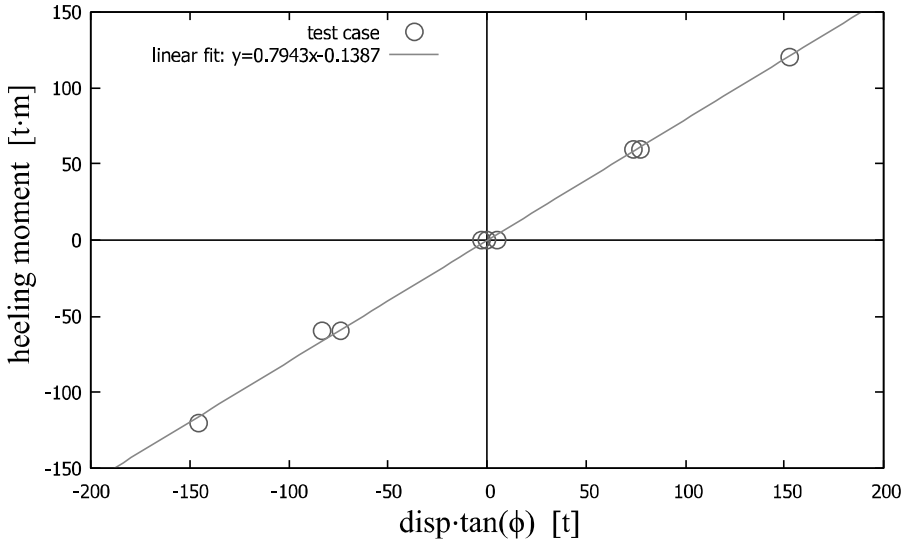

Figure 8.2 Example of results from an inclining test

During the inclining test, all tanks should be either empty or full in order to avoid the free surface effect. Therefore, the vertical centre of gravity is:

$$z_{\mathrm{G}} \equiv \overline{KG} = \overline{KM_0} - \overline{GM_0} = \overline{KB_0} + \overline{B_0M_0} - \overline{GM_0} \tag{8.4}$$

The longitudinal location of the centre of gravity can be evaluated based on the calculated centre of buoyancy at the measured floating position (with trim angle θ):

$$x_{\mathrm{G}} = x_{\mathrm{B}} - (\overline{B_0M_0} - \overline{GM_0}) \tan \theta \tag{8.5}$$

And similarly, for the transverse location, in case there is an initial heel angle ϕ:

$$y_{\mathrm{G}} = y_{\mathrm{B}} - (\overline{B_0M_0} - \overline{GM_0}) \tan \phi \tag{8.6}$$

Inclining test is typically carried out at shipyard when some structures and equipment may still be missing. Furthermore, there may be additional equipment and tools onboard or liquid loads in the tanks that need to be reduced from the actual lightweight of the ship. Consequently, the final centre of gravity for the lightweight is calculated by adding the missing masses $m_{\mathrm{m},i}$ and reducing the additional weights $m_{\mathrm{a},i}$:

$$z_{\mathrm{G}^*} = \frac{Mz_{\mathrm{G}} + \sum_i^{n_{\mathrm{m}}}(m_{\mathrm{m},i}z_{\mathrm{m},i}) - \sum_i^{n_{\mathrm{a}}}(m_{\mathrm{a},i}z_{\mathrm{a},i})}{M + \sum_i^{n_{\mathrm{m}}}(m_{\mathrm{m},i}) - \sum_i^{n_{\mathrm{a}}}(m_{\mathrm{a},i})} \tag{8.7}$$

where $M = W/g$ is the mass of the ship during the inclining test.

The lightweight and its centre of gravity are fundamental parameters for all stability analyses. Therefore, reliable and accurate assessment is essential. Consequently, the IMO IS Code has detailed requirements and recommendations for performing the inclining test. The most notable ones are listed below:

- ship should be as complete as possible
- all temporary material on board should be reduced to minimum
- all tanks should be either empty or full
- decks should be free of water
- calm weather and still water
- ship is free of any mooring restraints
- ship should be as upright as possible
- minimum inclination is 1° and maximum is 4°, to both sides
- density of water needs to be analysed

For cargo ships and Ro-Ro/Passenger (RoPax) ships, the inclining test can usually be done by shifting solid weights as described above. However, for some ship types, like cruise liners, this is not possible, and the inclining moments need to be achieved by transferring liquid (ballast water) between the tanks, Figure 8.3. The inclining tanks should be directly opposite in order to maintain trim. Exact movement of the water in the heeling tanks must be accounted for in the calculation of the heeling moment. Consequently, no free surface correction should be applied for these tanks.

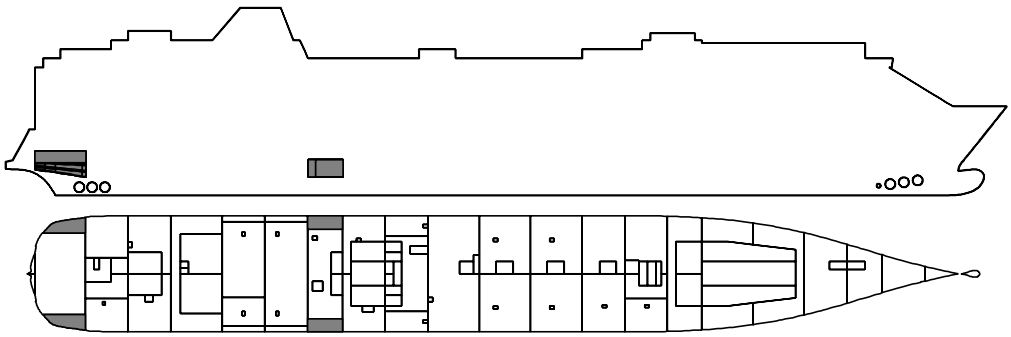

Figure 8.3 Heeling tanks on a cruise ship can be used in inclining test

8.3 Advanced analysis method

The standard method for analysis of inclining test results, equation (8.3), is based on the initial stability approximation. Most notably, it is assumed that the waterplane area and the centre of flotation remain unchanged during the test. For a conventional hull form these simplifications are usually valid, at least with very small heel angles (less than 2°). However, for certain hull forms this assumption may not be fully valid.

The inclining test results can also be analysed with more advanced methods, utilizing the 3D model of the hull form to evaluate the actual righting lever in the heeled conditions. Utilizing this value instead of the initial stability assumption, a more accurate estimate of the centre of gravity can be obtained.

An extensive comparison of various methods to analyse inclining test results for different hull forms was presented by Karolius and Vassalos (2018). In their study, increased error (up to 0.44%) was observed for the examined navy, container and RoPax ships with the standard method. Therefore, it is essential to evaluate also waterplane area changes in the test conditions to ensure that the applied simplifications are valid. Yet, the IMO IS Code does not acknowledge these more advanced analysis methods, so in practice the standard method needs to be used, unless otherwise agreed with the administration.

9 Dynamic stability

9.1 Background

The previous chapters have dealt with the stability of ships in calm water under static, or quasi-static, external moments. However, e.g. waves and gusty wind are dynamic, so the assumption of a static condition may result in a serious under-estimation of the maximum heel angle. Consequently, another approach is needed to estimate the maximum dynamic heel angle the ship can reach, when subjected to a dynamic external moment.

The concept of dynamic stability of ships was first discussed by Moseley (1850), and in the 20th Century this has become an essential part of stability criteria. In the following sections, the concept of a dynamic righting lever is derived, using a simplified one degree-of-freedom (DOF) equation for the roll motion of ship.

9.2 Roll motion

One degree of freedom (DOF) uncoupled roll motion can be presented as sum of moments:

$$M_{\text{inertia}} + M_{\text{damping}} + M_{\text{st}} + M_{\text{ext}} = 0 \tag{9.1}$$

In reality, roll motion is coupled with the other ship motions, but for simplicity, a simple 1-DOF model can be used. For ship-shaped objects, the roll direction is usually the most critical one concerning the safety. However, it should be noted that for offshore structures, this simplified approach is usually not valid.

Dynamic roll motion depends on the inertia of ship, and the angular acceleration of roll $\ddot{\phi}$:

$$M_{\text{inertia}} = -I'_{\text{xx}}\ddot{\phi} \tag{9.2}$$

The effective moment of inertia is:

$$I'_{\text{xx}} = I_{\text{xx}} + \delta I_{\text{xx}} \tag{9.3}$$

The *added mass* term δI_{xx} represents the additional moment of inertia due to the seawater around the ship that moves with the ship. And by using the radius of inertia, k_{xx}, the moment of inertia can be presented as:

$$I'_{\text{xx}} = \frac{\Delta}{g}\left(k_{\text{xx}}{}^2 + \delta k_{\text{xx}}{}^2\right) \tag{9.4}$$

The radius of inertia k_{xx} can be evaluated from detailed weight calculations or with approximate formulae, based on the main dimensions of the ship. The radius of inertia for the added mass δk_{xx} can be calculated with seakeeping software, or roughly estimated to be about 30%..40% of the breadth of a ship.

The second term in the equation (9.1) is *roll damping*, which involves complex phenomena related to wave making, eddy flows and viscosity. In general, all these components are proportional to the roll velocity $\dot{\phi}$. For simplicity, in this context a linear (equivalent) damping term is assumed, so that:

$$M_{\text{damping}} = -N_{\text{xx}}\dot{\phi} \tag{9.5}$$

Furthermore, by using the assumption of initial stability, the static righting moment can be approximated with:

$$M_{\mathrm{st}} = -\Delta\overline{GZ}(\phi) \approx -\Delta\overline{GM_0}\phi \tag{9.6}$$

Consequently, without any external excitation, the equation (9.1) can be presented as a simple homogenous linear second order differential equation:

$$I'_{\mathrm{xx}}\ddot{\phi} + N_{\mathrm{xx}}\dot{\phi} + \Delta\overline{GM_0}\phi = 0 \tag{9.7}$$

or in a non-dimensional form:

$$\ddot{\phi} + 2\xi\omega_\phi\dot{\phi} + \omega_\phi^2\phi = 0 \tag{9.8}$$

where the *critical damping ratio* is:

$$\xi = \frac{N_{\mathrm{xx}}}{2\omega_\phi I'_{\mathrm{xx}}} \tag{9.9}$$

and the natural angular frequency of roll motion is:

$$\omega_\phi = \sqrt{\frac{\Delta\overline{GM_0}}{I'_{\mathrm{xx}}}} \tag{9.10}$$

Consequently, the natural roll period is:

$$T_\phi = \frac{2\pi}{\omega_\phi} = 2\pi\sqrt{\frac{I'_{\mathrm{xx}}}{\Delta\overline{GM_0}}} \tag{9.11}$$

The equation (9.8) is in the form of a homogeneous second order ordinary differential equation. If the ship is initially heeled to an angle ϕ_0, the initial condition is $\phi(0) = \phi_0$ and $\dot{\phi}(0) = 0$. By assuming $\xi < 1$, the solution of this differential equation is:

$$\phi(t) = \phi_0 e^{-\xi\omega_\phi t}\cos\left(\omega_\phi(1-\xi^2)t\right) \tag{9.12}$$

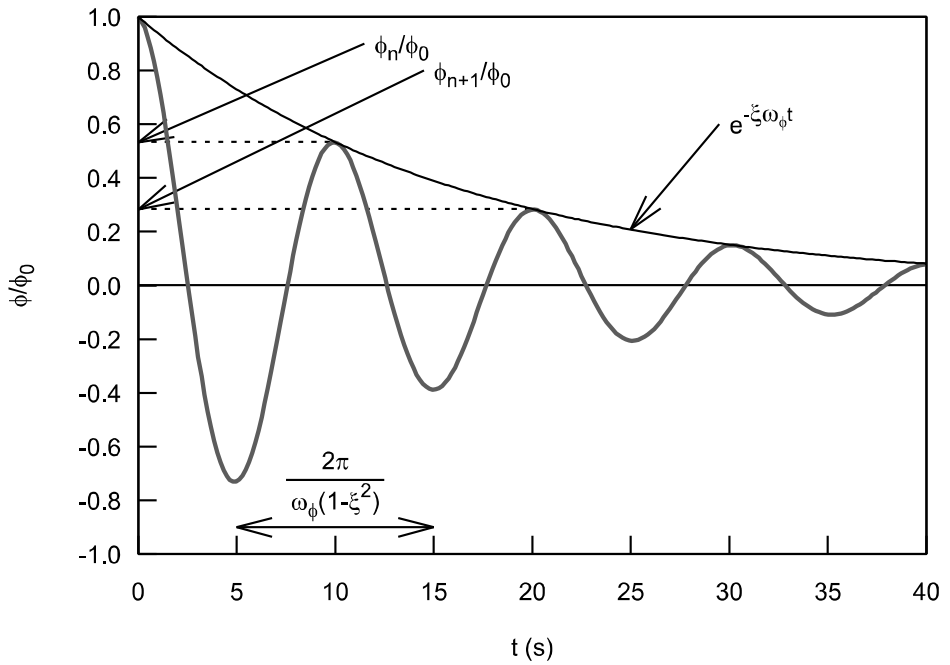

Figure 9.1 Example of roll decay

The roll response is shown in Figure 9.1. The natural roll period and critical damping ratio ξ can be evaluated experimentally in a *roll decay test*, based on the transient response:

$$\xi = \frac{1}{2\pi}\ln\left(\frac{\phi_n}{\phi_{n+1}}\right) \tag{9.13}$$

9.3 Roll response in waves

The most common cause of rolling is wave excitation. The *angular frequency of encounter* depends on the velocity of the ship V_s and on the encounter angle β, see Figure 9.2:

$$\omega_e = \omega\left(1 - \frac{\omega V_s}{g}\cos\beta\right) \tag{9.14}$$

In deep water the wave frequency ω and wavelength λ have the following relation:

$$\omega = \sqrt{\frac{2\pi g}{\lambda}} \tag{9.15}$$

From the stability point of view, the beam seas condition is the most severe one, although also other wave directions can be dangerous. In this chapter, only the beam seas situation is investigated.

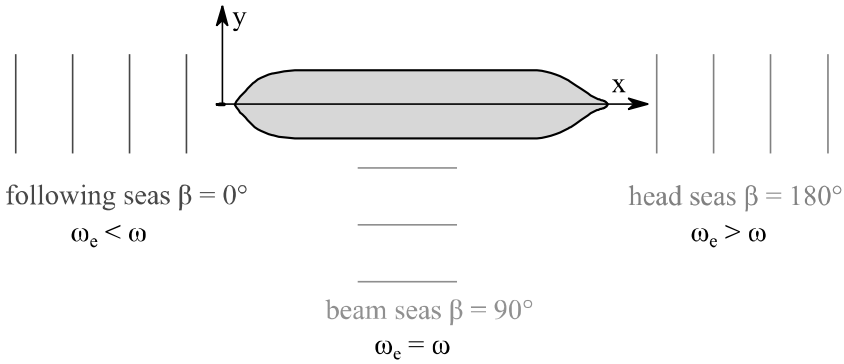

Figure 9.2 Wave directions and effect on the encounter frequency

Roll response in waves is a rather complex phenomenon. Several numerical models, with different levels of sophistication, have been developed for this. The simplest model of uncoupled roll motion in regular waves has been presented extensively by Bhattacharyya (1978), and shortly in Rawson and Tupper (2001). For convenience, the principles related to ship stability are presented in the following.

The approach is based on the so-called Froude-Krylov hypothesis, where it is assumed that the pressure acting on a ship in a wave is the same as the pressure in the wave in an absence of ship. The forces and moments are obtained by integrating the pressures over the constant wet surface of the ship. The first simplification means that diffraction of the waves (disturbance caused by a ship to the on-coming waves) is disregarded. This approximation is good for long waves (much longer than the ship breadth, i.e. $\lambda \gg B$). The other simplification (constant wet surface) means that the motions of the ship are disregarded when calculating the excitation. Consequently, the approximation is good for a small amplitude motion.

In case of the regular sinusoidal beam waves ($\omega_e = \omega$), the model of excitation is further simplified, Bhattacharyya (1978), and the exciting moment is:

$$M_{ext}(t) = a_w k \Delta \overline{GM_0} \sin(\omega t) \tag{9.16}$$

where a_w is wave amplitude and the *wave number* is:

$$k = \frac{2\pi}{\lambda} \tag{9.17}$$

where λ is wavelength. In deep water, the *dispersion relation*, couples the wave number and angular wave frequency ω:

$$k = \frac{\omega^2}{g} \tag{9.18}$$

The product of the wave amplitude and the wave number represents the maximum wave slope. By substituting the wave excitation moment (9.16) into the righthand side of the equation (9.7) yields a linear second order ordinary differential equation for the roll motion of a ship in beam regular waves. Similarly to the calm water case, this can be presented in non-dimensional form:

$$\ddot{\phi} + 2\xi\omega_\phi\dot{\phi} + \omega_\phi^2\phi = a_w k \omega_\phi^2 \sin(\omega t) \tag{9.19}$$

The steady state solution to roll motion in regular beam seas is, Bhattacharyya (1978):

$$\phi(t) = \phi_A \sin(\omega t - \varepsilon) \tag{9.20}$$

By using a *tuning factor*:

$$\Lambda = \frac{\omega}{\omega_\phi} \tag{9.21}$$

the roll amplitude is:

$$\phi_A = \frac{a_w k}{\sqrt{(1-\Lambda^2)^2 + (2\xi\Lambda)^2}} \tag{9.22}$$

and the tangent of the phase angle ε is:

$$\tan\varepsilon = \frac{2\xi\Lambda}{1-\Lambda^2} \tag{9.23}$$

The roll amplitude ϕ_A in relation to the wave slope $a_w k$ and phase angle ε are presented as a function of the ratio of wave frequency to the natural frequency of roll in Figure 9.3. This kind of graph is called *response amplitude operator*, i.e. RAO. For very long waves ($\omega \approx 0$), the roll motion of the ship follows the wave slope. Increasing wave frequency (decreasing wavelength) is followed by an increase in the roll amplitude. At resonance ($\omega \approx \omega_\phi$), the roll amplitude, in relation to the wave slope, is at the maximum. A further increase in the wave frequency (a decrease of wavelength) causes a decrease in the roll amplitude.

The large amplitude roll motion in beam seas at the resonance frequency ($\omega \approx \omega_\phi$ i.e. $\Lambda = 1$) is known as *synchronous rolling*. This can damage the cargo or cause injuries to the people on board. The roll motion can be decreased by increasing roll damping, and for example, bilge keels are often used for this purpose.

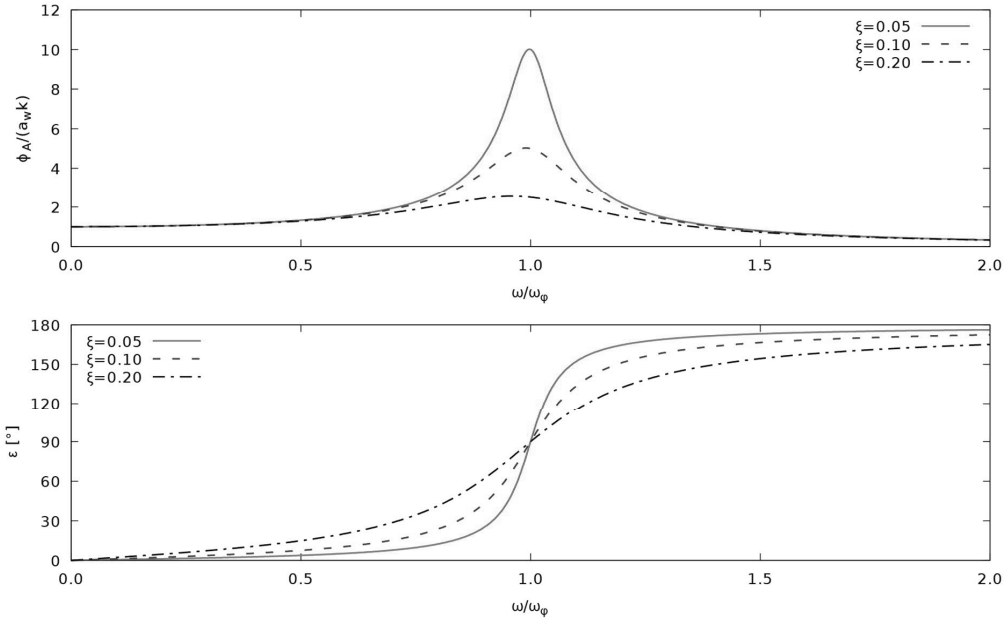

Figure 9.3 Roll response in regular beam waves with three different roll damping coefficients

9.4 Roll damping

The *roll damping* characteristics have a significant effect on the roll motion of the ship. In the previous sections the damping term was considered to be a linear function of the roll velocity. However, in reality some components are proportional to the square or cubic of the roll velocity, and consequently the roll motion equation (9.8) can be extended to:

$$\ddot{\phi} + 2\alpha\dot{\phi} + \beta\dot{\phi}|\dot{\phi}| + \gamma\dot{\phi}^3 + \omega_\phi^2\phi = 0 \tag{9.24}$$

where α, β and γ represent linear, quadratic and cubic damping, respectively.

In practice, so-called Ikeda's method is often used to estimate the roll damping characteristics of a ship. An extensive summary of this approach is given by Himeno (1981). Several enhancements have been presented, and roll damping is a widely studied subject, and updated recommendations for numerical estimation of roll damping have been presented in ITTC (2011).

Since roll damping has a fundamental role in the assessment of ship stability in waves, a brief introduction to some widely used devices for roll stabilization is presented next. A more comprehensive overview is given e.g. by Kula (2015).

Bilge keels

Most ships are equipped with *bilge keels* for increased roll damping characteristics. These keels are passive devices, permanently attached to the hull, as illustrated in Figure 9.4. The keels are located amidships, perpendicular to the hull surface, Typically, the length is 25%..50% of the

ship length, and usually the width is less than 1 m. The keels should not increase the draft or breadth of the ship.

The hydrodynamic resistance force is developed when the ship rolls. This force is opposite to the direction of the roll motion. In addition, the keels cause vortices that increase viscous damping of the roll motion. Also other hull appendages, such as rudders and skeg, increase the roll damping.

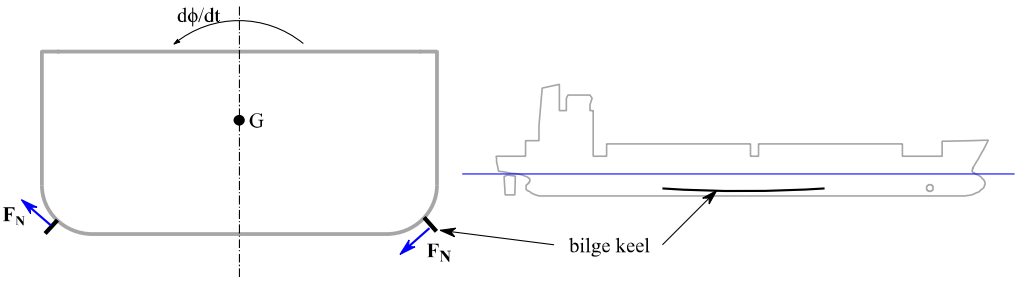

Figure 9.4 Bilge keels

Fin stabilizers

A more efficient way of increasing roll damping is to use active devices, such as *fin stabilizers*. Usually, these can be retracted inside the hull, and when in use, they extend transversally outside the waterline width, Figure 9.5. Large ships can also have two pairs of fins.

The angle of the fin α is automatically controlled, ensuring maximal lift force $\boldsymbol{F}_{\mathrm{N}}$ and roll damping. This system accounts for both the angular roll velocity $d\phi/dt$ and the velocity of the ship V. Consequently, these stabilizers are effective only when the ship has high enough velocity (at least 10 knots).

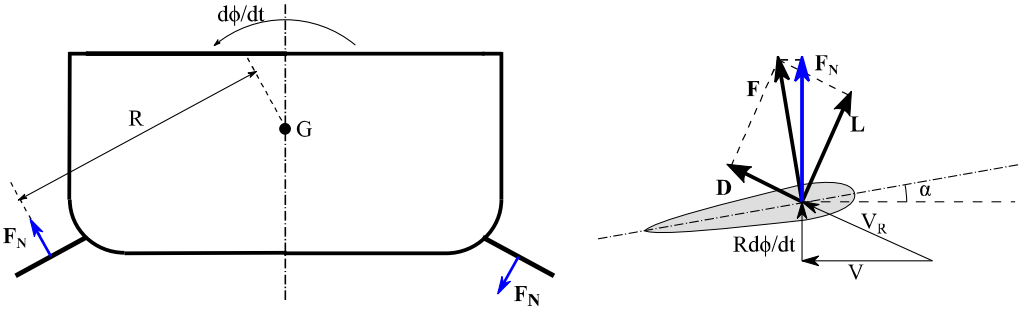

Figure 9.5 Principle of using fin stabilizers for roll damping

Antiroll tanks

Also movement of liquids, usually water, can be used to increase roll damping. Such a device is called an *antiroll tank*, Figure 9.6, These can be divided into active and passive antiroll tanks.

It is noteworthy, that the free surface effect of the antiroll tanks must be accounted for in the stability calculations.

In the passive antiroll tank, the tank is partly filled with liquid. When the natural frequency of the liquid in the antiroll tank is the same as the natural roll frequency, Passive antiroll tanks require large volumes of liquid in order to absorb a significant amount of roll energy.

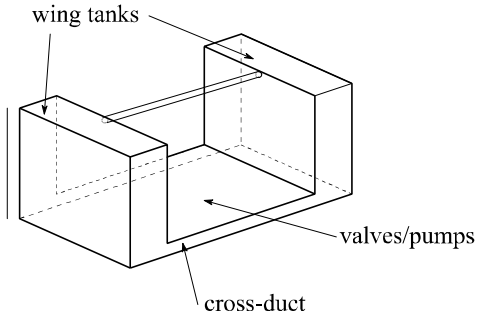

Figure 9.6 Schematic illustration of a U-shaped antiroll tank

In active antiroll tanks the movement of liquid is controlled by pumping. The tank is usually U-shaped, with valves and pumps in the bottom. The peak of the roll response amplitude can be significantly reduced with a passive antiroll tank. However, at other frequencies, the liquid in the tank can even slightly increase the rolling. With an active tank the roll response can be decreased at all frequencies. A schematic example is presented in Figure 9.7, for more details, see e.g. Hsueh and Lee (1997).

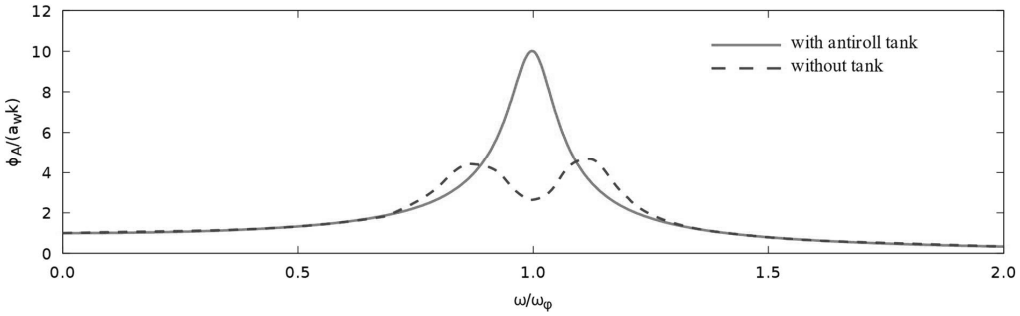

Figure 9.7 Schematic example of the effects of an antiroll tank on the roll response of a ship in beam seas,

9.5 Dynamic righting lever

From the point of view of ship stability, the weakness of the above-presented model for roll motion is its linearity. The concept of the dynamic righting lever makes it possible to investigate a ship's dynamic heeling (transient roll), taking properly into account nonlinearity of the righting lever. Especially the loading comprising a steady (slowly increasing) and a step-function type (suddenly growing) contribution can be taken into account when evaluating maximum heel angles, developing as a result of a complex heeling excitation.

In this section, the righting lever is marked, for simplicity, as:

$$h(\phi) \equiv \overline{GZ}(\phi) \tag{9.25}$$

The equation for roll motion (9.6), can be further simplified by ignoring the damping term, resulting in:

$$I'_{\mathrm{xx}}\ddot{\phi} + \Delta h(\phi) = M_{\mathrm{ext}}(\phi) \tag{9.26}$$

The roll acceleration can be presented as:

$$\ddot{\phi} = \frac{\mathrm{d}\dot{\phi}}{\mathrm{d}t} = \frac{\mathrm{d}\dot{\phi}}{\mathrm{d}\phi}\frac{\mathrm{d}\phi}{\mathrm{d}t} = \dot{\phi}\frac{\mathrm{d}\dot{\phi}}{\mathrm{d}\phi} = \frac{\mathrm{d}}{\mathrm{d}\phi}\left(\frac{1}{2}\dot{\phi}^2\right) \tag{9.27}$$

This is substituted into equation (9.26), and both sides are multiplied by $\mathrm{d}\phi$, resulting in:

$$I'_{\mathrm{xx}}\left(\frac{1}{2}\dot{\phi}^2\right) + \Delta h(\phi)\mathrm{d}\phi = M_{\mathrm{ext}}(\phi)\mathrm{d}\phi \tag{9.28}$$

The inertia moment (first term on the left-hand side) is the difference in kinetic energies of a dynamically heeling ship at the instant when the maximum heel angle ϕ_{d} is reached, and the one at the initial stage, i.e. $\phi = 0$. The kinetic energy is zero, both at the beginning and at the instant when the maximum heel is reached since the roll velocity, i.e. time derivative of roll angle, is zero, as visualized in Figure 9.8.

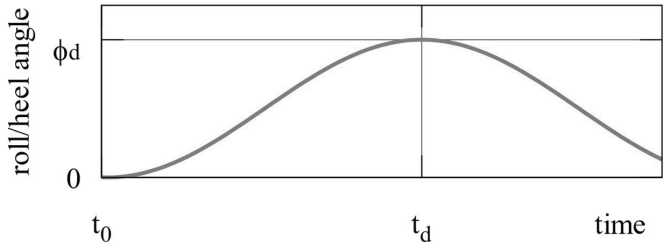

Figure 9.8 Visualization of roll velocity in heeling due to a stepwise external moment

The initial condition at time $t = t_0$ is $\phi(t_0) = 0$ and $\dot{\phi}(t_0) = 0$. The maximum roll angle ϕ_d is reached at time t_{d}, when the roll velocity is again zero, i.e. $\dot{\phi}(t_{\mathrm{d}}) = 0$.

Integration from a zero heel to an unknown maximum roll angle ϕ_d results in:

$$\Delta\int_0^{\phi_{\mathrm{d}}} h(\phi)\mathrm{d}\phi = \int_0^{\phi_{\mathrm{d}}} M_{\mathrm{ext}}(\phi)\mathrm{d}\phi \tag{9.29}$$

Note that the first term disappeared due to the initial conditions, as there is no change in the kinetic energy.

The left-hand side of equation (9.29) represents the increase of potential energy, absorbed by the ship when heeled. When this is divided by the displacement force Δ, the *dynamic righting lever* is obtained:

$$e(\phi) = \int_0^{\phi} h(\phi)\mathrm{d}\phi \tag{9.30}$$

It is the integral of the static righting lever. An example is shown in Figure 9.9.

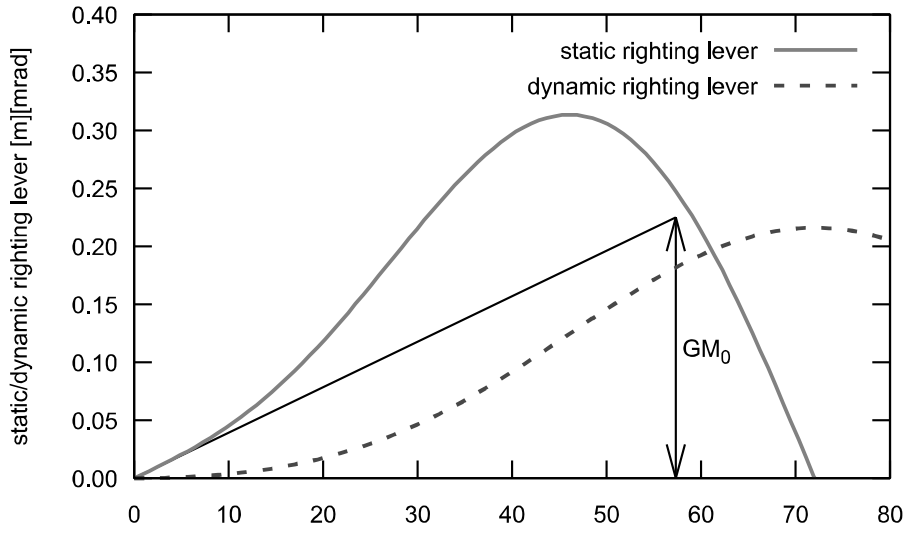

Figure 9.9 Example of static and dynamic righting lever curves

The right-hand side of equation (9.29) represents the work that is done by the external moment to heel the ship to the angle ϕ_d. This can be presented also by using the lever l_ext of the heeling moment:

$$\int_0^{\phi_\mathrm{d}} M_\mathrm{ext}(\phi)\mathrm{d}\phi = \Delta \int_0^{\phi_\mathrm{d}} l_\mathrm{ext}(\phi)\mathrm{d}\phi \tag{9.31}$$

Note that the lever $l_\mathrm{ext}(\phi)$ may be a function of the heel angle ϕ.

9.6 Dynamic heel due to a stepwise external moment

A stepwise heeling moment causes a dynamic heeling that can be significantly larger than the static heel angle, due to an equally large slowly exposed moment. Let us evaluate the maximum angle of heel the ship reaches, when subjected to stepwise heeling moment. Initially, the heel angle and its time derivative are both zero, i.e. $\phi = \dot{\phi} = 0$. At time t_0, an external stepwise loading starts to act on the ship. The lever of the heeling moment is $l_\mathrm{ext} = M_\mathrm{ext}/\Delta$. By substituting these into equation (9.29), the following relation is obtained:

$$e(\phi_\mathrm{d}) = l_\mathrm{ext}\phi_\mathrm{d} \tag{9.32}$$

A graphical solution for the maximum angle of heel ϕ_d, reached by the ship when subjected to this transient loading, is presented in Figure 9.10. If the external moment was static, the ship would heel to an angle ϕ_s. The work done by a heeling moment is represented by a constant $l_\mathrm{dyn} = l_\mathrm{ext}\phi$. The dynamic balance, which is the equality of the work done by ship resisting the loading and the work done by the external heeling moment, is reached at point ϕ_d, which is the maximum transient heel angle. If the straight line overshoots the e-curve, this means that the ship does not withstand the transient (stepwise) loading, and as a result the ship capsizes.

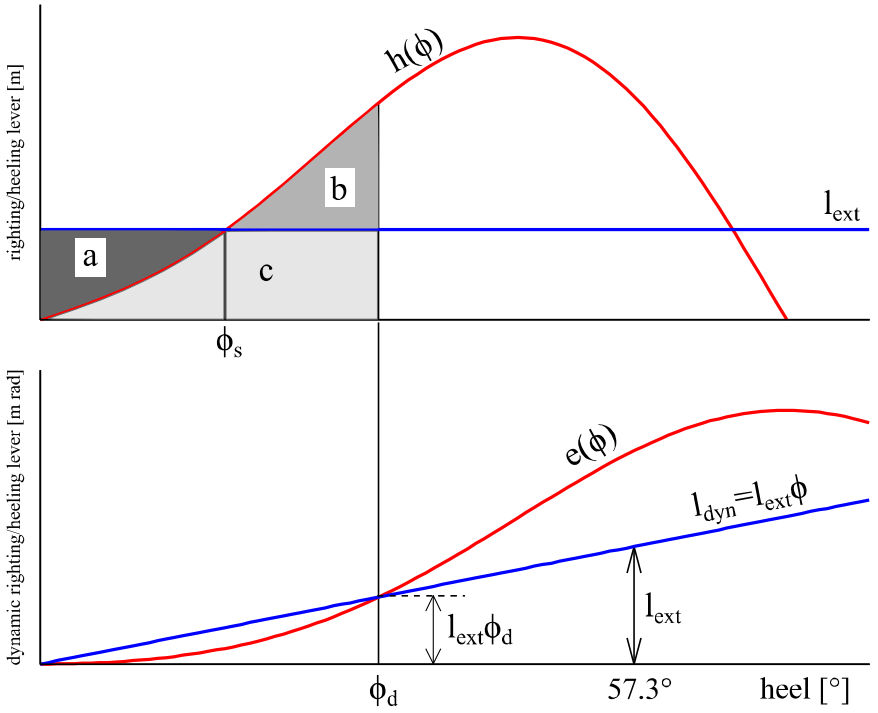

Figure 9.10 Evaluation of dynamic heel angle due to a stepwise external moment by using the dynamic stability lever

Dynamic heeling can be investigated with the aid of dynamic levers (lower graph in Figure 9.10), and by using the GZ-curve. In the latter case the areas "a+c" and "b+c" represent the work done by the external loading and that of the ship resisting it, respectively. Therefore, the areas "a" and "b" must be equal.

It is worth noting that for a linear restoring moment, dynamically reached heel angle is exactly twice as large as the one reached under a static heeling moment.

The required stepwise moment to cause a dynamic heeling up to the flooding angle ϕ_f (see section 10.2) can be solved from the value of the dynamic righting lever at this angle, as shown in Figure 9.11.

$$M_{ext,f} = \Delta \frac{e(\phi_f)}{\phi_f} \tag{9.33}$$

The maximum dynamic heeling moment the ship can withstand without capsizing can be evaluated graphically, as illustrated in Figure 9.12, so that the areas "a" and "b" are equal.

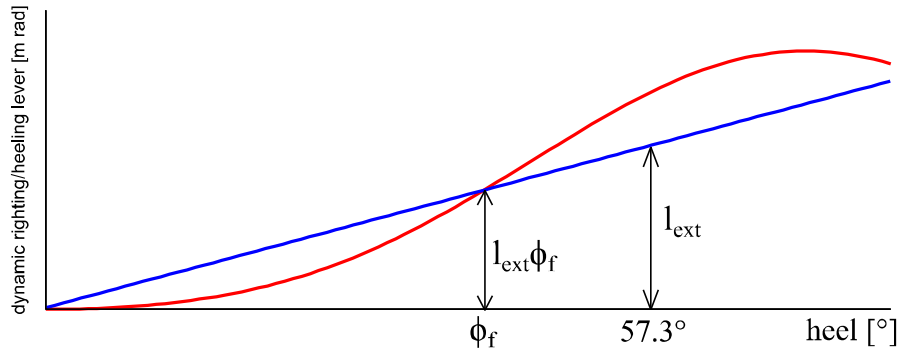

Figure 9.11 Evaluation of the stepwise moment that causes a dynamic heel angle that equals to the critical flooding angle

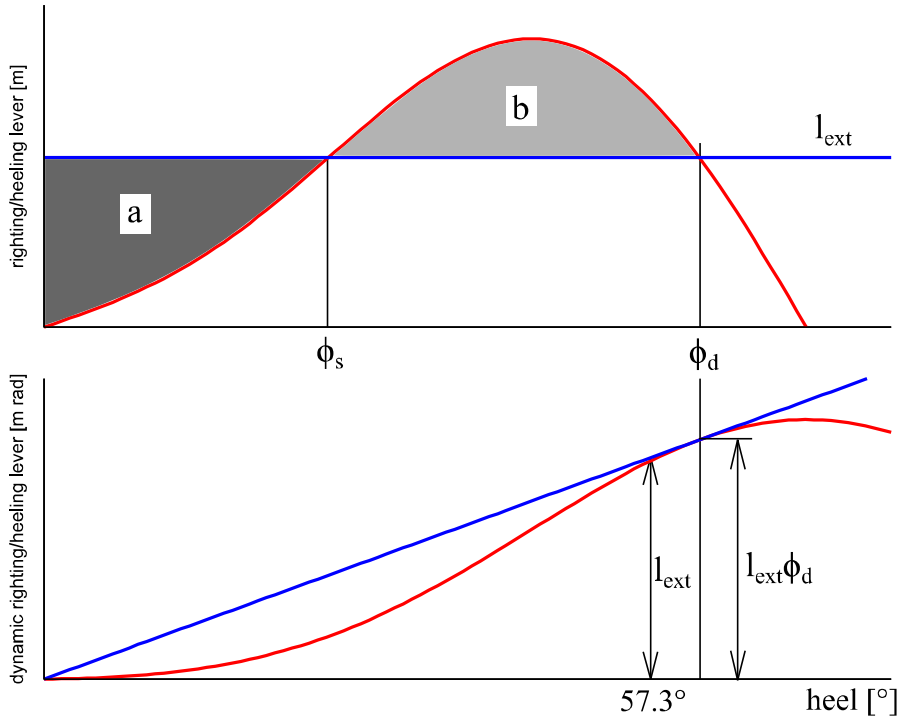

Figure 9.12 Evaluation of maximum stepwise moment the ship can withstand without capsizing

Time histories for the roll response of a ship after a stepwise heeling moment with and without roll damping are presented in Figure 9.13. The roll motion takes place around the heel angle due to an equal static external moment. Without roll damping, the maximum roll angle is twice the static heel angle if restoring moment is linear (initial stability assumption). In reality, the roll motion is dampened, and consequently the maximum roll angle is slightly smaller, and consequently, the adopted approach is somewhat conservative.

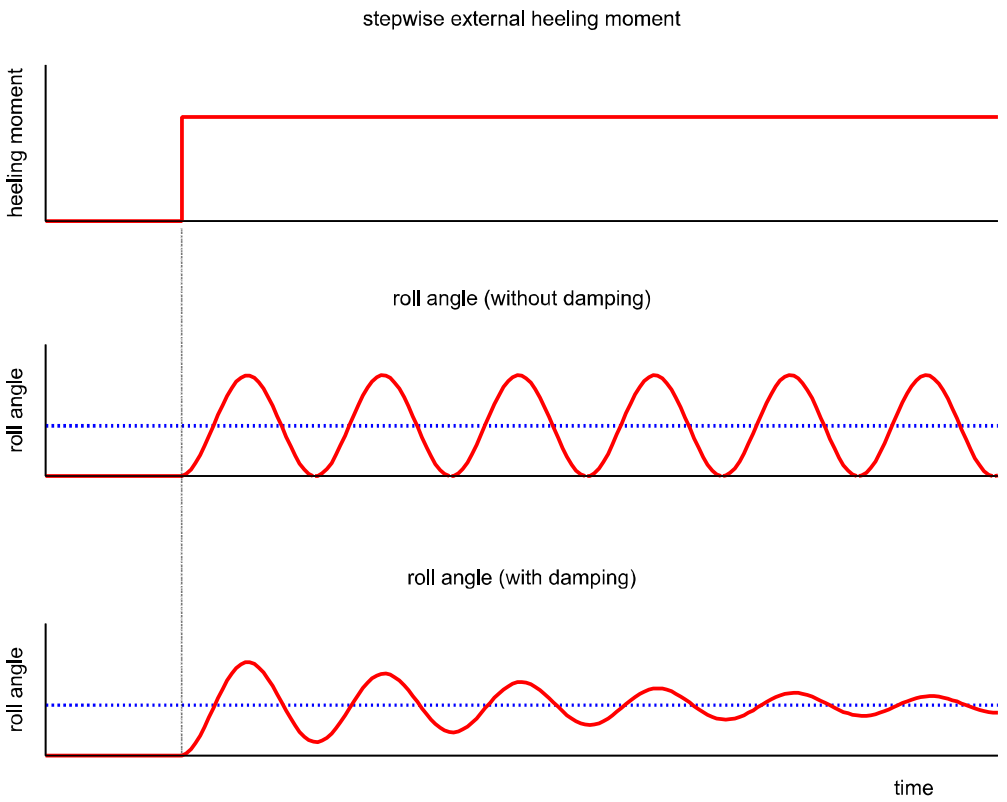

Figure 9.13 Roll response to a stepwise external moment with and without damping; the dotted line represents a static heel angle caused by an equal quasi-static external moment

9.7 Dynamic heel due to combined static and stepwise moments

The external moment can also be a combination of a static heeling moment and a stepwise moment. A practical example of such a case is gusty wind. Calculation of the heeling moment due to wind is explained later in section 10.5.

Under a static external moment $M_\mathrm{w} = \Delta l_\mathrm{w}$, the ship has a steady heel angle ϕ_w. While under this condition, an additional stepwise moment $M_\mathrm{wd} = \Delta l_\mathrm{wd}$, starts to act, and the ship rolls up to the angle ϕ_wd, as presented in Figure 9.14.

By using equation (9.29), the following is obtained:

$$\Delta \int_{\phi_\mathrm{w}}^{\phi_\mathrm{wd}} h(\phi)\mathrm{d}\phi = \int_{\phi_\mathrm{w}}^{\phi_\mathrm{wd}} (M_\mathrm{w} + M_\mathrm{wd})\mathrm{d}\phi \tag{9.34}$$

resulting in:

$$e(\phi_\mathrm{wd}) - e(\phi_\mathrm{w}) = (l_\mathrm{w} + l_\mathrm{wd})(\phi_\mathrm{wd} - \phi_\mathrm{w}) \tag{9.35}$$

A graphical solution is presented in Figure 9.14.

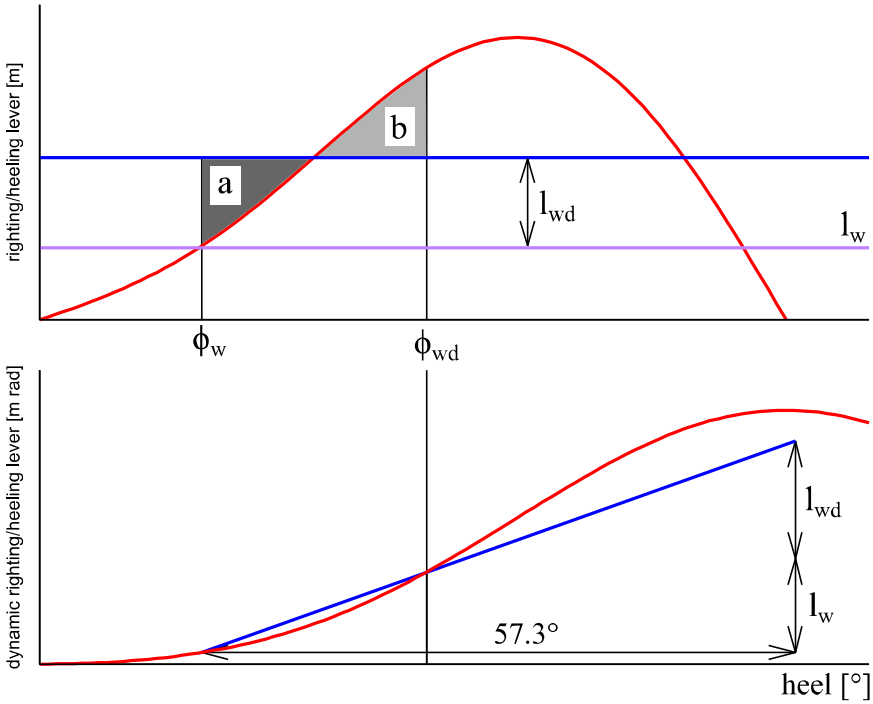

Figure 9.14 Dynamic heel due to a combination of steady and stepwise external moments

Usually when a ship is subjected to a gusty wind, there are also waves that cause roll motion, and the combined effect of gusty side wind and roll motion needs to be studied. Initially the ship is heeled windward from the steady heel angle ϕ_w, caused by a constant wind moment. The assumed amplitude of the roll motion is ϕ_A.

At the maximum roll angle to windward $(-\phi_A + \phi_w)$ and at the maximum dynamic heel angle (ϕ_{wd}), the roll velocity is zero and the inertia term disappears. Consequently:

$$\Delta \int_{-\phi_A+\phi_w}^{\phi_{wd}} h(\phi)\mathrm{d}\phi = \int_{-\phi_A+\phi_w}^{\phi_{wd}} (M_w + M_{wd})\mathrm{d}\phi \tag{9.36}$$

resulting in:

$$e(\phi_{wd}) - e(-\phi_A + \phi_w) = (l_w + l_{wd})(\phi_{wd} + \phi_A - \phi_w) \tag{9.37}$$

A graphical solution is presented in Figure 9.15. This is the physical background for the so-called weather criterion, which is discussed in detail in section 10.6.

It is worth noting that the presented graphical solutions are illustrative, and are included for educational purposes. In practice, the dynamic heel angle is solved numerically, and usually only the areas under the static righting lever curve (upper parts of the previous figures) are presented.

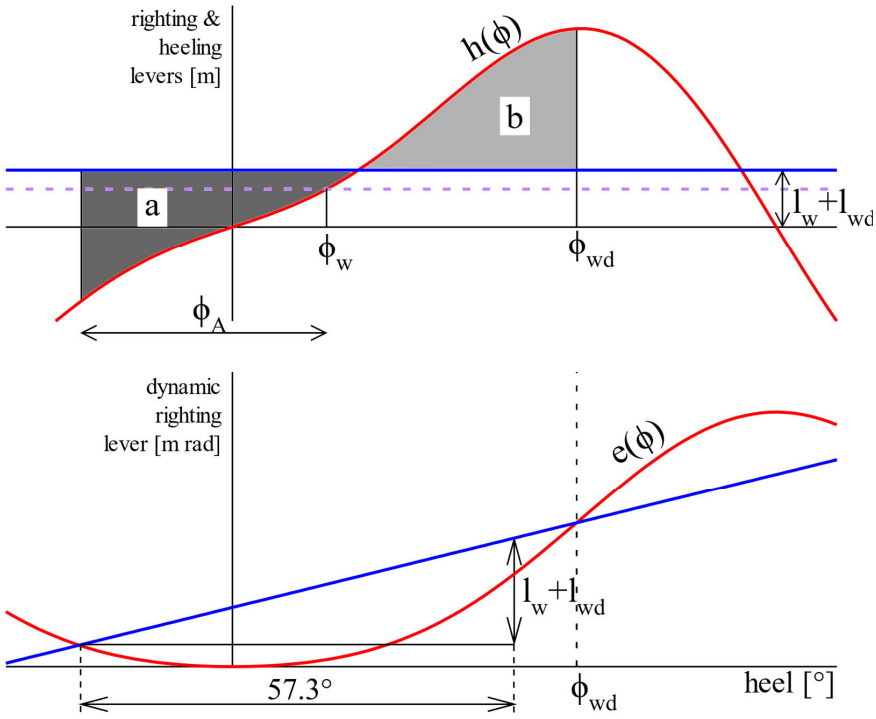

Figure 9.15 Maximum dynamic heel due to the combined action of waves and gusty wind

10 Intact stability criteria

10.1 Background

The first proper intact stability criteria were developed in Finland by Jaakko Rahola in 1939, based on a comparison of stability characteristics of ships that had capsized with those which had operated safely, Rahola (1939). The main outcome of this research was the so-called *Rahola criterion* for seagoing vessels, which is illustrated in Figure 10.1.

For static stability, Rahola defined requirements for the heel angle ϕ_{m}, where the maximum righting lever is reached, as well as for the values of the righting lever at heel angles of 20° and 30°. Rahola noted that the dynamic stability is usually more relevant, and based on the sample ship material, he concluded that the minimum dynamic righting lever is 0.08 m·rad at the limit heel angle, he had defined as $\phi_{\mathrm{r}} = \min(\phi_{\mathrm{m}}, \phi_{\mathrm{f}}, \phi_{\mathrm{s}}, 40°)$. Therefore, Rahola considered both the flooding angle ϕ_{f} and the possible dynamic angle of repose for the cargo ϕ_{s}.

These criteria were further developed and internationally adopted by IMO in 1960s. An extensive overview of the criteria development is given by Kobylinski (2014). In the following section, the physical background, and the practices for calculation of the current IMO Intact Stability Code criteria are presented.

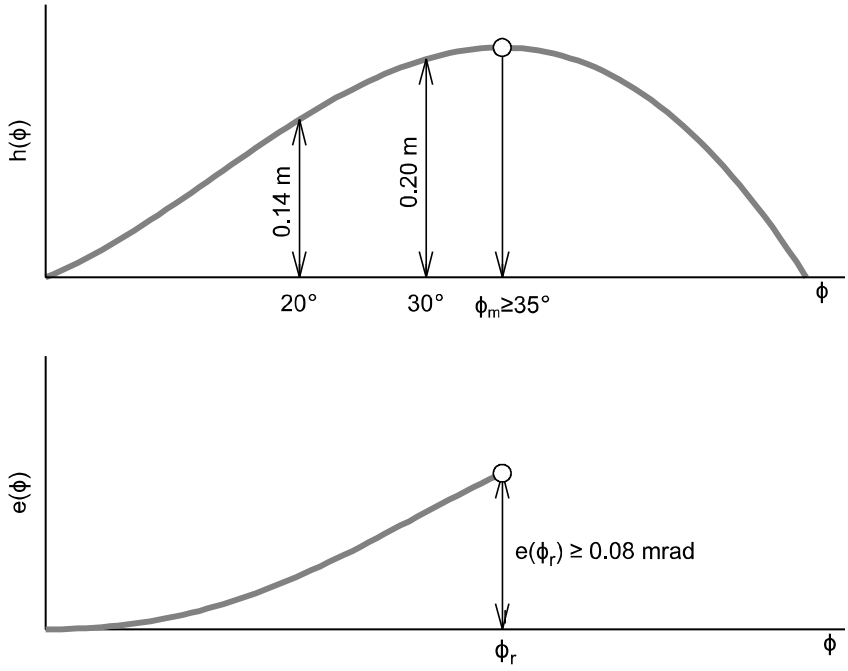

Figure 10.1 So-called "Rahola criterion" for judging stability of seagoing vessels

10.2 Righting lever curve characteristics

The stability criteria are usually calculated from the characteristics of the righting lever curve. The curve may be calculated either for a loading condition, accounting for the free surface corrections, or for a nominal condition with given floating position and centre of gravity.

The main parameters of the righting lever curve for use in the calculation of stability criteria are:

- steady heel angle
- maximum righting lever
- range of stability
- area under the righting lever

These are illustrated in Figure 10.2. The *range of positive stability* extends from the steady equilibrium heel angle (ϕ_{eq}) to the *angle of vanishing stability* ϕ_v. For criteria calculations the range is usually limited to $\min(\phi_v, \phi_f)$, where ϕ_f is the heel angle where the first unprotected opening is immersed, i.e. the *flooding angle*, Figure 10.3. For example, the maximum righting lever GZ_{max} is the maximum within the range, not necessary the absolute maximum of the curve. Similarly, the area under the curve is limited to the range. Thus, it is assumed that if the ship heels so much that an unprotected opening is submerged, there can be notable flooding, and the ship may be lost.

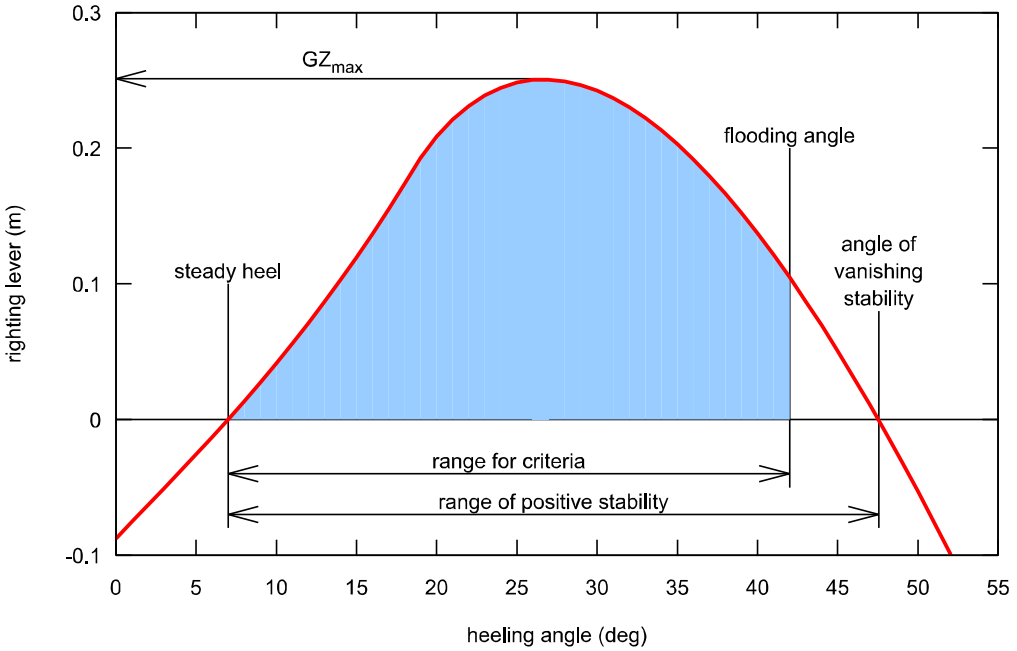

Figure 10.2 Key parameters of the righting lever curve for criteria calculations

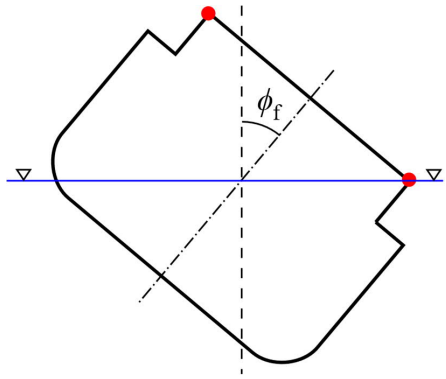

Figure 10.3 Flooding angle when the first unprotected opening is immersed

The righting lever can contain more than one *hump*, as illustrated in Figure 10.4. These may be caused by an increased reserve buoyancy high above the intact waterline. It is not always clear how the regulations should be interpreted in such cases. In general, the use of only the first hump is likely the conservative approach.

Some examples of various intact stability criteria, including their physical background are presented in the following subsections.

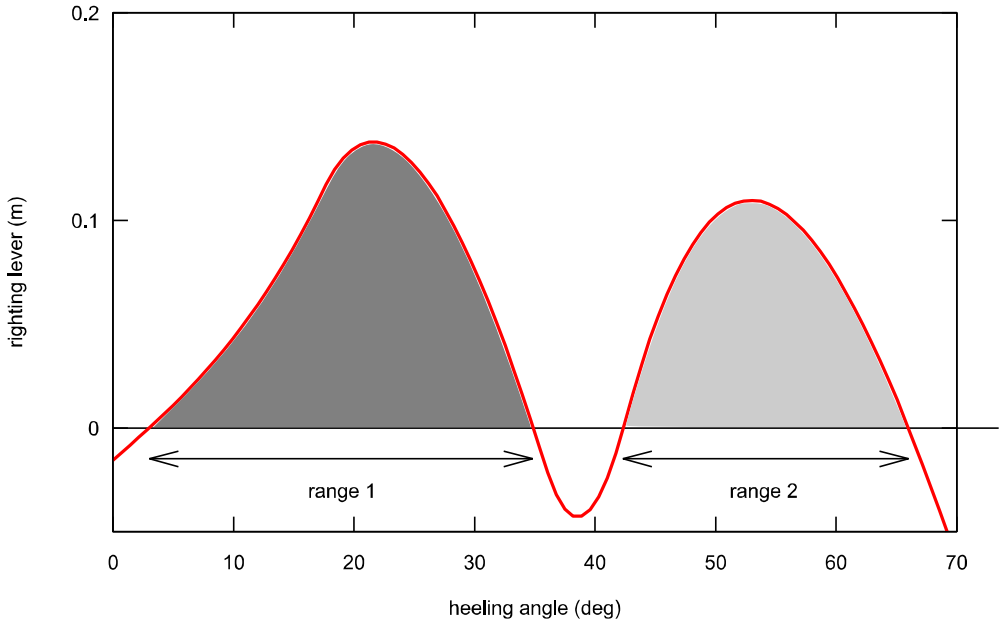

Figure 10.4 Example of two humps in the righting lever curve

10.3 General stability criteria

The IMO International Code on Intact Stability 2008 ("2008 IS Code") sets basic requirements for various parameters of the righting lever curve, IMO 2008. The origin for these criteria is in the pioneering work of Rahola (1939). These parameters are illustrated in Figure 10.5. As a summary, it is required that:

- area under GZ curve up to heel angle of 30° (*area1*) shall not be less than 0.055 m·rad
- area under GZ curve up to angle $\phi^* = \min(\phi_f, 40°)$, i.e. *area1*+*area2*, shall not be less than 0.09 m·rad
- area under GZ curve between 30° and ϕ^* (*area2*) shall not be less than 0.03 m·rad
- the righting lever shall be at least 0.2 m at an angle of heel greater or equal to 30°
- maximum righting lever shall occur at an angle of heel not less than 25°
- initial metacentric height shall not be less than 0.15 m

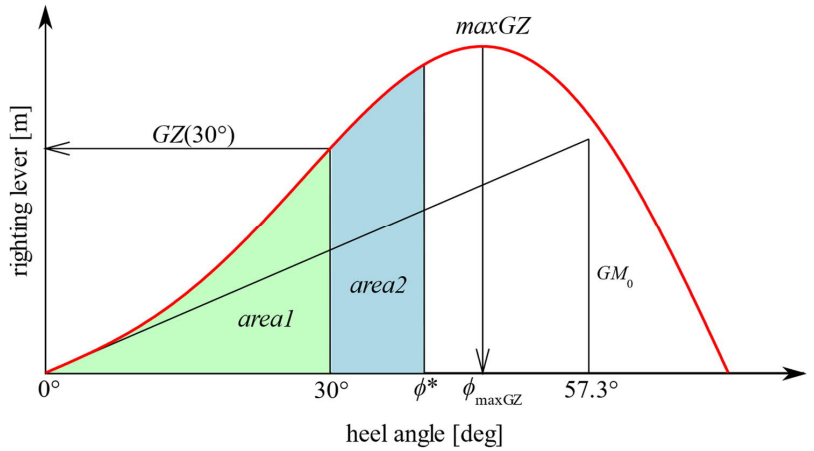

Figure 10.5 Parameters for righting lever curve criteria in IMO Intact Stability Code

10.4 Heel due to turning

Rapid turning, and the resulting forces can cause a large heeling moment. For example, in the SEWOL accident of 2014, the ship had too low initial stability, and the heeling in turning motion caused extensive heel and cargo shift that resulted in flooding, eventually capsizing and sinking the ship, Kim et al. (2019).

The traditional approach to heeling moment ignores transient phenomena and focuses on the steady turning motion. Let us consider a ship with a velocity V_s, when the diameter of the steady turning circle is D_s. The centrifugal force, acting on the centre of gravity G is:

$$F_{cf} = \rho \nabla \dot{\psi}^2 \frac{D_s}{2} = \rho \nabla \dot{\psi} V_s \tag{10.1}$$

where the angular turning velocity is:

$$\dot{\psi} = \frac{V_s}{D_s/2} \tag{10.2}$$

In addition, there is a lateral hydrodynamic reaction force F_h, acting on the hull and the rudder. It is a common practice to assume that the centre of this reaction force is in the middle between the baseline and the waterline (i.e. at $T/2$). The situation is illustrated in Figure 10.6.

These forces create a heeling moment:

$$M_{ext} = \rho \nabla \dot{\psi} V_s \left(\overline{KG} - \frac{T}{2} \right) \cos \phi \tag{10.3}$$

This needs to be compensated by the righting moment from the weight and buoyancy force. With the assumption of initial stability (i.e. $\phi < 10°$), equation (4.36), the heel angle due to a steady turning motion is:

$$\phi = \arctan \left(\dot{\psi} V_s \frac{(\overline{KG} - T/2)}{g \overline{GM}_0} \right) \tag{10.4}$$

The vertical centre of gravity has a large impact on the heeling in a steady turning motion since it affects both the metacentric height and the lever of the heeling moment.

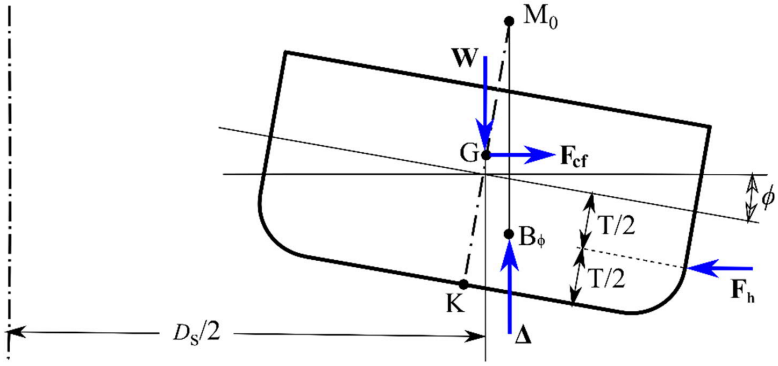

Figure 10.6 Forces on a ship in a steady turning motion

As an example, the IS Code sets a requirement for passenger ships that the heel angle in a steady turning motion shall not exceed 10° when the heeling moment is defined as:

$$M_{ext} = 0.2 \Delta \frac{V_S^2}{L_{wl}} \left(\overline{KG} - \frac{T}{2} \right) \tag{10.5}$$

By comparing this to the equation (10.3), it can be seen that the radius of the turning circle is assumed to be 5-times the waterline length, i.e. $D_s/2 = 5L_{wl}$, and the equation is further simplified since $\cos \phi \approx 1.0$ for small heel angles $\phi \leq 10°$.

10.5 Wind moment

From stability point of view, side wind is usually the worst condition. The wind force acts on the lateral exposed area (A_L) of the ship above the waterline, i.e. the *wind profile*. It is assumed that the wind velocity U_w is constant along this profile. Therefore, the wind force is:

$$F_w = \frac{1}{2} \rho_{air} {U_w}^2 A_L C_w \tag{10.6}$$

where ρ_{air} is the density of air (usually 1.225 kg/m^3) and C_{w} is a non-dimensional aerodynamic resistance coefficient. Typically, the value $C_{\mathrm{w}} = 1.2$ is adopted, but also detailed results from wind tunnel model tests can be used.

The effective wind force acts on the centroid of the wind profile area, and the lever of the wind moment (Z) is the vertical distance between this point and the centroid of underwater part of the ship. Usually, it is simply assumed that the latter point is located at $T/2$. The scenario is illustrated in Figure 10.7.

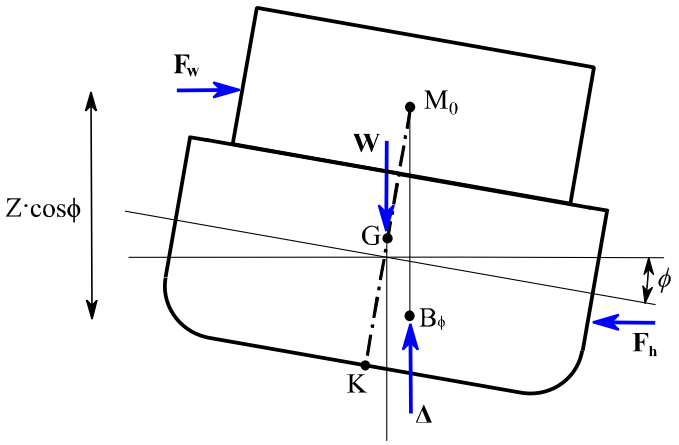

Figure 10.7 Wind moment calculation

If the ship is assumed to be (nearly) flat, both the actual exposed area and the lever are proportional to $\cos\phi$. Consequently, the heeling moment due to the wind is:

$$M_{\mathrm{w}}(\phi) = F_{\mathrm{w}} Z \cos^2\phi \tag{10.7}$$

However, this is not very realistic at large heel angles, when the bilge is emerged from water. The wider the ship, the bigger the effect is. Therefore, a conservative approach with a constant *wind moment* is often used, so that:

$$M_{\mathrm{w}} = F_{\mathrm{w}} Z \tag{10.8}$$

In regulations, usually the wind pressure P is defined instead of a wind velocity. In such case, the wind moment is presented as:

$$M_{\mathrm{w}} = P A_{\mathrm{L}} Z \tag{10.9}$$

It is essential to use correct wind profile, which may be dependent on the loading condition. Especially for container ships, the deck load can increase the lateral area significantly, as illustrated in Figure 10.8.

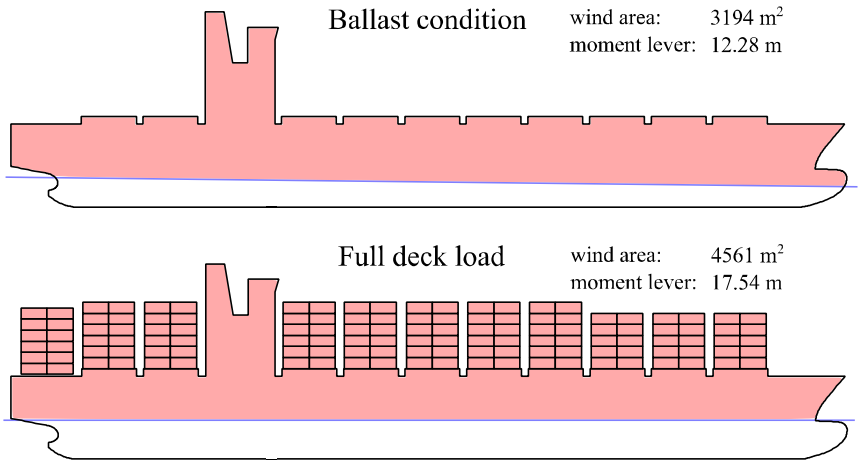

Figure 10.8 Comparison of wind profiles of a container ship with different loading conditions

10.6 Weather criterion

The *weather criterion,* in the IMO Intact Stability Code, attempts to model a combined action of the resonant beam waves with a gusty wind on the transient heeling of ship. The situation is also known as a *dead ship condition*, since it may result from a blackout and loss of steering. The current IMO weather criterion has been developed based on Japanese and Russian research from the 1950s and 1960s, as presented in Kobylinski and Kastner (2003). In the following, the details of the criterion are presented, along with discussion on the applicability and physical background.

In the studied condition ship is rolling in beam seas. Initially the ship is subjected to a steadily acting wind, given by a lever l_{w1}, that suddenly changes to a gusty one when ship is heeled to windward by an angle $\phi_{\mathrm{w}} - \phi_{\mathrm{A}}$, where ϕ_{w} is heel due to the steady wind and ϕ_{A} is the amplitude of the roll motion due to waves.

The total moment lever of the wind gust is taken as $l_{\mathrm{w2}} = 1.5 l_{\mathrm{w1}}$. The applied steady wind pressure is 504 Pa on the lateral wind profile area, and the moment is obtained by applying the equation (10.9). It should be noted that the wind moment levers are assumed to be constant for all heel angles. Moreover, by using equation (10.6) and assuming $\rho_{\mathrm{air}} = 1.225\ \mathrm{kg/m^3}$ and $C_{\mathrm{w}} = 1.2$, it can be seen that the given pressure corresponds to a wind velocity $U_{\mathrm{w}} \approx 26\ \mathrm{m/s}$.

The criterion is illustrated in Figure 10.9. The ship survives without capsizing, when the area "b" is larger than area "a". The area "b" is limited to an angle $\min(\phi_{\mathrm{f}}, \phi_{\mathrm{v}}, 50°)$, where ϕ_{f} is the flooding angle and ϕ_{v} is the second intercept of the righting lever curve and the moment lever, i.e. the angle of vanishing stability.

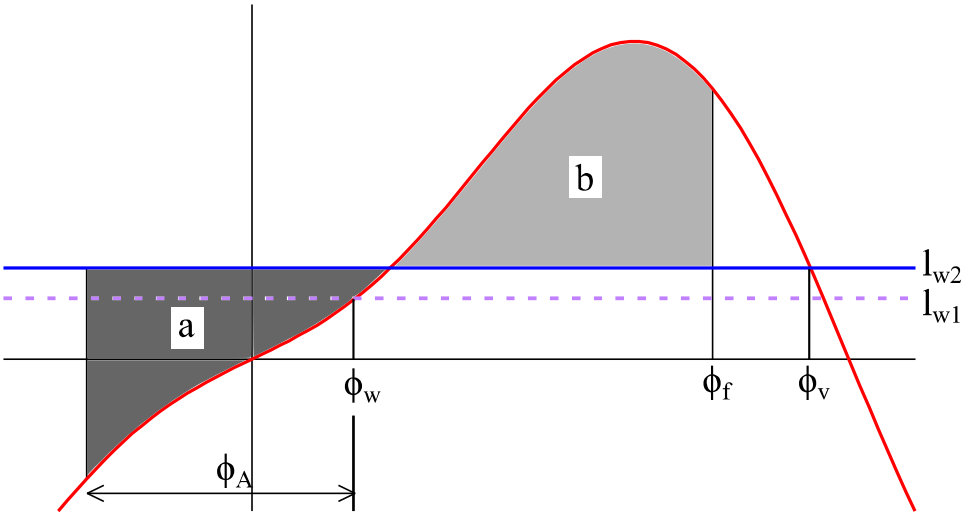

Figure 10.9 Weather criterion

In regular sinusoidal waves the maximum wave slope is $r = \pi 2a_w/\lambda$ and the wave steepness is $s = 2a_w/\lambda$. Furthermore, in the resonance condition $\omega = \omega_\phi$, the equation (9.22) for roll amplitude (in radians) in regular beam waves reduces to:

$$\phi_A = \frac{a_w \pi}{\xi \lambda} \tag{10.10}$$

Therefore, roll amplitude can be considered proportional to $\sqrt{rs}$ and inversely proportional to the roll damping ξ:

$$\phi_A \sim \frac{\sqrt{rs}}{\xi} \tag{10.11}$$

The ship is rolling in irregular beam seas, and furthermore, since the roll amplitude can be large, the linearized model in section 9.3 cannot be directly applied. Instead, approximations based on semi-empirical factors, considering both the hull form and roll damping characteristics, are used. Consequently, in the IMO weather criterion, the roll amplitude ϕ_A (in degrees) is approximated from the following equation:

$$\phi_A = 109 K X_1 X_2 \sqrt{rs} \tag{10.12}$$

The correction coefficients X_1 and X_2 are evaluated based on the hull form (breadth/draft ratio and block coefficient) as shown in Table 10.1, by using linear interpolation. The coefficient K accounts for decreased amplitude due to roll damping. If the ship has a round bilge and no bilge keels, then $K = 1$, and if the ship has a sharp bilge $K = 0.7$. For ships fitted with bilge keels $0.7 \leq K \leq 1$, and the value is interpolated based on the total bilge keel area A_k.

The effective slope factor is estimated based on the distance between the centre of gravity and the waterplane, $\overline{KG} - T$, and it is defined as:

$$r = 0.73 + 0.6\frac{\overline{KG} - T}{T} \tag{10.13}$$

Also the wave steepness factor s is interpolated from a predefined table, based on the natural roll period. Initially, this table covered only roll periods between 6 and 20 s, but an extended

table (up to 30 s) was introduced in MSC.1/Circ.1200, IMO (2006). With longer periods the factor is reduced, and the old approach penalizes especially large passenger ships.

The roll period (in seconds) is usually estimated from the following equation:

$$T_\phi = \frac{2CB}{\sqrt{GM}} \tag{10.14}$$

where the coefficient is:

$$C = 0.373 + 0.023\frac{B}{T} - 0.043\frac{L_{\mathrm{wl}}}{100} \tag{10.15}$$

Here B is breadth, T is draft and L_{wl} is length of waterline. Also alternative methods to approximate the roll period can be used, if approved by the administration.

Table 10.1 Definition of parameters for calculation of the roll amplitude in the weather criterion; both for 2008 IS Code and alternative method in MSC.1/Circ.1200, IMO (2006)

B/T	X_1
≤2.4	1.00
2.5	0.98
2.6	0.96
2.7	0.95
2.8	0.93
2.9	0.91
3.0	0.90
3.1	0.88
3.2	0.86
3.4	0.82
≥3.5	0.80

C_b	X_2
≤0.45	0.75
0.50	0.82
0.55	0.89
0.60	0.95
0.65	0.97
≥0.70	1.00

$\frac{100A_k}{L_{wl}B}$	K
0.0	1.00
1.0	0.98
1.5	0.95
2.0	0.88
2.5	0.79
3.0	0.74
3.5	0.72
≥4.0	0.70

T_ϕ [s]	s	
	IS 2008	Circ1200
≤6	0.100	0.100
7	0.098	0.098
8	0.093	0.093
12	0.065	0.065
14	0.053	0.053
16	0.044	0.044
18	0.038	0.038
20	0.035	0.032
22	0.035	0.028
24	0.035	0.025
26	0.035	0.023
28	0.035	0.021
≥30	0.035	0.020

The weather criterion has been derived from sample ships with:

- $B/T < 3.5$
- $-0.3 \leq \overline{KG}/T - 1 \leq 0.5$
- $T_\phi < 20\mathrm{s}$

Therefore, some deviation is allowed by IMO for ships with parameters outside these limits. The roll period can be determined from model test experiments, as described in MSC.1/Circ1200, IMO (2006). In practice, this is relevant especially for large passenger ships with large B/T ratio, and long natural roll period. Model tests can be conducted to determine:

- steady wind heeling lever as a function of the heel angle, $l_{w1}(\phi)$, in wind tunnel
- natural roll period
- roll back angle ϕ_A based on tests in regular waves (wave steepness s is based on the natural roll period)

Furthermore, the introduction of the dead ship failure mode within the Second Generation Intact Stability Criteria (SGISC), IMO (2020), should enable more realistic assessment without the need for expensive model tests.

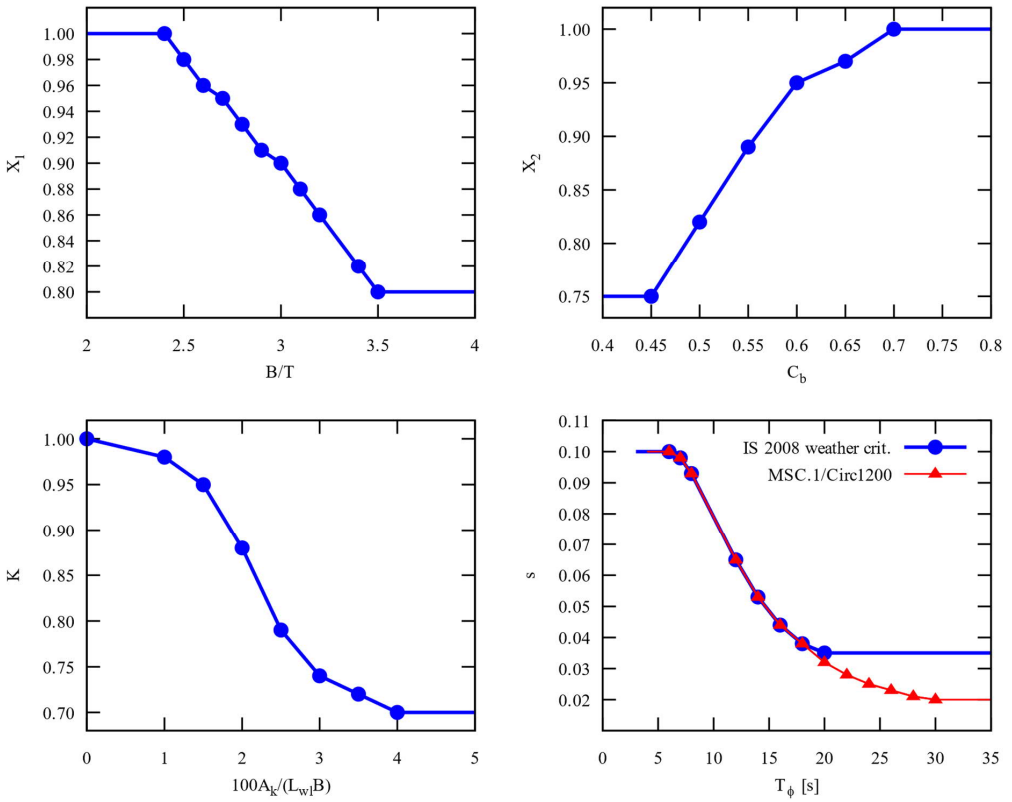

Figure 10.10 Visualization of the parameters for roll amplitude calculation in the weather criterion

10.7 Limit curves

For planning of safe operation of the ship, limit curves for maximum allowed KG, or minimum allowed GM, are usually prepared. These are presented as functions of draft or displacement. An example is shown in Figure 10.11.

If trim variation is notable in different operational loading conditions, separate curves for different trim values are needed. On board the ship, the actual loading condition can easily be checked against the limit curves. However, modern ships are equipped with a loading computer, as discussed in chapter 15. Such software can calculate various stability criteria for the real loading condition including a realistic treatment of free surface effects from the partially filled tanks, and therefore, providing a better assessment of intact stability than what can be achieved by applying limit curves.

Minimum GM is first calculated for all relevant stability criteria at the whole operational range of drafts and trims. The actual limit curve is then obtained as the envelope curve of the separate curves for each individual criterion.

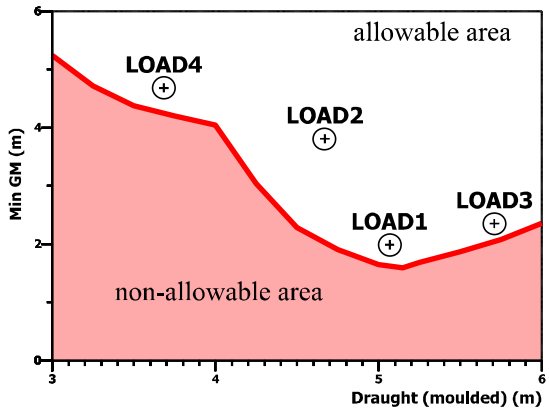

Figure 10.11 Example of a minimum GM curve, with marked loading conditions

The righting lever can be presented as a sum of two components, see equation (5.2). In the evaluation of the minimum $\overline{GM_0}$ that is needed to pass a stability criterion, the residual stability $\overline{M_0S}$ as a function of heel is unchanged, but $\overline{GM_0}$ is iterated until the "new" GZ curve reaches the requirement of the criterion:

$$\overline{GZ}_{\text{new}}(\phi) = \overline{GM_0}\sin\phi + \overline{M_0S}(\phi) \tag{10.16}$$

The assumption that the residual stability lever $\overline{M_0S}$ does not depend on the centre of gravity implies that the trim as a function of heel angle is not changed. For ships with large length/breadth ratio, this assumption is usually valid, but especially for floating offshore structures iterative calculation of the whole righting lever curve is needed.

An example is shown in Figure 10.12, for the requirement that the righting lever is at least 0.2 m at a heel angle of 30° or larger.

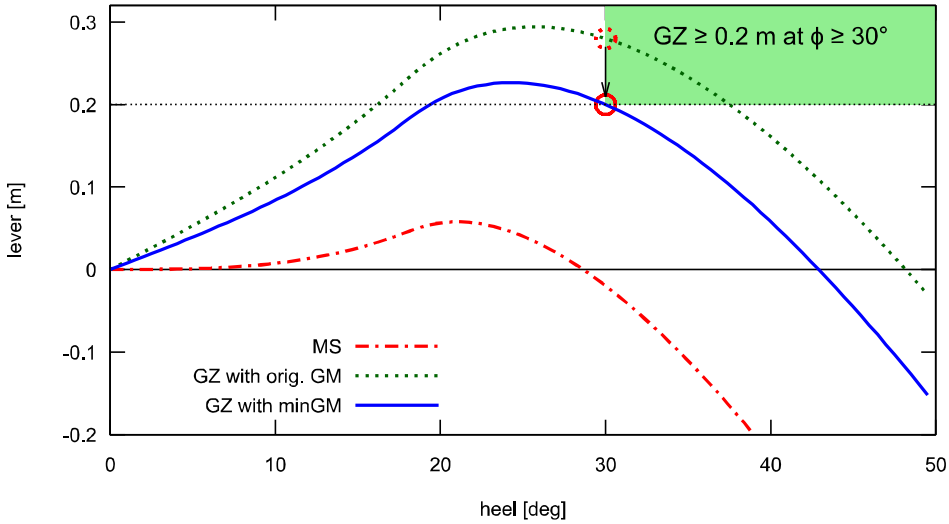

Figure 10.12 Example of minimum GM for a criterion that the righting lever is at least 0.2 m at an angle that is 30° or more

For this kind of simple stability criterion, the minimum GM can be evaluated analytically. For the presented example criterion, the required righting lever value can be written as:

$$\overline{GZ}_{\text{new}}(30°) = \overline{GM_0}\sin 30° + \overline{M_0S}(30°) \geq 0.2\text{m} \tag{10.17}$$

Since the residual stability $\overline{M_0S}(30°)$ is known, this criterion is passed if:

$$\overline{GM_0} \geq \frac{0.2\text{m} - \overline{M_0S}(30°)}{\sin 30°} \tag{10.18}$$

Iteration is often needed for more complex criteria. Moreover, if the trim changes are notable, further iteration, starting from the initially obtained minimum GM condition, should be performed in order to account for the changes in the residual stability lever. Also note that for some criteria the minimum GM may be negative if they are passed also with an angle of loll.

11 Stability failure modes in waves

11.1 Background

In the previous chapters, the ship has been considered to float in calm water, and the environment, including wind and waves, has been taken into account as external heeling moments, and the righting lever curve in calm water has been applied. In the following sections, various stability failure modes in waves are presented, along with some simplified methods for assessing the vulnerability of the ship to these phenomena. First, some basic concepts, common for several stability failure modes, are introduced.

Ship stability can be evaluated in a longitudinal stationary wave, exactly the same way as in calm water, as described in chapters 4 and 5. However, the waterplane area quantities need to be calculated from a projected area of the intersection between the wave surface and the buoyant hull of the ship, as illustrated in Figure 11.1.

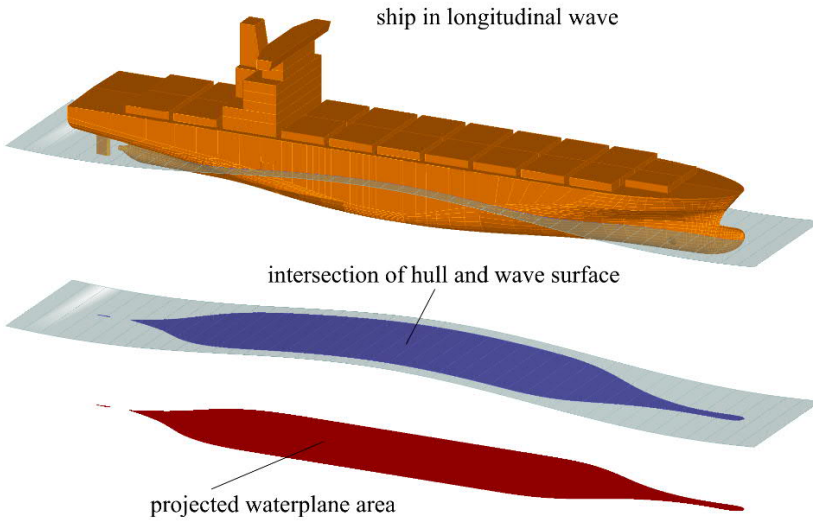

Figure 11.1 Projected waterplane area for a ship in a longitudinal stationary wave

Furthermore, an essential aspect of analysing stability failures in waves it the probability of occurrence of such a dangerous condition. A conservative approach is to apply the wave statistics for the North Atlantic, Figure 11.2, which is considered the harshest sea area. For ships with restricted operation area, more relevant wave statistics can be used instead.

Based on the wave scatter data, an index representing the probability of a specified stability failure can be calculated:

$$CR = \sum_{i=1}^{N} W_i C_i \tag{11.1}$$

where W_i is the probability of a sea state with significant wave height $H_{s,i}$ and zero up-crossing period $T_{z,i}$. The coefficient C_i equals 1 if the specified stability failure can occur in this sea state, otherwise it is taken as zero.

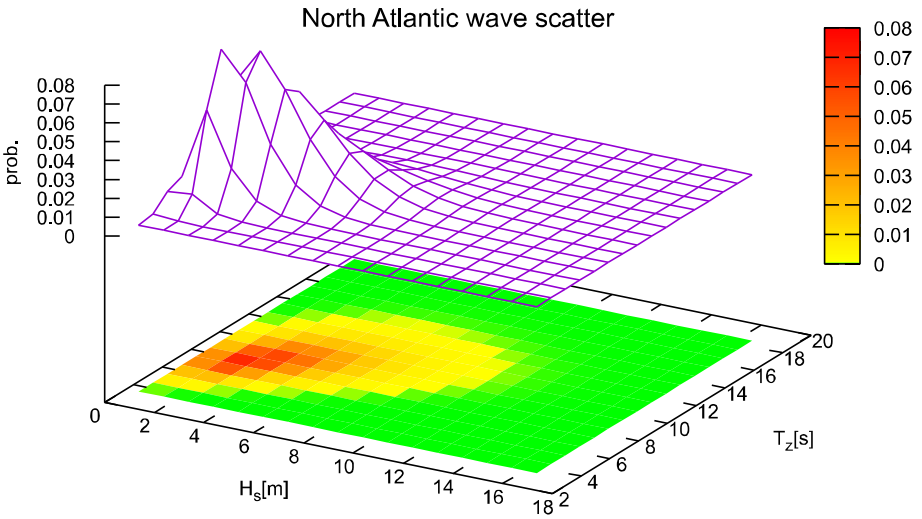

Figure 11.2 Visualization of wave scatter data for the North Atlantic; the values present the probability of occurrence for the given sea state with significant wave height H_s and zero up-crossing period T_z.

11.2 Pure loss of stability

Stability of the ship may be seriously decreased in high following waves if the length of the wave is roughly equal to the ship length. This due to the reduced waterplane area when the wave crest is close to amidships. Also, if the ship and wave velocities are almost equal, the condition of reduced stability is prolonged, and the ship may heel notably (angle of loll, or due to an external heeling moment), see Figure 11.3. This phenomenon is known as *pure loss of stability*. This condition rarely results in direct capsizing, but it can still cause cargo shift or flooding through unprotected openings, which may develop further into capsizing and loss of ship.

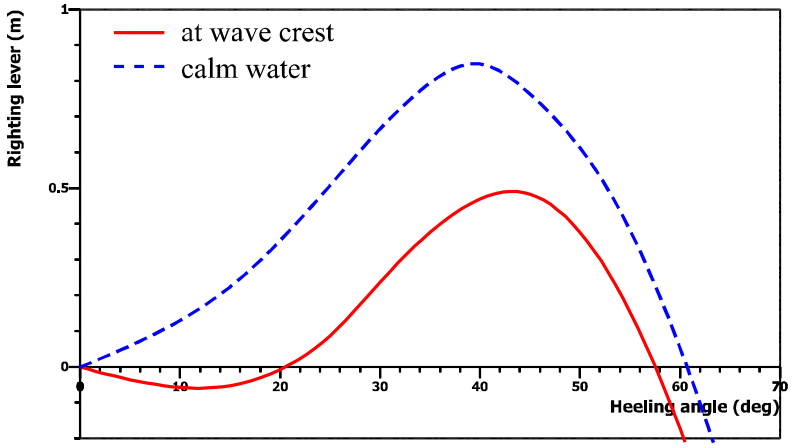

Figure 11.3 Reduced stability at wave crest can result in large angle of loll

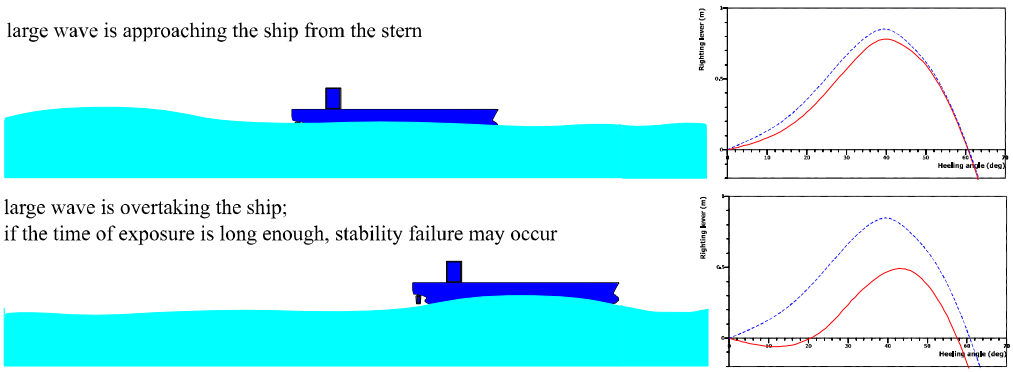

Figure 11.4 Development of pure loss of stability in following seas

The development of pure loss of stability is illustrated in Figure 11.4. This phenomenon cannot occur for slow ships since the reduced stability condition does not last long enough when the waves pass the ship. Therefore, detailed vulnerability assessment is required only if:

$$Fn = V_s/\sqrt{gL} > 0.24 \tag{11.2}$$

where V_s is velocity of the ship and L is the length of the ship.

Moreover, for ships with large block coefficient, such as bulk carriers and tankers, the changes in the waterplane area are so small that the reduction of stability at wave crest is minimal. In general, the first check for possible vulnerability to pure loss of stability according to IMO (2020) can be calculated based on simple hydrostatic quantities, by evaluating a representative metacentric height:

$$\overline{GM}^* = \overline{KB} + \frac{I^*}{\nabla} - \overline{KG} \tag{11.3}$$

where $\overline{KB}$, ∇ and $\overline{KG}$ are the vertical centre of displacement, volume of displacement and vertical centre of gravity at the studied loading condition. The characteristic transverse moment of inertia of the waterplane area I^*, calculated at a characteristic reduced draft:

$$T^* = T - \min\left(T - 0.25T_{\text{full}}, \frac{0.0334L}{2}\right) \tag{11.4}$$

where T is the draft of the studied loading condition, T_{full} is draft corresponding to the fully loaded departure condition and L is the length of the ship. The ship, at the studied loading condition, is potentially vulnerable to pure loss of stability if $\overline{GM}^*$ is less than 0.05 m. Note that the constant 0.0334 represents the maximum assumed wave steepness.

11.3 Parametric roll resonance

Another stability failure mode in waves is related to a periodic variation of the righting lever curve in waves. This is called *parametric roll resonance*, or often simply parametric roll. The phenomenon can be observed in head, following, bow or stern-quartering seas at certain critical encounter frequencies. For simplicity, longitudinal regular waves are assumed in the following description. When a wave trough is amidships stability is increased, and when a wave crest is amidships stability is decreased, as visualized in Figure 11.5.

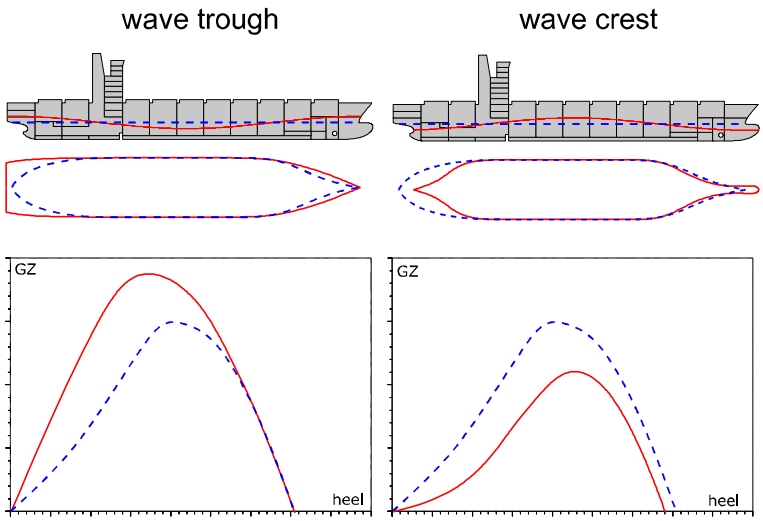

Figure 11.5 Variation of waterplane area and righting lever curve in following/head seas, compared to the calm water condition (dashed curves)

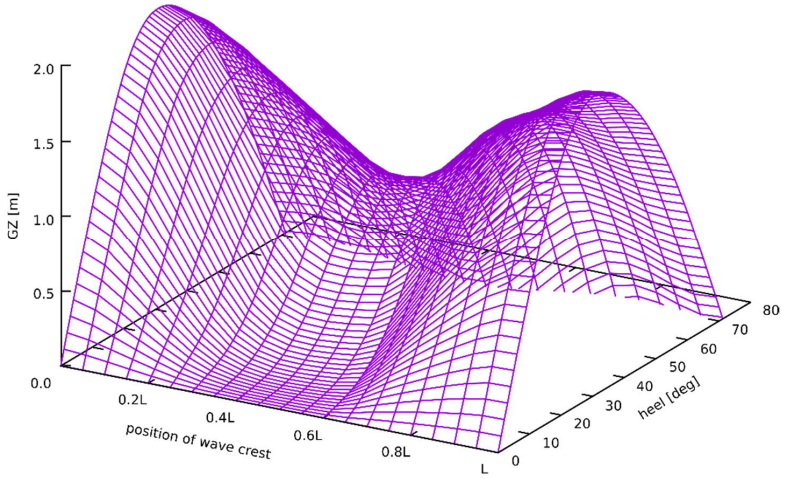

Figure 11.6 Righting lever surface with different longitudinal position of the wave crest for a container ship; wave steepness is 0.05 and wavelength equals the length of the ship

The righting lever curve at different positions of the wave crest can also be plotted as a surface, Figure 11.6, in a longitudinal wave, with wavelength equal to the ship length. Depending on the hull form, the variation can be very large if the wave is steep enough.

A ship with non-zero heel angle and wave trough located amidships is experiencing a strong restoring force. As the ship is up-righted it has a greater roll-rate due to the strong restoring force. If the ship is up-righted at the time when the wave crest is at mid-ship, the stability is decreased and the ship will roll further to the opposite side due to the increased roll-rate and reduced restoring force to rolling. Then, if the maximum roll angle is attained at wave trough

amidships, stability is increased again and the process will start again, Peters et al. (2011). The development of parametric roll on a ship is shown in Figure 11.7. This means that two waves pass during each roll period of ship, Figure 11.8.

The time dependency of the restoring moment is caused by changes in the water plane inertia moment I_T at the encounter frequency ω_e. A simplified model, based on the approximation of initial stability can be presented as:

$$M_{st}(t) \approx -\Delta\overline{GM_0}(1 + \delta \cos \omega_e t)\phi \tag{11.5}$$

The parameter δ depends on the wave height and length, along with the shape of the hull. It is practically linearly dependent on the wave height, and it reaches maximum when the wavelength is equal to ship length. For hull forms with V-shaped lines and flat bottom stern, e.g. container, Ro-Ro and RoPax ships, the parameter has larger values.

Substituting (11.5) into the homogenous roll motion equation (9.7) results in:

$$I'_{xx}\ddot{\phi} + N_{xx}\dot{\phi} + \Delta\overline{GM_0}(1 + \delta \cos \omega_e t)\phi = 0 \tag{11.6}$$

which can be presented as:

$$\ddot{\phi} + 2\xi\omega_\phi\dot{\phi} + \omega_\phi^2(1 + \delta \cos \omega_e t)\phi = 0 \tag{11.7}$$

This is the so-called *Mathieu's equation*. Its solution is very unstable at certain values of the encounter frequency ω_e, resulting in large amplitude roll motion if the parameter δ is large. The unstable situation in the Mathieu's equation is known as parametric roll resonance.

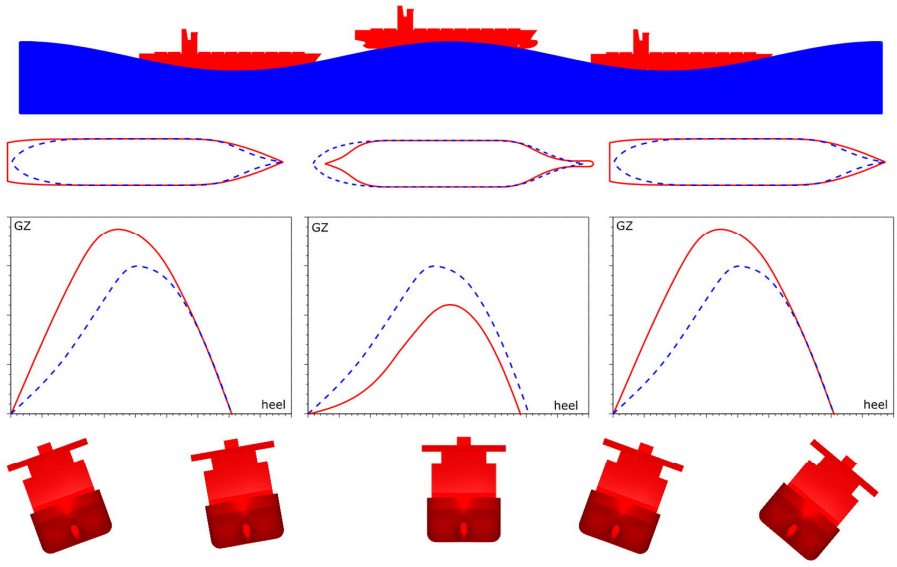

Figure 11.7 Development of parametric roll

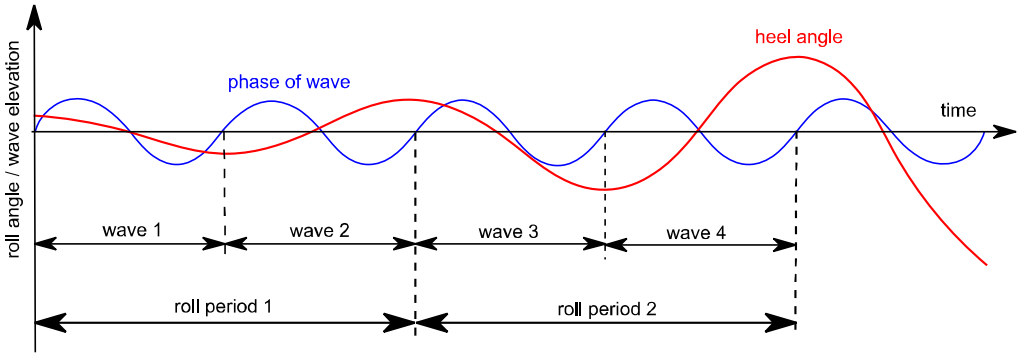

Figure 11.8 Correlation between wave phase and roll angle in the development of parametric roll resonance

The main resonance, with largest roll motion, occurs at:

$$\omega_e = 2\omega_\phi \quad \text{or} \quad T_e = \frac{T_\phi}{2} \tag{11.8}$$

Also weaker resonances are possible, namely:

$$\omega_e = \omega_\phi \quad \text{and} \quad 3\omega_e = 2\omega_\phi \tag{11.9}$$

A rough estimation on the vulnerability to parametric roll can be evaluated from the maximum change of metacentric height ($\delta\overline{GM} = \overline{GM}_{\text{trough}} - \overline{GM}_{\text{crest}}$) in a high wave having a length equal to the ship length. If this change is large, when compared to the metacentric height in calm water, the ship is potentially vulnerable. According to IMO (2020), the ship with the given loading condition is potentially vulnerable to parametric roll if:

$$\frac{\delta\overline{GM}}{\overline{GM}_0} > R_{\text{PR}} \tag{11.10}$$

The threshold value is defined based on the total overall projected area of the bilge keels A_k and midship section coefficient at the fully loaded condition in calm water C_m:

$$R_{\text{PR}} = \begin{cases} 1.87 & \text{sharp bilge} \\ 0.17 + 0.425\left(\frac{100A_k}{LB}\right) & \text{if } C_m \geq 0.96 \\ 0.17 + (10.625C_m - 9.775)\left(\frac{100A_k}{LB}\right) & \text{if } 0.94 < C_m < 0.96 \\ 0.17 + 0.2125\left(\frac{100A_k}{LB}\right) & \text{if } C_m \leq 0.94 \end{cases} \tag{11.11}$$

Here L and B are the length and moulded breadth of the ship, respectively. The function is visualized in Figure 11.9.

Note that $\left(\frac{100A_k}{LB}\right) \leq 4$ and other appendices than bilge keels are not included in A_k.

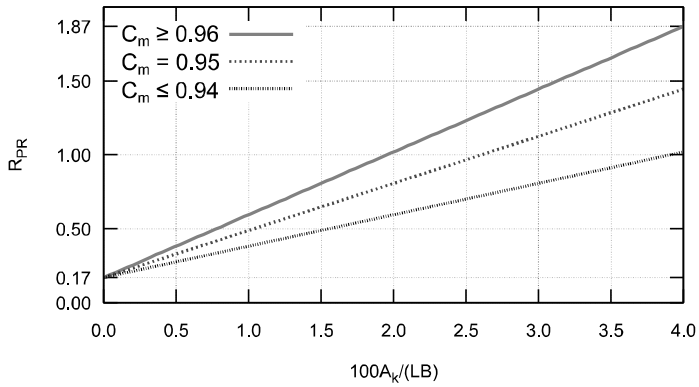

Figure 11.9 Threshold value for checking potential vulnerability to parametric roll based on total bilge keel area and midship coefficient

A very simple approach can be used to estimate the amplitude of the GM variation in waves:

$$\delta\overline{GM} = \frac{I_\mathrm{u} - I_\mathrm{l}}{2\nabla} \tag{11.12}$$

where ∇ is the volume of displacement at the studied loading condition, I_u and I_l are moments of inertia for waterplane areas, calculated at the following characteristic draft values:

$$\begin{aligned} T_\mathrm{u} &= T + \delta T_\mathrm{u} \\ T_\mathrm{l} &= T - \delta T_\mathrm{l} \end{aligned} \tag{11.13}$$

where T is the draft of the studied loading condition and:

$$\delta T_\mathrm{u} = \min\left(D - T, \frac{0.0167L}{2}\right) \tag{11.14}$$

$$\delta T_\mathrm{l} = \min\left(T - 0.25T_\mathrm{full}, \frac{0.0167L}{2}\right) \tag{11.15}$$

Here D is the moulded depth of the hull and T_full is draft corresponding to the fully loaded departure condition and the constant 0.0167 refers to the assumed maximum wave steepness.

More realistic assessment of vulnerability to parametric roll in can be obtained by simulation of roll motion with a simple 1-DOF equation:

$$\ddot{\phi} + 2\delta_\mathrm{L}\dot{\phi} + \delta_\mathrm{Q}\dot{\phi}\left|\dot{\phi}\right| + \delta_\mathrm{C}\dot{\phi}^3 + \omega_\phi^2 f(\phi, t) = 0 \tag{11.16}$$

where δ_L, δ_Q and δ_C represent linear, quadratic and cubic roll damping. The function $f(\phi, t)$ represents non-linear restoring moment, evaluated from a righting lever curve in a static wave. The studied waves are longitudinal, i.e. either head or following seas. A worst-case scenario with the wavelength equal to the ship length is assumed. The encounter frequency is calculated with equation (9.14), accounting for the ship velocity. The initial condition is a small heel angle, e.g. 5°, with a zero roll velocity.

As an example, simulation results at two different velocities of the vessel are shown in Figure 11.10. The zero-speed condition is close to the main resonance frequency, and parametric roll with an amplitude of over 25° develops very rapidly. With a forward speed of 5 knots the roll motion is damped.

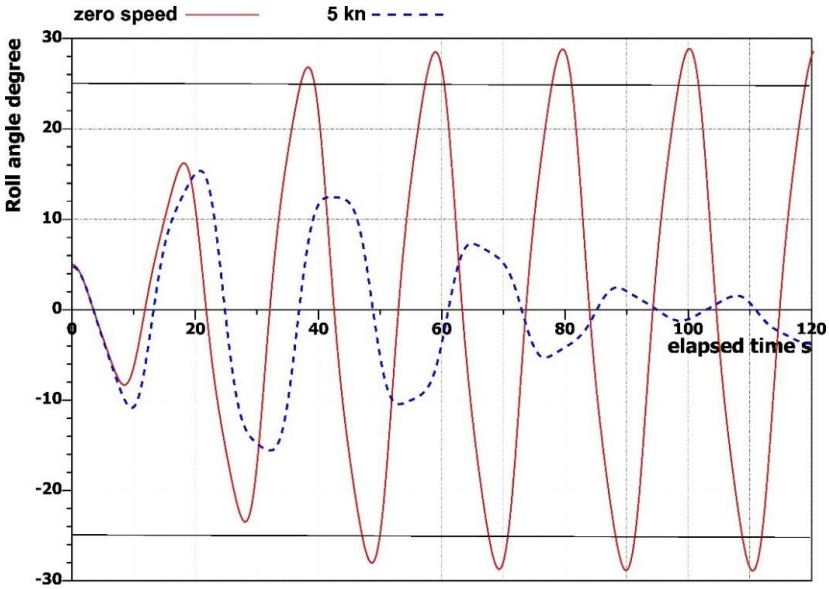

Figure 11.10 Simulated roll motion of a RoPax vessel with zero and 5 knot speeds in regular following waves of 5 m height, adopted from Tompuri et al. (2014)

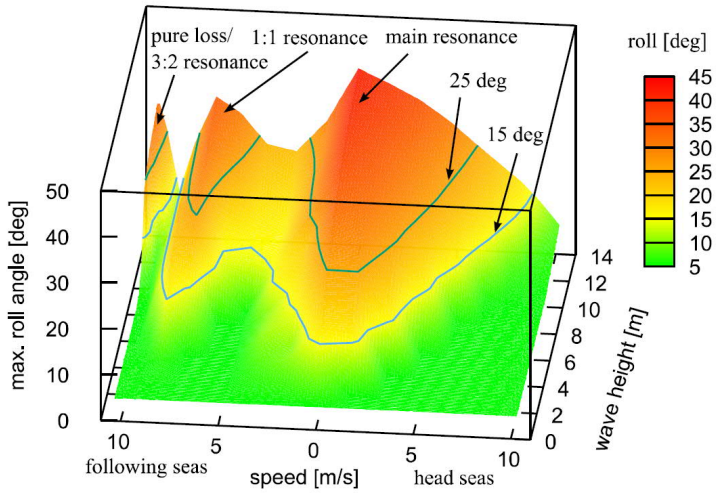

Figure 11.11 Simulated maximum roll angle for a short-sea Ro-Ro vessel, adopted from Tompuri et al. (2016)

The same approach can be used for a range of ship speeds and wave heights, as illustrated in Figure 11.11, which clearly demonstrates the resonance conditions. Based on the probabilities for various sea states, see Figure 11.2, the actual vulnerability to parametric roll can be estimated.

In practice, container ships and pure car/truck carriers (PCTC), in particular, are often vulnerable to parametric roll due to a fine hull form and relatively fast speed. Real measurements of parametric roll have been presented e.g. by Rosen et al. (2013). The

phenomenon very rarely results in capsizing, but significant damage to the cargo and injuries to the crew are more common. Consequently, it is essential that the risk of parametric roll is properly accounted for already in the design stage, and proper operational guidelines are prepared for these vessel types.

11.4 Broaching

The term *broaching* is used to describe a violent uncontrollable turn that occurs despite maximum steering efforts to the opposite side. The uncontrollable turn is often accompanied with a large roll angle that can lead to partial or total stability failure (capsize). Broaching is a dangerous phenomenon, because the occurrence of significant heel angles caused by circulation and wave heeling moment are acting in the same direction, Belenky and Sevastianov (2007).

Broaching can occur in following or stern-quartering waves, and it is a known problem mainly in fishing vessels and fast monohull ships, such as navy vessels. There is no uniformly accepted mathematical definition of a broaching. However, since broaching is always preceded by surf-riding, the vulnerability checks can be established based on this phenomenon. However, it is worth noticing that surf-riding does not always lead to broaching.

In *surf-riding*, a wave captures the ship and accelerates it, so that the ship begins to move with the speed of the wave celerity. To an outside observer, surf-riding can be seen as a transition from a periodical surging motion to a situation, where ship appears to move with the wave, Peters et al. (2011). Surf-riding is an equilibrium situation, where the wave-induced surge-force, propeller thrust and resistance are in balance, meaning that the ship speed is equal to the wave celerity. The forces acting on a ship in following waves are visualized in Figure 11.12.

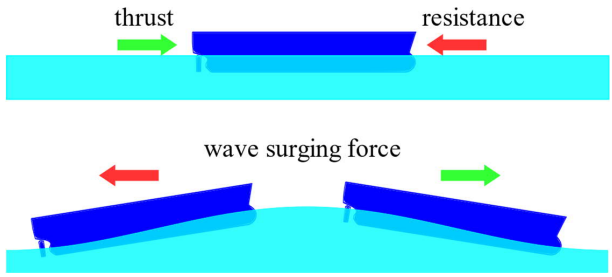

Figure 11.12 Forces acting on a ship in following seas

For surf-riding to occur, the wavelength must be comparable to the length of the ship (0.75~2 times) while ship speed is around 75% of the wave celerity. Large ships are less prone to surf-ride because longer waves are simply too fast compared to the speed of the ship, Belenky et al. (2011). Consequently, detailed assessment of surf-riding is needed only if the length of the ship is less than 200 m and the Froude number is larger than 0.3, IMO (2020).

Detailed assessment of the probability of surf-riding requires information on both ship resistance as function of speed, and propeller open water curves (thrust coefficient as a function of propeller advance ratio). This procedure (Level 2) is presented in IMO (2020).

11.5 Excessive accelerations

Large lateral forces are more dangerous to people than vertical inertial forces, since they can cause loss of balance or fall. In the worst case, people can be thrown against structures and equipment. Large accelerations on ships are mostly caused by roll motion.

Large amplitude roll motion can be caused by parametric roll, as described in section 11.3. A more common situation is synchronous rolling, where the wave encounter frequency is equal to the natural roll frequency. Beam seas is usually most dangerous, and thus the level of accelerations should be considered in this situation to ensure safety of the people on board.

When the ship is rolling in a seaway, a point located high in the superstructure or deckhouse of the ship can move a notably long distance, as illustrated in Figure 11.13. The period of roll motion is the same for all locations, and therefore, the linear velocity must be larger for higher locations in order to cover the longer distance during the same time. Obviously, larger linear velocity means also larger linear acceleration.

As shown in the equation (9.11), the natural roll period is inversely proportional to the square root of the metacentric height. Therefore, a very large GM inevitably means a very short roll period, and consequently, the accelerations on board can be dangerous to people and cargo. For example, container ships in ballast condition can have a very high GM (over 10 m). At the navigation bridge, which is located high above the centre of gravity, even a small amplitude roll motion can cause large accelerations that are dangerous to the crew. Fatal accidents have occurred on the CHICAGO EXPRESS in 2008 and the CCNI GUAYAS in 2011. Both ships suffered large amplitude roll motion with a very short period of about 8 s. Consequently, ships should be designed so that the stability is not "too good" in any real operational loading condition.

According to IMO (2020), a ship is considered not vulnerable to excessive accelerations if:

$$\phi_{\mathrm{A}} k_{\mathrm{L}} \left(g + \frac{4\pi^2 h}{T_{\Phi}} \right) \leq 4.65 \frac{\mathrm{m}}{\mathrm{s}^2} \tag{11.17}$$

where ϕ_{A} is characteristic roll amplitude (rad), coefficient k_{L} takes into account simultaneous action of roll, pitch and yaw, h is the height of the studied point from the assumed roll axis and T_{ϕ} is natural roll period. Note that:

- ϕ_{A} is calculated based on effective wave slope coefficient r, wave steepness s based on roll period and non-dimensional logarithmic decrement of roll decay
- k_{L} is larger in the stern and bow of the ship than amidships
- the roll axis may be assumed to be located at the midpoint between the waterline and the vertical centre of gravity

Detailed guidance and equations are given in the IMO Circ.1627, IMO (2020), where also a more detailed calculation method (Level 2) is presented.

Too large initial stability, and the resulting excessive accelerations, are especially typical for container ships in ballast condition. However, also bulk carriers with a heavy load, such as steel coils in the bottom of the holds, can have a very large metacentric height. It is also worth noting

that, for large passenger ships this can also be a problem, at least from the passenger comfortability point of view. These ships are wide, resulting in a very large metacentric radius and good initial stability. In addition, the superstructure is high, and thus there is a notable risk of excessive accelerations. Some examples of high locations, where the vulnerability to excessive accelerations should be evaluated are illustrated in Figure 11.14 for different ship types.

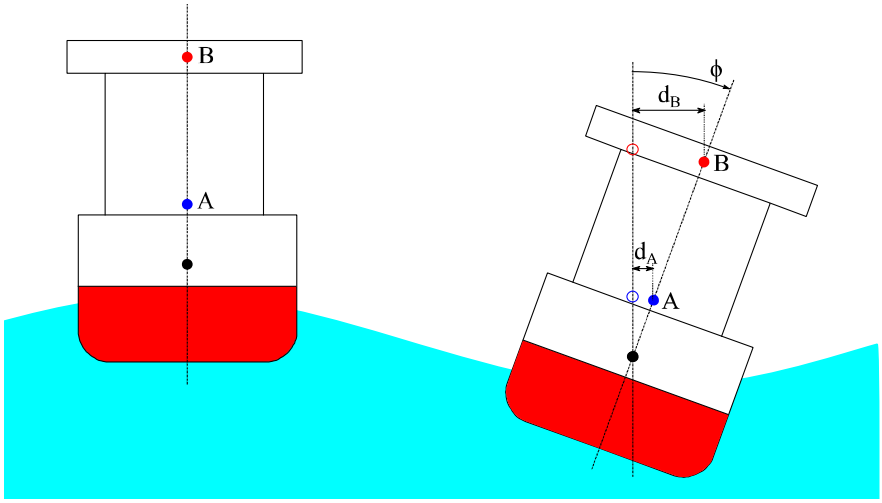

Figure 11.13 Illustration of failure mode for excessive accelerations in high locations in the deckhouse, the lateral acceleration at point A is much larger than lower in the deckhouse at point B

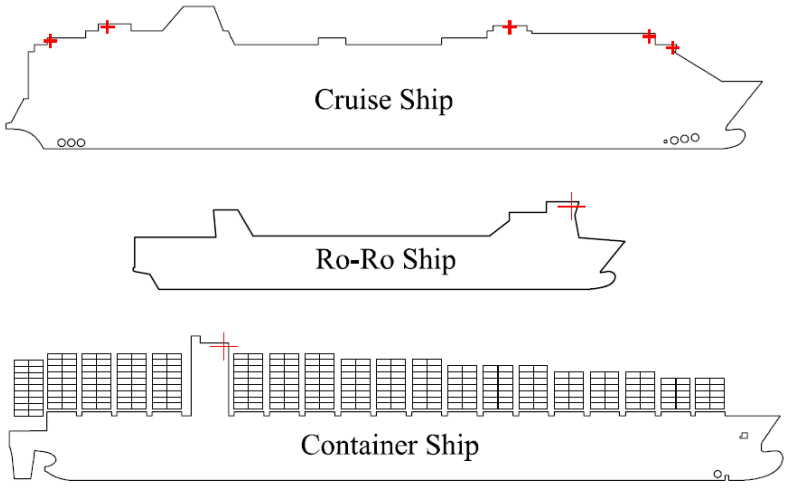

Figure 11.14 Examples of high locations on different ship types, where the level of accelerations needs to be evaluated, adopted from Tompuri et al. (2016)

11.6 Second Generation Intact Stability criteria

The origin of the "first generation intact stability criteria" (IMO IS Code), presented in chapter 10, can be traced to the pioneering works of Rahola (1939), as well as the early versions of weather criterion developed in the 1950s. The history of development and the background of these criteria are described in detail by Kobylinski and Kastner (2003).

The introduction of ships with characteristics and operational modes that differ significantly from the reference ships on which the first generation of intact stability criteria are based challenges the assumption that adequate stability is always provided. A series of stability accidents, e.g. APL CHINA and CHICAGO EXPRESS, clearly demonstrate that a revision or upgrade of the intact stability criteria was needed. Therefore, the development of the *Second Generation Intact Stability Criteria* (SGISC) was initiated at IMO.

Five different stability failure modes in waves are studied independently, IMO (2020):

- Parametric roll
- Pure loss of stability
- Broaching/surf-riding
- Dead ship condition
- Excessive accelerations

Four of these failure modes have been presented in the previous sections. In the dead ship condition ship has lost steering capability and is rolling in beam seas, subjected to a gusty wind. This is situation is already governed in the weather criterion of the IS Code, see section 10.6. Within the SGISC framework, more advanced methods are applied for analysis of potential vulnerability in dead ship condition. The main reason for this is that the original weather criterion was developed using model test data for sample ships from 1950/60s, and therefore, the derived equations are not very realistic for modern hull forms, especially for large cruise ships. See Figure 10.10 on page 94 for the differences in the applied wave steepness.

The SGISC concept is multi-tiered, as presented in Figure 11.15, and it is applied separately for each of the above-mentioned failure modes. The level 1 contains conservative simple checks for vulnerability to each failure mode. If a ship is found to be vulnerable, more advanced level 2 analysis is needed. Also these are based on simplified methods, but considering more physics than level 1. The third level is *direct stability assessment* (DSA), with 6-DOF simulations of ship motions in different sea states. Based on the results, *operational guidelines* (OG) can be derived so that dangerous conditions can be avoided. These ship specific guidelines, either based on DSA results, or simplified by utilizing level 1 and level 2 methods. In addition, the actual operational profile can be considered by using local wave statistics for the planned operational areas of the ship.

For a long time, IMO has issued generic guidance to masters for avoiding dangerous conditions in adverse weather and sea conditions, IMO (2007). One major advantage is of SGISC is that real ship specific operational guidelines can be developed and used for ensuring safe operation.

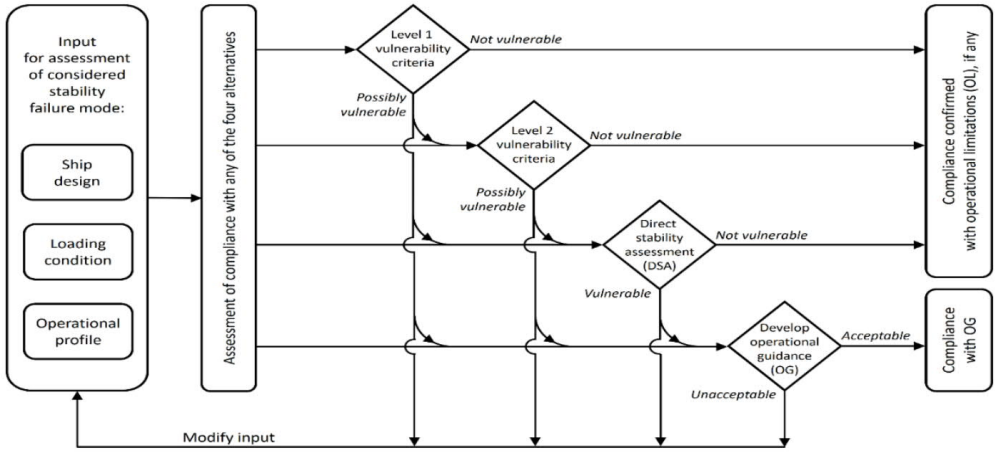

Figure 11.15 Multitier concept of proposed Second Generation Intact Stability Criteria, adopted from IMO (2020)

For some ship types, the proposed new criteria would significantly increase the required minimum GM. In addition, an upper limit for allowed GM is introduced by the failure mode of excessive accelerations. At some draft values the allowed GM range may be quite limited. An example is shown in Figure 11.16 for a short-sea Ro-Ro ship, based on the Level 2 methods and threshold values. Most notably the maximum allowed GM values are quite small, since the studied ship design has a bridge in the forward part, where the accelerations are larger. In addition, the increased minimum GM due to the risk of pure loss of stability in following seas means that the original full load condition fails the requirement.

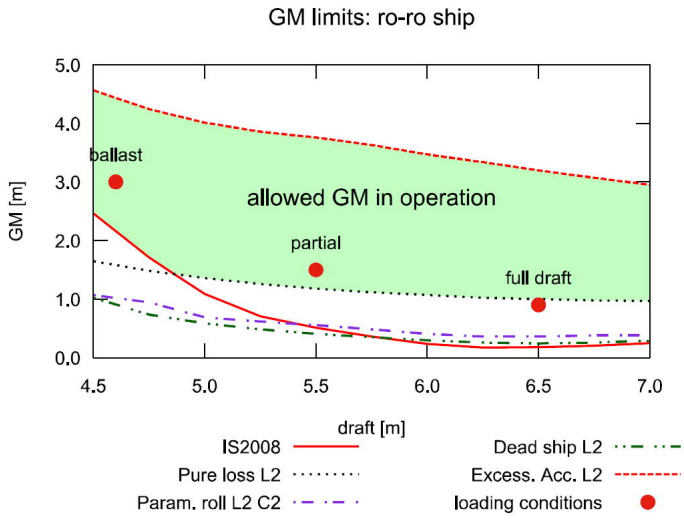

Figure 11.16 Allowed operational GM as a function of draft for a short sea Ro-Ro ship based on the level 2 of the Second Generation Intact Stability Criteria, adopted from Tompuri et al. (2016)

It should be noted that the traditional GM-limit curve approach is not very suitable for some of the failure modes, since the same GM value can be reached with different natural roll periods, depending on the mass moment of inertia of the deadweight.

At the time of writing, the explanatory notes on applying the Second Generation Intact Stability Criteria are being finalized. These new criteria have been developed envisioning a future incorporation into the Intact Stability Code. However, they require testing before using them as mandatory criteria. This is because the robustness of the new criteria is not the same for the different stability failure modes, IMO (2020). Consequently, improvements and revisions to the methods and threshold values can be expected in the future.

Finally, it is noteworthy that the five studied failure modes are idealized conditions, and the loss of stability in waves can be caused by a combined effect of different modes. In addition, the occurrence of roll resonance in stern quartering seas can result in very large amplitude roll motion, Matusiak and Stigler (2012).

12 Subdivision and damage stability

12.1 Background

The previous chapters have presented buoyancy and stability of an intact ship. Collision with another ship or grounding can cause a breach in the hull, flooding of the damaged compartments, and consequently, compromise the stability of the ship. Three damage types, with different characteristics, are illustrated below in Figure 12.1.

Flooding of the ship usually results in decreased freeboard and reduced stability due to the free surfaces in the flooded compartments. Moreover, the static heel angle can be large if the flooding case is asymmetric. Consequently, damage stability also needs to be considered, both in the design and operation of ships. In general, damage stability means the capability to maintain a stable floating position in the case of a damage. The requirements regarding the capability of the ship to withstand external moments are much smaller than in intact stability criteria.

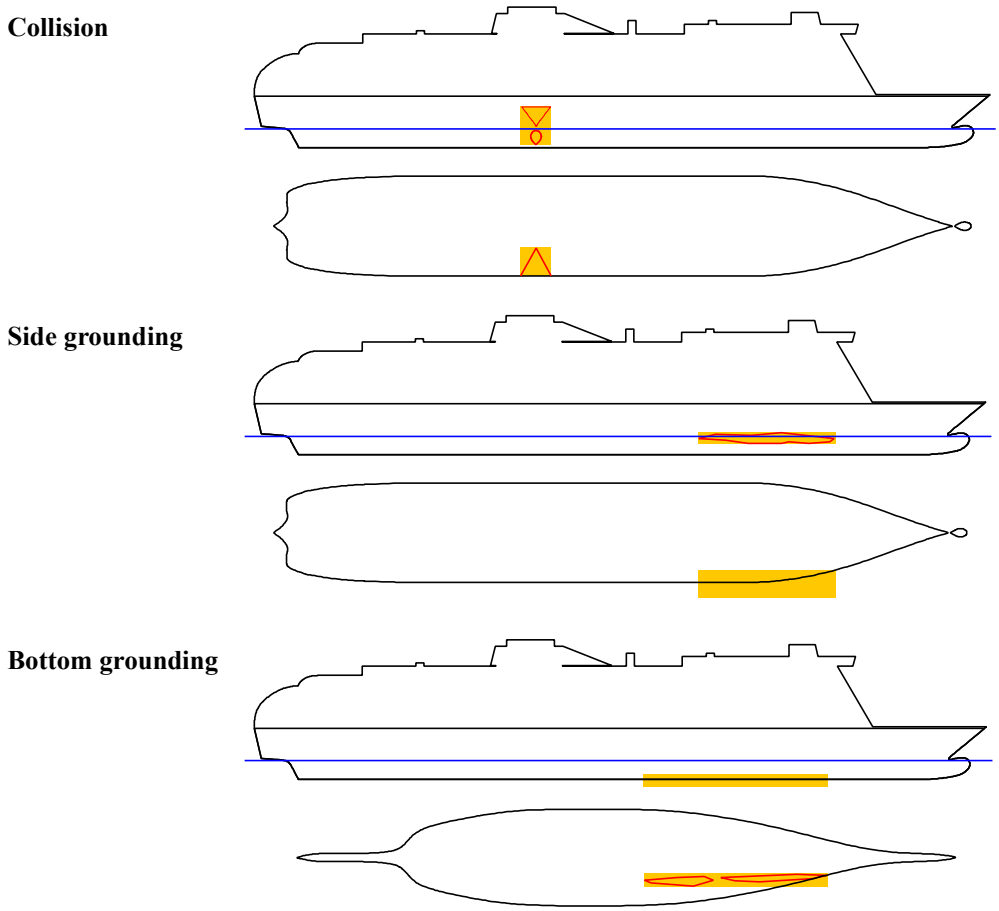

Figure 12.1 Schematic examples of different damage types

In principle, the flooding process can be divided into three separate stages with different characteristics:

- transient flooding
- progressive flooding
- steady state

These stages are visualized in Figure 12.2 for development of roll motion. Naturally, the later stages can only occur if the ship survives the previous stage without capsizing or sinking. The transient flooding stage involves complex dynamics and fluid-structure interaction, Manderbacka et al. (2015). Usually this stage lasts only a couple of roll cycles (about a minute), and it is followed by progressive flooding through internal openings to other rooms. This process can last from a couple of minutes to even several days, depending on the damage case and arrangement of the flooded compartments. Especially non-watertight doors inside watertight (WT) compartments have a significant effect on this, Ruponen (2017). Eventually, if the ship does not sink or capsize, a steady equilibrium is reached.

In regulatory framework, a *flooding stage* refers to any discrete step in the flooding process. Physically, flooding is a continuous process, and the aforementioned characteristic stages each last for a certain time period.

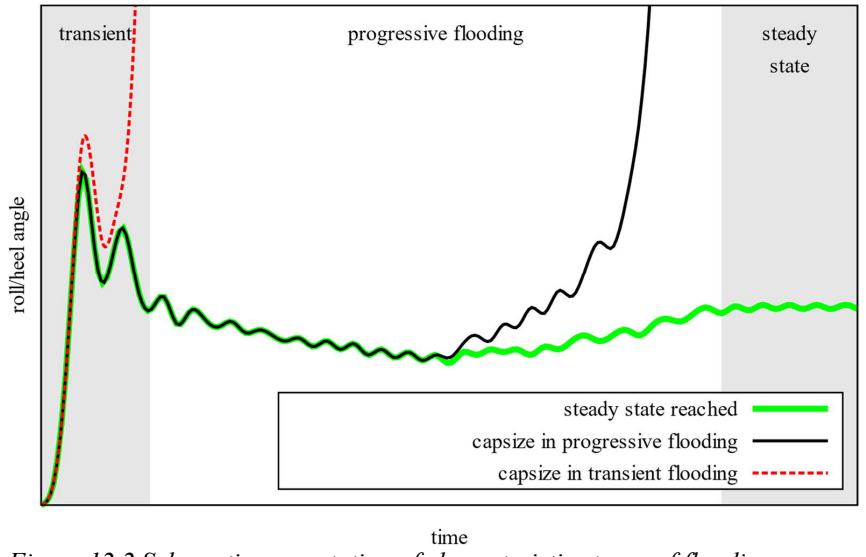

Figure 12.2 Schematic presentation of characteristic stages of flooding process

12.2 Regulatory framework

The sinking of the TITANIC in 1912 emphasized the need for international regulations, and in 1914 the first *Safety of Life at Sea* (*SOLAS*) convention was established. Initially, only reserve buoyancy was considered, but later requirements for reserve stability were also developed. The sinking of the ANDREA DORIA in a collision accident in 1956 was a notable driver for the

SOLAS 1960. The focus was on the stability criteria for the final (steady) state after flooding. After SOLAS 1974, even larger changes have been applied as amendments.

With the increased computing capacity, it is nowadays possible to perform extensive damage stability analyses for a large number of different damage scenarios. Consequently, also regulatory requirements have become more complex. Today, also the intermediate flooding stages are accounted for, and advanced methods have been developed to evaluate the transient and progressive flooding stages. In this chapter, the principles of subdivision and the calculation methods for damage stability assessment are presented.

12.3 Subdivision

In order to limit the consequences of flooding, a *subdivision* of the buoyant hull into smaller watertight (WT) compartments is necessary. Vertically the subdivision extends up to the *bulkhead deck*. Above this level, there is no WT subdivision. As a protection for grounding damages, the ship needs to have a watertight double bottom. Sometimes also other watertight decks are used. Longitudinal bulkheads (double side) can be used to protect e.g. engine room compartments against minor damages, and this kind of arrangement has been commonly applied on new cruise ships after the COSTA CONCORDIA accident. The main elements of subdivision are illustrated in Figure 12.3.

The watertight subdivision is essential for the survivability of the ship in the event of a flooding accidents since it limits the progression of the floodwater. It is allowed to install *watertight doors* (WT doors) in the watertight bulkheads to enable easy passage between the compartments. SOLAS Chapter II-1 states that:

> *"the number of openings in watertight bulkheads shall be reduced to the minimum compatible with the design and proper working of the ship".*

And this concerns also the doors. All watertight doors should be closed at sea, except in certain limited circumstances, e.g. when work in the immediate vicinity of the door necessitates it being opened. However, normally these doors should be opened only temporarily to allow passage of crew between the compartments, since an open WT door compromises the watertight integrity of the ship.

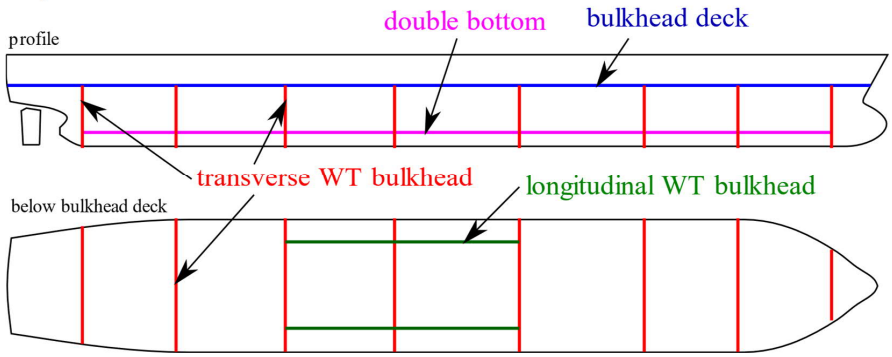

Figure 12.3 Basic elements of a watertight subdivision of a ship

12.4 Permeability

The flooded compartments are not normally empty. In addition to structures, also machinery, equipment and cargo limit the volume that can be filled with floodwater. The *permeability* of a compartment is the portion of the volume which may be occupied by seawater if the compartment is flooded:

$$\mu = \frac{V_{\text{net}}}{V_{\text{tot}}} \tag{12.1}$$

where the volume V_{net} may be flooded and the total geometrical volume is V_{tot}.

The standard permeabilities according to SOLAS are given in Table 12.1, and for various cargo compartments in

Table 12.2. Other values may also be used, based on a detailed analysis of the structures, equipment and cargo in the room. It should be noted that a too small permeability may give too optimistic results.

Recently, Luhmann et al. (2019) calculated the permeability of real ship compartments based on detailed 3D CAD models. For engine rooms, the results varied between 0.91 and 0.94, which is larger than what SOLAS defines, whereas for cabin areas the results were smaller, ranging between 0.894 and 0.930. For stores, the permeability is a difficult concept, since it can vary during a voyage. Luhmann et al. (2019) also calculated the average permeabilities for different stores, indicating that 0.90 would be more realistic than the 0.60 assumed in SOLAS.

Table 12.1 Permeabilities according to SOLAS Ch. II-1 Reg. 7-3

Purpose	**Permeability**
Accommodation	0.95
Machinery	0.85
Void spaces	0.95
Stores	0.60
Tanks	0 or 0.95

Table 12.2 Permeabilities for cargo compartments according to SOLAS Ch. II-1 Reg. 7-3

Purpose	**Permeability**		
	Loading condition:		
	Full:	Partial:	Ballast:
Dry cargo spaces	0.70	0.80	0.95
Container spaces	0.70	0.80	0.95
Ro-Ro spaces	0.90	0.90	0.95
Cargo liquids	0.70	0.80	0.95

12.5 Damage extent

Flooding detection involves some terminology that is often confused. The actual extent of the breach(es) in the hull is the *damage extent*, and the so-called *flooding extent* comprises of all flooded spaces, thus including also flooding to undamaged compartments through internal openings. These are illustrated in Figure 12.4.

An example of a real breach is shown in Figure 12.5, along with typical simplifications. Normally, damage extents are considered by assuming a box-shaped penetration. In regulatory damage stability analyses, a zonal approach is used, so that the whole WT zone that is breached is considered to be flooded instantaneously, thus considering only the breached compartments instead of the actual size and location of the breach opening.

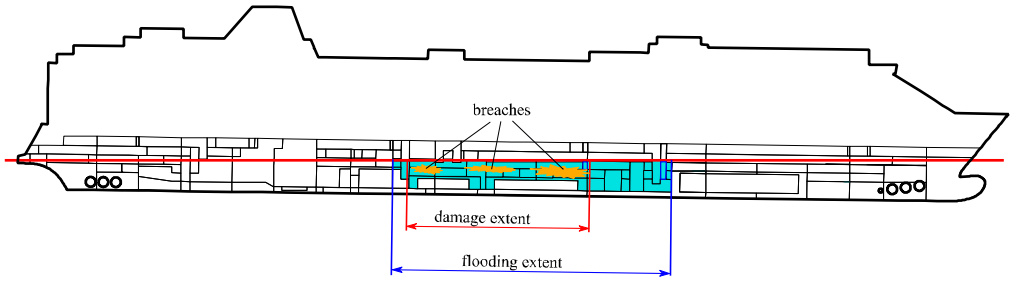

Figure 12.4 Schematic definition of damage extent and flooding extent

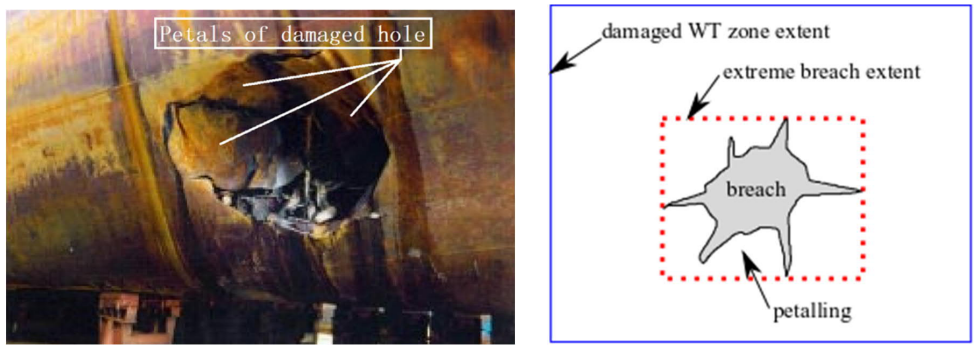

Figure 12.5 Real breach extent compared to regulatory damage extent, photo on left has been adopted from Li et al. (2014)

12.6 Floodable length

The initial approach to survivability of damaged ships was based on ensuring a sufficient watertight subdivision, which would provide enough reserve buoyancy and prevent the ship from sinking. The *floodable length* at any point along the length of the ship is defined as the greatest part of the ship, centred at that point, which can be flooded with the given permeability without submerging the margin line. The *margin line* is an imaginary line on the hull surface. In the SOLAS 90 regulation, the margin line is 3 inches (76 mm) below the bulkhead deck.

An example of a floodable length curve is shown in Figure 12.6. Typically, both axes in the plot have the same scale, so that the forward and aft terminals are at an angle $\arctan(2)$ to the baseline. Therefore, an isosceles triangle, with the top at the floodable length curve will set the maximum allowed distance between the watertight bulkheads.

The floodable length curves were used for deterministic damage stability checks of previous international regulations, including SOLAS 90. Thus, the concept is still relevant, especially for minor conversions of old ships. In addition, the floodable length curves can be used in the early stages of the design process to determine a suitable initial transverse subdivision.

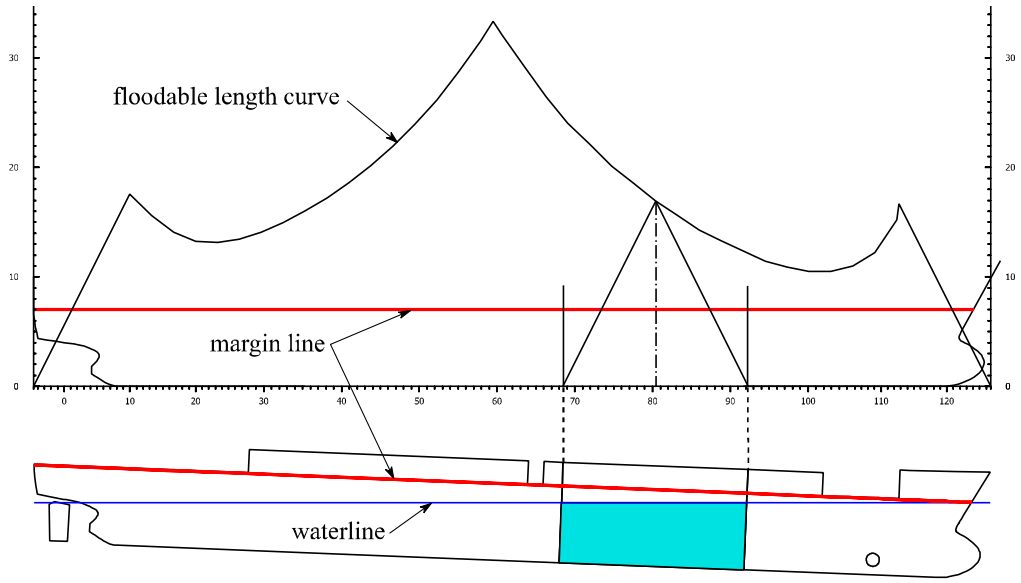

Figure 12.6 Example of a floodable length curve

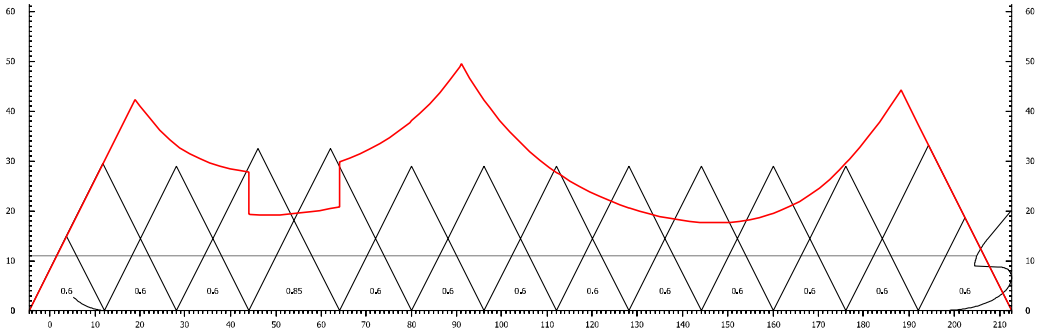

Figure 12.7 Floodable length curve based on average permeabilities in the compartments and transverse subdivision, based on two-compartment standard

In this context, a fully symmetrical flooding condition is assumed, and each compartment, divided by the transverse bulkheads is considered to have a uniform permeability. The floodable length curve is usually plotted together with subdivision triangles, see Figure 12.7, so that it is easy to visually check that the transverse subdivision is dense enough. In the example figure, the machinery room compartments have a larger permeability, and thus the floodable length curve is located lower in this part of the ship. The older SOLAS editions, such as IMO (2001), contained detailed instructions and equations for calculation of representative permeability values.

12.7 Permissible length and compartment standards

Especially in the past, the damage stability characteristics of a ship have been described by referring the number of subsequent compartments that can be flooded without sinking the ship, i.e. so-called *compartment standard*. The *permissible length* between the transverse bulkheads is obtained when the floodable length is multiplied by the *factor of subdivision*. For example, value 0.5 means that a two-compartment standard is applied since flooding of any two adjacent compartments will not result in immersion of the margin line. In practice, the compartment standard is the inverse of the factor of subdivision.

The factor of subdivision depends on the length of the ship and the *criterion of service numeral*, which is calculated based on the enclosed volumes and number of passengers. The detailed instructions and equations are given in the older editions of SOLAS, such as IMO (2001). It should be noted that these old regulations can still be relevant when an existing ship, built according to these regulations, is slightly modified.

12.8 Calculation methods

Similarly to conventional intact stability analyses, conventional damage stability calculations are also done in calm seas. The principles are practically the same, but the floodwater requires special handling. There are two alternative approaches for handling this, the *lost buoyancy method* and the *added weight method*.

With the lost buoyancy method, the flooded compartments are reduced from the buoyant hull, with permeability taken into account. This situation is illustrated in Figure 12.8. The mass and centre of gravity of the ship remain unchanged, unless there are liquid loads in flooded tanks that flow out. Thus, the flooded compartments are in free communication with the sea, meaning that the floodwater can freely flow between the flooded compartments and the sea if the ship moves, e.g. due to an external heeling moment. This assumption implies that the time available for equalizing the water levels in the flooded compartments is infinite, as the water levels are in hydrostatic balance with the sea. Furthermore, the method cannot account for accumulated water above the sea level, such as firefighting water or accumulated water on a Ro-Ro deck.

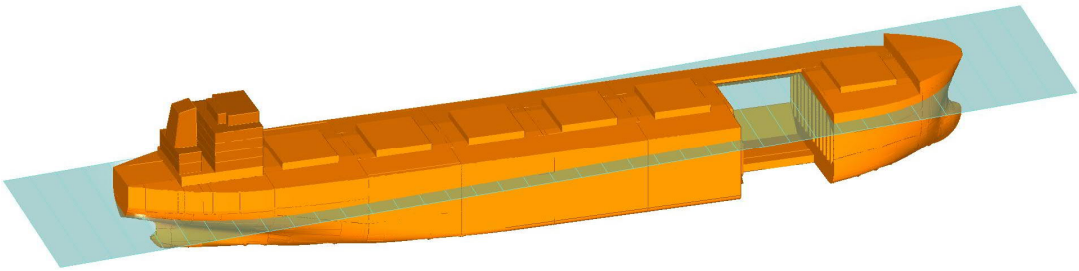

Figure 12.8 Concept of the lost buoyancy method, where the damaged compartments are reduced from the buoyant hull

In the added weight method, the floodwater is treated as additional liquid cargo, Figure 12.9. For compartments that are connected to the sea, this method requires iterations to find the final equilibrium condition. For example, the accumulated water on the vehicle deck must be treated as an added weight, since the method of lost buoyancy would result in an immediate draining of the water back to the sea, if the floodwater level is above the sea level. The same applies also for firefighting water.

The initial volume of floodwater V_w below the intact water line needs to be compensated by the reserve buoyancy, and consequently, the draft is increased, with the trim and heel also usually affected, Figure 12.10; subsequently, the amount of floodwater is also increased by δV_w. With the lost buoyancy method this is easy to calculate, using a modified hull, where the flooded compartments have been reduced. However, with the added weight method the volume of floodwater, $V_w + \delta V_w$, needs to be solved iteratively, making this method cumbersome for the final stage of flooding.

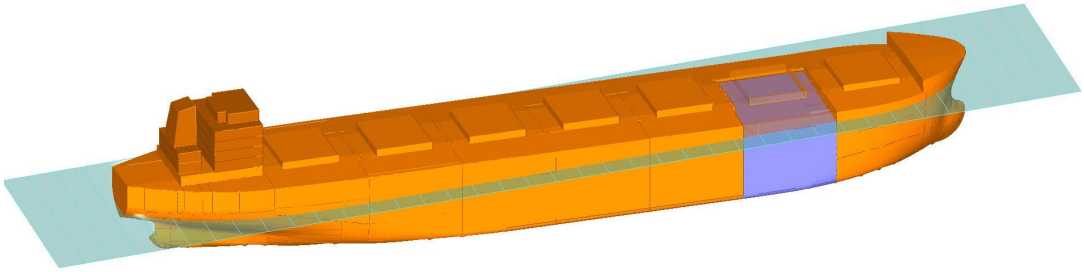

Figure 12.9 Concept of the added weight method, where floodwater is treated as unwanted liquid cargo in the damaged compartments

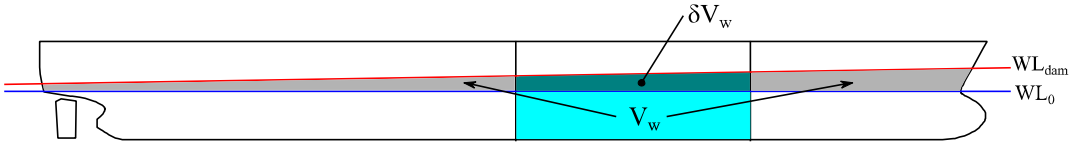

Figure 12.10 Use of reserve buoyancy in a flooded ship

The principle for calculating the floating position of a damaged ship with the lost buoyancy method is illustrated in Figure 12.11. The damaged compartments are reduced from the buoyant hull, with the permeability taken into account. The weight and centre of gravity are unchanged. As a result, the displacement is smaller than the weight, and the centre of buoyancy is moved. Consequently, the lost buoyancy of the flooded compartments is compensated by the reserve buoyancy, draft is increased and the trim and heel are increased so that the centre of buoyancy and centre of gravity are aligned again.

The real shift of floodwater is always considered in the calculation of the righting lever curve, and thus there is no need for any artificial free surface corrections as described in section 7.1 for partially filled tanks. This approach applies also for the use of the added weight method.

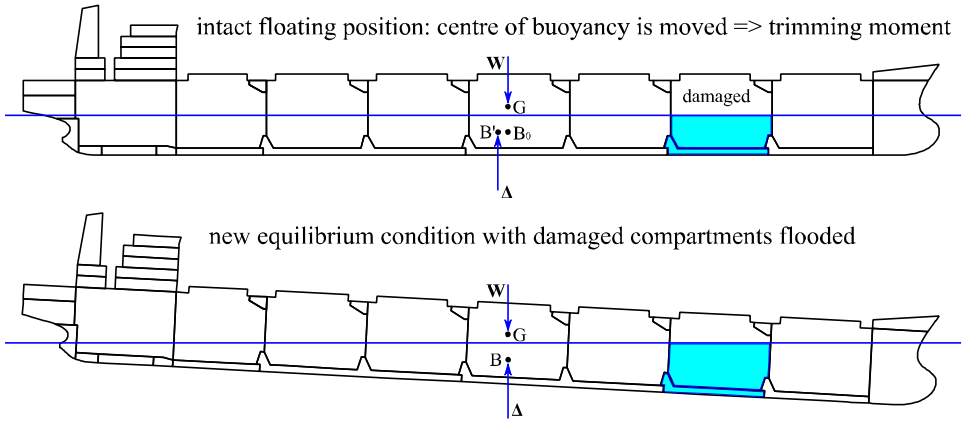

Figure 12.11 Illustration of balancing to find out the equilibrium floating position by applying the lost buoyancy method

12.9 Intermediate stages of flooding

The conventional regulatory approach for damage stability analyses is based on the assumption that the damaged compartments are filled simultaneously, with a single common free surface. The intermediate filling phases are normally based on a selected number of height steps, but alternatively, volume steps can also be used. The former approach is illustrated in Figure 12.12.

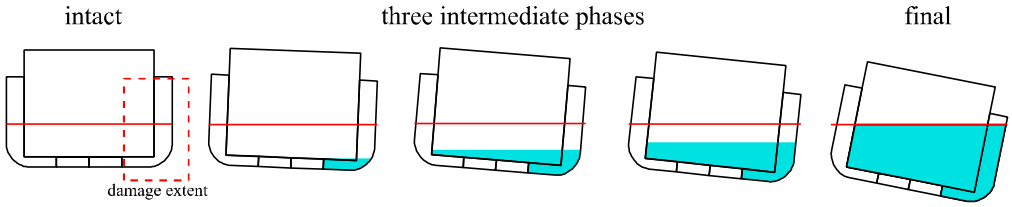

Figure 12.12 Example of intermediate filling phases based on height steps and a single common free surface in the flooded compartments

The situation, where undamaged compartments are flooded through internal openings and pipes, is known as *progressive flooding*. The time-to-flood depends on the size of the openings and the pressure head of the floodwater. Consequently, the flooding process can be very slow, up to several hours or even days. In the current regulatory context, the focus is on the final condition after flooding, but especially while dealing with an emergency onboard, the actual progress and flooding time are more relevant.

Non-watertight boundaries inside the watertight compartments can have a significant effect on the flooding process. Some examples of these structures are illustrated in Figure 12.13. Based on the SOLAS Explanatory Notes, IMO (2017b), only so-called A-class fire rated structures need to be considered.

Leakage and collapse of non-watertight structures were studied with full-scale experiments in the EU FP7 project FLOODSTAND. Closed A-class fireproof doors withstand notable water pressure (2.0 m .. 3.5 m), albeit leakage is notable. On the other hand, tests showed that typical B-class fireproof wall panels leak extensively, and therefore, the assumption of SOLAS to ignore these boundaries seems to be justified. Some examples are show in Figure 12.14, and the analyses and recommendations are summarized by Jalonen et al. (2017).

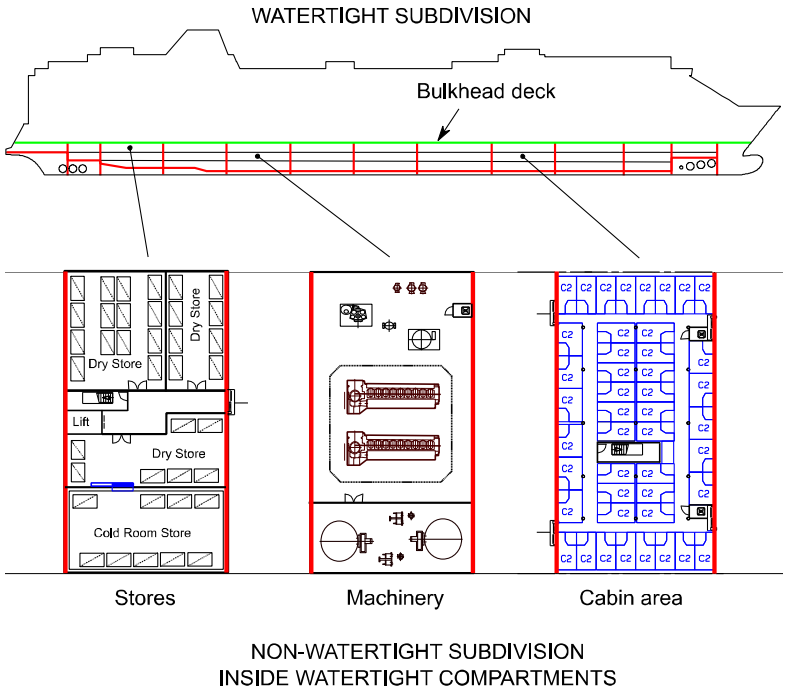

Figure 12.13 Examples of typical non-watertight structures in passenger ships, adopted from Jalonen et al. (2017)

Figure 12.14 Leakage through A-class hinged door (left) and B-class wall (right) in full-scale tests at CTO, photos adopted from Jakubowski and Bieniek (2010)

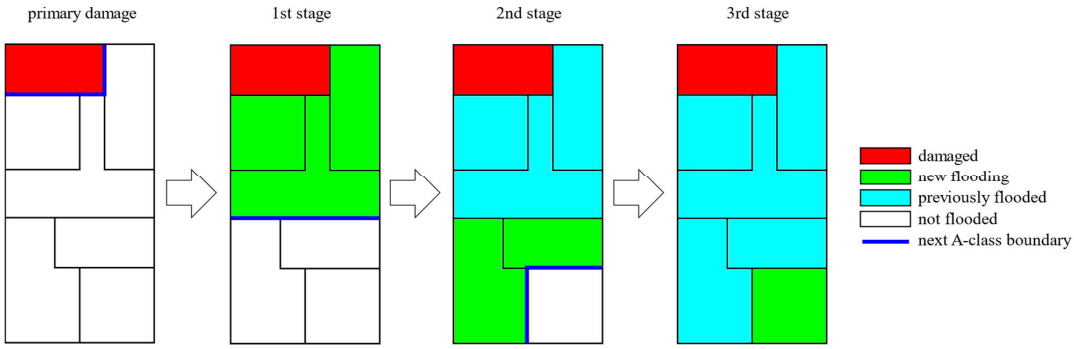

Figure 12.15 Simplified method for considering intermediate flooding stages due to progressive flooding through A-class boundaries, adopted from Bulian et al. (2020)

A very conservative, but frequently applied method, is to study all combinations of intact and collapsed boundaries. However, this may result in a very large number of alternative intermediate stages of flooding, and consequently the computation time may be very long, Ruponen et al. (2018). An alternative, simpler approach, has been implemented in NAPA software, based on the idea that flooding progresses simultaneous to all "neighbouring" rooms with A-class boundary. The approach is visualized in Figure 12.15.

For ships with several decks, such as passenger ships, the real intermediate phases of flooding may consist of multiple free surfaces. The current SOLAS approach does not account for this effect. However, realistic progress of flooding can be calculated with time-domain flooding simulation, where Bernoulli's equation is used to calculate the flooding rates on internal openings, as described in chapter 14.3. Furthermore, this approach enables also the assessment of time-to-flood, or time-to-capsize. With increasing number of persons on the largest passenger ships, these kinds of first principle tools are becoming more popular as shipyards and cruise operators are investing in the design of safer ships, beyond the regulatory requirements.

12.10 Righting lever curve for a flooded ship

The definition of the righting lever is the static righting moment divided by the displacement of the ship. Thus, for damage stability analyses, the applied displacement needs to be clarified. Normally, e.g. in SOLAS, this is always the intact displacement, i.e. constant displacement method. If a real loading condition, with liquid loads in tanks, is studied, the out-flown liquids from the damaged tanks may be reduced from the applied displacement in the calculation of the righting lever curve. This approach is known as the variable displacement method.

The flooding of a damaged ship is a time-dependent process, where the time scale can vary from a couple of minutes to even several days. This time dependency makes it difficult to provide a unique interpretation for the GZ curve during the flooding process.

The conventional approach is to consider various filling degrees for the flooded compartments in intermediate stages. However, in order to evaluate the GZ curve along the flooding process, the time needs to be frozen, while the ship is heeled to different angles, and the righting moment lever is calculated based on the centres of buoyancy and mass. Thus during the progressive flooding, each GZ curve is associated to a frozen snapshot in time, whereas the real situation is a continuous process, Figure 12.16. This assumption indicates that the heeling of the ship is done instantaneously when calculating the GZ values. Consequently, it would be reasonable to assume that there is no flow between the flooded compartments and the sea.

The internal structures in the flooded compartments will restrict the free flow of water. If the ship is heeled very rapidly, the volumes of water will remain practically unchanged since there is no time for water to flow to other rooms through the openings. On the other hand, if the heeling is an extremely slow process, the water levels in all flooded compartments will eventually be in hydrostatic balance with the sea, i.e. part of the lost buoyancy. These interpretations are illustrated in Figure 12.17. The treatment of floodwater can have a notable effect on the GZ curve characteristics, Figure 12.18. A comprehensive discussion on this topic, with several examples, is given in Ruponen et al. (2018).

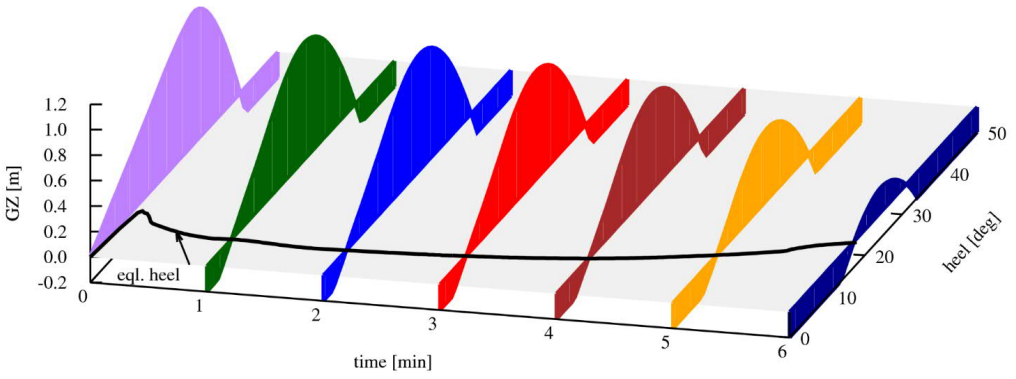

Figure 12.16 Schematic presentation of the GZ curve for a flooded ship as a function of time, adopted from Ruponen et al. (2018)

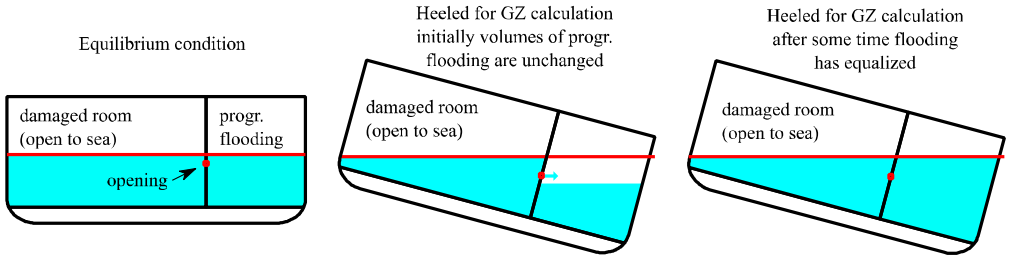

Figure 12.17 Schematic presentation of the effect of an opening on the amount of floodwater in the calculation of GZ curve, adopted from Ruponen et al. (2018)

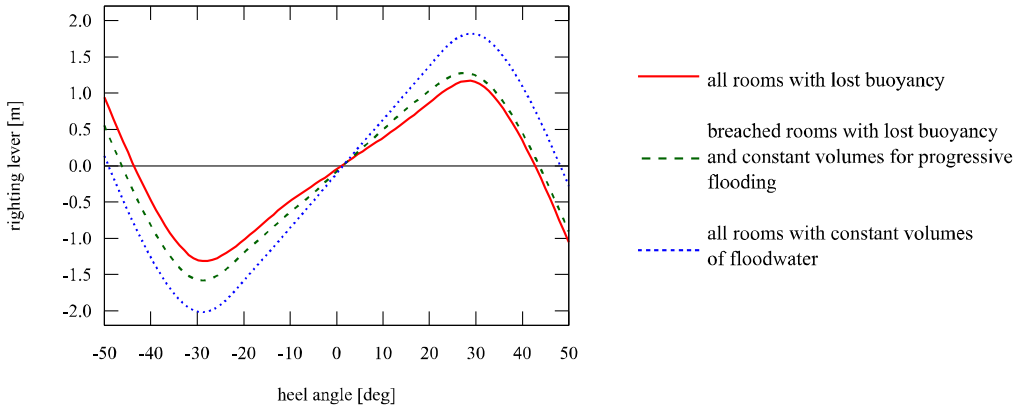

Figure 12.18 Examples of GZ curve for the same final stage after flooding with different treatment methods for floodwater in the flooded compartments

12.11 Deterministic damage stability criteria

Deterministic damage stability criteria set requirements for the residual stability for a set of damage cases. For example, SOLAS 90 considers damages with a maximum length of 11 m or 3 m plus 3% of the ship length, whichever is less, and a penetration up to $B/5$. Similarly to the intact stability criteria, requirements are set for the steady heel angle, range of stability, area and maximum righting lever. In practice, this means that the ship must survive all one and two compartment damages with sufficient reserve stability. The approach is straight forward but there is no benefit for designs that can survive more extensive damages. Moreover, it practically defines the subdivision with transverse bulkheads and centre compartments, protected by longitudinal WT bulkheads at a distance $B/5$ from the side shell.

The evolution of the SOLAS damage stability standards is described in Francescutto and Papanikolaou (2011). Many ships designed according to the SOLAS 90 edition are still in operation, and the older regulations are to be applied in the case of minor conversion. Therefore, the main stability requirements for SOLAS 90 are briefly introduced in the following:

- In case of symmetrical flooding, the ship must have a minimum metacentric height of 0.05 m, calculated with the constant displacement (i.e. lost buoyancy) method.
- In the case of asymmetric flooding, the steady heel angle shall not be greater than 7°. If permitted by the administration, a greater limit of 12° can be applied for damages of more than one WT compartment.
- The positive residual righting lever curve shall have a minimum range of 15° beyond the angle of equilibrium
- The area under the righting lever curve shall be at least 0.015 m·rad, measured from the equilibrium to $\min(\phi_f, \phi_m)$, where ϕ_f is the angle where progressive flooding occurs and ϕ_m is 22° for one-compartment damages and 27° for damages with multiple WT compartments.
- Furthermore, it is required that $GZ_{max} - M/\Delta + 0.04\text{m} \geq 0.10\text{m}$
- For intermediate flooding stages the range shall be at least 7° and maximum righting lever value at least 0.05 m.

Similar to the intact stability criteria, it is trivial to calculate a minimum GM value that is required to pass the criteria, but an iterative procedure is needed (see section 10.7) since the stable floating position is normally highly dependent on the centre of gravity.

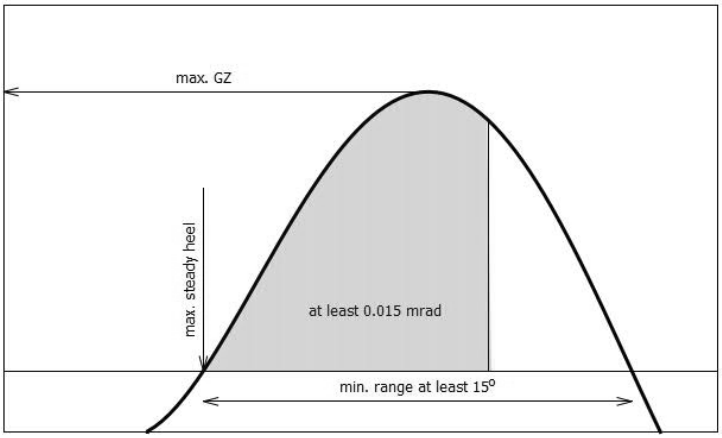

Figure 12.19 Requirements for residual stability after damage in the older deterministic SOLAS 90

13 Probabilistic damage stability

13.1 Background

The alternative approach to a set of deterministic damage stability criteria is a probabilistic damage stability analysis, which is based on the assessment of the survival probability after a flooding incident. This is expressed by an attained index. The calculation of this index requires the assessment of damage stability for a group of different damage cases, using different predefined loading conditions. For each case a weight factor is applied, representing the estimated probability of the occurrence of a particular damage scenario. The attained index, representing the overall survivability of the ship, should be greater than a required index, specified by the applied regulation.

The principles of probabilistic damage stability assessment methodology were introduced by Kurt Wendel, Wendel (1960, 1968). This approach was further developed, and eventually, IMO adopted the first probabilistic regulations as an equivalent alternative to the deterministic rules in 1973. However, the Resolution A.265(VIII) concerned only passenger ships, and in practice it was very rarely applied. A further step was taken in 1992 with the amendments to SOLAS 90, where a probabilistic damage stability method, Regulation 25 in a new part B-1, became effective for all cargo ships with a length over 100 m. This was later extended to cover also cargo ships with length between 80 m and 100 m.

In the 1990s there were three separate damage stability requirements in SOLAS:

- deterministic SOLAS 90 requirements for passenger ships,
- alternative probabilistic method A.265(VIII) for passenger ships, and
- probabilistic Regulation 25 for cargo ships.

Consequently, within the research project HARDER, a common harmonized probabilistic damage stability criterion was developed. The intention was to retain the existing safety level, while harmonizing the previous deterministic and probabilistic requirements. Based on this research, IMO adopted the so-called SOLAS 2009 damage stability regulation. Recently, some amendments, known as SOLAS 2020, have been introduced, emphasizing an increase in the required safety level, especially for passenger ships.

In the following sections, the principles of the probabilistic damage stability assessment of SOLAS Chapter II-1 are presented, based on the latest amendments, IMO (2017a) and explanatory notes, IMO (2017b), commonly known as SOLAS 2020. It should be noted that this regulation covers only collision damages, but a similar framework could be used basically for any damage types. Currently, the SOLAS regulations contain deterministic requirements for bottom (grounding) damages. In addition, for passenger ships, so-called minor damages need to be studied with a deterministic method. Basically, this additional requirement prevents designs with a single “weak spot”, where the ship could sink or capsize following a very small damage extent.

13.2 Definitions

In this section, some basic terminology and definitions that are needed in the probabilistic damage stability analyses are explained. Most notably, from regulatory perspective, any ship that carries more than 12 passengers is a *passenger ship*, otherwise the ship is considered to be a *cargo ship*.

The deepest subdivision draft corresponds to the summer load line, see chapter 3.6. The maximum possible vertical extent of damage above the baseline is limited to 12.5 m above this draft.

The *subdivision length* L_s of the ship is the greatest projected moulded length of that part of the ship at or below deck or decks limiting the vertical extent of flooding with the ship at the deepest subdivision draft, Figure 13.1.

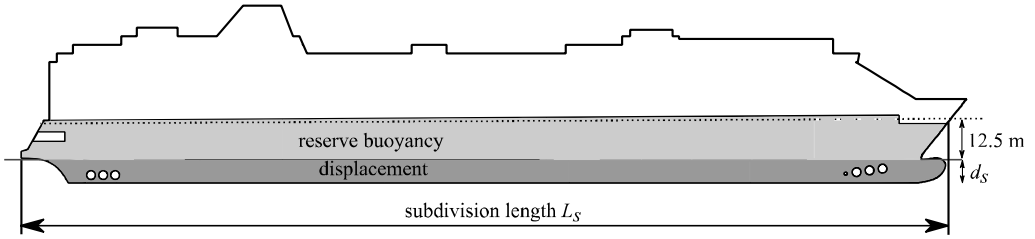

Figure 13.1 Example of subdivision length for a passenger ship

13.3 Required and attained indices

The *required subdivision index* represents the benchmark level of survivability. The requirement for passenger ships was changed in SOLAS 2020, so that R depends only on the number of persons on board (passengers and crew), Figure 13.2. Partly as a result of the COSTA CONCORDIA accident in 2012, it was decided that better survivability is needed, especially for large passenger ships with thousands of people on board. For cargo ships, the required index R is notably lower, and it depends on the subdivision length L_s, as illustrated in Figure 13.3.

The calculations are done with three different initial conditions, Figure 13.4, namely:

- deepest subdivision draft, d_s
- partial subdivision draft, d_p
- lightest service draft, d_l

In all cases a “dry ship” is assumed. This means that the liquid loads are taken into account in the centre of gravity (or metacentric height) of the intact ship, but the tanks are modelled as empty and can be flooded.

If the subdivision is not symmetric, port side and starboard need to be calculated separately, and the actual attained index is the average of them.

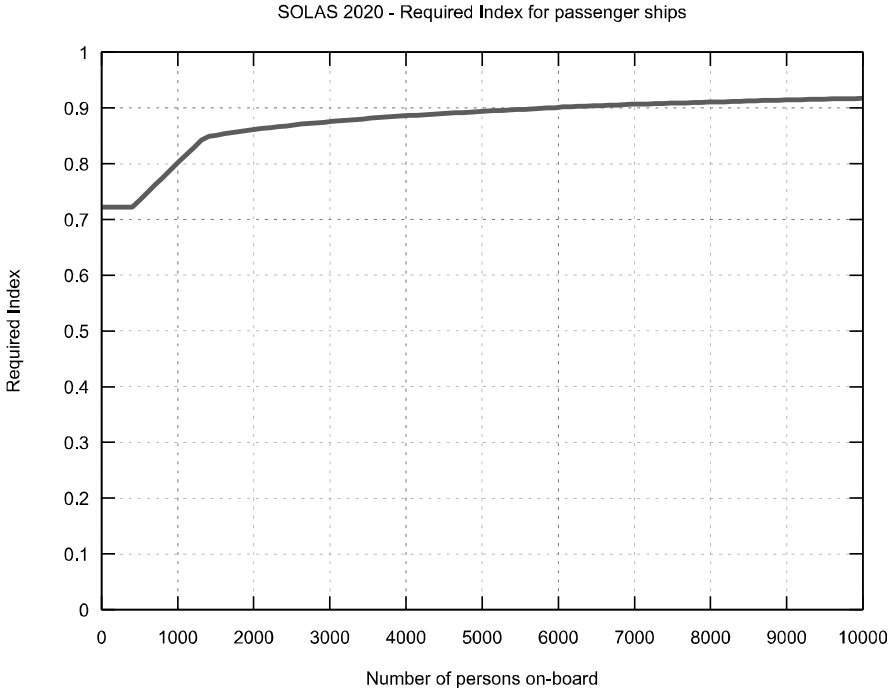

Figure 13.2 Required subdivision index for passenger ships

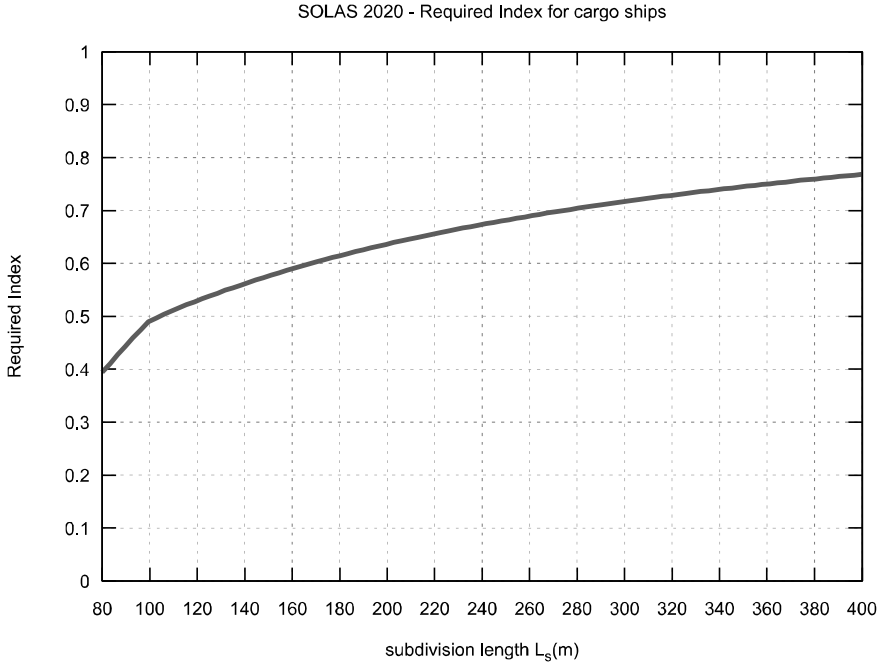

Figure 13.3 Required subdivision index for cargo ships

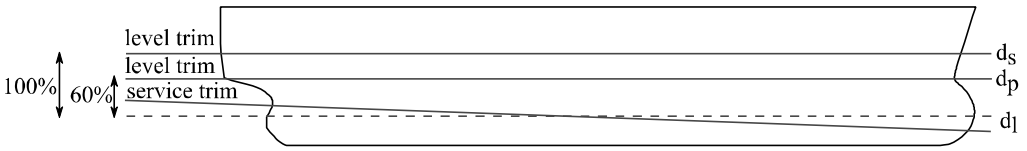

Figure 13.4 Initial conditions for probabilistic damage stability in SOLAS II-1

The *attained subdivision index*, representing the survivability level of the ship in the event of a collision damage, is calculated as:

$$A = 0.4A_s + 0.4A_p + 0.2A_l \tag{13.1}$$

where the subscripts s, p and l present the applied initial condition (deepest subdivision draft, partial and lightest service draft). Consequently, this equation also implies the assumed probabilities for these three initial conditions. It is worth noting that, for example, bulk carriers may have a significantly larger variation in the loading conditions, and for cruise ships, there is not that much deviation, Paterson et al. (2019). Yet, the regulatory approach is the same.

For each initial condition, $c \in \{s, p, l\}$, the attained *partial subdivision index* is:

$$A_c = \sum p_i s_i \tag{13.2}$$

where p_i is the probability of the damage and s_i is the "probability" of survival. When there is also horizontal watertight subdivision above the waterline, this extends to:

$$A_c = \sum p_i s_i v_i \tag{13.3}$$

where the additional factor v_i accounts for the probability that the damage has a vertical extent that will flood only the spaces below a given horizontal boundary, such as a watertight deck. The probability of penetration, i.e. the transverse damage extent, is embedded in the p-factor.

It is required that:

$$A \geq R \tag{13.4}$$

In addition, it is required that each partial attained index A_c is at least $0.9R$ for passenger ships, and for cargo ships at least $0.5R$. This ensures that all initial conditions have a large enough contribution to the total index, and thus provide a sufficient safety level in all operational conditions.

13.4 Probability of damage

The current SOLAS Chapter II-1 regulation 7 is based on a zonal approach, where the ship is subdivided into zones. An example is shown in Figure 13.5. In addition to transverse bulkheads, also longitudinal and horizontal limits can be used. Based on this definition, the damage cases for calculation can be generated ant the probabilities can be evaluated.

The transverse bulkheads are primary, and damages are generated from single to multiple zones. Each damage case has a certain group of rooms that are damaged, based on the damage extents and the used subdivision zone limits. Thus, each case also has a probability that the damage is

limited to these zones. This probability is calculated inversely, using the equations given in the regulation. An example of the underlying probability distributions is shown in Figure 13.6. When damages are created for more adjacent zones, the sum of probabilities eventually approaches 1.0. Note that the maximum length of a damage is limited, depending on the length of the ship, and all damages that are longer than this limit have a zero probability. The absolute maximum damage length is 60 m.

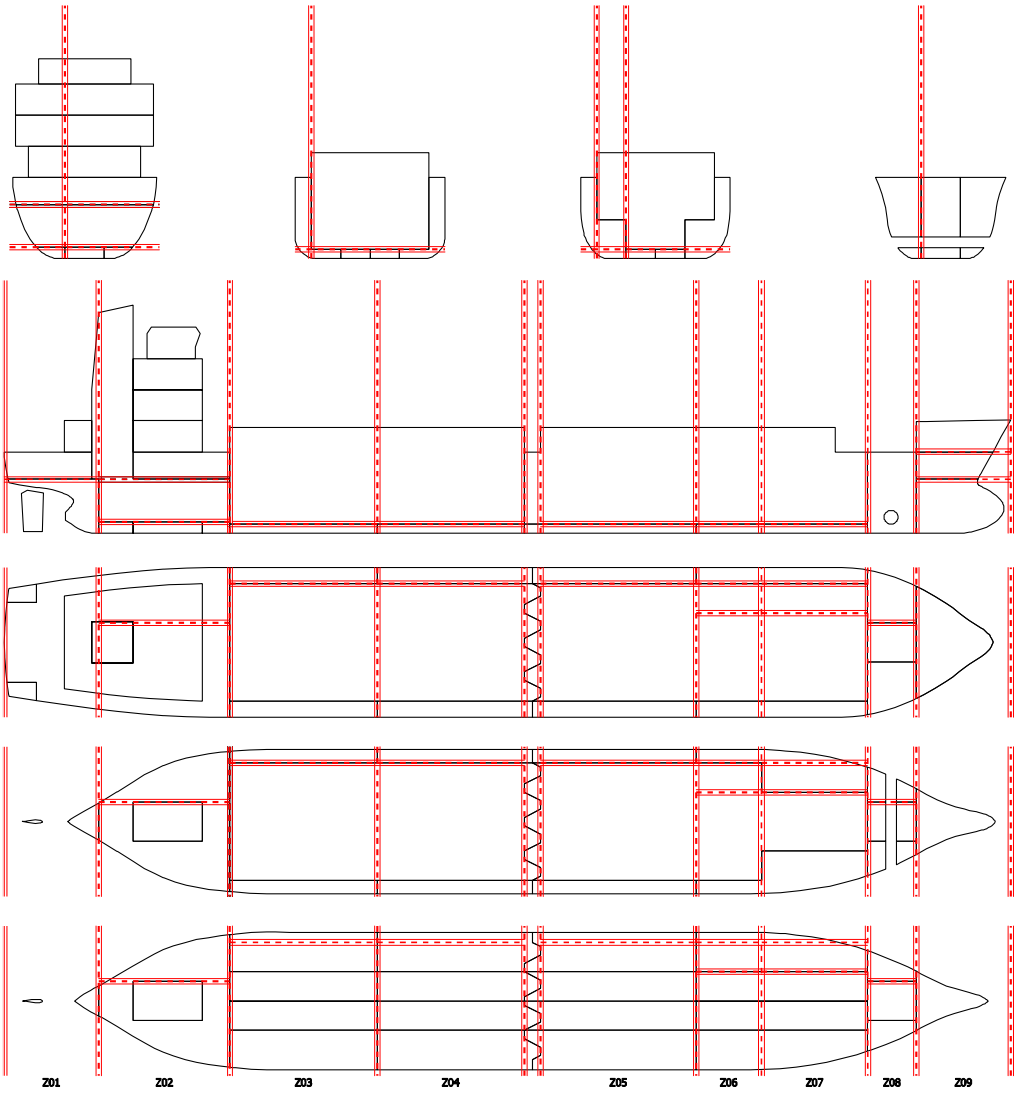

Figure 13.5 Example of a zonal subdivision for probabilistic damage stability calculations

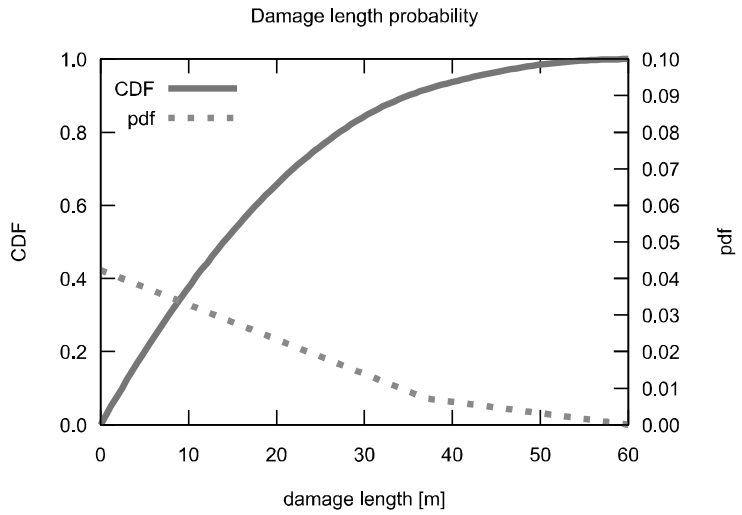

Figure 13.6 Probability density function (pdf) and cumulative density function (CDF) for damage length in collision damages according to SOLAS for a ship with a subdivision length of over 260 m

13.5 Survivability

The probabilistic concept requires an assessment of survivability for each studied damage case, i.e. the s-factor. Theoretically, this can be considered the probability of survival, and the values are limited between 0 and 1. However, in practice, this is merely a measure of residual stability, and therefore the ship can actually survive even if $s = 0$. Consequently, also the A-index is not the actual probability of surviving a collision damage. In fact, the original probabilistic framework by Wendel (1960) introduced the term "sicherheitsgrad", which translates to "safety degree".

According to research in the HARDER project, most of the collision accidents have occurred in sea states with a significant wave height less than 4 m, Tagg and Tuzcu (2003). Consequently, a survivability for 30 min in this limiting sea state was the basis for the development of the s-factor, using results from systematic model test.

If the flooding of the compartments is not instantaneous, intermediate flooding stages need to be studied. According to the explanatory notes, IMO (2017b):

> *"Where intermediate stages of flooding calculations are necessary in connection with progressive flooding, flooding through non-watertight boundaries or cross-flooding, they should reflect the sequence of filling as well as filling level phases. Calculations for intermediate stages of flooding should be performed whenever equalization is not instantaneous, i.e. equalization is of a duration greater than 60 s."*

Consequently, there are also two different equations for the s-factor, separately for intermediate and final stages. Intermediate flooding stages need to be considered for passenger ships. For cargo ships this is relevant only if cross-flooding devices (see section 14.1) are used, IMO (2017a). According to SOLAS Chapter II-1, for intermediate flooding stages:

$$s_{\text{intermediate}} = \left(\frac{GZ_{\max}}{0.05} \cdot \frac{range}{7}\right)^{1/4} \tag{13.5}$$

where:

$GZ_{\max}$ is not to be taken as more than 0.05 m
$range$ is not to be taken as more than 7°

In addition, $s_{\text{intermediate}} = 0$, if the heel angle exceeds 15° for passenger ships and 30° for cargo ships.

For final stage of flooding, the s-factor is:

$$s_{\text{final}} = K\left(\frac{GZ_{\max}}{TGZ_{\max}} \cdot \frac{range}{Trange}\right)^{1/4} \tag{13.6}$$

where:

$GZ_{\max}$ is not to be taken as more than $TGZ_{\max}$
$range$ is not to be taken as more than $Trange$

For Ro-Ro/passenger ships in damage cases that involve a Ro-Ro space:

$TGZ_{\max} = 0.20$ m
$Trange = 20°$

Otherwise:

$TGZ_{\max} = 0.12$ m
$Trange = 16°$

In this context, a Ro-Ro space is either a vehicle deck or a lower hold beneath the bulkhead deck, Figure 13.7. A room is involved in a damage, if it is located within the damage extensions, or can be flooded progressively from another compartment.

According to the SOLAS Explanatory Notes, IMO (2017b):

"the instantaneous transverse moment of this floodwater is calculated by assuming a constant volume of water at each heeling angle".

And furthermore:

"the righting lever curve is calculated with a constant intact displacement at all stages of flooding".

The heel angle is accounted for with the factor:

$$K = \sqrt{\frac{\phi_{\max} - \phi_{\text{e}}}{\phi_{\max} - \phi_{\min}}} \tag{13.7}$$

For passenger ships:

$$\phi_{\max} = 15°$$

$$\phi_{\min} = 7°$$

And for cargo ships:

$$\phi_{\max} = 30°$$

$$\phi_{\min} = 25°$$

Schematic righting lever curves for different flooding stages and ship types with a minimum stability still resulting in $s = 1$ are illustrated in Figure 13.8. The requirement for additional reserve stability for cases where a Ro-Ro space is involved for RoPax ships is quite notable. Furthermore, it can be seen that during intermediate stages, the maximum s-factor can be easily achieved, even with minimal reserve stability. For cargo ships, $s = 1$ can be achieved even with a very large heel angle, and consequently the risk of cargo shift may be notable, although this is not considered in the SOLAS framework.

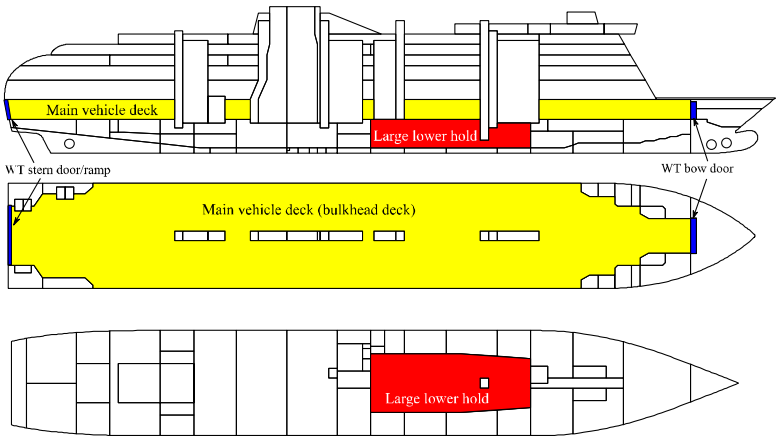

Figure 13.7 Examples of Ro-Ro spaces in a RoPax vessel

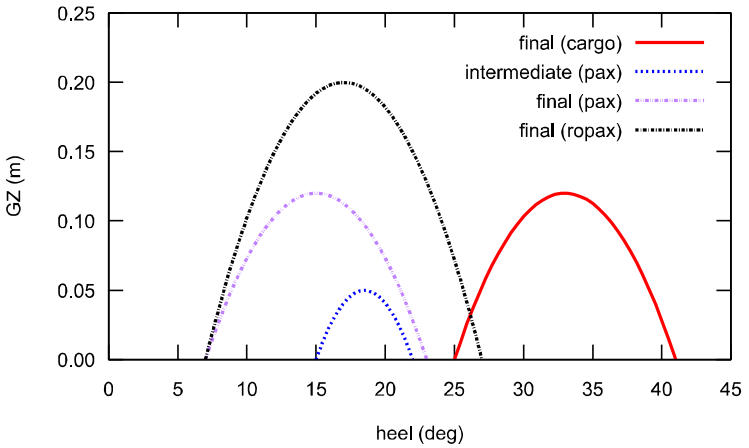

Figure 13.8 Illustration of minimum stability (range and GZmax) and maximum heel angle that result in s = 1 for different flooding stages and ship types

The s-factor is first calculated for each flooding stage and intermediate filling phase. The actual applied s-factor of the case for index calculation is then evaluated as:

$$s = \min(s_{\text{intermediate}}, s_{\text{final}} \cdot s_{\text{mom}}) \tag{13.8}$$

For cargo ships $s_{\text{mom}} = 1$, but for passenger ships, this factor accounts for the external moments in the final condition, so that:

$$s_{\text{mom}} = \min\left(\frac{(GZ_{\max} - 0.04) \cdot Disp}{M_{\text{heel}}}, 1.0\right) \tag{13.9}$$

Here $Disp$ is the displacement of the ship at the subdivision draft (in tons), and the applied heeling moment (in ton·m) is:

$$M_{\text{heel}} = \max(M_{\text{pass}}, M_{\text{wind}}, M_{\text{survcraft}}) \tag{13.10}$$

The heeling moment (in ton·m) due to passenger crowding is:

$$M_{\text{pass}} = (0.075 N_{\text{p}})(0.45 B) \tag{13.11}$$

where N_{p} is the number of passengers and B is the breadth of the ship.

The wind heeling moment (in ton·m) is:

$$M_{\text{wind}} = \frac{PAZ}{9.806} \tag{13.12}$$

where the wind pressure P is 120 N/m^2, A is the lateral area exposed to wind and Z is the vertical distance between the centroid of the area A and half draft at relevant intact condition. The equation also gives an explicit value for the gravitational acceleration.

$M_{\text{survcraft}}$ is the maximum assumed heeling moment (in ton·m) due to a fully loaded survival craft on one side of the ship.

The s-factor is taken as zero if any unprotected opening is submerged, resulting in progressive flooding that is not accounted for in the calculations, i.e. as a progressive flooding stage. In addition, the s-factor is also affected by elements that are not directly related to stability and buoyancy of the damaged ship. If a vertical escape hatch is immersed, then the s-factor is nullified. Also, immersion of a horizontal escape route on a passenger ship, Figure 13.9, or a control station for watertight doors, results in a zero s-factor, although in such cases the real survivability of the ship, and the people on-board, may be much better.

Also, alternative approaches for estimation of the survivability level, i.e. the s-factor, have been developed, e.g. within the GOALDS project, Papanikolaou et al. (2013), aiming at a better measure of the probability of surviving a collision damage with flooding in a seaway. However, the current standard SOLAS approach is still considered to be suitable, although in some cases it may be quite conservative, especially for large passenger ships.

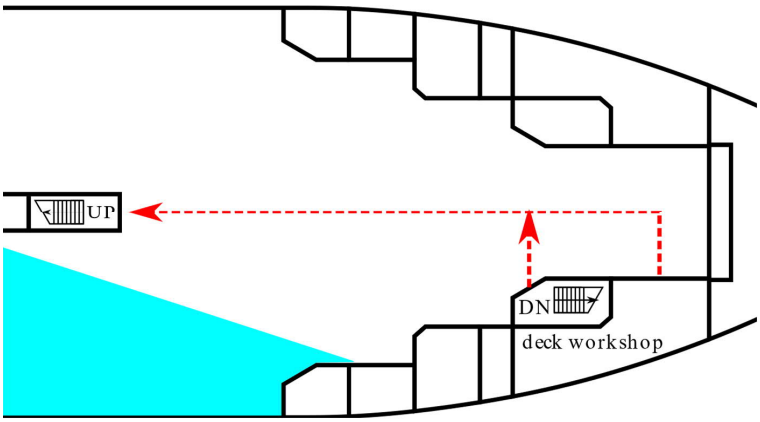

Figure 13.9 Horizontal escape routes on the vehicle deck of a RoPax ship

13.6 V-lines

One important output from the probabilistic damage stability calculations is the envelope surface of all waterplanes from the cases that are contributing to the A-index, i.e. with $s_i > 0$. The results are usually presented in cross-sections of the ship, where the surface is V-shaped, and thus these are often called *V-lines*. If the compartments and relevant openings are not fully symmetric, the portside and starboard cases need to be studied separately, and consequently, also the V-lines are not always symmetric. The concept is visualized in Figure 13.10.

The V-lines are usually drawn at the locations of the transverse bulkheads. This helps in ensuring that the part of the bulkhead that is below the V-line is kept watertight, also above the bulkhead deck level. Figure 13.10 includes final stages after flooding, but a similar envelope surface can be prepared also for intermediate flooding phases, and doors that may be temporarily submerged during flooding should ensure certain level of watertightness (so-called semi-watertight doors) to prevent progressive flooding that is not accounted for the in the probabilistic damage stability analysis.

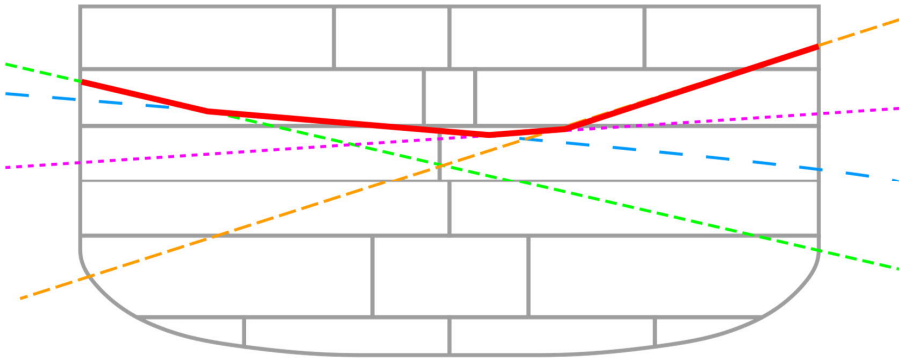

Figure 13.10 Principle of preparing the envelope (thick red line) of waterplanes (dashed lines) to form V-lines.

13.7 Analysis of probabilistic damage stability calculations

In general, the analysis of probabilistic damage stability results is very straight forward; the attained subdivision index must be larger than the required index. If this is not reached, and the sum of the p-factors is not close to unity, it might be possible to increase the index by generating damages for more zones. However, for long damages the probability (p-factor) is usually small, and furthermore and many of these extensive damages are not survivable. Alternatively, the design must be improved. This may be done e.g. by:

- improving the subdivision
- lowering the centre of gravity
- avoiding asymmetric flooding with more efficient cross-flooding arrangements
- increasing the freeboard height
- rearrangement of openings
- adding watertight decks that limit flooding extent

The attained subdivision index represents the survivability level of the ship for collision damages. However, it is not the actual probability of survival. It should be noted that although the s-factor formulae have been derived from extensive model tests in the HARDER project, it actually represents the characteristics of the righting lever curve, compressed into a single value instead of a real probability. Furthermore, the s-factor is nullified if an escape route or a control station is immersed. Consequently, the probability of survival of the ship is usually much larger than the A-index, especially for large passenger ships. Moreover, the probability of survival for the people on board is even better, since the time-to-sink/capsize can be long enough to enable orderly evacuation and abandonment.

A summary of probabilistic damage stability calculations for a RoPax ship is presented in Table 13.1. The damage cases were generated with up to 6 zones, but only 5 zones or less contribute to the attained index.

A more detailed analysis of these results is shown in Figure 13.11 with up to 4 zone damages. Each point in this diagram represents one damage case. Along the x-axis is the location of the longitudinal centre of damage and the quantity on the y-axis is $p(1-s)$. The cases with high values have the largest potential for improvement, since the s-factor value is small, and the p-factor is notable. The effect of the v-factor, see equation (13.3), is also considered. In the presented example the 2 and 3 zone damages in the forward shoulder area are the most notable ones, indicating that some improvement in the subdivision on this part of the ship would likely increase the attained index considerably.

Table 13.1 Example of probabilistic damage stability results

```
Required subdivision index R: 0.803428

PROBABILISTIC DAMAGE STABILITY
---------------------------------
DAMAGES                   W*P*V*S
---------------------------------
1-ZONE DAMAGES            0.32024
2-ZONE DAMAGES            0.38758
3-ZONE DAMAGES            0.12005
4-ZONE DAMAGES            0.01030
5-ZONE DAMAGES            0.00070
6-ZONE DAMAGES            0.00000
---------------------------------
A-INDEX TOTAL             0.83886
---------------------------------
THE SUM OF WCOEF*PFAC*VFAC EQUALS 0.958417
```

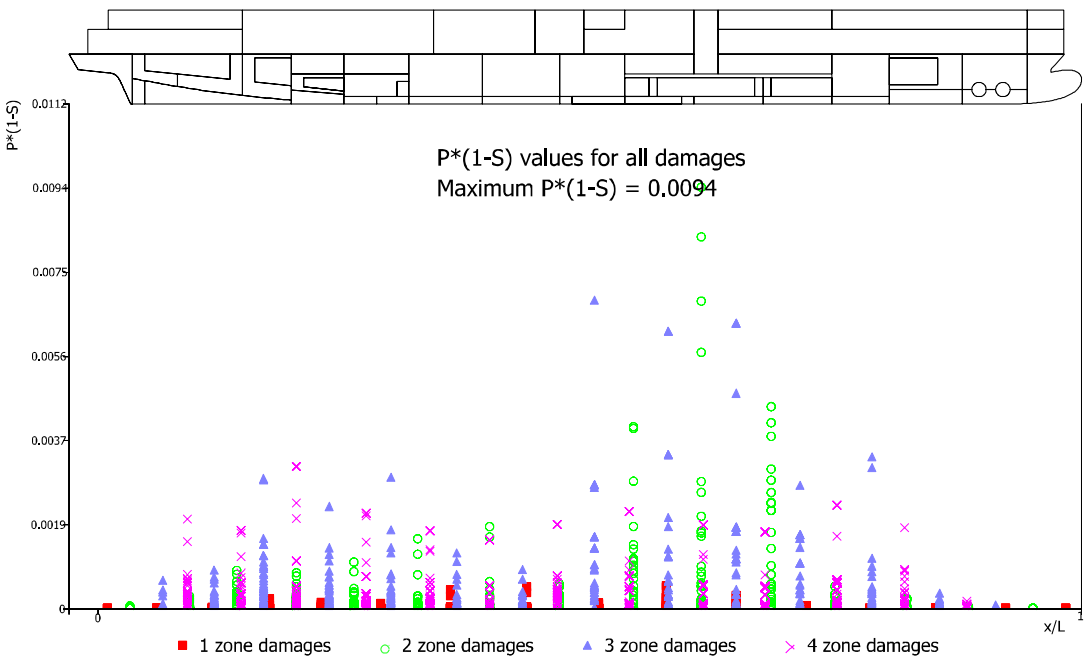

Figure 13.11 Example of a so-called p(1-s) diagram from probabilistic damage stability calculation results for a RoPax vessel

13.8 Minor damages

A ship design may pass the probabilistic requirements, i.e. the A-index is larger than the R-index, even if there is a vulnerable spot in some part along the ship length, causing the ship to sink or capsize (i.e. s-factor equals zero) if a certain critical compartment is breached. A schematic example is visualized in Figure 13.12, where even a minimal damage at the location of a critical transverse bulkhead would result in zero s-factor.

This situation was considered unacceptable for passenger ships, and therefore, additional deterministic requirements for so-called *minor damages* were included in the SOLAS Ch. II-1 Regulation 8. In practice, this means that passenger ships need to survive ($s \geq 0.9$) all one and two compartment damages with limited penetration. The considered damage length and penetration depend on the number of persons onboard. For ships designed for 400 or more persons, the damage length is $0.03L$ and penetration is $0.1B$.

It is worth noting that compared to the previous deterministic SOLAS 90 requirements ($B/5$), the considered maximum damage penetration is much smaller. Still the requirement for minor damages is significantly affecting the design of the watertight subdivision for passenger ships.

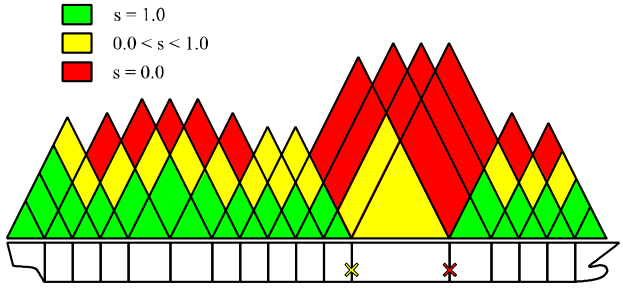

Figure 13.12 Visualization of a simplified case, where the probabilistic requirement is met ($A > R$) but even a small damage to critical transverse bulkheads (marked with X) would result in serious flooding

13.9 Monte Carlo methods for damage stability

As mentioned in section 13.1, the probabilistic damage stability framework was originally introduced in 1960s. At the time, the computing capacity was limited, and therefore the zonal approach, with inversely calculated probabilities for the damages, was adopted. An alternative to the zonal approach for generation of damages and evaluation of probabilities is the generation of large number of random damage cases based on probability distributions (Monte Carlo simulation). This requires more computations, but it is already feasible with modern computers.

In the Monte Carlo method, cumulative density functions (CDF) for the damage location and extensions are needed. A large set of random numbers are generated, while the damage parameters are generated based on the CDFs, as illustrated in Figure 13.13.

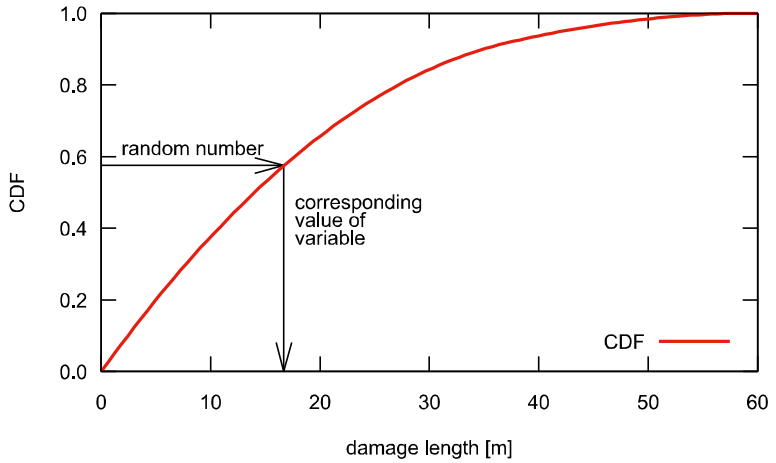

Figure 13.13 Principle of using Monte Carlo simulation for the length of a collision damage

It is not necessary to calculate all the generated damage cases individually. Instead, the cases can be grouped based on the set of rooms that are damaged, Figure 13.14. Each group with the same damaged rooms has the probability (p-factor):

$$p_{\text{group},i} = \frac{N_{\text{group},i}}{N_{\text{tot}}} \tag{13.13}$$

where $N_{\text{group},i}$ is the number of damage cases with the same group of rooms, and N_{tot} is the total number of generated cases.

The main benefit of this kind of a non-zonal approach is the capability to apply basically any probability distribution for the damage characteristics. The principles of this approach and example of grounding damages were developed within the EMSA III project (EMSA/OP/10/2013). Details are presented in Bulian et al. (2016, 2020). Non-zonal approach also allows for easy modifications to the applied probability distributions, and for example crashworthiness of ship structures can be considered, Conti et al. (2021).

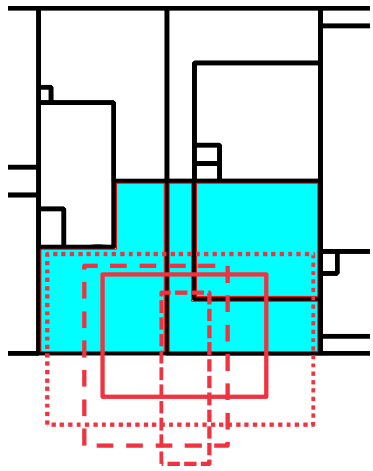

Figure 13.14 Different damage extents (red rectangles) breaching the same set of rooms

For collision damages the SOLAS Ch. II-1 Reg. 7 provides only the equations for calculating the p-factors with a zonal approach, but the underlying probability density functions can be derived. Moreover, in SOLAS a conservative interpretation has been adopted for the lower vertical damage extent. Consequently, Bulian et al. (2019) have complemented the SOLAS framework with a distribution for the vertical lower limit of the damage. This development enables the use of the non-zonal method also for collision damages.

14 Specific damage stability calculations

14.1 Cross-flooding and time-to-flood

An asymmetric flooding condition can be dangerous, as it increases the risk of capsizing, and also can hinder, or even prevent, evacuation and abandonment of the ship. Consequently, equalization of flooding usually improves the survivability, although the total amount of floodwater is increased. The process to equalize asymmetric flooding is known as *cross-flooding*. Typically, this is arranged with ducts and/or pipes, as shown in Figure 14.1.

The cross-flooding process must be fast enough to minimize the negative impact of a large heel. In regulatory calculations the rooms in way of damage are treated as lost buoyancy. Water flows through the cross-flooding device(s) until an equilibrium condition is reached. This is illustrated in Figure 14.2. In general, a detailed analysis of the cross-flooding process requires time-domain flooding simulation, Ruponen et al. (2012), but for simple cases with a single pair of compartments, a simplified estimate of the cross-flooding time can be calculated.

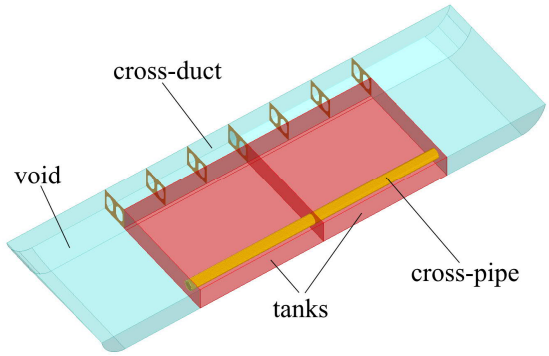

Figure 14.1 Cross-flooding arrangement with a structural duct and pipe in the double bottom

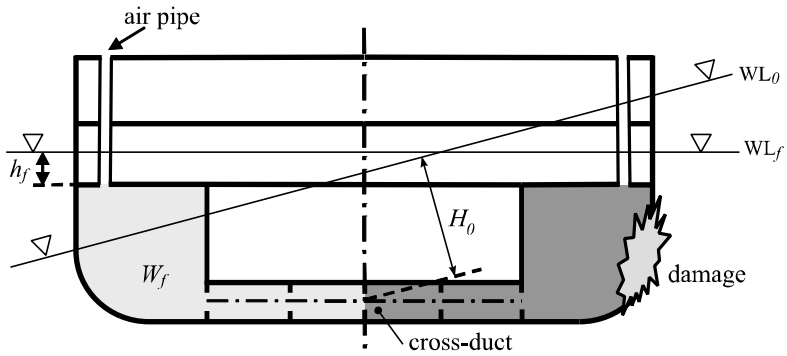

Figure 14.2 Principles of cross-flooding in a large U-shaped void (dark shaded area is treated as lost buoyancy)

The instantaneous flooding rate through an opening can be calculated by applying Bernoulli's theorem for a streamline between the points A and B, as illustrated in Figure 14.3. The velocity is considered to be zero at point A (far away from the opening). Furthermore, by assuming constant air pressure, i.e. $p_A = p_B$, the volumetric flow rate through a small opening is:

$$Q = C_{\mathrm{d}} A \sqrt{2g(h_{\mathrm{A}} - h_{\mathrm{B}})} \tag{14.1}$$

where h is the water level height, measured from a common reference level, A is the area of the opening, and C_{d} is a discharge coefficient that represents the pressure losses, e.g. due to friction and flow contraction. In cross-flooding calculations, the structural duct is usually considered as a single opening, and the effects of the girders are accounted for in the discharge coefficient. For large openings, the flow rate is obtained by integrating equation (14.1) over the submerged area.

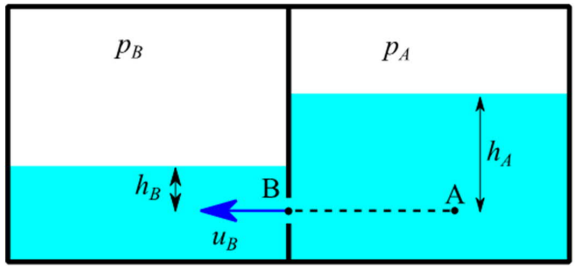

Figure 14.3 Use of Bernoulli's theorem for a streamline in calculation of the flooding rate

For a simple case, Figure 14.2, the cross-flooding time can be approximated as:

$$T_{\mathrm{f}} = \frac{2W_{\mathrm{f}}}{S \cdot F} \cdot \frac{1}{\sqrt{2gH_0}} \cdot \frac{1}{\left(1 + \sqrt{\frac{h_{\mathrm{f}}}{H_0}}\right)} \tag{14.2}$$

where W_{f} is the cross-flooded volume, S is the effective area of the device, and the flow reduction coefficient equals to the effective discharge coefficient of the cross-flooding device, i.e. $F = C_{\mathrm{d}}$. The initial pressure head of floodwater is H_0, and the pressure head at the end of cross-flooding is h_{f}. If the tank extends above the water level, as in Figure 14.2, it equals to zero. Note that the pressure heads are in metres, and thus air compressibility is not considered.

This simple method was introduced by Solda (1961), and it has later been adopted as a recommended procedure MSC.362(92), IMO (2013). It should be noted that this simplified approach is valid only when a single room is flooded through a single connection, directly from the sea.

Air compression in the flooded tanks can be notable, Ruponen et al. (2013), and therefore it is essential that the cross-flooded tanks and void spaces are equipped with large enough air pipes. Proper analysis of ventilation effects requires time-domain simulation, but alternatively the counter air pressure can be accounted for by increasing the effective flow resistance in the cross-flooding duct/pipe, IMO (2013).

According to SOLAS, asymmetric flooding should be kept to a minimum consistent with the efficient arrangements, IMO (2017a), and further that:

> *"For passenger and cargo ships, where cross-flooding devices are fitted, the time for equalization shall not exceed 10 min."*

In addition, the explanatory notes, IMO (2007b), state that if the cross-flooding time exceeds 60 s, the intermediate flooding stage at 60 s needs to be calculated. This requirement encourages designs, where notable asymmetric flooding conditions are properly equalized.

Within the current regulatory framework of SOLAS, cross-flooding devices are the only exception, where the actual time-to-flood is directly considered. Especially with passenger ships, the watertight compartments often contain a lot of non-watertight boundaries, usually referred to as A-class structures, based on the fire-proof rating. These structures can have a significant effect on the flooding process, and time-domain simulation can be used for a more realistic assessment of progressive flooding.

14.2 Accumulation of water on deck

Flooding of the large open vehicle decks on Ro-Ro ships is extremely dangerous. The tragic accidents of HERALD OF FREE ENTERPRISE in 1987 and ESTONIA in 1994 prove this. Therefore, several North-Western European countries soon adopted regional specific additional damage stability requirements, known as the *Stockholm Agreement*. This was later reinforced as an EU directive 2003/25/EC. Contrary to a common practice, this regulation concerned also existing Ro-Ro/passenger (RoPax) ships.

The new water on deck requirements were added to the deterministic damage stability regulations for passenger ships in SOLAS 90. In practice, this means one and two compartment damages with penetration up to $B/5$.

The principle of accumulation of water on deck due to waves is illustrated in Figure 14.4. Flooding of damaged compartments decreases the residual freeboard, and if the breach extends to the vehicle deck, the “pumping” effect of waves can cause accumulation of water on the deck.

The height of accumulated water on deck is evaluated from the diagram in Figure 14.5, based on the residual freeboard height and the significant wave height, H_S. For an unrestricted operational area, $H_\mathrm{S} = 4$ m. The maximum height of water on deck is 0.5 m. Most notably, if the residual freeboard is at least 2.0 m, no water is considered to be accumulated. If the residual freeboard is negative, so that the vehicle deck is submerged, the accumulated height is added on top of the “normal” floodwater on the vehicle deck, Figure 14.6. In practice, new RoPax ships have been designed with a higher freeboard, whereas for older ships, sponsons (see section 5.9) were often needed to ensure sufficient residual stability.

Although the IMO has replaced the deterministic SOLAS 90 regulation with the probabilistic SOLAS 2009/2020 approach, within the European Union and some other countries, the deterministic Stockholm Agreement requirements still need to be passed. Furthermore, recently Cichowicz et al. (2019) have concluded that for RoPax ships with number of passengers $N_\mathrm{p} < 1350$, the new SOLAS 2020 requirements may not ensure the same safety standard as the Stockholm Agreement.

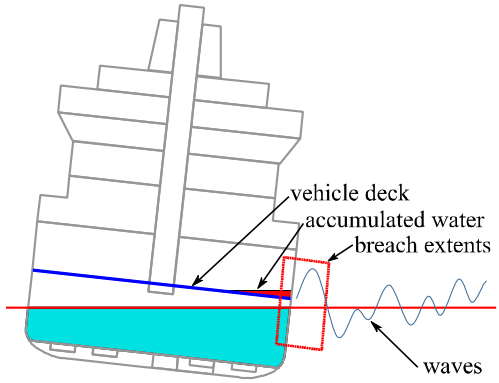

Figure 14.4 Accumulation of water on vehicle deck due to waves

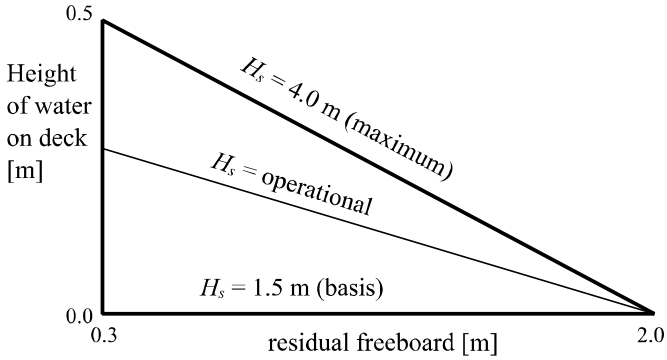

Figure 14.5 Height of accumulated water on the vehicle deck based on residual freeboard and operational significant wave height (H_s) for the Stockholm Agreement

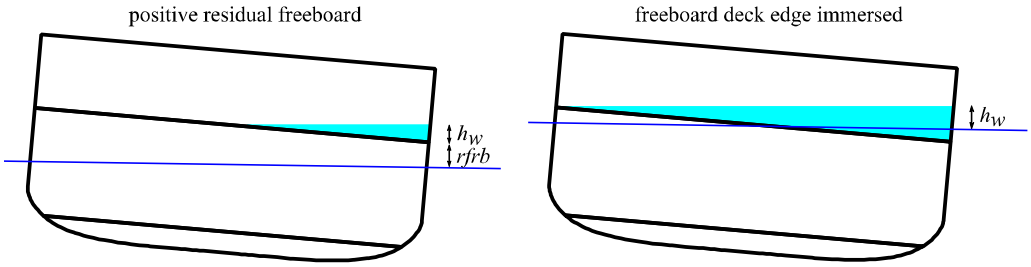

Figure 14.6 Height of accumulated water h_w, depending on the residual freeboard height $rfrb$

The vehicle deck may also become flooded by *firefighting water*. Even a small amount of water in a large open space will result in negative initial metacentric height. With increased heel and trim the free surface area rapidly decreases, and the ship has a stable floating position with an angle of loll. An example is shown in Figure 14.7. Large amounts of firefighting water on the vehicle deck may even cause extensive heeling or even capsizing. For example, in the fire on-board the RoPax ship LISCO GLORIA in 2010, firefighting activities had to be temporarily halted to avoid capsizing.

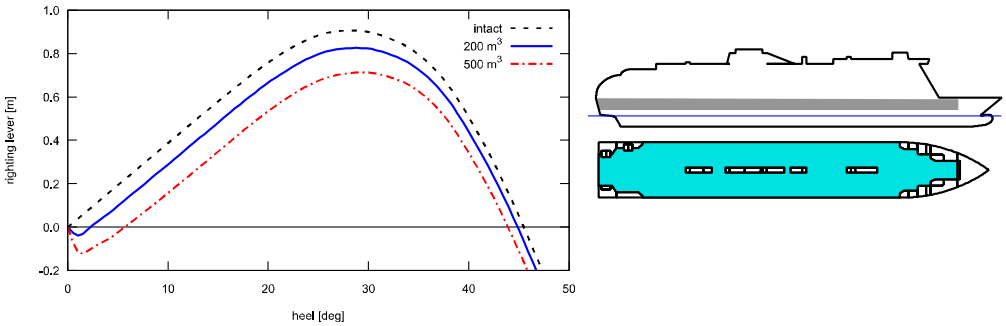

Figure 14.7 Water on deck effect on the righting lever curve; volume 500 m^3 corresponds to about 10 cm of water at upright position

14.3 Time-domain flooding simulation

The regulatory methods are based on a predefined order of intermediate stages of flooding. However, similar to the cross-flooding calculation between a pair of tanks, the whole flooding process can be simulated in time-domain by applying Bernoulli's equation (14.1) for the flow rate through each opening. With increased computing capacity and new advanced simulation methods, the trend of damage stability analyses is towards the time-domain approach, as noted by Papanikolaou (2007). For this reason, the generic principles of a typical hydraulic model for flooding simulation are briefly presented in this section.

The basic governing equations for the flooding process are conservation of mass and momentum, that need to be satisfied at each time step. Considering a constant air pressure and water as incompressible fluid, the volumetric net flow to each compartment must be equal to the sum of the volumetric flow rates $Q_{i,j}$ through the openings that are connected to this compartment:

$$\frac{\mathrm{d}V_i}{\mathrm{d}t} = \sum_{\mathrm{j}} Q_{i,j} \tag{14.3}$$

Here inflow to room i is positive and outflow is negative.

The continuity equation couples the flow rates in the openings to the change of floodwater levels in the compartments. If the time step is short, the free surface area $S_{w,i}$ in the room does not change significantly, and therefore:

$$\frac{\mathrm{d}V_i}{\mathrm{d}t} \approx S_{\mathrm{w},i} \frac{\mathrm{d}H_{\mathrm{w},i}}{\mathrm{d}t} \tag{14.4}$$

where $H_{\mathrm{w},i}$ is the height of water level in the room i. Note that all the heights need to be measured from a common horizontal zero level.

The volumetric flow rates in the openings can be calculated from Bernoulli's equation (14.1), which also represents conservation of momentum. For a small opening with area A and discharge coefficient C_{d} the flow rate is:

$$Q = \mathrm{sign}\left(\max\left(H_{\mathrm{w},i}, H_{\mathrm{o}}\right) - \max\left(H_{\mathrm{w},j}, H_{\mathrm{o}}\right)\right) C_{\mathrm{d}} A \sqrt{2g\left|\max\left(H_{\mathrm{w},i}, H_{\mathrm{o}}\right) - \max\left(H_{\mathrm{w},j}, H_{\mathrm{o}}\right)\right|} \tag{14.5}$$

where H_o is the height of the opening, perpendicular to the sea level in the same coordinate system as the water levels $H_{w,i}$ and $H_{w,j}$, Figure 14.8. The sign function defines the direction of the flow, which is positive from room i to j. For larger openings, the flow rate is obtained by integration over the submerged opening area.

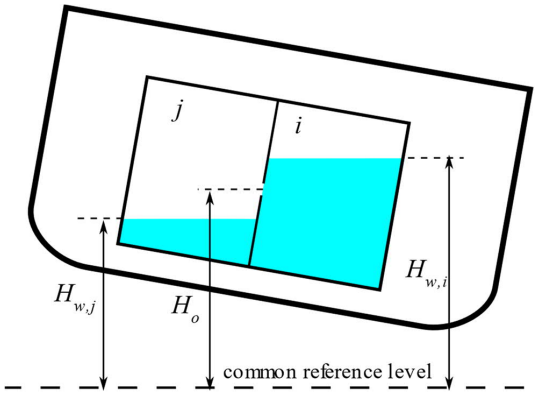

Figure 14.8 Water level and opening heights for calculation of flow rate through a small opening connecting two flooded compartments

For rooms that are filled up with floodwater, the effective (hydrostatic) pressure is larger than the distance from the common reference level to the top of the room. An example is shown in Figure 14.9, where the rooms B and C are filled up, but there is still flow from room A to D. Bernoulli's equation can be used to calculate the flow rate in each opening, A→B, B→C and C→D, if the effective pressure heights $H_{w,B}$ and $H_{w,C}$ are known.

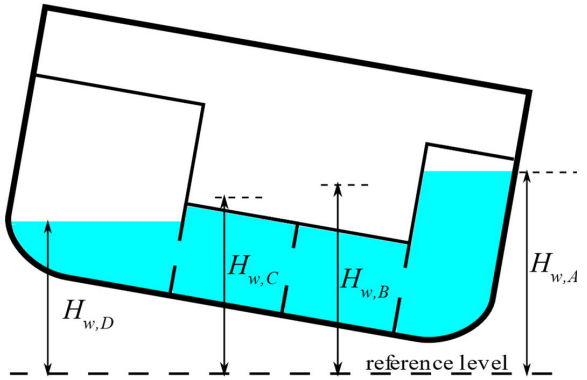

Figure 14.9 Effective hydrostatic pressure levels for filled up rooms

The volumes of floodwater in each compartment can be solved as functions of time with numerical integration. Based on the floodwater distribution, the new floating position of the ship can be solved for each time step. In calm water, a quasi-static model can be applied. Alternatively, dynamic motions can be solved either for roll motion only or for full six degrees-of-freedom. Furthermore, the effects of waves can be considered, as presented e.g. by van't

Veer et al. (2004). This means that the stability of the flooded ship is not considered, only the time-to-capsize or survival for the simulated period of time. In irregular waves, a different realisation of the same sea state, can result in different outcome.

Recently, CFD (Computational Fluid Dynamics) methods have also been used for detailed calculations of the flooding process in simplified scenarios, such as Cheng et al. (2017), but these methods are still much too slow for practical applications. Coupling of CFD for flooding and a potential theory method for damaged ship motions, as presented by Bu and Gu (2020), can improve the computational performance. However, the Bernoulli-based simulation methods are considered accurate enough, especially for modelling progressive flooding, based e.g. on full scale validation results by Ruponen et al. (2010). In the transient flooding stage, the so-called lump mass model can be used to capture the transient dynamics of floodwater, considering also the momentum of the floodwater, Manderbacka et al. (2015).

The assumption of quasi-static ship motions allows for calculation of the righting lever curve at each time step, Ruponen et al. (2018). Therefore, the simulation can also be used for various statutory calculations, as presented in Lindroth et al. (2018), and for example the s-factor can be evaluated. This kind of quasi-static simulation enables a more realistic assessment of the intermediate flooding stages, especially for ships with a complex internal non-watertight subdivision with several A-class fireproof boundaries or cross-flooding devices. However, this approach also requires a much more detailed modelling of the arrangement, including all internal openings, such as doors, with proper characteristics for leakage and collapse, Jalonen et al. (2017).

As an example, an extensive side grounding damage on a large passenger ship, Figure 14.10, is investigated wit time-domain flooding simulation. Time histories for the heel angle with all fire doors open and closed are presented in Figure 14.11. All watertight doors are closed. In addition, detailed analyses on the progress of flooding can be done, and Figure 14.12 shows the difference of the flooding progression after 60 min for the two studied configuration of fire door statuses (open/closed). This example demonstrates that the non-watertight structures, such as closed fire doors, can have a significant effect on the timescale of progressive flooding.

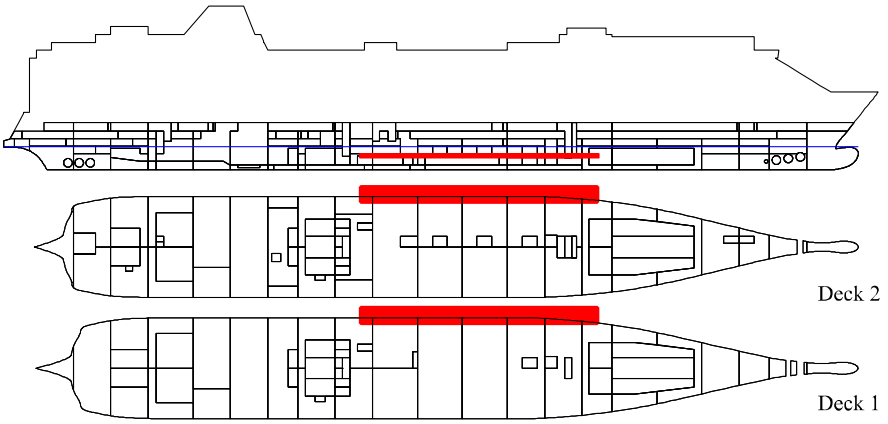

Figure 14.10 Extensive side grounding damage

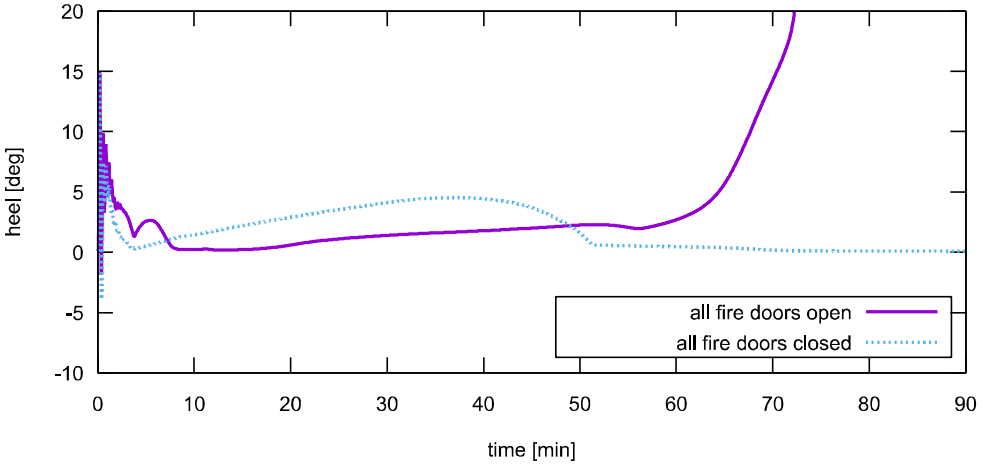

Figure 14.11 Example of flooding simulation results for heel angle; comparison between all fire doors open and closed

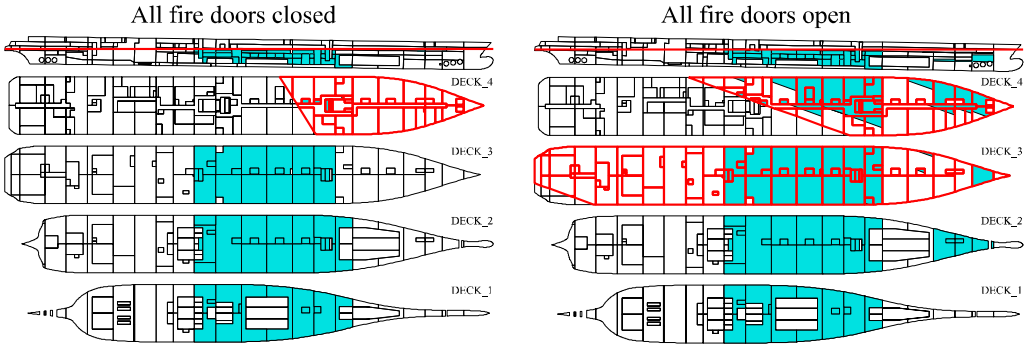

Figure 14.12 Example of detailed analysis of flooding simulation results, 60 min after damage

15 Ship stability in operation

15.1 Loading computer

For safe operation of the ship, it is essential to ensure sufficient stability at all conditions. Therefore, stability calculations and criteria checks are done frequently on board. SOLAS Chapter II-1 Reg. 5-1 defines stability information to be supplied to the master:

> *"The master shall be supplied with such information satisfactory to the Administration as is necessary to enable him by rapid and simple processes to obtain accurate guidance as to the stability of the ship under varying conditions of service."*

In the past the stability of a ship in different loading conditions has been studied manually, using various pre-calculated tables and curves, as described in section 3.2. Nowadays, such basic hydrostatic results have only a little importance since practically all larger vessels are equipped with a *loading computer* on board. This software can typically perform stability calculations and criteria checks, based on a 3D model of the ship or preloaded hydrostatic tables.

The actual filling ratios of various tanks and cargo holds can be obtained from sounding devices, either automatically or manually. Consequently, the centre of gravity of the total weight (lightweight and deadweight) can be calculated. The floating position of the ship is obtained either from draft sensors or read from the draft marks on the hull. Based on this *draft survey*, the actual displacement can be calculated from the hydrostatics. The difference between the actual displacement based on draft survey and the calculated displacement is called *unknown deadweight*.

A loading computer is a statutory instrument, requiring approval. IACS (International Association of Classification Societies), currently identifies four different types of loading computers, IACS (2017):

- Type 1: Software calculating intact stability only (for vessels not required to meet a damage stability criterion).
- Type 2: Software calculating intact stability and checking damage stability on basis of a limit curve (e.g. for vessels applicable to SOLAS Part B-1 damage stability calculations, etc.), or checking all the stability requirements (intact and damage stability) on the basis of a limit curve.
- Type 3: Software calculating intact stability and damage stability by direct application of pre-programmed damage cases based on the relevant Conventions or Codes for each loading condition (for some tankers etc.).
- Type 4: Software calculating damage stability associated with an actual loading condition and actual flooding case, using direct application of user defined damage, for the purpose of providing operational information for safe return to port (SRtP).

15.2 Use of GM limit curves

For the intact stability criteria, the minimum required metacentric height can be solved either analytically or iteratively, by assuming that the residual stability lever curve $\overline{M_0 S}(\phi)$ is independent of the centre of gravity, as presented in section 10.7, and the envelope limit curve can be generated from the limit curves for each individual criterion.

In principle, the same procedure can also be applied to deterministic damage stability requirements at different draft values. However, for probabilistic assessment with a very large number of damage cases this is not viable. Moreover, in a damaged condition, the iteration should include a full calculation of the righting lever curve, since the residual stability lever may also change significantly. Consequently, SOLAS Ch. II-1 Reg. 5-1 states that the metacentric height values for the three characteristic draft values, as used in the probabilistic damage stability calculations (see section 13.3), define the limiting GM curve.

Linear interpolation of the limiting values is applied between the drafts d_s, d_p and d_l. If multiple GM limiting curves are obtained from damage stability calculations with different trim values, an envelope curve covering all calculated initial conditions must be prepared, as shown in Figure 15.1. According to the explanatory notes, IMO (2017b), the limit curve can be extrapolated outside the range of calculated draft values by assuming a constant value. This can be relevant, e.g. when operating in brackish water, Pennanen et al. (2019).

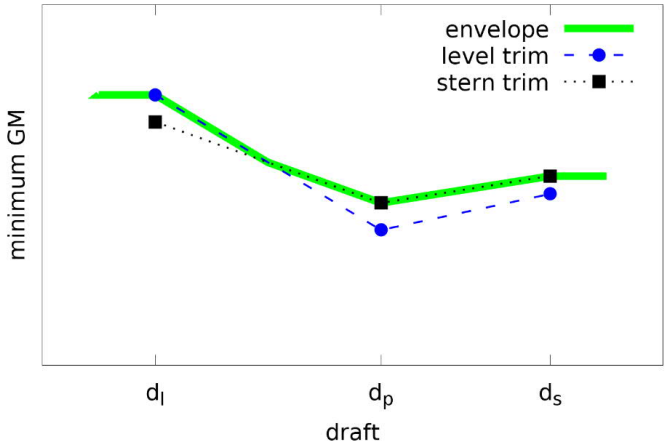

Figure 15.1 Definition of the envelope GM limit curve for probabilistic damage stability requirements

Evaluation of various intact stability criteria for the actual loading condition of the ship is trivial, and it can be done in most loading computers. However, probabilistic damage stability calculations are time-consuming, and cannot be done on board. Therefore, the compliance with damage stability requirements for the actual loading condition is done by comparing the GM value against the limit curve. The damage stability calculations on board (Type 4 loading computer) are intended for use in the event of an accident. A step further is a dedicated decision support system (DSS) for flooding emergencies, as discussed in Ruponen et al. (2019).

15.3 Adverse weather and sea conditions

In adverse weather and sea conditions, a ship may encounter dangerous phenomena, as described in chapter 11. As a result, the ship can experience severe roll motions or even capsize, with significant damage to cargo, equipment, and persons on board. The potential vulnerability of a ship to these phenomena depends on the actual stability parameters, hull geometry, ship size, speed and heading, as well as on the prevailing weather and sea conditions.

IMO has issued circular MSC.1/Circ.1228, IMO (2007), as a general guidance for masters to avoid dangerous conditions at sea. It is recommended to observe the sea state, wave height and period, as well as the ship speed and heading, and to avoid conditions, where surf-riding, pure loss of stability, synchronous rolling or parametric roll resonance could occur.

The concept of the new Second Generation Intact Stability Criteria (see section 11.6) provides methods for preparation of ship specific operational guidance, as outlined in MSC.1/Circ.1627, IMO (2020). In practice, the combinations of ship speed and heading relative to mean wave direction that should be avoided are defined for each relevant sea state and loading condition. A review of recent developments in operational measures for intact stability has been presented in Shigunov et al. (2021).

16 Special stability problems

16.1 Grounding

Ship grounding is the impact of a ship on the seabed. As a result, the ship may be stranded, with or without a breach in the hull. In addition to possible flooding, contact with the seabed can also compromise the stability of a grounded ship. The simplest grounding case is a single point of contact situation, as shown in Figure 16.1.

Another grounding type is often referred to as *shelf grounding* since the ship is supported by a larger contact area with the sea bottom, Figure 16.2. This kind of grounding case can result in tipping over one edge or corner of the shelf, e.g. due to tidal changes in the sea level. As a result, the shelf grounding can develop into a single point of contact case.

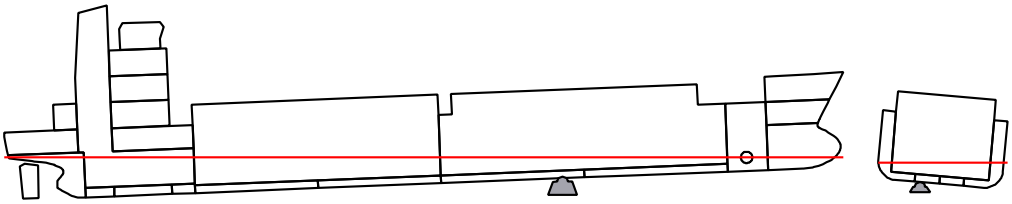

Figure 16.1 Grounding with a single point of contact

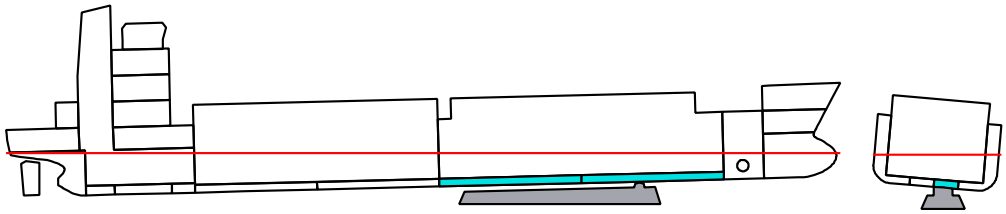

Figure 16.2 Shelf grounding with breach to the double bottom

Let us consider the transverse stability of a grounded ship with a single point of contact, Figure 16.3. The hull is intact and there is no flooding. The displacement in this condition is denoted with Δ_1. In addition to the displacement force and weight W, there is also the contact force P of the ground affecting on the ship hull. The distance between the centre of buoyancy and the point of contact is denoted with a. The weight of the ship and the centre of gravity are unchanged, and the distance between the centre of gravity and point of contact is b.

The force and moment balance results in the following equations:

$$\Delta_1 = W - P \tag{16.1}$$

$$\Delta_1 a = Wb \tag{16.2}$$

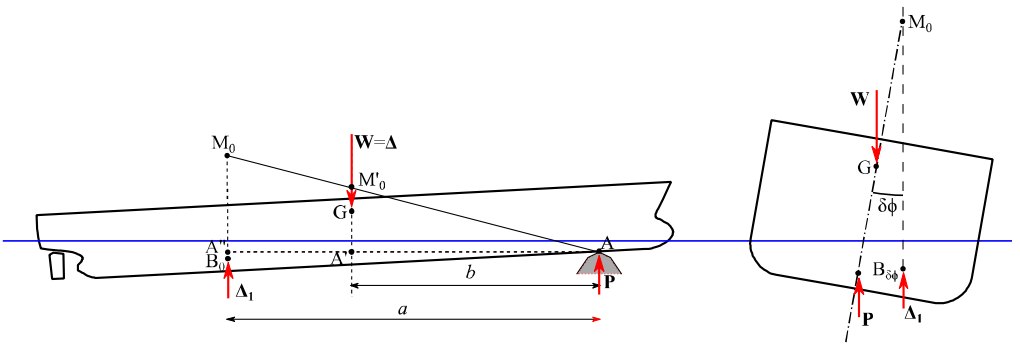

Figure 16.3 Effective metacentre in single point of contact grounding

By assuming a small heel angle $\delta\phi$, the initial stability approximation can be used, and consequently, the static righting moment is:

$$M_{\mathrm{st}} = -\left(\Delta_1 \overline{A''M_0} - W\overline{A'G}\right)\sin\delta\phi \tag{16.3}$$

By substituting the new displacement, solved from equation (16.2), and since $W = \Delta$, the righting moment can be presented as:

$$M_{\mathrm{st}} = -\left(W\frac{b}{a}\overline{A''M_0} - W\overline{A'G}\right)\sin\delta\phi = -\Delta\left(\frac{b}{a}\overline{A''M_0} - \overline{A'G}\right) \tag{16.4}$$

Based on Figure 16.3 and the similarity of the triangles $AA'M_0$ and $AA''M'_0$:

$$\frac{b}{a}\overline{A''M_0} = \overline{A'M_0} \tag{16.5}$$

and therefore, the effective metacentric height is:

$$\overline{GM'_0} = \frac{b}{a}\overline{A''M_0} - \overline{A'G} = \overline{A'M_0} - \overline{A'G} \tag{16.6}$$

Consequently, a grounding with a single point of contact decreases the initial stability of the ship.

Tidal changes are important in the assessment of stability for a grounded ship. High tide may help to re-float the ship, but on the other hand, low tide may compromise the stability.

The previous analysis is based on the assumption that the point of contact is known. In emergency response and salvage operations this is usually not known accurately before inspections have been performed by divers. However, the displacement and floating position can also be evaluated from draft survey results. Using the equations (16.1) and (16.2), the point of contact can be solved when the weight is known, and the displacement is calculated based on the observed floating position.

Similar grounding calculations can also be done for a flooded ship. If the lost buoyancy method (see section 12.8) is used, the damaged compartments need to be reduced from the buoyant hull for calculation of the displacement in the grounded condition. Moreover, it should be noted that the point of contact may be within this region of lost buoyancy.

16.2 Launching

In this section, the mechanics of commonly used longitudinal launching, with stern first, are presented. Using this arrangement, the ship slides on a slipway under her own weight from the building site into water, Figure 16.4. In general, the launching process can be divided into four characteristic phases:

1. Dry sliding
2. Wet sliding (ship parallel to the slipway)
3. Sliding with ship rotation
4. Free floating

From a stability point of view, the third phase is the most critical one, Figure 16.5. Usually, it can be assumed that the speed of the ship is low, as she moves along the slipway, and therefore, the influence of the hydrodynamic forces is negligible. Consequently, the stability in this stage can be evaluated with the same approach as in the case of a single point of contact grounding damage, described in section 16.1.

If the slipway is not long enough, the ship leaves it before the displacement is close to the weight of the ship. As a result, the bow drops suddenly, and there must be enough water depth to avoid damages. Also tipping, where the stern goes down, is possible if the slipway is not long enough. Therefore, the moment of the buoyancy force about the slipway edge must always be larger than the moment of weight about that point.

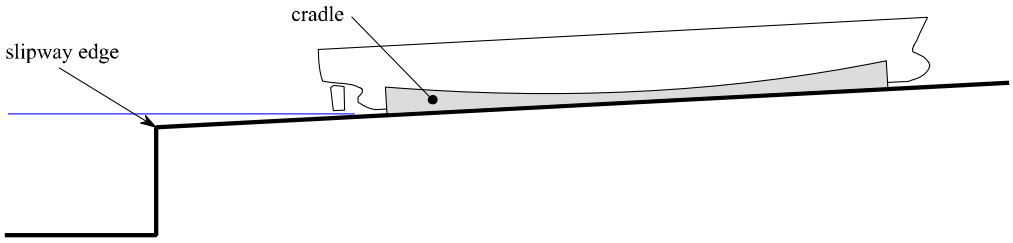

Figure 16.4 Schematic presentation of launching on a longitudinal slipway

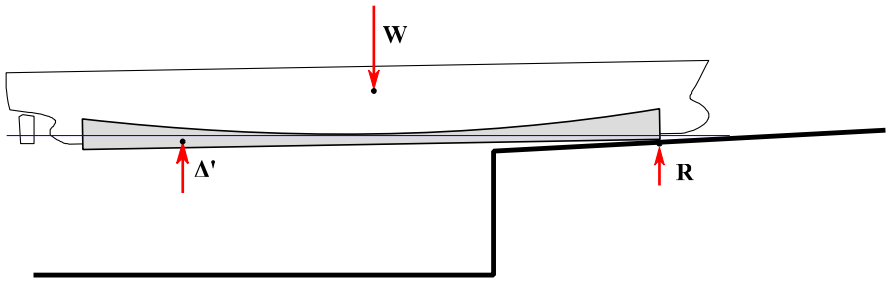

Figure 16.5 Critical moment of end launching with ship rotating around the single point of contact with the slipway

Sometimes side launching is used, especially for small ships and at shipyards located at riverbanks. A schematic presentation of the process is shown in Figure 16.6. This type of launching is a very dynamic process that needs to be carefully planned and analysed, to avoid capsizing. Roll angle can exceed 30° and the watertightness of the hull must be ensured since some openings may temporarily be immersed during the launching process. In addition, the generated waves may cause damage on the adjacent shoreline.

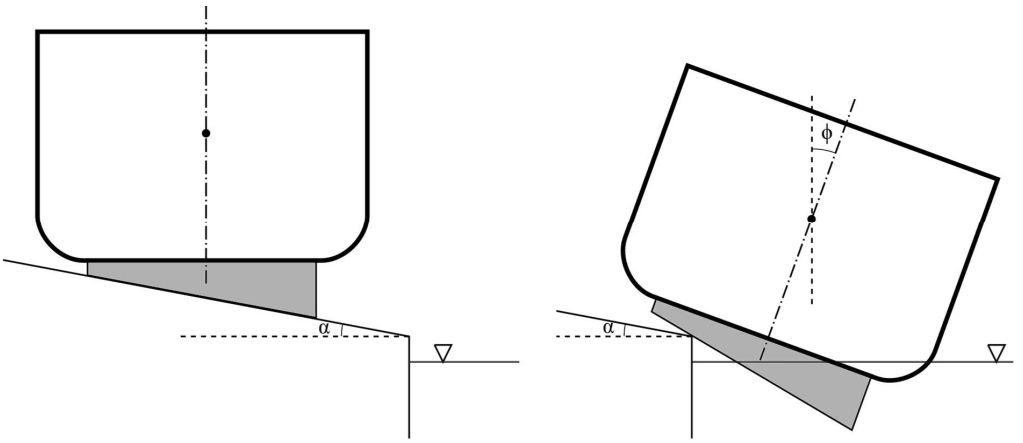

Figure 16.6 Visualization of side launching

16.3 Stability of high-speed craft

This book concentrates on displacement ships, where the weight of the ship is supported by the hydrostatic lift, i.e. buoyancy. At zero speed, the weight of the vessel is always borne entirely by the buoyancy force. Independent of the hull form, at low speeds the buoyancy force is mainly responsible for supporting the vessel. However, with increased speed, the hydrodynamic lift increases as well. In contrast, the buoyancy force decreases since the hull is lifted out of the water, thus decreasing the volume of displacement. At a certain speed, the dynamic lift becomes the predominant upward force, and the vessel is *planing*.

The approximate upper limit of displacement ships is $Fn < 0.5$ and the lower limit for full planing craft is $Fn > 1.0$, Molland et al. (2011). The intermediate condition, where both buoyancy and dynamic lift are notable, is called either semi-displacement or semi-planing speed.

The stability of a fast craft can be studied with a dynamic inclining test for a scale model. The model is towed with different speeds and exposed to an external heeling moment. The actual GM at this speed can be evaluated, as presented for a static inclining test in chapter 8. A schematic example of the GM, as a function of the Froude number for a fast ship with round bilge, is presented in Figure 16.7.

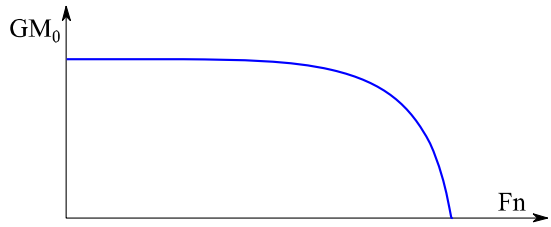

Figure 16.7 Schematic example of GM as function of Froude number for a ship with round bilge

At a certain threshold velocity, the ship loses her transverse stability completely. This velocity is highly dependent on the hull form, especially the part where the dynamic lifting force acts. A comprehensive discussion on dynamic stability of planning crafts is given by Blount and Codega (1992). In principle, the reduction of stability due to the resultant force of the dynamic pressure, Figure 16.8, is very similar to a single point of grounding condition, presented in Figure 16.3.

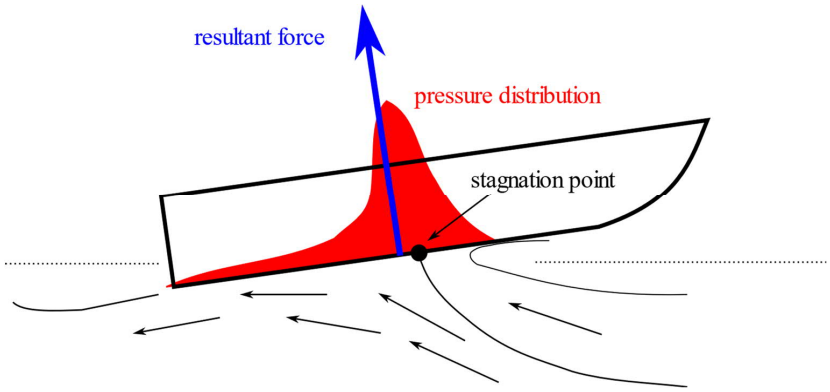

Figure 16.8 Schematic presentation of dynamic pressure on a semi-planing fast craft

It should also be noted that instead of Froude number, the IMO interpretation for a high-speed craft is that the maximum velocity (m/s) is:

$$V_s \geq 3.7\nabla^{0.1667} \tag{16.7}$$

where ∇ is the volume of displacement corresponding to the design waterline (m^3).

One special catamaran type is known as *SWATH* (small waterplane area twin hull), Figure 16.9. This concept minimizes the waterplane area, while the twin hull design provides a stable platform with broad decks. Most of the displacement volume is located deep beneath the waterline, thus minimizing the wave effects, and ensuring good seakeeping characteristics.

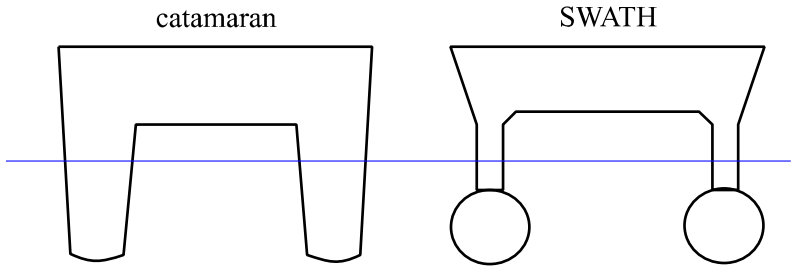

Figure 16.9 Schematic comparison of conventional catamaran design and SWATH

A comparison of the righting lever curves for generic conventional catamaran and SWATH concept, with the same displacement and vertical centre of gravity, is presented in Figure 16.10. Due to the much smaller water plane area, the SWATH has much smaller initial metacentric height, thus avoiding excessive accelerations (see chapter 11.5). For both concepts, the maximum righting lever is achieved at a quite small heel angle (about 22°), when one of the hulls emerges from the water. Yet, the range of positive stability is large.

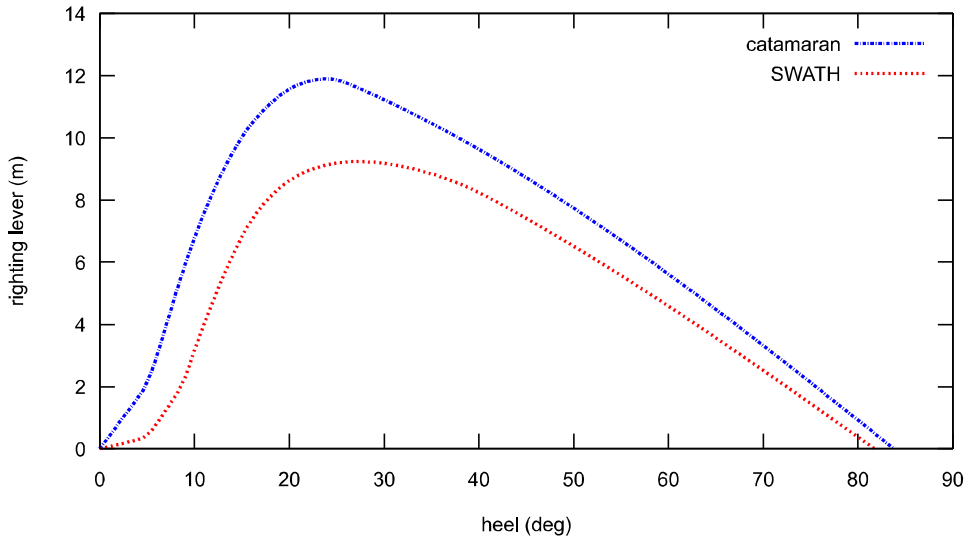

Figure 16.10 Comparison of righting lever curves for a catamaran and SWATH vessels with the same displacement and vertical centre of gravity

16.4 Towing operations

Ships engaged in towing operations can be subjected to large heeling moments, and various administrations have issued specific stability criteria for these operations. Recently, guidance and stability criteria for towing operations were introduced with the amendments to the 2008 IS Code, as presented in IMO (2016).

The main principles of these stability criteria are very similar to the general intact stability criteria, presented in chapter 10, but including an external heeling moment lever. In the case of towing, two separate heeling moments are considered:

- *tow-tripping*: the towline force is caused by the tow, dragging the ship; moment depends on the lateral underwater area of the ship (drag) and velocity and angle of the tow
- *self-tripping*: the towline force is caused by the action of the towing vessel; moment depends on the bollard pull force of the propellers

The regulation, IMO (2016), gives detailed equations for calculation, based on the geometry of the ship arrangement, namely:

- coordinates of the towing point
- coordinates of the propulsion point (intersection of propeller axis and propeller plane)

For the self-tripping condition, the heeling lever as a function of the heel angle ϕ is defined as:

$$l(\phi) = \frac{F_{\mathrm{bp}} C_{\mathrm{T}}}{\Delta} (h \cos\phi - r \sin\phi) \tag{16.8}$$

where F_{bp} is bollard pull in kN, coefficient $C_{\mathrm{T}} \in [0.5, 0.9]$ depends on the propulsion arrangement, with value 0.5 for conventional units and higher values for azimuthing propulsors, Δ is the displacement force (kN), h is the vertical distance between the towing point and the horizontal centreline of the propulsion unit(s), and r is the transverse distance between the centreline and the towing point. The condition is visualized in Figure 16.11. Note that with an asymmetric towing point, the opposite direction produces a larger moment since in that case r is negative.

The self-tripping is a dynamic phenomenon that requires consideration of a dynamic stability reserve when the ship is subjected to a stepwise heeling moment, see section 9.6. In principle, the area "a" between the righting lever curve and heeling moment lever curve, bounded by the static equilibrium heel angle ϕ_{e} and the minimum of the second interception angle ϕ_{c} and the flooding angle ϕ_{f} should be greater than the area "b" between the heeling moment lever and righting lever curves from upright to equilibrium heel, Figure 16.12.

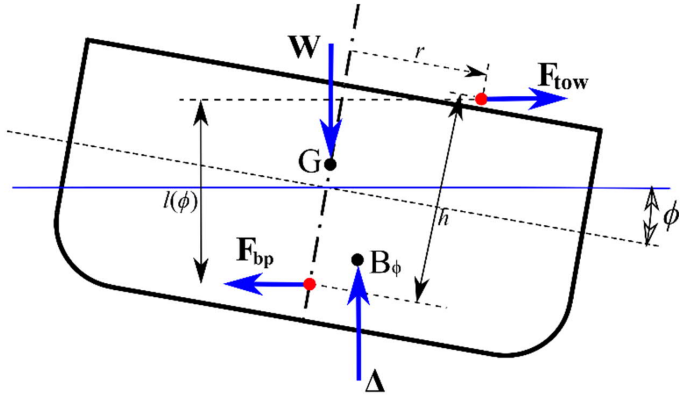

Figure 16.11 Forces and definitions for self-tripping in towing operation

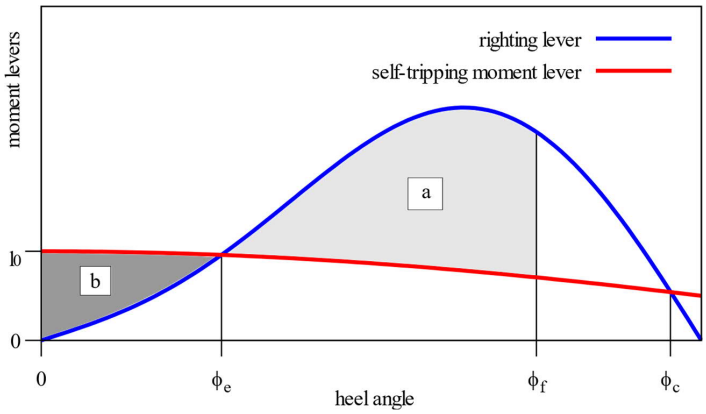

Figure 16.12 Stability criterion for self-tripping condition in towing operation

The tow-tripping moment is calculated based on the towing velocity, and lthe ateral area of the underwater hull. The condition can be considered quasi-static, Figure 16.13, and therefore, IMO (2016) requires that the steady equilibrium heel under this external moment should be less than the down-flooding angle.

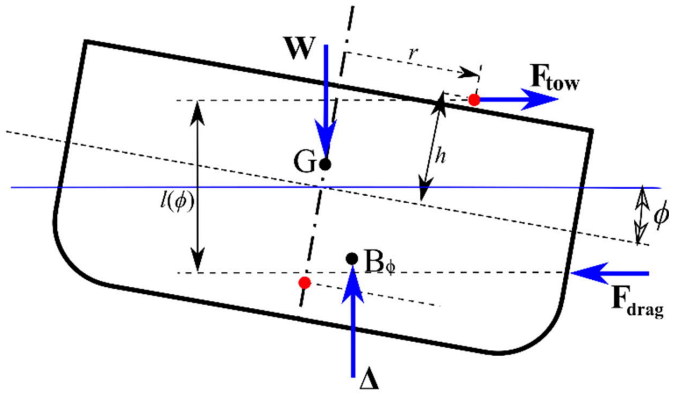

Figure 16.13 Forces and definitions for tow-tripping in towing operation

16.5 Anchor handling operations

Anchor handling operations are similar to towing, and the AHTS (anchor handling tug supply) vessels can be subjected to large heeling moments. The capsize of the AHTS BOURBON DOLPHIN, while anchoring a semisubmersible drilling platform in 2007, was a major driver for development of improved stability criteria, which were recently issued in the amendments to the IS Code, IMO (2016).

For anchor handling criteria, the heeling lever is defined similarly to the towing criteria:

$$l(\phi) = M_{AH} \cos \phi / \Delta_2 \quad (16.9)$$

The displacement force Δ_2 includes also the action of vertical loads added at the centreline in the stern of ship. Moreover, the moment M_{AH} is evaluated based on the vertical and horizontal components of the tension applied to the wire, as well as the permissible wire tension, as explained in IMO (2016).

The stability requirements are illustrated in Figure 16.14, and include:

- The residual area between the righting lever curve and the heeling lever should not be less than 0.070 m·rad between the static equilibrium heel angle ϕ_e and the minimum of the second interception angle ϕ_{c} and the flooding angle ϕ_{f}
- The maximum *residual righting lever* $\overline{GZ}(\phi) - l(\phi)$ should be at least 0.2 m
- The static equilibrium heel angle ϕ_{e} should be less than the minimum of the following:
    - the angle at which the righting lever equals 50% of the maximum righting lever;
    - deck edge immersion angle; or
    - 15°

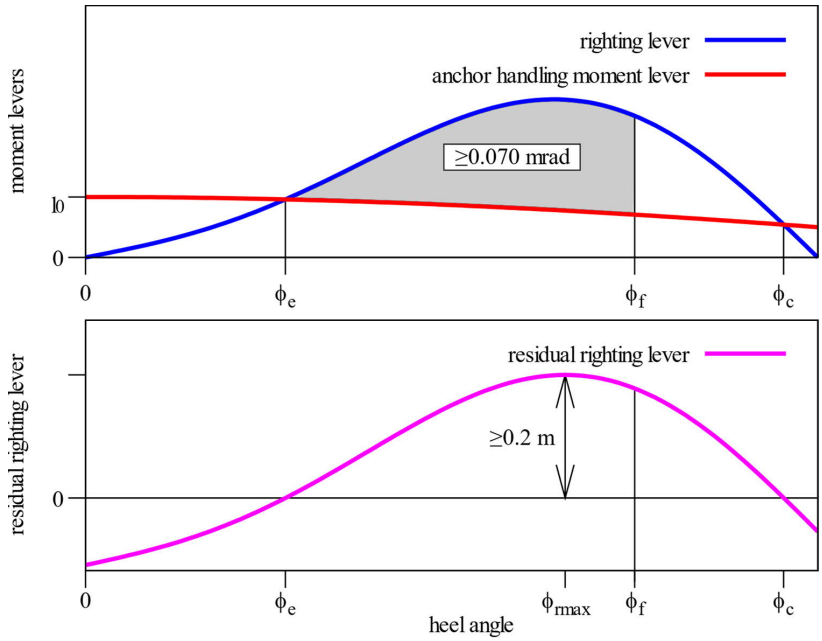

Figure 16.14 Stability criteria for anchor handling operations

16.6 Heavy lift operations

Lifting a heavy weight with crane(s) usually requires counter ballasting in order to avoid extensive heeling of the ship. A typical situation is illustrated in Figure 16.15. The amount of ballast water is controlled for each phase of the lifting process. However, large asymmetric ballasting can compromise the stability of the ship in a situation, where the cable breaks and the load is dropped.

The stability of heavy lift vessels has been extensively studied, e.g. by Hatecke (2016). With the recent amendments to the IS Code, IMO (2016), international stability criteria for lifting operations are now included. Physically, the most interesting stability requirement concerns a sudden loss of the hook load, and this criterion is explained in the following.

Consider a situation, where counter ballasting is used in a lifting operation, and suddenly the cable breaks, and the heavy load is dropped, Figure 16.16. Obviously, a dynamic stability analysis is needed, and it is not sufficient to study only the static equilibrium after the event.

An example case is illustrated in Figure 16.17. The steady heel angle before the load drop is 1.9° and after the event it is -19.6°. The ship avoids capsizing if the area “a”, limited by the immersion angle and the steady equilibrium heel, is larger than the area “b”, limited by the initial heel angle before the load drop and the final steady heel angle.

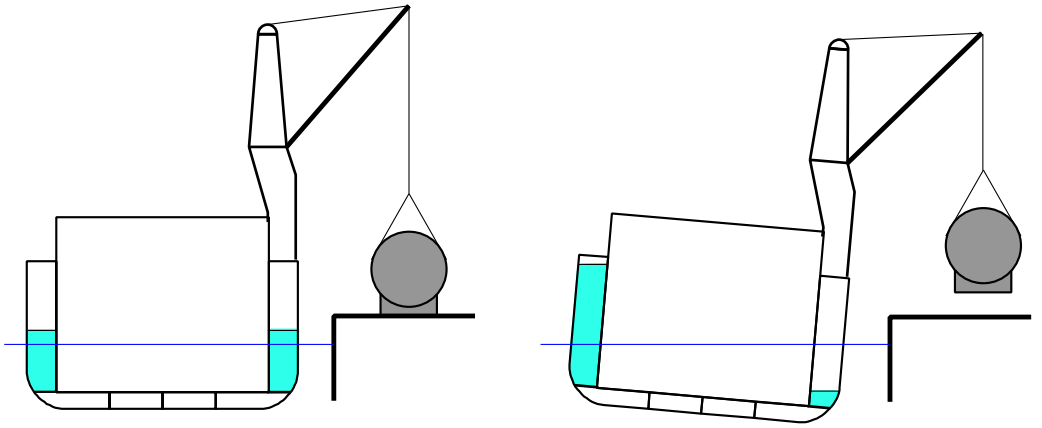

Figure 16.15 Counter-ballasting to reduce heeling during a heavy lift operation

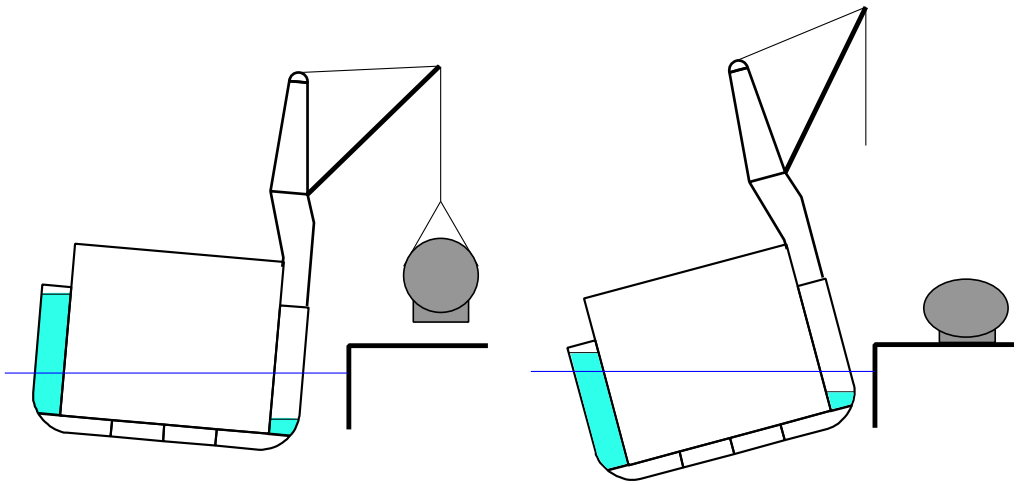

Figure 16.16 Drop of load in a heavy lift operation

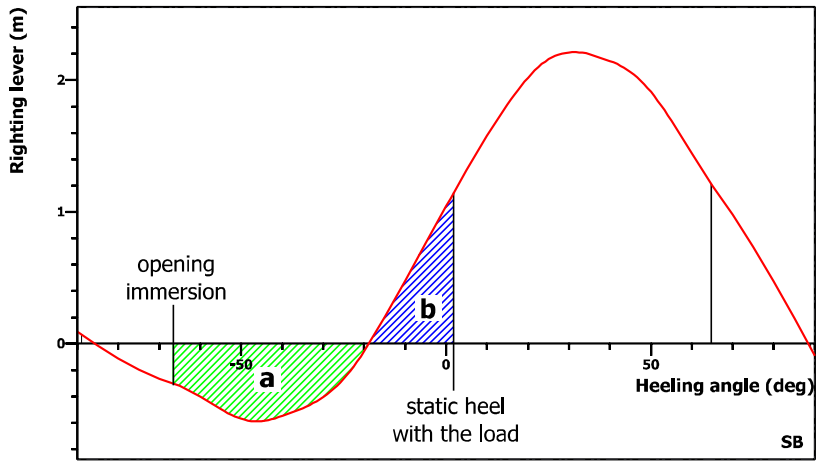

Figure 16.17 Criterion to ensure sufficient stability in case of a sudden load drop

Stability criteria for lifting operations have been included in the recent amendments to the IS Code, IMO (2016), requiring area ratio $a/b \geq 1.4$ for operation in exposed waters, otherwise the requirement for the ratio is 1.0. In the presented example, the area ratio is 1.74, so the presented lifting condition passes this criterion.

16.7 Submerging operations

Semisubmersible heavy lift ships are intentionally "sank" to allow loading of floating cargo, and then lifted with the cargo on deck, Figure 16.18. This kind of operation needs careful planning and stability calculations. A failure in the controlled sinking process can have disastrous consequences, as in the MIGHTY SERVANT 3 accident, analysed in detail by Dankowski and Dilger (2013).

.

Figure 16.18 Semisubmersible heavy lift ship BLUE MERLIN preparing to offload (Photo credit: Jim Hatter, Wikimedia Commons, cc-by-2.0)

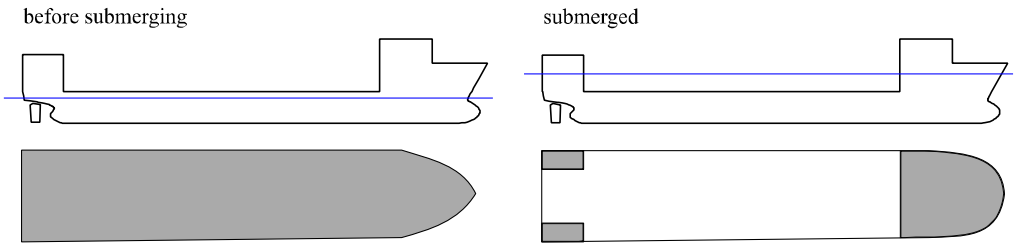

Figure 16.19 Change of waterplane area in the submerging

Changes in the waterplane area can be extremely large, as illustrated in Figure 16.19. Consequently, the stability of the ship must be calculated for all stages of the submerging process. It is favourable to use a small heel angle when the deck is immersed in order to avoid extensive changes in the waterplane area, Wang and Ko (2019).

16.8 Stability of floating offshore structures

There is a large variety of different offshore structure types, with somewhat different stability characteristics. For example, for jack-up rigs the stability needs to be considered for transits, and usually the range of positive stability is quite small. For semisubmersible rigs the stability range is large, but in flooded conditions the tilting can be a major problem.

For ships, the length/breadth ratio is usually large, and therefore, it is usually sufficient to study only the transverse stability (around the x-axis). However, for floating offshore structures, this simplification is not valid. Moreover, even in intact conditions, the waterplane area can be asymmetric. The principal stability axis may be evaluated with equation (4.13). Based on the waterplane area quantities, it is trivial to evaluate the weakest direction. However, as the structure is heeled to this direction, the waterplane may change significantly, and another direction may become much more critical.

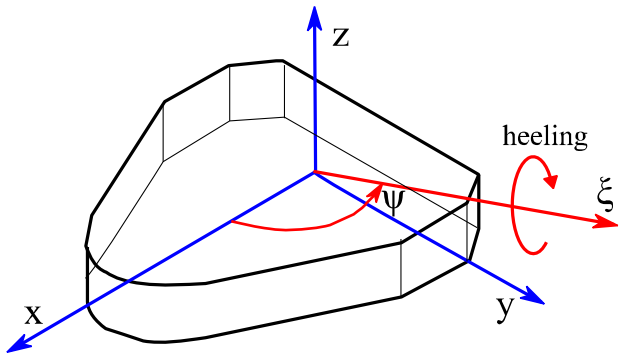

Figure 16.20 Azimuth angle ψ for the studied stability axis ξ

A common practice for floating offshore stability analyses is to assume constant heeling direction, and repeat the calculations for all azimuth angles with a certain step, e.g. 10°.

An alternative approach for stability of floating offshore structures, the so-called *free twist* method, has been developed by van Santen (1986). In this method, the direction of the heeling axis is varied such that the moment around the initial vertical axis is zero. By doing this, the trimming moment (being the horizontal component of the moment around the inclined twist axis) is zero whilst the trim angle is nil. In general, it results in the lowest energy build-up in the system, van Santen (2009).

An example of the righting lever curves with different calculation methods for a "triangular-shaped" floating jack-up platform is shown in Figure 16.21. This case clearly demonstrates that the critical heeling direction is not trivial. The free twist method seems to be rather robust and reliable. However, some administrations may not approve this approach, and a traditional free trim method with different azimuth angles is required instead.

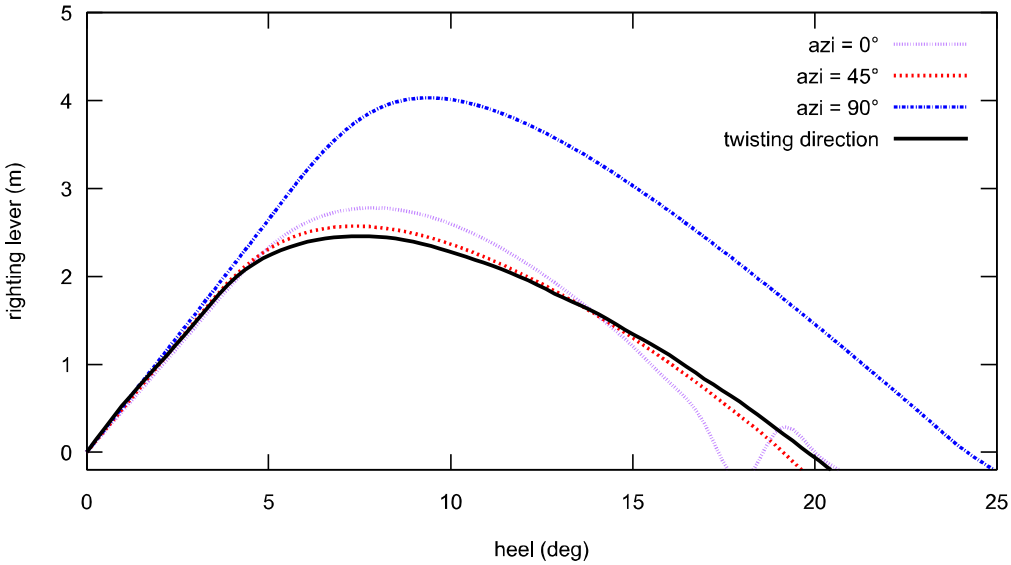

Figure 16.21 Comparison of righting lever curves for a jack-up platform, calculated with three different constant directions and with the so-called free twist method

16.9 Stepped righting lever curve

The normal approach for calculation of stability criteria is to consider the immersion angle of an unprotected opening as the upper limit for the range of stability, as presented in section 10.2, and consequently the righting lever curve at larger heel angles is ignored. However, in rare cases, it may be allowed to account for the additional reserve stability by considering flooding through the immersed openings. In this approach, all enclosed spaces are considered to provide buoyancy in the calculation of the righting lever curve up to the heel angle when an unprotected opening is immersed. Beyond the immersion angle, the connected space is considered as lost

buoyancy. This approach results in distinctive steps in the righting lever curve. An example of this is IMO Resolution A.651(16), IMO (1989).

An example of a stepped righting lever curve is presented in Figure 16.22. The studied case is a column-stabilized platform, where one of the pontoons is damaged. The first unprotected opening OP1 is immersed at a heel angle of 11.5° before the equilibrium floating position is reached. Therefore, at the equilibrium heel of 14.9°, part of the platform is also flooded. There is another step in the righting lever curve at a heel angle of 32.2° when the opening OP2 is immersed, resulting in more extensive flooding and reduced buoyancy.

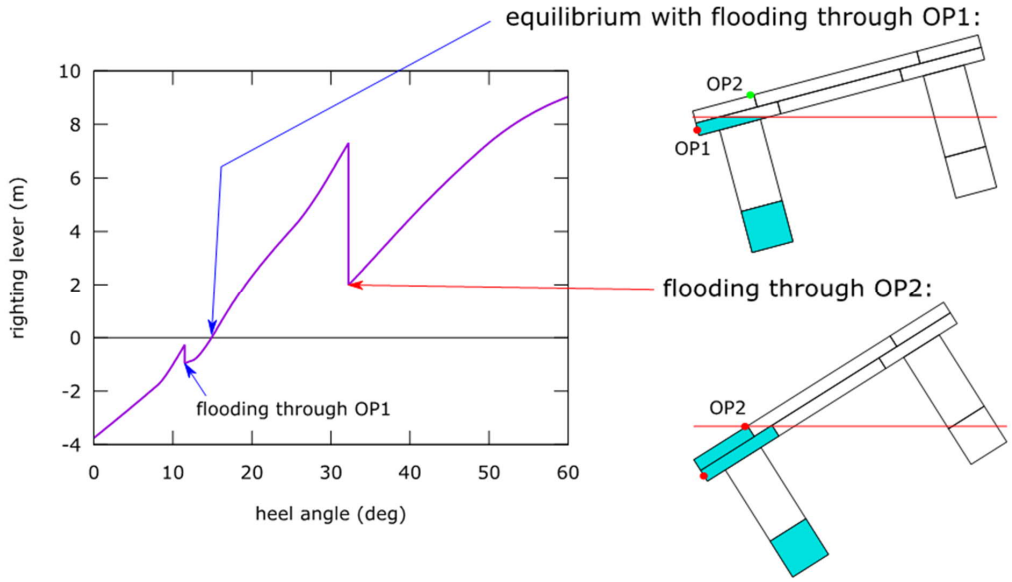

Figure 16.22 Example of a righting lever curve with steps due to progressive flooding; at equilibrium the opening OP1 is submerged and when heel reaches 32.2° also the opening OP2 is immersed, resulting in a reduction of the righting lever

References

Andrei, C., Hanzu Pazara, R. 2013. The Impact of Bulk Cargoes Liquefaction on Ship's Intact Stability, *U.P.B. Sci. Bull., Series D*, Vol. 75, Issue 4, 2013.

Bhattacharyya, R. 1978. Dynamics of Marine Vehicles, John Wiley & Son, 498 p.

Belenky V., Sevastianov N.B., 2007. Stability and Safety of Ships: Risk of Capsizing, 2nd ed., Society of Naval Architects and Marine Engineers, Jersey City, NJ. USA. 449 p.

Belenky, V., Bassler, C. G., Spyrou, K. J., 2011. Development of Second Generation Intact Stability Criteria (No. NSWCCD-50-TR-2011/065). Naval Surface Warfare Center Carderock Div Bethesda Md Hydromechanics Dept.

Blount, D. L., Codega, L. T. 1992. Dynamic stability of planing boats. *Marine Technology*, Vol. 29(1), pp. 4-12.

Bu, S., Gu, M. 2020. Unified viscous and potential prediction method for the coupled motion of damaged ship and floodwater in calm water. *Ocean Engineering*, 210, 107441. https://doi.org/10.1016/j.oceaneng.2020.107441

Bulian, G., Lindroth, D., Ruponen, P., Zaraphonitis, G. 2016. Probabilistic assessment of damaged ship survivability in case of grounding: development and testing of a direct non-zonal approach, *Ocean Engineering*, Vol. 120, pp. 331-338. https://doi.org/10.1016/j.oceaneng.2016.02.018

Bulian, G., Cardinale, M., Francescutto, A., Zaraphonitis, G. 2019. Complementing SOLAS damage ship stability framework with a probabilistic description for the extent of collision damage below the waterline. *Ocean Engineering*, Vol. 186, 106073. https://doi.org/10.1016/j.oceaneng.2019.05.055

Bulian, G., Cardinale, M., Dafermos, G., Lindroth, D., Ruponen, P., Zaraphonitis, G. 2020. Probabilistic assessment of damaged survivability of passenger ships in case of grounding or contact. *Ocean Engineering*, 218, 107396. https://doi.org/10.1016/j.oceaneng.2020.107396

Cheng, H., Zhang, A. M., Ming, F. R. 2017. Study on coupled dynamics of ship and flooding water based on experimental and SPH methods, *Physics of Fluids* 29, 107101

Cichowicz, J., Olufsen, O., Vassalos, D. 2019. Ro-Ro passenger ships – from Stockholm Agreement to SOLAS2020, *Proceedings of the 17th International Ship Stability Workshop (ISSW2019)*, Helsinki, Finland 10-12 June 2019, pp. 199-207.

Conti, F., Le Sourne, H., Vassalos, D., Kujala, P., Lindroth, D., Kim, S.J., Hirdaris, S. 2021. A comparative method for scaling SOLAS collision damage distributions based on ship crashworthiness–application to probabilistic damage stability analysis of a

passenger ship. *Ships and Offshore Structures*, (pre-print published online) pp. 1-17. https://doi.org/10.1080/17445302.2021.1932023

Dankowski, H., Dilger, H. 2013. Investigation of the Mighty Servant 3 accident by a progressive flooding method, Proceedings of the ASME 2013 32nd International Conference on Ocean, Offshore and Arctic Engineering OMAE2013, June 9-14, 2013, Nantes, France.

Ferreiro, L.D. 2020. Bridging the Seas – The Rise of Naval Architecture in the Industrial Age, 1800-2000, MIT Press, 386 p.

Francescutto, A., Papanikolaou, A. 2011. Buoyancy, Stability, and Subdivision: From Archimedes to SOLAS 2009 and the Way Ahead, *Proc IMechE Part M: J Engineering for the Maritime Environment*, Vol. 225(1) pp. 17-32. https://doi.org/10.1177/14750902JEME238

Hatecke, H. 2016. Dynamic Stability of Heavy Lift Vessels during Loss of Tandem Load, Doctoral Dissertation, Technical University of Hamburg.

Himeno, Y. 1981. Prediction of ship roll damping-a state of the art. University of Michigan.

Hsueh, W.J., Lee, Y.J. 1997. A design for ship stabilization by activated antiroll tanks, *J Mar Sci Technol*. Vol. 2, Issue 2, pp. 77-86. https://doi.org/10.1007/BF02491522

IACS 2017. Computer software for onboard stability calculations, UICS Unified Requirement L5 Rev.3, June 2017. http://iacs.org.uk/download/4196

IMO 1989. An Example of Alternative Stability Criteria for a Range of Positive Stability after Damage or Flooding for Column-Stabilized Semisubmersible Units, Resolution A.651(16), adopted on 19 October 1989.

IMO 1991. International Code for the Safe Carriage of Grain in Bulk (International Grain Code).

IMO 2001. SOLAS Consolidated Edition 2001.

IMO 2006. Interim Guidelines for Alternative Assessment of the Weather Criterion, MSC.1/Circ.1200, 24 May 2006.

IMO 2007. Revised Guidance to the Master for Avoiding Dangerous Situations in Adverse Weather and Sea Conditions, MSC.1/Circ.1228, 11 January 2007.

IMO 2008. Adoption of the International Code on Intact Stability 2008 (2008 IS Code), Resolution MSC.268(85).

IMO 2013. Revised Recommendation on a Standard Method for Evaluating Cross-Flooding Arrangements, Resolution MSC.362(92), Adopted on 14 June 2013.

IMO 2016. Amendments to Part B of the International Code on Intact Stability, 2008 (2008 IS Code), Resolution MSC.415(97), adopted on 25 November 2016.

IMO 2017a. Amendments to the International Convention for the Safety of Life at Sea 1974, as amended, Resolution MSC.421(98).

IMO 2017b. Revised Explanatory Notes to the SOLAS Chapter II-1 Subdivision and Damage Stability Regulations, Resolution MSC.429(98).

IMO 2020. Interim Guidelines on the Second Generation Intact Stability Criteria, MSC.1/Circ.1627, 10 December 2020.

Intercargo 2019. Bulk Carrier Casualty Report - Years 2009 to 2018 and trends, International Association of Dry Cargo Shipowners. https://www.intercargo.org/wp-content/uploads/2019/02/Bulk-Carrier-Casualty-Report-2018-publisher-version-10Apr2019.pdf

ITTC 2011. Numerical Estimation of Roll Damping, Recommended Procedures and Guidelines 7.5-02-07-04.5, International Towing Tank Conference. https://www.ittc.info/media/8151/75-02-07-045.pdf

Jakubowski, P., Bieniek, N. 2010. Experiments with leaking and collapsing structures, FLOODSTAND Deliverable D2.1b. http://floodstand.aalto.fi/Info/Files/FLOODSTAND_Deliverable_D2.1b_final_v.1.6.pdf

Jalonen, R., Ruponen, P., Weryk, M., Naar, H., Vaher, S. 2017. A study on leakage and collapse of non-watertight doors under floodwater pressure, *Marine Structures*, Vol. 51, pp. 188-201. https://doi.org/10.1016/j.marstruc.2016.10.010

Karolius, K.B., Vassalos, D. 2018. Weight and buoyancy is the foundation in design: Get it right, *Marine Design XIII*, pp. 727-736.

Kim, Y., Seo, M.-G., Lee, J.-H. 2019. Numerical simulation of Sewol ferry capsize. *Proceedings of the Institution of Mechanical Engineers, Part M: Journal of Engineering for the Maritime Environment*, Vol. 233(1), pp. 186–208. https://doi.org/10.1177/1475090217729045

Kobylinski, L., Kastner, S., 2003. Stability and Safety of Ships, Volume 1: Regulations and Operation, Vol. 9, Elsevier Engineering Book Series, Elsevier, Amsterdam, Netherlands. 412 p.

Kobylinski, L. 2014. Stability Criteria - Present Status and Perspectives of Improvement, *TRANSNAV the International Journal on Marine Navigation and Safety of Sea Transportation*, Vol. 8, Number 2, pp. 281-286.

Kula, K.S. 2015. An Overview of Roll Stabilizers and Systems for Their Control, *TransNav: International Journal on Marine Navigation and Safety of Sea Transportation*, Vol. 9, Number 3, pp. 405-414.

Li, Y., Sobey, A.J., Tan, M., 2014. Investigation into the effects of petalling on coefficient of discharge during compartment flooding. *Journal of Fluids and Structures*, Vol. 45, pp. 66–78. https://doi.org/10.1016/j.jfluidstructs.2013.11.016

Lindroth, D., Ruponen, P., Tompuri, M. 2018. Application of Flooding Simulation for a Detailed Analysis of SOLAS Damage Stability Results, *Proceedings of the 13th International Conference on the Stability of Ships and Ocean Vehicles*, 16-21 September 2018, Kobe, Japan, pp. 608-615.

Luhmann, H., Cardinale, M., Wettstein, N., Routi, A-L., Bertin, R. 2019. Analysis of Permeabilities, Deliverable D2.3, Project FLARE. https://flare-project.eu/images/downloads/191125_FLARE_Deliverable_2.3_Final.pdf

Manderbacka, T., Mikkola, T., Ruponen, P., Matusiak, J., 2015. Transient response of a ship to an abrupt flooding accounting for the momentum flux. *Journal of Fluids and Structures*, Vol. 57, pp. 108–126. https://doi.org/10.1016/j.jfluidstructs.2015.06.001

Matusiak, J. 2000. Laivan kelluvuus ja vakavuus, 4th edition, Otatieto, 180 p. (in Finnish)

Matusiak, J., Stigler, C. 2012. Ship Roll Motion in Irregular Waves During a Turning Circle Maneuver, *Proceedings of the 11th International Conference on the Stability of Ships and Ocean Vehicles*, 23-27 September 2018, Athens, Greece, pp. 291-297.

Mégel, J., Kliava, J. 2010. Metacenter and ship stability, *American Journal of Physics*, Vol. 78, No. 7, pp. 738-747.

Molland, A.F., Turnock, S.R., Hudson, D.A. 2011. Ship Resistance and Propulsion, Cambridge University Press, 537 p.

Moseley, H. 1850. On the dynamical stability and on the oscillations of floating bodies, *Philosophical Transactions of the Royal Society of London*, Vol. 140, pp. 609-643.

Nowacki, H. Ferreiro, L.D. 2003. Historical Roots of the Theory of Hydrostatic Stability of Ships, *Proceedings of the 8th International Conference on the Stability of Ships and Ocean Vehicles, STAB2003*, Madrid, Spain.

Papanikolaou, A.D. 2007. Review of Damage Stability of Ships – Recent Developments and Trends, *Proceedings of the 10th Int. Symposium on Practical Design of Ships and Other Floating Structures* (PRADS 2007), Houston, U.S.A.

Papanikolaou, A., Hamann, R., Lee, B.S., Mains, C., Olufsen, O., Vassalos, D., Zaraphonitis, G. 2013. GOALDS—Goal Based Damage Ship Stability and safety standards, *Accident Analysis & Prevention*, Vol. 60, pp. 353–365. https://doi.org/10.1016/j.aap.2013.04.006

Paterson, D., Vassalos, D., Atzampos, G., Boulougouris, E., Luhmann, H. 2019. Impact of drafts
on the damage survivability of cruise ships. *Ocean Engineering*, Vol. 187, Article 106136. https://doi.org/10.1016/j.oceaneng.2019.106136

Pennanen, P., Lindroth, D., Ruponen, P. 2019. GM limiting curve for operation in brackish water, *Proceedings of the 17th International Ship Stability Workshop (ISSW2019)*, Helsinki, Finland 10-12 June 2019, pp. 191-197.

Rahola, J. 1939. The Judging of the Stability of Ships and the Determination of the Minimum Amount of Stability – Especially Considering the Vessels Navigating Finnish Waters, Doctoral Thesis, https://aaltodoc.aalto.fi/handle/123456789/15149

Rawson, K.J., Tupper, E.C. 2001. Basic Ship Theory, 7th Edition, Butterworth-Heinemann, 727 p.

Rosen, A., Huss, M., Palmquist, M. 2012. Experience from Parametric Rolling of Ships, *Parametric Resonance in Dynamical Systems*. Springer, New York. p. 147-165.

Ruponen, P., Kurvinen, P., Saisto, I., Harras, J., 2010. Experimental and numerical study on progressive flooding in full-scale. *Transactions of the Royal Institute of Naval Architects, International Journal of Maritime Engineering*, Vol. 152, Part A4, pp. A-197–207.

Ruponen, P., Queutey, P., Kraskowski, M., Jalonen, R., Guilmineau, E. 2012. On the calculation of cross-flooding time, *Ocean Engineering*, Vol. 40, February 2012, pp. 27-39.
https://doi.org/10.1016/j.oceaneng.2011.12.008

Ruponen, P., Kurvinen, P., Saisto, I., Harras, J. 2013. Air compression in a flooded tank of a damaged ship, *Ocean Engineering*, Vol. 57, pp. 64–71.
https://doi.org/10.1016/j.oceaneng.2012.09.014

Ruponen, P., 2017. On the effects of non-watertight doors on progressive flooding in a damaged passenger ship. *Ocean Engineering*, Vol. 130, pp. 115–125.
https://doi.org/10.1016/j.oceaneng.2016.11.073

Ruponen, P., Manderbacka, T., Lindroth, D. 2018. On the calculation of the righting lever curve for a damaged ship, *Ocean Engineering*, Vol. 148, pp. 313-324.
https://doi.org/10.1016/j.oceaneng.2017.12.036

Ruponen, P., Pennanen, P., Manderbacka, T. 2019. On the alternative approaches to stability analysis in decision support for damaged passenger ships. *WMU Journal of Maritime Affairs*, 18(3), 477-494. https://doi.org/10.1007/s13437-019-00186-8

van Santen, J. 1986. Stability calculations for jack ups and semi-submersibles, Conference on computer Aided Design, Manufacturer and Operation in the Marine and Offshore Industries CADMO 1986, Washington.

van Santen, J. 2009. The use of energy build up to identify the most critical heeling axis direction for stability calculations for floating offshore structures, *Proceedings of the 10th International Conference on Stability of Ships and Ocean Vechicles (STAB2009)*, St. Petersburg, Russia, 22-26 June 2009, pp. 65-76.

Shigunov, V., Themelis, N., Backalov, I., Begovic, E., Eliopoulou, E., Hashimoto, H., Hinz, T., McCue, L., Miguez Gonzalez, M., Rodriguez, C.A. 2021. Operational measures for intact ship stability, *Proceedings of the 1st International Conference on the Stability and Safety of Ships and Ocean Vehicles*, 7-11 June 2021, Glasgow, Scotland, UK.

Solda, G.S. 1961. Equalisation of Unsymmetrical Flooding, *Transactions of the Royal Institute of Naval Architects*, Vol. 103, pp. 219-225.

Tagg, R., Tuzcu, C. 2003. A Performance-Based Assessment of the Survivability of Damaged Ships: Final Outcome of the EU Research Project HARDER, *Marine Technology*, Vol. 40, No. 4, pp. 288-295.

Tompuri, M, Ruponen, P, Forss, M, Lindroth, D 2014. Application of the Second Generation Intact Stability Criteria in Initial Ship Design, *SNAME Transactions*, Vol. 122, pp. 20-45.

Tompuri, M., Ruponen, P., Lindroth, D. 2016. Second Generation Intact Stability Criteria and Operational Limitations in Initial Ship Design, *Proceedings of PRADS2016*, 4-8 September 2016, Copenhagen, Denmark.

van't Veer, R., de Kat, J., Cojeen, P. 2004. Large Passenger Ship Safety: Time-to-Flood Simulations, *Marine Technology*, Vol. 41, No. 2, pp. 82-88.

Wang, X., Ko, W.J. 2019. Study on submerging operation design for heavy-lift barges based on a real case analysis, *Proc IMechE Part M: J Engineering for the Maritime Environment*, Vol. 233(1) pp. 363–371.

Wendel, K. 1960. Die Wahrscheinlichkeit des Überstehens von Verletzungen, *Schiffstechnik*, 36(7), pp. 47–61.

Wendel, K. 1968. Subdivision of Ships, *Proceedings of the 1968 Diamond Jubilee Int. Meeting – 75th Anniversary*, SNAME, New York, paper N.º 12. 1968.

Keywords

Buoyancy and stability are the most important technical parameters of a ship. These must be carefully considered throughout the design process. Furthermore, relevant stability criteria are frequently checked also on board the ship. In this book the theory of ship buoyancy and stability are presented with several practical applications. The relevant regulations of the International Maritime Organization (IMO), for both intact and damage stability, are also briefly reviewed. The focus is on the underlying physics and description of the applied assumptions and simplifications in the regulations. Therefore, the material is believed to be useful also for graduated naval architects in the industry.

Aalto-ST 8/2021

ISBN 978-952-64-0579-7 (printed)
ISBN 978-952-64-0580-3 (pdf)
ISSN 1799-4896 (printed)
ISSN 1799-490X (pdf)

Aalto University
School of Engineering
Mechanical Engineering
www.aalto.fi